The Use of Driven Equilibrium Conditions

in the Measurement of NMR Relaxation Times

JOHN KENNETH ROBERTS

Doctor of Philosophy

THE UNIVERSITY OF ASTON IN BIRMINGHAM

March 1989

The University of Aston in Birmingham

The Use of Driven Equilibrium Conditions in the Measurement of NMR Relaxation Times.

JOHN KENNETH ROBERTS

Doctor of Philosophy

1989

The further development of the use of NMR relaxation times in chemical, biological and medical research has perhaps been curtailed by the length of time these measurements often take. The DESPOT (Driven Equilibrium Single Pulse Observation of T_1) method has been developed, which reduces the time required to make a T_1 measurement by a factor of up to 100. The technique has been studied extensively herein and the thesis contains recommendations for its successful experimental application. Modified DESPOT type equations for use when T_2^* relaxation is incomplete or where off-resonance effects are thought to be significant are also presented. A recently reported application of the DESPOT technique to MR imaging gave good initial results but suffered from the fact that the images were derived from spin systems that were not driven to equilibrium. An approach which allows equilibrium to be obtained with only one non-acquisition sequence is presented herein and should prove invaluable in variable contrast imaging.

A DESPOT type approach has also been successfully applied to the measurement of $T_1\rho$. $T_1\rho$'s can be measured, using this approach significantly faster than by the use of the classical method. The new method also provides a value for T_1 simultaneously and therefore the technique should prove valuable in intermediate energy barrier chemical exchange studies. The method also gives rise to the possibility of obtaining simultaneous T_1 and $T_1\rho$ MR images.

The DESPOT technique depends on rapid multipulsing at nutation angles, normally less than 90°. Work in this area has highlighted the possible time saving for spectral acquisition over the classical technique $(90°-5T_1)_n$. A new method based on these principles has been developed which permits the rapid multipulsing of samples to give T_1 and M_0 ratio information. The time needed, however, is only slightly longer than would be required to determine the M_0 ratio alone using the classical technique. In ^1H decoupled ^{13}C spectroscopy the method also gives nOe ratio information for the individual absorptions in the spectrum.

NMR, DESPOT, T_1 measurement, Rapid multipulsing, Spin-lock

DEDICATION

This thesis is dedicated to my Uncle, the late John F. Roberts whose interest and support throughout this and other projects was much appreciated, and will be sadly missed in the future.

ACKNOWLEDGEMENTS

CONTENTS

INDEX TO TABLES

INDEX TO FIGURES

CHAPTER 1

INTRODUCTION

1.1. Introduction

Many atomic nuclei behave as though they are spinning. As a result of this spin the nuclei possess angular momentum and magnetic moments. These propeties were first proposed by Pauli (1) to explain some hyperfine splittings observed in atomic spectra. Nuclei possessing magnetic moments will experience a torque when placed in an external magnetic field that causes them to preferentially align with the applied field. This alignment process can be observed indirectly by the ability of the orientated magnetic moments to absorb energy from a magnetic field oscillating in the radio frequency region of the electromagnetic spectrum. This absorption of energy by the nuclear moments forms the basis of the nuclear magnetic resonance (NMR) technique.

The magnitudes of nuclear magnetic moments were first measured by Stern and Estermann (2) in 1933, but it was not until 1939 that Rabi (3) and his co-workers actually observed the NMR phenomenon. They passed a beam of hydrogen molecules through an homogeneous magnetic field. Whilst the molecules were passing through the homogeneous field they applied radio frequency electromagnetic radiation to the beam of molecules. At a sharply defined frequency of the radiation, energy was absorbed and the molecular beam was deflected. The phenomenon was not detected in bulk matter until 1946 when Purcell and his co-workers (4) detected the proton NMR absorption of solid paraffin wax and Bloch and

his co-workers (5) detected the proton absorption of liquid water.

NMR techniques, however, attracted scant attention from chemists until it was discovered (6) that the precise resonant frequency of a particular nucleus was dependent on its chemical environment: Separate resonant positions for different protons in a molecule were observed in 1951 (7). It was realised at this point that the NMR technique could act as a sensitive probe to the structure of molecules and consequently the NMR technique has grown in the last 40 years from a physical curiosity to arguably the most useful and diversely applicable analytical technique available to the modern chemist.

1.2.   An Isolated Nucleus in a Magnetic Field

Atomic nuclei which act   as though they are spinning possess angular momentum. Angular momentum is quantized in units of $\hbar$, where $\hbar$ is Planck's constant (h) divided by 2π. It's magnitude, P, can be written in terms of a quantum number, I, as

$$P = \hbar \sqrt{I(I+1)} \tag{1.1}$$

where I is the spin quantum number of the atomic nucleus. Angular momentum is actually a vector property and therefore the direction as well as the magnitude must be specified. This is accomplished by the use of another quantum number,

m, such that the component of the angular momentum along the z direction, P_z, is given by (Fig. 1.1)

$$P_z = \hbar m \qquad (1.2)$$

Quantum mechanically it can be shown (8) that there are $(2I+1)$ allowed values of m. These allowed values are as in Eqn. 1.3 and illustrated in Fig. 1.1

$$m = I, I-1, I-2, \ldots, -I \qquad (1.3)$$

If a charged body is in motion then it will have associated with that motion a magnetic field. As angular momentum on the atomic scale is quantised so is the magnetic moment, μ associated with it. The magnetic moment of a nucleus may be related to the angular momentum by Eqn 1.4

$$\mu = \gamma P \qquad (1.4)$$

where γ is the gyromagnetic ratio and is a physical constant for a particular nucleus and depends on the charge, mass and a factor analogous to the Landé splitting factor for electrons. Eqn. 1.4 shows that similar equations to 1.1, 1.2 and 1.3 can be written relating μ to the spin quantum number, I.

In the absence of a magnetic field the allowed energy of an isolated nucleus is independent of the quantum

$P_z = \hbar I$

z

$P = \hbar \sqrt{[I(I+1)]}$

θ

$\cos \theta = I/\sqrt{[I(I+1)]}$
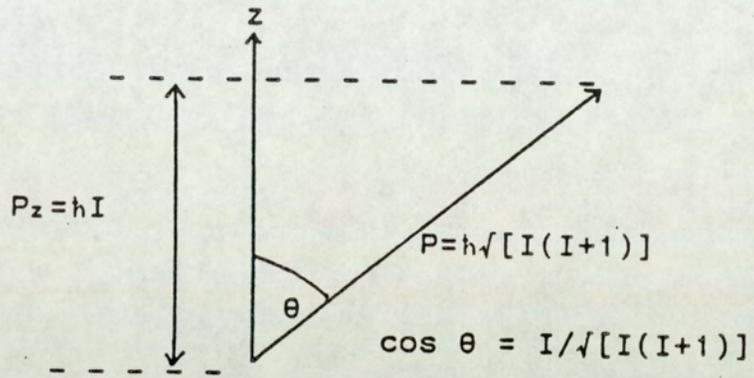
The Maximum Angular Momentum Component P_z

z

I = 1

I = 0

I = -1
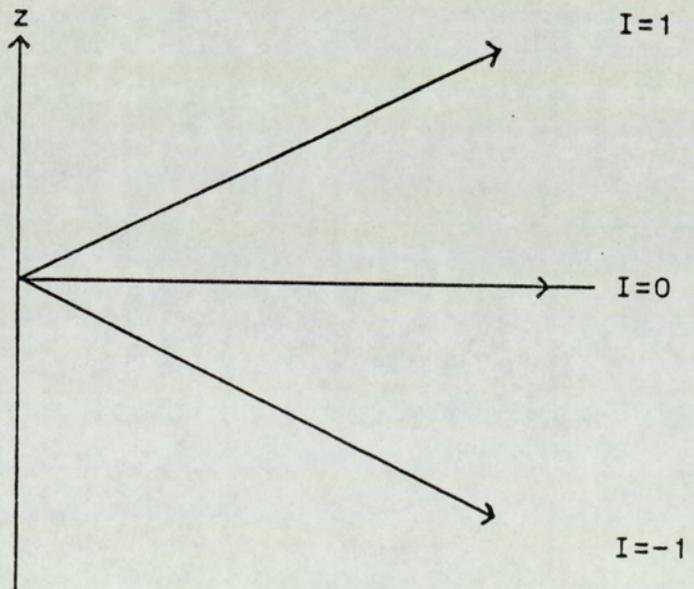
The Possible Orientations for an Angular Momentum Vector
(I=1) in a Static Magnetic Field

Fig. 1.1 Quantization of Angular Momentum

number m. When a field B_0 is applied in the z direction a magnetic moment μ will have an extra energy, U, relative to that in zero field given by 1.5

$$U = \mu \cdot B_0 = -\mu_z B_0 \qquad (1.5)$$

where μ_z is the component of μ in the z direction. Combination of 1.5 with 1.4 and bearing in mind 1.3 and 1.2 leads to

$$U = -\gamma h m B_0 \qquad (1.6)$$

In the presence of the magnetic field the energy of the isolated nucleus is now dependent upon the quantum number m, (see Fig 1.2). It can be seen from Fig 1.2 that each energy level is separated by $h B_0$ and in principle transitions between the levels may be induced by the use of electromagnetic radiation. These transitions will occur when the energy of the applied electromagnetic radiation is equal to the energy between the levels (U). Transitions, however, are only permitted between energy levels when $\Delta m = \pm 1$ (8) and consequently NMR transitions for a single nucleus are given by

$$\nu = \frac{\gamma B_0}{2\pi} \qquad (1.7)$$

where ν is the frequency of the electromagnetic radiation.

1.3 <u>The NMR Experiment</u>
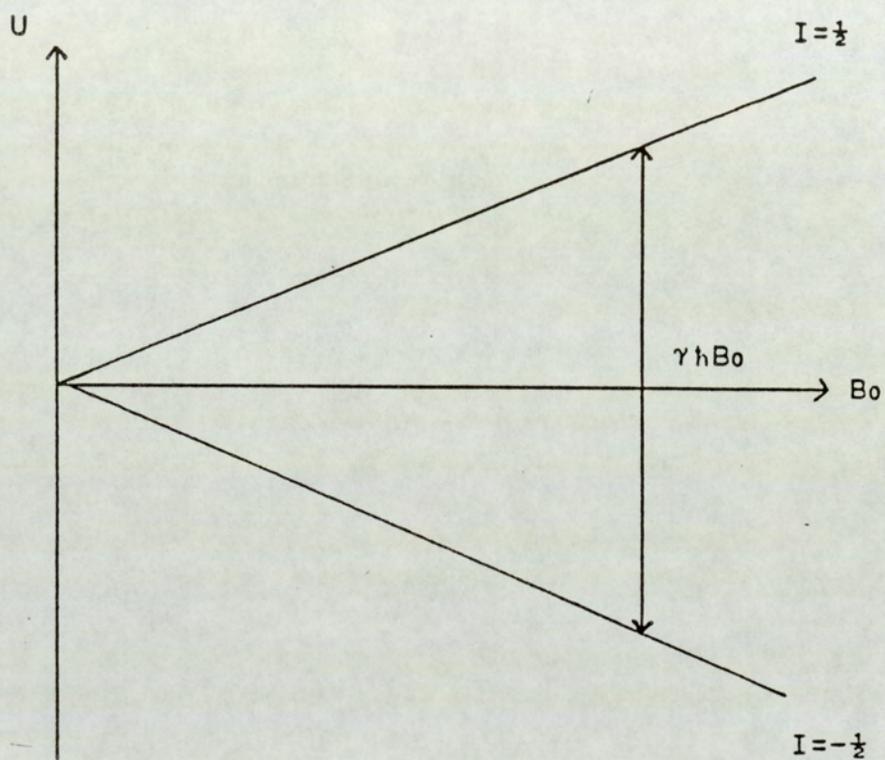
Fig. 1.2 <u>Energy of a Nucleus in a Static Magnetic Field</u>

The NMR experiment can be described both classically and by the use of quantum mechanics. The classical description is better suited to derive a physical picture of the experiment whereas the quantum mechanical approach deals with the expected absorption of energy during the experiment.

1.3.1 The Classical Description of NMR

A nuclear magnetic moment, μ, in a magnetic field, B_0 will lie at some angle θ with respect to the field direction (Fig. 1.1). The interaction between μ and B_0 leads to a torque on the magnetic moment tending to tip it towards the field direction. As the nucleus is spinning the torque does not change θ, but causes the magnetic moment to precess about the field direction.

The torque, L, is given (9) by

$$L = \mu \times B_0 = \frac{dP}{dt} \qquad (1.8)$$

Substituting from 1.4 gives us

$$\frac{d\mu}{dt} = \gamma\mu \times B_0 \qquad (1.9)$$

Since the magnitude of μ cannot change the above equation describes the precession of a magnetic moment about the direction of B_0. This precession of μ with angular velocity given by ω_0 can be expressed by

$$\frac{d\mu}{dt} = \omega_0 \times \mu \qquad (1.10)$$

Comparison of 1.9 and 1.10 shows that

$$\omega_0 = -\gamma B_0 \qquad (1.11)$$

The precessional frequency of μ about B_0 is given by

$$\gamma = \frac{\omega_0}{2\pi} = \frac{\gamma B_0}{2\pi} \qquad (1.12)$$

The above equation is often called the Larmor equation. A vectorial representation of Larmor precession is given in Fig. 1.3.

If a second smaller field B_1 is applied in the xy plane (Fig. 1.3) and is rotating in the same direction as μ an interaction between μ and B_1 occurs. If the field B_1 and μ are rotating at different frequencies then the torque experienced by μ due to B_1 is constantly changing and all that occurs is a slight perturbation of the angle θ. When the field B_1 is rotating at the Larmor frequency, large perturbations of the angle θ occur as μ is tipped towards the xy plane. This corresponds to an absorption of energy, consequently, equations 1.7 and 1.12 are seen to be identical.

In practice the rotating field is produced by applying an A.C. current at a frequency, γ, through a coil surrounding the sample. This corresponds to equal field
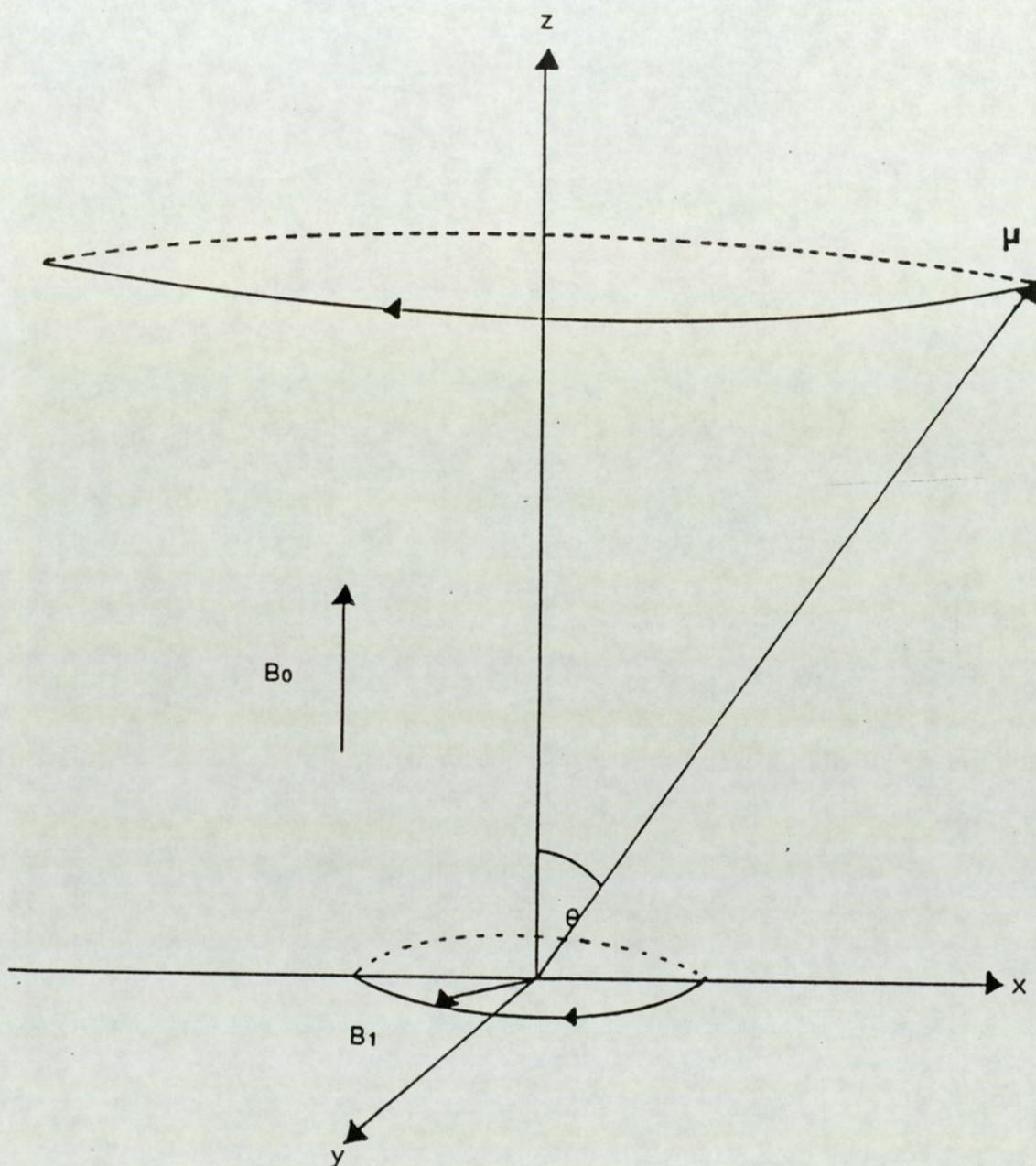
Fig. 1.3 <u>Vectorial Representation of the Classical Larmor Precession</u>

components counterrotating in the xy plane. Only the field
rotating in the same sense as μ will cause NMR transitions;
the other field rotating in the opposite sense to μ is too
far from the Larmor condition to be of significance.

1.3.2. The Quantum Mechanical Treatment of NMR

The energy of interaction between the magnetic
moment and the applied field appears in the Hamiltonian
operator,

$$\mathcal{H} = -\gamma\hbar\mathbf{B_0} \cdot \mathbf{I}$$ (1.13)

In this context I is interpreted as an operator. The
solution of this Hamiltonian yields the discrete (2I+1)
energy levels (8) for the system

$$E_m = -\gamma\hbar m B_0$$ (1.14)

where m can have the values I, I-1, ..., -I. Hence, as in
Eqn 1.3, we can think of the system being described by
(2I+1) discrete energy levels arising from different
orientations of μ with respect to B_0 (Fig. 1.2). The energy
separation of the states is also linearly dependent on the
magnetic field (Eqn. 1.6).

Transitions are induced between the energy levels
by the absorption of energy from the applied electromagnetic
field. The presence of this extra field, B_1, is expressed by

the addition of an extra term to the Hamiltonian.

$$\mathcal{H}' = 2\mu_x B_1 \cos 2\pi\nu t \qquad (1.15)$$

where $2B_1$ is the amplitude and ν is the frequency of the oscillating electromagnetic radiation in the x direction. By the use of transition probability theory (10) the probability of a transition per unit time between the energy levels m and m' is

$$P_{mm'} = \gamma^2 B_1^2 |(m|I_x|m')|^2 \delta(\nu_{mm'} - \nu) \qquad (1.16)$$

where $(m|I_x|m')$ is the quantum mechanical matrix element of I_x between the energy states m and m' corresponding to the absorption or emission of radiation. This element is zero unless the selection rule m=m'±1 is fulfilled. δ is the Dirac δ function which is zero unless $\nu_{mm'} = \nu$. The frequency $\nu_{mm'}$ is given by the Bohr relation previously seen in Eqns. 1.7 and 1.12. Three points should be noted from Eqn 1.16. First the transition probability is proportional to and B_1. Second, due to the selection rule only a single line is observed at a frequency ν. Thirdly the δ function predicts an infinitely sharp resonance line: This is unrealistic due to other factors and so the δ function is replaced by a line-shape function $g(\nu)$ which is

$$\int_0^\infty g(\nu) \, d\nu = 1 \qquad (1.17)$$

Hence for nuclei of spin $\frac{1}{2}$ Eqn. 1.16 becomes

$$P = \tfrac{1}{4}\gamma^2 B_1^2 g(\gamma) \qquad\qquad (1.18)$$

1.4. The Population of Spin States

So far the case of one isolated nucleus has been treated, in a real sample however, there are many different nuclei, each possessing their own magnetic moment. For simplicity in this respect the case of spin $\frac{1}{2}$ nuclei will be treated. One would expect the moments to preferentially align with the field direction in the lowest energy state. This alignment process is opposed by thermal motions which tends to equalise the populations of the two energy states. The actual equilibrium population between the states α (low energy) and β (high energy) is given by the Boltzmann equation.

$$\frac{n_\beta}{n_\alpha} = \exp - \left[\frac{\Delta E}{kT} \right] \qquad\qquad (1.19)$$

where ΔE is the energy difference between the α and β energy states, k is the Boltzmann constant and T the absolute temperature. By combination of 1.2, 1.4 and 1.6, Eqn. 1.19 can be rewritten as

$$\frac{n_\beta}{n_\alpha} = \exp \frac{-2\mu B_0}{kT} \approx 1 - \frac{2\mu B_0}{kT} \qquad\qquad (1.20)$$

Even for ^1H which has a large magnetic moment, the predicted

excess of nuclear moments in the α energy state is only 1.5 x 10^{-5} at room temperature in a field of 2.35T (11). Hence it can be observed readily that the NMR technique is inherently insensitive. The excess of moments in the α state gives rise to a very small macroscopic moment directed along B_0, $\Sigma\mu$. This translates into a volume magnetic susceptibility χ_0

$$\chi_0 = \frac{N\mu^2}{kT} \qquad (1.21)$$

where N is the number of nuclei per unit volume.

This small paramagnetic nuclear susceptibility is ordinarily masked by the larger diamagnetic susceptibility of the electrons associated with the nucleus. Consequently, detection for the purposes of NMR is carried out using the resonance technique. Nuclear paramagnetic susceptibilities, however, have been measured directly in solid hydrogen at low temperature (12).

Eqn. 1.16 predicts the probability of the absorption or emission of radiation. Spontaneous emission has been shown (13) to be dependent on the cube of the transition frequency. Due to the small energies involved in NMR transitions the probability of spontaneous emission is negligible (14). This contrasts with visible spectroscopy where spontaneous emission is the primary relaxation process.

1.4.1 Intensity of NMR absorptions

It was stated above that the NMR technique is inherently insensitive because of the small excess population of magnetic moments in the α energy state. The spin system can absorb energy from the B_1 field at a rate, R, which is dependent on three factors. Firstly, the rate is dependent on the probability, P, per unit time of a transition being induced (Eqn 1.18). Secondly, the rate depends on the population difference between the energy states (Eqn 1.20). Finally, the rate is also dependent on the energy change appropriate to the transition (Eqn. 1.7). Appropriate combination of the various equations shows that the rate of energy absorption is given by

$$R \; \alpha \; \gamma^4 B_0{}^2 N B_1{}^2 g(\gamma)/T \tag{1.22}$$

where T is the absolute temperature. NMR spectrometers, however, do not detect R directly but rather the rate of induced magnetization change in the y direction. This turns out to be equal to R/B_1 and so the observed signal intensity, S, is given by

$$S \; \alpha \; \gamma^4 B_0{}^2 N B_1 g(\gamma)/T \tag{1.23}$$

providing that $n_\alpha - n_\beta$ remains relatively constant. Four points are worth noting from inspection of Eqn 1.23. The signal intensity is proportional to N and therefore NMR is a quantitative technique. Nuclei with low values of γ will

give small signals due to the significant depedence of S on γ. The observed signal is also theoretically proportional to the square of the static field, hence the modern trend towards higher static field spectrometers. Inspection of Eqn 1.23 also shows that the observed signal is inversely proportional to the absolute temperature. Spectra obtained at low temperature, though, often give broad lines due to increased solvent viscosity.

1.5   Relaxation Processes

Although this thesis will be primarily concerned with the use, measurement, and implications of relaxation processes it is necessary to give an initial indication of what relaxation processes are. Relaxation processes, their mechanisms and some of their uses will be discussed in more detail in Chapter 2.

1.5.1   Spin-Lattice Relaxation

For simplicity in the discussion the case of spin $\frac{1}{2}$ nuclei only will be considered. Spin-lattice relaxation is concerned with the establishment of the Boltzmann distribution (Sec. 1.4). When the sample is outside the polarizing magnetic field the energy states α and β are degenerate and hence the populations n_α and n_β are equal. When the sample is placed in the polarizing field the two different energy levels are created instantaneously but the population distribution is not similarly achieved. As

spontaneous emission is negligible the equilibrium excess number of nuclei in the ß state must fall to the α state via interaction with their surroundings (the lattice). This first order rate process is characterised by a "rate constant" $1/T_1$ where T_1 is known as the spin-lattice relaxation time. Let $n = (n_\alpha - n_\beta)$, $n_0 = (n_\alpha + n_\beta)$, $W_{\alpha\beta}$ is the probability of a transition from the α to the ß level and $W_{\beta\alpha}$ is the probability of the reverse transition. The probabilities $W_{\alpha\beta}$ and $W_{\beta\alpha}$ are not equal, but at equilibrium where the number of upward and downward transitions are equal Eqn 1.24 can be written.

$$n_\alpha \, W_{\alpha\beta} = n_\beta \, W_{\beta\alpha} \qquad (1.24)$$

From Eqn. 1.20

$$\frac{W_{\alpha\beta}}{W_{\beta\alpha}} = \frac{n_\beta}{n_\alpha} \approx 1 - \frac{2\mu B_0}{kT}$$

Now putting W = to the average of $W_{\alpha\beta}$ and $W_{\beta\alpha}$, we can write

$$\frac{W_{\alpha\beta}}{W} = \frac{n_{\beta\,eq}}{n_0/2} = 1 - \frac{\mu B_0}{kT}$$

$$\frac{W_{\beta\alpha}}{W} = \frac{n_{\alpha\,eq}}{n_0/2} = 1 + \frac{\mu B_0}{kT}$$

$$(1.25)$$

The rate of change of n is given by

$$\frac{dn}{dt} = \frac{dn_\alpha}{dt} - \frac{dn_\beta}{dt} = 2\frac{dn_\alpha}{dt} \qquad (1.26)$$

From the definition of $W_{\alpha\beta}$ and $W_{\beta\alpha}$

$$\frac{dn_\alpha}{dt} = n_\beta W_{\beta\alpha} - n_\alpha W_{\beta\alpha} \qquad (1.27)$$

Hence by combination of 1.25 to 1.27 together with 1.20 it may be shown that

$$\frac{dn}{dt} = 2W (n_{eq} - n) \qquad (1.28)$$

This is obviously a first order process with a rate constant equal to 2W. From Eqn. 1.28 the spin-lattice relaxation time, T_1 is defined as,

$$T_1 = 1/2W \qquad (1.29)$$

Integration of 1.28 with respect to t and with the inclusion of 1.29 yields

$$n_{eq} - n = (n_{eq})_{t=0} \exp - \left[\frac{t}{T_1} \right] \qquad (1.30)$$

Hence T_1 is a measure of the time required to achieve the Boltzmann distribution of nuclei between the states α and β, and the reason for the name spin-lattice relaxation time becomes evident. Inspection of Eqn. 1.30 reveals that for the actual distribution to be achieved a time, t, of the order of $5T_1$'s is required.

1.5.2 Spin-spin Relaxation

Spins not only exchange energy with the lattice but they can also exchange energy amongst themselves. Unlike spin-lattice relaxation such an exchange of energy does not change the energy of the system and hence does not help the establishment of the Boltzmann equilibrium distribution. The quantum mechanical description of NMR in Sec 1.3.2 predicted infinitely sharp resonance lines. This was stated to be impractical and consequently the line shape function was introduced into Eqn. 1 17. It can be seen from the discussion of 1.5.1 that resonance lines must have a finite width of the order of $1/T_1$ due to the uncertainty principle. In practice NMR lines are often broader than this and it is convenient to define another characteristic time T_2 which is smaller than T_1 to account for this. T_2 is then defined in terms of the maximum value of the line shape function.

$$T_2 = \tfrac{1}{2}[g(\nu)]_{max} = 1/\pi\nu_{\tfrac{1}{2}}$$ (1.31)

where $\nu_{\tfrac{1}{2}}$ is the half height width of a Lorentzian NMR absorption .

The actual value of T_2 is often equal to that of T_1, however, where molecules are large or where solutions are viscous the value of T_2 departs from the value of T_1 (See chapter 2). A relaxation parameter T_2^* often replaces T_2 in Eqn 1.31 for practical NMR line widths. The parameter T_2^* accounts for the broadening of resonance lines due to

inhomogeneity in the polarizing magnetic field. A further relaxation parameter $T_1 \rho$ has a physical significance and will be discussed further in Chapters 2 and 7.

1.6 Macroscopic Magnetization

As pointed out in Sec 1.4, in a real sample we do not deal with a single nucleus but with an ensemble of identical nuclei. Even in the least concentrated samples a large number of nuclei will be present. In dealing with this it is helpful to define **M** as the sum of the individual μ's,

$$M = \Sigma \; \mu_i \hspace{5cm} (1.32)$$

As shown in Fig. 1.4 an ensemble of identical nuclei precessing about the field direction have random phase in the xy direction. This leads to a macroscopic magnetization, **Mo**, aligned along the field axis (usually taken as the z direction): This macroscopic magnetization is responsible for the small nuclear magnetic susceptibility in Eqn. 1.21. From the classical description of NMR presented in Sec. 1.3, the vector μ can now be replaced by **M**. For example an electromagnetic field oscillating at the Larmor frequency in the x direction will cause the magnetization vector **M** to be tipped towards the y axis. This will provide a magnetization component in the xy plane. Such a component corresponds to phase coherence along the y axis which was absent in the equilibrium condition (Fig.1.4). The decay of this phase coherence occurs via energy exchange between the individual

Bo

z

M
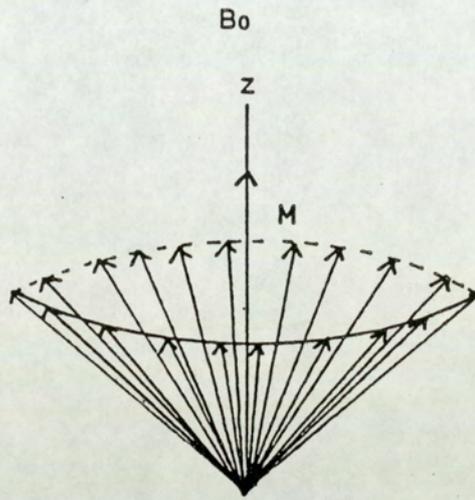
Phase incoherence of individual moments giving rise to a
total magnetic moment M along z axis

z

y

My
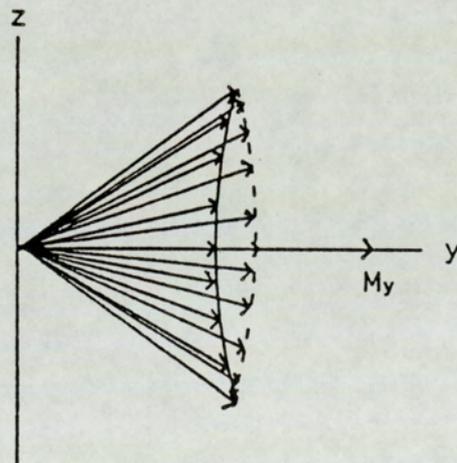
Phase coherence of individual moments when resonance occurs

Fig. 1.4 Phase Coherence of Individual Nuclear Moments away
from Resonance and at Resonance

moments and is characterized by T_2. At the same time the
nuclei will lose the energy they absorbed from the B_1 field
to the surroundings (lattice) and M_z will decay back to its
equilibrium value, M_0, in a time characterised by T_1.

1.6.1 The Bloch Equations

Bloch (15) used the ideas discussed in Sec. 1.6 to
successfully predict the behaviour of a macroscopic
magnetization vector, **M**, in the presence of a fixed magnetic
field, B_0, in the z direction and an oscillating rf field in
the x direction.

By combination of Eqn's 1.9 and 1.32, Eqn. 1.33 can be
written

$$\frac{d\mathbf{M}}{dt} = \gamma \mathbf{M} \times \mathbf{B} \qquad (1.33)$$

where **B** is the total magnetic field experienced by the
macroscopic magnetization vector, **M**. Expansion of the cross
product of Eqn. 1.33 reveals

$$\frac{dM_x}{dt} = \gamma (M_y B_z - M_z B_y)$$

$$\frac{dM_y}{dt} = \gamma (-M_x B_z + M_z B_x) \qquad (1.34)$$

$$\frac{dM_z}{dt} = \gamma (M_x B_y - M_y B_x)$$

The field B_z can be equated to the fixed strong applied field, B_0. The fields B_x and B_y are the components of the rotating field along the x and y axes respectively given by

$$B_{xy} = B_{1x} \cos\omega t - B_{1y} \sin\omega t \qquad (1.35)$$

It should be noted that the above equation only includes the component rotating in the correct sense for absorption to occur. Relaxation has to be accounted for in the equations, Bloch assumed that M_z would decay to its equilibrium value M_0 exponentially (Sec. 1.5.1) with a time constant T_1, whilst M_x and M_y would decay exponentially to zero with a different time constant T_2. Overall then the Bloch equations can be written as

$$\frac{dM_x}{dt} = \gamma(M_y B_0 + M_z B_1 \sin\omega t) - \frac{M_x}{T_2}$$

$$\frac{dM_y}{dt} = \gamma(M_z B_1 \cos\omega t - M_x B_0) - \frac{M_y}{T_2} \qquad (1.36)$$

$$\frac{dM_z}{dt} = -\gamma(M_x B_1 \sin\omega t + M_y B_1 \cos\omega t) - \frac{(M_z - M_0)}{T_1}$$

1.6.2. The Rotating Frame of Reference

The equations represented by Eqn. 1.36 take a considerably simpler form if they are related to a frame of reference (x',y',z) rotating at an angular velocity $-\omega$ about the z axis. The components of magnetization perpendicular to

the z axis will be designated u and v where u represents the component along the x' axis and v represents the component along the y' axis.

$$u = M_x \cos \omega t - M_y \sin \omega t$$

(1.37)

$$v = M_x \sin \omega t + M_y \cos \omega t$$

Using these equations the Bloch equations (Eqn. 1.36) can be rewritten

$$\frac{dM_z}{dt} = -\gamma B_1 v - \frac{(M_z - M_0)}{T_1}$$

$$\frac{du}{dt} = (\omega_0 - \omega)v - \frac{u}{T_2}$$

(1.38)

$$\frac{dv}{dt} = -(\omega_0 - \omega)u + B_1 M_z - \frac{v}{T_2}$$

It is worth taking some time to consider a physical picture of the rotating frame. The frame is considered to be rotating at an angular velocity, ω, which means the B_1 field is stationary in this frame of reference. Moreover, the precessional rotation of the magnetization vector in this frame can be regarded as $(\omega_0 - \omega)$ as opposed to ω_0 in the laboratory frame. Recalling Eqn. 1.12 this corresponds to precession in an apparent field, B_{app}, given by

$$B_{app} = (\omega_0 - \omega)/\gamma = B_0 (1 - \omega/\omega_0)$$

(1.39)

Now the total field, B_t experienced by M_z is the vector sum of B_0 and B_1, but as $B_0 \gg B_1$ the approximation $B_t \approx B_0$ holds in practice. It is useful, however, to define an effective field, B_{eff} which is the vector sum of the apparent field of Eqn 1.39 and the field B_1 (Fig. 1.5). In the rotating frame the magnetization vector, **M** will precess about B_{eff}. When ω and ω_0 differ significantly B_{eff} will tend to B_0 and precession about the static field direction will occur. When ω tends towards ω_0 precession about B_{eff} will tend towards precession about B_1 (i.e. **M** will precess at a rate γB_1 in the zy' plane). B_1 will only have a significant effect on B_{eff} when ω is close to ω_0 (i.e. resonance) and the difference ($\omega - \omega_0$) can be interpreted as an off-resonance parameter. As the signal detected in the NMR experiment is induced by the rate of change of M_y (Sec 1.4.1) then a signal will be detected when $\omega \approx \omega_0$ as the M_y component will be finite (Fig. 1.4).

1.6.3 <u>Steady State NMR Experiments</u>

If the time derivatives of Eqn's 1.38 are equated to zero then the Eqn's 1.38 can be solved to give

$$M_z = \frac{M_0 \left[1 + T_2^2 (\omega_0 - \omega)^2 \right]}{T_2^2 (\omega_0 - \omega)^2 + 1 + T_1 T_2 \gamma B_1^2}$$

$$(1.40)$$

$$u = \frac{M_0 B_1 T_2^2 (\omega_0 - \omega)}{T_2^2 (\omega_0 - \omega)^2 + 1 + T_1 T_2 \gamma B_1^2}$$
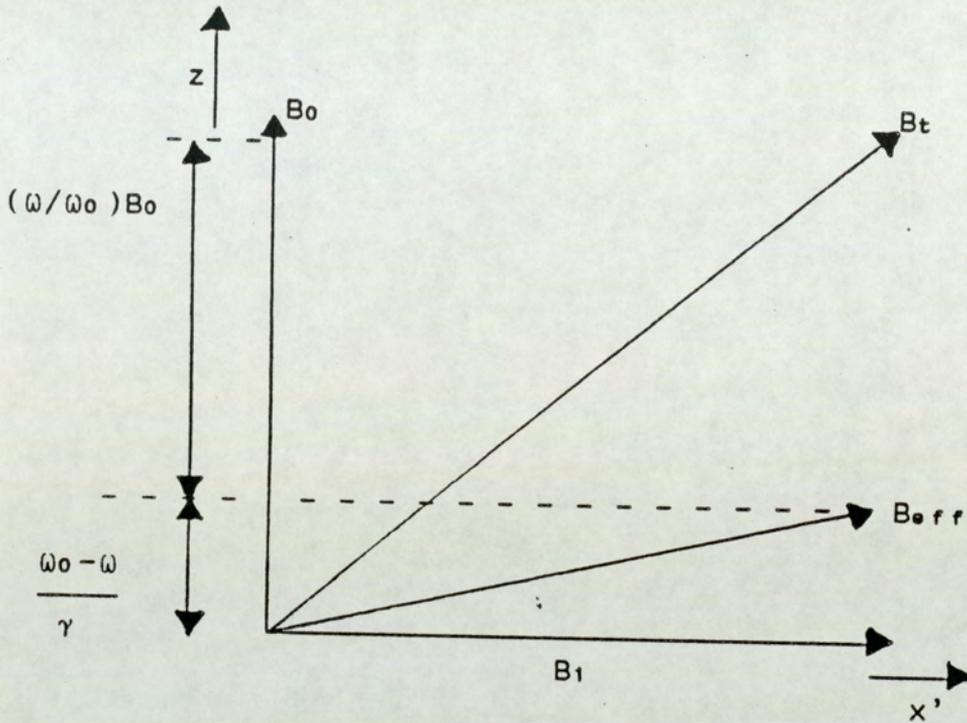
Fig. 1.5 **Magnetic Fields in the Rotating Frame of Reference**
(See text)
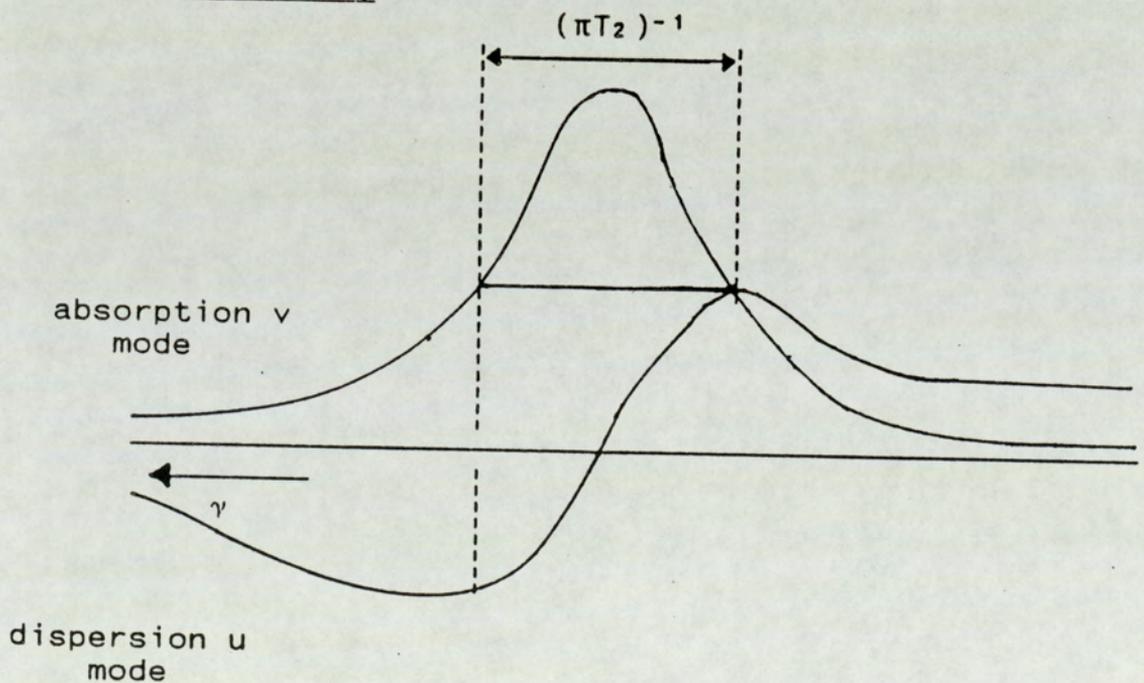
Fig. 1.6 **Shapes of u and v Mode Signals from Bloch**
Equations

$$v = \frac{M_0 \ B_1 \ T_2}{T_2{}^2 \ (\omega_0 - \omega)^2 + 1 + T_1 \ T_2 \ \gamma B_1{}^2} \qquad (1.40)$$

Figure 1.6 shows the shapes of the u and v mode signals as predicted by the Bloch equations when the condition $\gamma B_1 \ll (T_1 T_2)^{-\frac{1}{2}}$ is fulfilled. The absorption (v mode) signal is proportional to

$$g(\nu) = \frac{2T_2}{1 + 4\pi^2 T_2{}^2 (\nu_0 - \nu)^2} \qquad (1.41)$$

This is the lineshape factor mentioned in Eqn (1.31) and shows the relationship between the observed line width and the relaxation parameter T_2 (Fig. 1.6). Eqn 1.41 predicts that the observed line shape in NMR experiments is Lorentzian (15,17).

1.6.3.1 Practical Steady State NMR Experiments

It is worth at this point considering the practical consequences of equating the time derivatives of Eqn's 1.38 to zero. When using continuous wave techniques (i.e. scanning the frequency range at fixed field or vice-versa) (Sec. 3.1) the practical consequence of equating the time derivatives to zero is that the frequency or field must be scanned very slowly. This is called the slow passage approximation and the resulting spectrum gives NMR resonance absorptions of the shapes predicted by Bloch. The upshot of scanning the frequency or field very slowly is that the

spectrum takes a very long time to record. If the field or
frequency is scanned too quickly then the observed NMR
absorption lines are distorted from the shapes predicted by
Bloch. This distortion usually takes the form of wiggle
beats on the upscan side of the absorption. NMR spectra can
also be obtained by applying a square wave pulse of
frequency close to the Larmor frequency along the x axis
for a sample in a static field (Sec 3.1). The resulting
interferrogram can then be fourier transformed to yield the
NMR spectrum. Ernst and Anderson (16) showed that on fourier
transformation the resulting spectrum gave absorptions of
the shape predicted by Bloch and could be equated to a slow
passage spectrum. Consequently, the use of fourier
transformation techniques has increased rapidly in the last
20 years (Chap. 3).

1.6.4. <u>Factors Affecting Line Widths</u>

Section 1.5.2 showed that resonance lines have a
finite width due to the uncertainty principle. It can be
seen from Eqn. 1.41 that the lines should be Lorentzian in
shape with the half height width being described by Eqn.
1.31. The resonance lines are often not Lorentzian in shape
and their half height widths do not follow from Eqn. 1.31.
There are several reasons for this which will be discussed
below.

1.6.4.1 Paramagnetic Species

Paramagnetic species, be they unpaired electrons, or other magnetic nuclei cause fluctuations in the static field at the observed nucleus. These fluctuating fields are proportional to the magnetic moment, μ, of the paramagnetic species and inversely proportional to the distance, r, between the paramagnetic species and the observed nucleus. The main effect of this is to cause an increase in the efficiency of nuclear relaxation and hence a subsequent increase in the width of the resonance line. In cases where μ is large (e.g. for an unpaired electron) the resonance line may not be observable at all. It is, therefore, of paramount importance to remove as far as possible all paramagnetic impurities from the sample under investigation. The principles described above will be described more fully in Chapter 2.

1.6.4.2 Quadrupole Effects

Nuclei with spin quantum number, I, greater than $\frac{1}{2}$ possess a nuclear quadrupole moment arising from a non spherical distribution of nuclear charge. Quadrupoles may precess in the presence of an electric field gradient enabling transitions to occur among the nuclear quadrupole energy levels. This process is often more efficient than the dipole relaxation processes (Chapter 2) exhibited by spin $\frac{1}{2}$ nuclei. Consequently, the relaxation times are reduced and the resonance lines tend to be broad.

1.6.4.3 Magnetic Field Inhomogeneity

The NMR resonance condition depends on the value of B_0, if this value is not constant across the sample volume then the resonance line will consist of a superposition of many resonance lines due to the value of B_0 at particular points in the sample. As, in practice, NMR magnets are generally very homogeneous the observed line is approximately lorentzian in shape but with a half height width greater than that predicted by Eqn. 1.31. The observed half height width is related to the parameter T_2^* which gives an indication of the homogeneity of the polarizing magnetic field. Spinning of the sample averages out the field gradients across the sample to a large extent thus increasing T_2^* but can lead to the observation of spinning side bands in the spectrum.

1.6.4.4 Digital Resolution

Fourier transform NMR relies on the digitisation of an analogue signal to eventually yield the spectrum (See Chap 3). If there are an insufficient number of data points across the spectral width then the peak shape will be determined by the data point resolution to a large extent.

1.7 The Chemical Shift

Although this thesis is not primarily concerned with chemical shifts, the chemical shift is so important to the

NMR technique that a brief discussion of its concepts will be given below.

1.7.1 Nuclear Screening

When a magnetic nucleus is placed in a magnetic field, the electrons surrounding the nucleus precess in the field in the opposite way to the nucleus (Lenz's law). As electrons are charged this motion leads to a secondary magnetic field, opposing the static field, B_0, at the nucleus. Consequently the field "felt" by the nucleus, B_{eff}, is smaller than the applied polarizing field and is given by

$$B_{eff} = B_0 (1 - \sigma) \tag{1.42}$$

where σ is the screening or shielding constant. The screening constant is small and has different values for different nuclei. In general it ranges between the values of 10-1000 ppm of the static field for NMR active nuclei in varying chemical environments. The screening constant, however, cannot be measured directly and so all measurements are taken relative to a reference compound.

1.7.2 Spectral Referencing

Chemical shifts are reported in ppm of the carrier frequency on a fixed field spectrometer. As ν determines B_0 and vice-versa, the reported value in ppm is independent of

the spectrometer field strength. For a fixed field spectrometer the chemical shift, δ, of a species, a, from a reference, r, in ppm units is given by

$$\delta \equiv \frac{\nu_a - \nu_r}{\nu_r} \times 10^6 \approx (\sigma_r - \sigma_a) \times 10^6 \qquad (1.43)$$

where ν represents the resonance frequencies of the sample and reference. The definition in Eqn 1.43 could have been reversed so that the value of δ increases with increased shielding. For a long time both conventions were in exsistence but the definition above has now been approved by I.U.P.A.C. (18). The choice of a reference compound is important. For ^1H and ^{13}C spectroscopy a popular reference is T.M.S. (Tetramethyl silane) whereas for ^{31}P the usual reference is 85% phosphoric acid in water. Obviously different references are required for different applications and so the reference used should always be quoted. The referencing technique is also important ie, whether an internal or external reference is used. Internal referencing is possibly the most accurate but suffers from possible association of the reference with the compound under study. External referencing overcomes this problem but requires the chemical shifts to be corrected for volume magnetic susceptibility (19) and the disadvantage of this is that the volume magnetic susceptibilities are not always known. Homer (20) has accurately measured chemical shifts by dispersed phase referencing which combines the advantages of both internal and external referencing techniques.

1.7.3. Use of Chemical Shifts

The sheilding constant and hence the chemical shift is affected by the electron distribution around the observed nucleus. Theoretically, it is very difficult to predict a chemical shift and it is therefore necessary to rely on empirical correlations between observed chemical shifts and structure. Much work has been carried out on such correlations for many nuclei (21,22,23,24,25), allowing chemical shifts to be related to structure in most cases.

1.7.4 Theory of Chemical Shifts

Although in general NMR chemical shifts cannot be predicted with precision the effect of substituents and the chemical shifts of NMR active nuclei in differing chemical environments can often be understood. Ramsey (26) produced an expression for σ which depended on two parameters. The first σ_d is called the diamagnetic term and is always >0. This term takes account of nuclear screening resulting from the motion of electrons around the nucleus. The second σ_p is the temperature independent paramagnetic term and is always negative. This term takes account of any mixing of low lying electronic levels of the same symmetry due to the presence of B_0 and is therefore considerably affected by p and d orbitals near the nucleus. The fact that the ^1H nucleus has no suitable low lying orbitals is primarily reponsible for its small chemical shift range. Apart from these two terms, an observed chemical shift can be affected by the

electronegativity of neighbouring functional groups (27,28),
magnetic anisotropy (29), induced ring currents (30) and
solvent effects (31,32).

1.8 Spin-spin Coupling

NMR spectra, as may have been implied so far do not
just consist of single lines at varying chemical shifts. NMR
absorption lines often appear as multiplets. These
multiplets appear due to interactions between nuclei that
cause changes in the value of B_{eff} at a particular nucleus.
This interaction is known as spin-spin coupling and
provides valuable information on chemical structure and
stereochemistry (33,34). As for chemical shifts the basic
concepts will be outlined below.

1.8.1 Origin of Spin-spin Coupling

Spin-spin coupling is independent of the B_0 field
strength and is not averaged out by rapid random motion of
molecules in solution as are the interactions due to the
presence of other magnetic nuclei surrounding a particular
nucleus in solution (Sec 2.4.1). Ramsey and Purcell (35)
explained spin-spin coupling on the basis of the spin
orientation of nuclei being transmitted through the
electrons forming the chemical bond. Consider two magnetic
nuclei, A and B, of spin ½ chemically bonded via a covalent
bond. If A is aligned parallel with the B_0 field then an
electron close to nucleus A will tend to align in the anti-

parallel fashion. An electron close to nucleus B but in the same orbital as the electron close to nucleus A will align in a parallel fashion due to the Pauli exclusion principle. Consequently nucleus B will tend to align anti-parallel with the B_0 field and thus the spin orientation of A is transmitted to B via the bonding electrons. The difference in energy between A and B being anti-parallel as opposed to parallel with each other is small and therefore the observed lines tend to be of equal intensity. The coupling constant, J_{AB}, is measured in Hertz.

1.8.2 First Order Analysis

When first order conditions are fulfilled a nucleus coupled to n nuclei of spin I will have its resonance split into $2nI + 1$ lines. For the case of $I=\frac{1}{2}$ the intensities of the n+1 lines correspond to the coefficients of the binomial theorem. The lines are separated by J Hz, the coupling constant. Spin-spin coupling is only observed between magnetically non-equivalent nuclei. For first order analysis to be applicable the criteria $|(\gamma_a-\gamma_b)|\gg J_{AB}$ must be fulfilled and departure from this criterion results in the distortion of the intensities from the expected binomial distribution.

1.8.3 Use of Coupling Constants

As with chemical shifts the theoretical calculation of the magnitude and sign of coupling constants is not

realistically possible. Coupling constants are affected by the hybridisation of chemical bonds (36), dihedral bond angles (37) and the electronegativity of substituents (36). As for chemical shift values extensive tables of structural moieties with their observed coupling constants have been prepared as an aid to structural analysis. Recently, coupling constants have been used to great effect in spectral editing techniques such as D.E.P.T. (38) and ^{13}C-^{13}C coupling constants have been obtained (39) as an aid to the structural determination of the carbon skeleton of peptides.

CHAPTER 2

NMR RELAXATION

2.1 Introduction

In Sec. 1.6 the rate of transfer of energy between the nuclear spins and the lattice were found to be instrumental in governing NMR line widths. In this chapter the mechanisms leading to NMR relaxation will be discussed in more detail. A survey of the use of relaxation times in solving chemical, biological and medical problems will also be presented.

2.2 The Origins of Relaxation for Spin $\frac{1}{2}$ Nuclei

Transitions between nuclear spin states (α and β) for spin $\frac{1}{2}$ nuclei can only be induced by magnetic fields. In order to establish the Boltzmann distribution of Eqn. (1.20) in a liquid sample, fluctuating magnetic fields must be present in the bulk of the sample. Such fluctuating magnetic fields are present within the sample due for example to the thermal motion of molecules containing nuclei possessing magnetic moments. This randomly fluctuating field may be resolved into frequency components via fourier analysis and may be further divided into contributions parallel and perpendicular to the static field, B_0. As would be expected from the discussion in Sec. 1.3, the component of the field fluctuating at the Larmor frequency, perpendicular to the static field, induces transitions similar to those induced by an electromagnetic field, thus causing relaxation towards the Boltzmann distribution. The component of the fluctuating field perpendicular to the static field also causes T_2

relaxation by changing the average life time of a moment in the α or β state and hence, via the uncertainty principle, effecting the line width and T_2 (Sec. 1.5.2). It should be noted that fluctuations in the x and y directions can effect T_1 whereas a component M_y can only be affected by fluctuating fields at the Larmor frequency in the x direction. Hence from fluctuations perpendicular to the applied field alone we would expect $T_2 = 2T_1$. However, there is a further contribution to T_2 relaxation from the component of the fluctuating field in the z direction. This has no effect on T_1 relaxation but causes T_2 relaxation by causing an inhomogeneity in the applied field (Sec. 1.6.4.3). For a mobile liquid this extra contribution makes $T_1 \approx T_2$.

2.3 The Theory of Relaxation

For simplicity we will consider a system of isolated spins being acted upon by an isotropic random magnetic field in a time varying fashion. The x component of this field may be written as

$$B_{x1} = B^o_{x1} f(t) \qquad\qquad (2.1)$$

where $f(t)$ has an average equal to zero and a root mean square average of unity. B^o_{x1} is the rms amplitude of the field. A similar expression may be written for the y component of the field. The interaction Hamiltonian may be written as

$$\mathcal{H}' = -\gamma\hbar I . B'(t) \qquad (2.2)$$

where $B'(t) = \sqrt{(B_{x1}^2 + B_{y1}^2)}$

Perturbation theory (10) shows that this induces transitions at a rate

$$W = \tfrac{1}{2}\gamma^2 [B^0{}_{x1}]J(\omega_0) \qquad (2.3)$$

where $J(\omega_0)$ is the power available from the fluctuating magnetic field at the Larmor frequency ω_0. W is the transition probability used in Eqn. (1.29). Combination of 2.3 with 1.29 reveals

$$\frac{1}{T_1} = 2W = \gamma^2 [B^0{}_{x1}] J(\omega_0) \qquad (2.4)$$

Further development of the theory requires some information about the nature of the fluctuations. Under certain specialised conditions it is possible to make use of the theory of Brownian motion. This procedure was first adopted by Bloembergen et al. (40) who considered the fluctuating field $B'(t)$ to arise from the rotational and translational motion of individual molecules perturbed in time by molecular collisions. For the Brownian motion approximation to be valid many such collisions must occur during the mean time it takes a molecule to rotate or translate through a distance characteristic of one molecular spacing. In the liquid state this is a reasonable approximation. In the

gaseous state however, the approximation is invalid. The nature of the fluctuations is governed by f(t). The important point in the discussion is the "memory" which is expressed in terms of an auto-correlation function $G(\tau)$, defined as

$$G(\tau) = \overline{f(t)f(t+\tau)} \qquad (2.5)$$

where the horizontal bar denotes an ensemble average. The function is independent of t but indicates how f(t) changes. The value of $G(\tau)$ must decay with τ, as "memory" is lost. The term "memory" requires some explanation and can perhaps be best explained in terms of a given molecule. Suppose a molecule is at a certain position (x,y,z) in space at a certain time (t). At a time (t+τ) the molecule will have moved to another position (x',y',z'). The "memory" expresses the dependence of the co-ordinates (x',y',z') on (x,y,z). If the time τ is large there will be little dependence whereas if the time τ is small the co-ordinates (x',y',z') will be more dependent on the original co-ordinates (x,y,z). Bloembergen et al assumed that this decay of "memory" was an exponential process

$$G(\tau) = \exp -(\tau/\tau_c) \qquad (2.6)$$

where τ_c is the correlation time and is a characteristic time representing the decay of the "memory". In the case of Brownian motion controlled processes this roughly corresponds to the time required for a molecule to move through one radian. Obviously a more mobile solution will

have a smaller value of τ_c. Extending Debye's theory (41) Bloembergen et al (40) related the correlation time to the viscosity of the solution by assuming that the molecule was a sphere of radius, r, turning in a viscous fluid.

$$\tau_c = \frac{4\pi \eta r^3}{3kT} \tag{2.7}$$

where η represents the viscosity of the medium

The auto-correlation function $G(\tau)$ is obviously a time domain function which by fourier transformation (42) corresponds to $J(\omega)$.

$$J(\omega) = \int_{-\infty}^{\infty} G(\tau) \exp(-i\omega\tau) \, d\tau \tag{2.8}$$

Substitution of Eqn. 2.6 into Eqn. 2.8 followed by integration reveals a Lorentzian form for $J(\omega)$

$$J(\omega) = 2\tau_c / (1 + \omega^2 \tau_c^2) \tag{2.9}$$

Further substitution into Eqn. 2.4 gives

$$\frac{1}{T_1} = \gamma^2 [B^0{}_{x1}]^2 \frac{2\tau_c}{1 + \omega_0{}^2 \tau_c{}^2} \tag{2.10}$$

Figure 2.1 shows a plot of the form $J(\omega)$ against $\log(\omega)$. The plot is noticeably flat in the region where $1 \gg \omega\tau_c$, and this is known as the extreme narrowing condition. In this region Eqn. 2.10 can be rewritten as
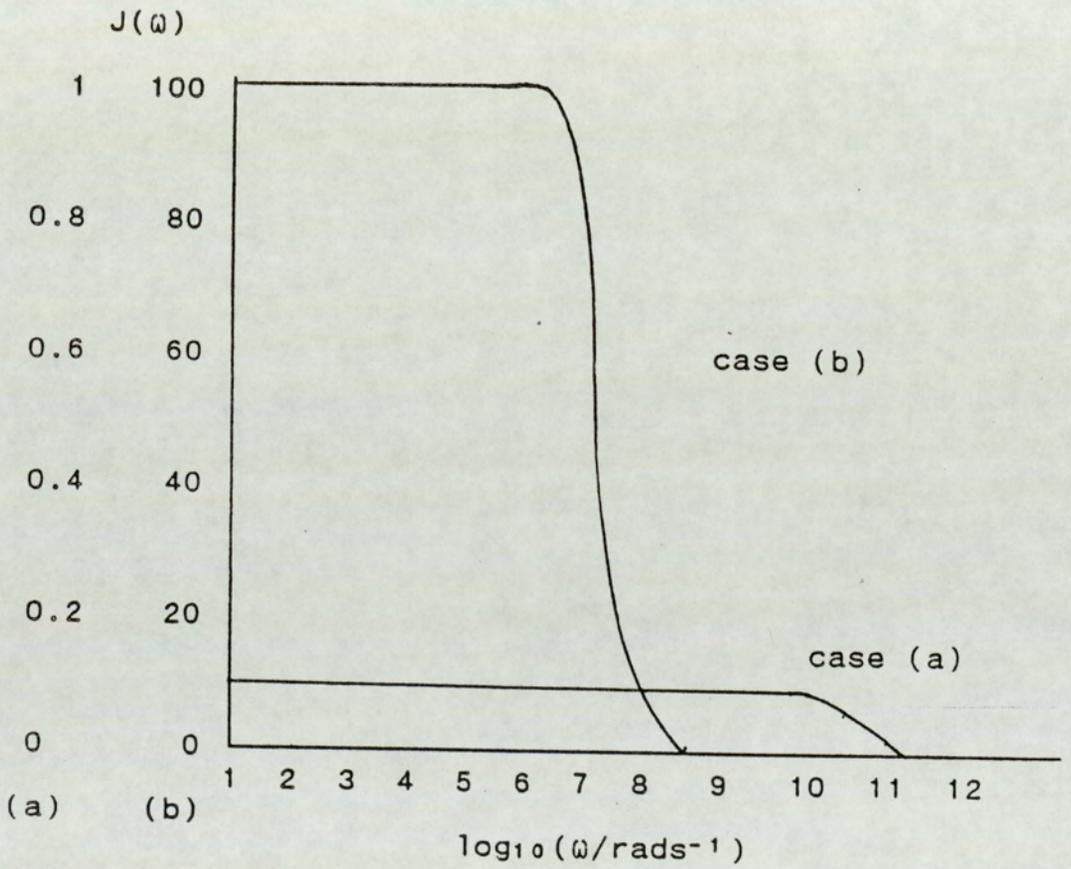
Fig. 2.1 <u>Plot of Spectral Density (arb. units) as a function of frequency ω/rad s^{-1} (a) in the extreme narrowing region, τ_c=30ps (b) away from extreme narrowing, τ_c=30ns</u>

$$T_1{}^{-1} = 2\gamma^2 [B^0{}_{x1}]^2 \tau_c \qquad (2.11)$$

Molecular tumbling in mobile solutions gives τ_c a value of approximately 1×10^{-12} secs., so for the usual magnitude of resonance frequencies the extreme narrowing condition holds. Eqn. (2.11) predicts that T_1 will fall as τ_c increases i.e. as mobility falls or as the temperature is decreased. If, however, τ_c becomes long so that the extreme narrowing condition no longer holds then T_1 must be predicted from Eqn. (2.10). This predicts a minimum value for T_1 when the condition $\tau_c = \omega_0{}^{-1}$ is fulfilled (Fig 2.2). This condition can realistically occur for macromolecules in solution and T_1(min) can be predicted from Eqn. 2.12

$$T_1(\text{min})^{-1} = \gamma^2 [B^0{}_{x1}]^2 / \omega_0 \qquad (2.12)$$

Equation (2.12) clearly shows that T_1(min) will be dependent on the spectrometer operating frequency and hence as the static field B_0 increases the minimum value of T_1 increases (Fig. 2.2). Fig. 2.2 shows the variation in T_2 and $T_1 \rho$ with the log τ_c also. It was stated in Sec 2.2 that T_2 also depended on the fluctuating fields perpendicular to the static field, B_0, and consequently the T_2 curve follows the T_1 curve whilst the extreme narrowing condition holds. T_2 also depends on the fluctuations in the z direction which cannot effect T_1; this contribution involves no energy exchange, and the appropriate spectral density function describing it is $J(0)$. The influence of the $J(0)$ term causes T_2 to decrease monotonically as τ_c increases in contrast to
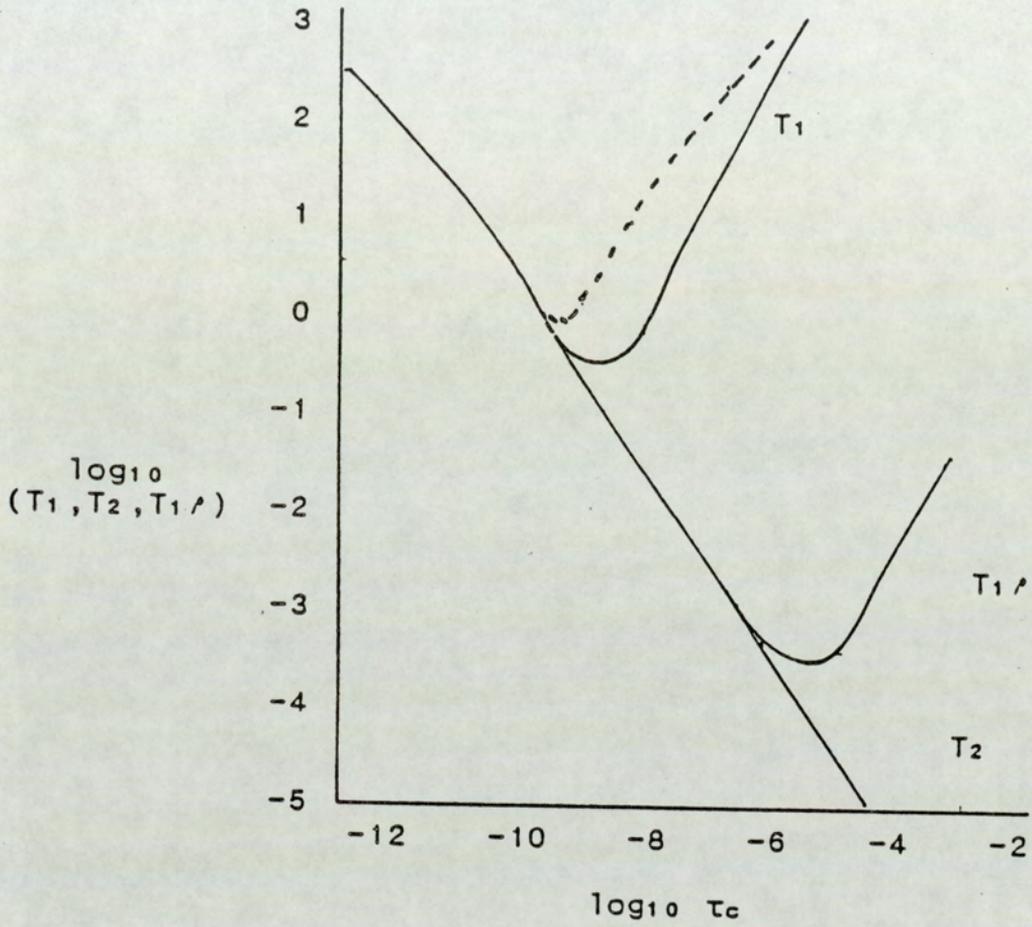
Fig 2.2 <u>Plot of $\log_{10}(T_1, T_2, T_1\rho)$ against $\log_{10}(\tau_c)$ solid curve represents $\gamma_0 = 100$ MHz, dotted curve $\gamma_0 = 400$ MHz. $T_1\rho$ curves are based on $\gamma B_1/2\pi = 40$ KHz. RMS random field based on 0.2 mT.</u>

T_1. $T_{1\rho}$ also shows a minimum but at a much longer correlation time than T_1, this is because $T_{1\rho}$ depends on the spectral density function $J(\Omega)$ where $\Omega = \gamma B_1$. As Ω lies between zero and ω_0, $T_{1\rho}$ represents the situation between T_1 and T_2. The parameter $T_{1\rho}$ is very useful in chemical exchange and large molecule studies as it effectively extends the extreme narrowing region. Proton T_2 measurements are often not possible due to spin-spin coupling (Sec 7.2.1). The equations for $T_{1\rho}$ and T_2 used in the derivation of Fig. 2.2 are presented as Eqn. 2.13 and 2.14 respectively.

$$\frac{1}{T_{1\rho}} = \frac{1}{6} \gamma^2 \{[B^0_{x1}]^2 + [B^0_{y1}]^2 + [B^0_{z1}]^2\}\{J(\Omega) + J(\omega_0)\} \quad (2.13)$$

$$\frac{1}{T_2} = \frac{1}{2T_1} + \frac{1}{2} \gamma^2 [B^0_{z1}]^2 J(0) \quad (2.14)$$

2.4 Relaxation Mechanisms

2.4.1 Dipolar Relaxation

In Sec. 1.6.4.1 it was stated that other magnetic nuclei in a system could lead to line broadening and hence relaxation. At a molecular level a given magnetic nucleus will be affected by the local field due to its neighbours. This field of course will be constantly changing due to the motion of the nuclei relative to each other in a liquid sample both intra-and intermolecularly.

Consider the relaxation of a nucleus I by another

magnetic nucleus S (an unpaired electron or another nucleus). The local field, B^{dd}, due to S at I is given classically by

$$B^{dd} = \pm\mu_s \, (3 \cos^2 \theta -1) \, r^{-3} \qquad (2.15)$$

where r is the distance between I and S and θ is the angle between the static field and the axis joining I and S. These local fields are quite large (larger than those due to chemical shifts or coupling constants) but as a rule have no bearing on high resolution spectra as the molecular motion results in the averaging of B_{dd} to zero (43). In solids and liquid crystals such averaging does not occur and large splittings due to the dipoles are observed. It should be emphasised that the mean squared value of B_{dd}, however, is non zero. As dipolar interactions occur mutually between the spins they cannot strictly be treated via the random field model of Sec 2.2. Solomon (44) treated the case of two spin $\frac{1}{2}$ nuclei with a scalar coupling constant $J_{is} \ll \delta_{is}$ and showed that the rates of relaxation were mutually dependent on each other.

$$d\langle I_z \rangle/dt = -\rho_i [\langle I_z \rangle - I_0] - \sigma[\langle S_z \rangle - S_0]$$

$$\qquad (2.16)$$

$$d\langle S_z \rangle/dt = -\rho_s [\langle S_z \rangle - S_0] - \sigma[\langle I_z \rangle - I_0]$$

The terms ρ and σ are defined in terms of transition probabilities previously described in Sec. 1.5.1.

$$\rho_i = 2W_1{}^I + W_0 + W_2 = 1/T_1{}^I$$

$$\rho_s = 2W_1{}^S + W_0 + W_2 = 1/T_1{}^S \qquad (2.17)$$

$$\sigma = W_2 - W_0 = 1/T_1{}^{IS}$$

where the subscripts on the W's represent the change in the quantum number, m, involved in the transition between the energy levels. The terms W_0, $W_1{}^i$, and W_2 have been calculated in terms of the correlation time, τ_c (45)

$$W_1{}^i = \frac{3}{20} \frac{\gamma_i{}^2 \gamma_s{}^2 \hbar^2}{r^6} \frac{\tau_c}{1 + \omega_i{}^2 \tau_c{}^2}$$

$$W_0 = \frac{1}{10} \frac{\gamma_i{}^2 \gamma_s{}^2 \hbar^2}{r^6} \frac{\tau_c}{1 + (\omega_i + \omega_s)^2 \tau_c{}^2} \qquad (2.18)$$

$$W_2 = \frac{3}{5} \frac{\gamma_i{}^2 \gamma_s{}^2 \hbar^2}{r^6} \frac{\tau_c}{1 + (\omega_i + \omega_s)^2 \tau_c{}^2}$$

When the extreme narrowing condition is fulfilled the frequency terms in the denominator can be neglected.

The four energy level system is presented in Fig. 2.3. Several points should be noted from eqn's 2.16. The selection rule $\Delta m = \pm 1$ is not obeyed for dipole-dipole relaxation in contrast to transitions occurring between energy levels due to r.f. pulses (Sec. 1.2). T_1 relaxation is now no longer a single exponential process, indeed in coupled systems T_1 has no particular meaning at all. For the relaxation to be exponential the cross relaxation term, σ, must to be zero and then equation 2.17 reduces to equation 1.29. This only occurs when there is no coupling between the spins I and S. Equations 2.16 represent a set of coupled differential equations whose solutions depend on the boundary conditions used (46). In the case where only the I (or S) spins are excited the recovery is strictly non
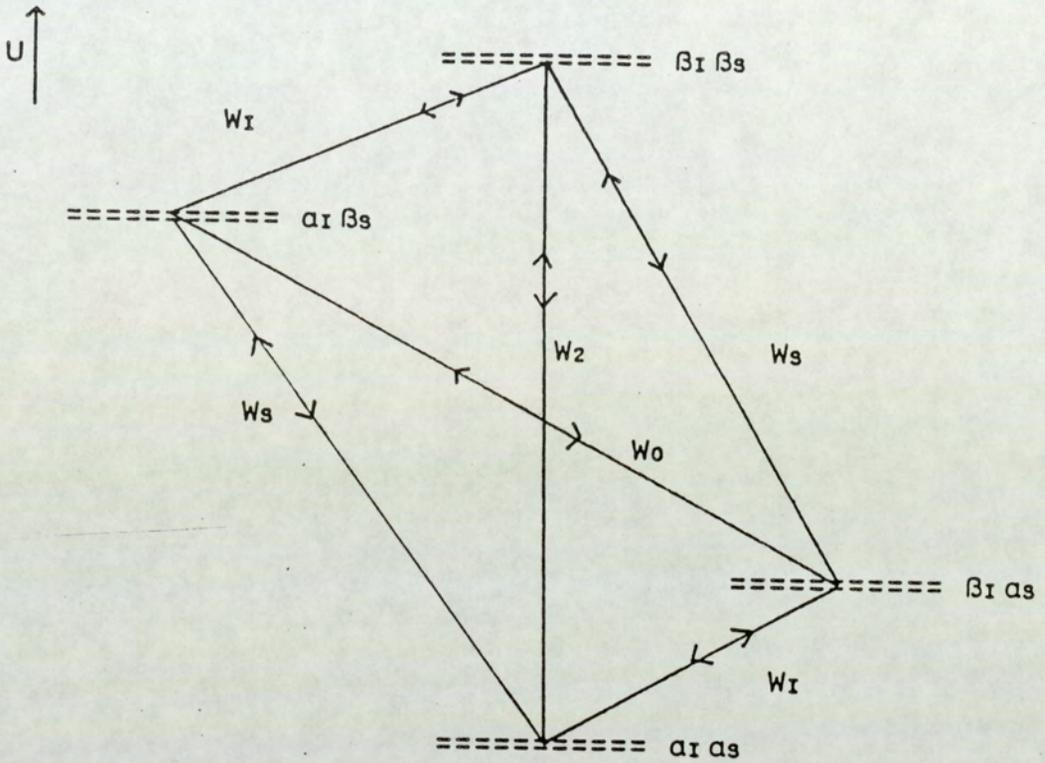
(a) Heteronuclear case
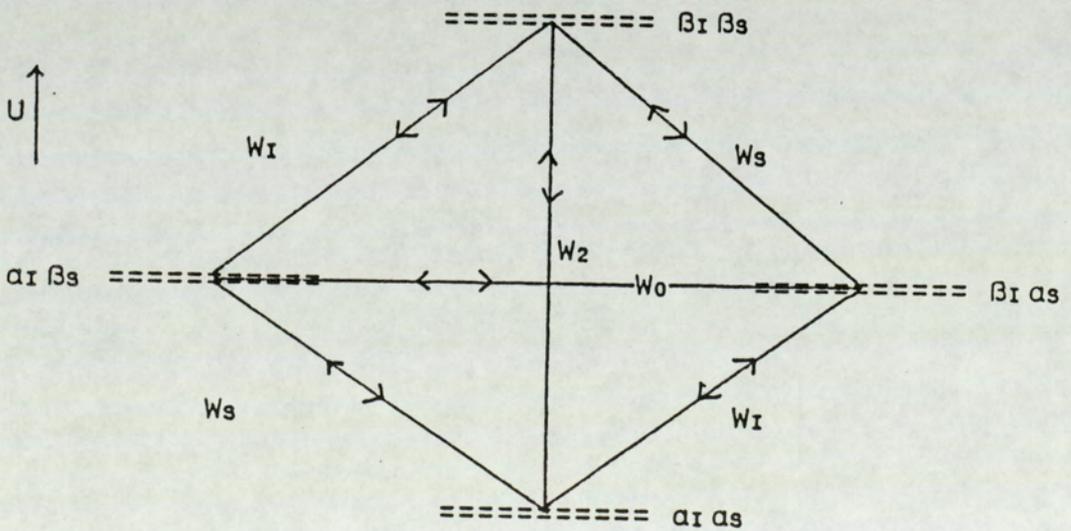
(b) Loosely Coupled Homonuclear Case

Fig. 2.3 <u>Energy Level Diagrams and Transition Probabilities</u>
<u>for a Two Spin System, I and S, of Spin ½ (a)</u>
<u>Heteronuclear Spins and (b) Homonuclear Spins</u>

exponential. Noggle et al (45) have shown, however, that where $\rho_i \approx \rho_s$ with $|\rho_i - \rho_s| \ll \sigma$ and where $\rho_i \neq \rho_s$ with $|\rho_i - \rho_s| \gg \sigma$, the recovery is essentially exponential. Campbell et al. (46) have shown that the initial rate of recovery is approximately exponential as long as $\sigma t \ll 1$ where t is the recovery time. T_1 in the above instances is given by Eqn. 2.19

$$1/T_1 \approx \rho_i = 2W_1 + W_2 + W_0 \qquad (2.19)$$

In the case where the I spin is observed with the S spins continuously irradiated (as is common for ^{13}C spectroscopy) the recovery of the I spin has been shown to be exponential (46) with $1/T_1 = \rho_i$. Saturation of the S spins causes S_z in Eqn 2.16 to equal zero, at the steady state when dI_z/dt equals zero, Eqn 2.16 can be rearranged to give Eqn 2.20 as $\gamma_i S_0 = \gamma_s I_0$

$$\frac{(I_z - I_0)}{I_0} = \eta = \frac{\gamma_s \sigma}{\gamma_i \rho} \qquad (2.20)$$

where η is the nuclear Overhauser enhancement (n.O.e) so called due to the discovery of the effect, in metals when the spin resonance of the electrons was saturated, by Overhauser (47). The n.O.e. which has great potential in NMR spectroscopy is a purely dipolar effect and has a theoretical maximum of $\gamma_s/2\gamma_i$ for spin $\frac{1}{2}$ nuclei. In cases where the saturated spin (S) has a high γ value, of the same sign as γ_i, and the relaxation is predominantly dipolar in

origin, the effect can lead to a large enhancement in the observed signal. In the case of ^{13}C spectroscopy with the coupled ^1H spins strongly irradiated, the maximum value of η is approximately 2. As the effect is only due to the dipolar relaxation mechanism (see below) then the observed value of the n.O.e. is dependent upon the relative amount of dipolar relaxation as shown in Eqn 2.21.

$$\eta = \frac{\gamma_s}{2\gamma_i} \frac{\rho_{dd}}{\rho} \qquad (2.21)$$

where ρ_{dd} is the dipole-dipole relaxation rate and ρ is the total relaxation of the I nucleus.

The third boundary condition that requires discussion as a result of the Solomon equations is the case where both the I and S spins are excited simultaneously, this case is very common in ^1H FTNMR. In this case the equations of 2.16 are added together and providing that $\rho_i = \rho_s$, T_1 is given by (45)

$$1/T_1 = \rho + \sigma = 3\rho/2 \qquad (2.22)$$

provided relaxation occurs via the dipole-dipole mechanism only. In cases where other relaxation mechanisms are possible, recovery is once again non exponential (46).

So far the discussion has implicitly suggested that only intramolecular dipole-dipole relaxation occurs.

Dipole-dipole relaxation can, however, occur intermolecularly also. The most common source of such relaxation is due to paramagnetic impurities in solution (40), especially oxygen (48). The solvent, however, can also provide some intermolecular dipole-dipole relaxation, Kaiser (49) observed an intermolecular n.O.e. between the protons of cyclohexane and chloroform. For intermolecular relaxation the term, r, in Eqn. 2.15 and the correlation time τ_c have to be redefined. Nuclei are considered whose distances lie between r and r+dr from the central molecule. τ_c is then estimated as the time a molecule takes to diffuse across a relative distance r. This is estimated from the diffusion coefficient, D, which can be related to the viscosity of the solution by the Stokes-Einstein relation (50). The intramolecular, heteronuclear, dipole-dipole relaxation contribution to T_1 relaxation in a two spin system is

$$\frac{1}{T_1} = \frac{\gamma_i^2 \gamma_s^2 h^2}{20 r^6_{is}} \{J_0(\omega_s - \omega_i) + 3J_1(\omega_i) + 6J_2(\omega_s + \omega_i)\} = \frac{\gamma^2_i \gamma^2_s h^2}{r^6_{is}} \tau_c$$

where $J_0(\omega_s - \omega_i) = \dfrac{20 \, W_0}{K^2}$

$$J_1(\omega_i) = \frac{40 \, W_1^i}{3K^2} \qquad\qquad (2.23)$$

$$J_2(\omega_s + \omega_i) = \frac{10 \, W_2}{3K^2}$$

where K is given by $\gamma_s \gamma_i h r^{-3}_{is}$

Similar equations for T_2 and $T_{1\rho}$, both homonuclear and heteronuclear, are given in (51). The equations have also been extended to systems of many nuclei by Gutowsky and

Woessner (52).

Nuclei of small magnetic moment such as ^{13}C are primarily relaxed by intramolecular interaction with nearby nuclei of high γ, usually protons (53). It has been shown (54), however, that intermolecular dipole-dipole relaxation for ^{13}C can be significant. Protons, on the other hand are relaxed both inter-and intramolecularly depending on the distances involved. The inter-and intramolecular contributions to dipole-dipole relaxation were originally separated via dilution studies (55,56). However, recent work by Homer et al. (54) has facilitated the separation of the inter-and intramolecular dipole-dipole contributions by the use of intermolecular ^{1}H-^{1}H n.O.e's.

2.4.2 Electron-Nuclear Relaxation

As mentioned above paramagnetic ions such as Mn^{2+} and Cr^{3+}, as well as organometallic complexes of these or other metals with unpaired electrons can provide very efficient intermolecular dipolar relaxation in solution. Chromium (acac)$_3$ and Fe (acac)$_3$ are particularly useful reagents for ^{13}C NMR spectroscopy; the non labile trisacetylacetonate (acac) ligand increases the solubility of the complex in organic solvents and prevents interaction of the metal with the sample. Paramagnetic pseudo-contact shifts are not observed with these complexes. Initial studies using such complexes (57) were involved with the reduction of the n.O.e. for quantitative ^{13}C NMR and in the

observation of ^{15}N NMR where γ_N is negative. Electron nuclear dipole-dipole relaxation becomes more efficient with increasing paramagnetic complex concentration. ^{13}C NMR relaxation data for organic molecules in Cr (acac)$_3$ doped solutions have been obtained (58). The electron-nuclear relaxation observed in these solutions is different to that observed in diamagnetic solutions. Abragam (59) gives an equation derived for dipole-dipole electron-nuclear relaxation between hard shell spheres of equal size, as

$$\frac{1}{T_1} = \frac{16\pi^2}{15} N^2 \hbar^2 s(s+1) \frac{\gamma^2 \eta}{kT} \cdot \tag{2.24}$$

where N is the density of the paramagnetic species per unit volume, $N^2 \hbar^2 s(s+1)$ represents the square of the magnetic moment of the paramagnetic species, γ is the gyromagnetic ratio of the nucleus being relaxed, η is the viscosity of the solution, k is the Boltzmann constant and T is the absolute temperature. The interesting aspect of Eqn. 2.24 is that there is no distance dependence as there is for normal dipole-dipole relaxation. The equation has been verified for ^{13}C relaxation in several organic compounds, even where nuclei are quite inaccessible (58).

2.4.3 Spin Rotation Relaxation

The fluctuating magnetic fields associated with this mechanism arise from magnetic fields generated at a nucleus by the motion of a molecular magnetic moment due to the

electron distribution in the molecule. Consider a nucleus with an associated electron at a distance, r, from it. The rotational frequency, V, of the molecule, which is considered to be in its Jth rotational state, is given by

$$V = hJ/2\pi I \tag{2.25}$$

where I is the moment of inertia of the molecule.

The current, i, generated by the electron due to this motion is then

$$i = (e/c)V \tag{2.26}$$

where e is the electronic charge and c the speed of light. The magnetic moment, μ_j, associated with this current is then

$$\mu_j = i(\pi r^2) = (eh/2\pi Mc)J \approx \mu_n J \tag{2.27}$$

where M is the nuclear mass and μ_j is the nuclear magneton. The motion of the electron thus causes a magnetic field at the nucleus of approximate magnitude $\mu_n J r^{-3}$. Molecular collisions which cause changes in both direction and rotation will modulate this field and provide a relaxation pathway. As there is no mutual interaction between the electron and the nucleus, the random field model of Sec 2.3 is applicable. For molecules undergoing isotropic molecular re-orientation the spin-lattice relaxation due to this

mechanism is

$$T_1^{-1} = 2\pi IkT/h^2 C^2_{eff}\tau_j \qquad (2.28)$$

where C^2_{eff} is the average component of the spin-rotation tensor and τ_j is the angular momentum correlation time, which is a measure of the length of time a molecule spends in any given angular momentum state. τ_j can be related to the isotropic molecular correlation time by (60)

$$\tau_c . \tau_j = I/6kT \qquad (2.29)$$

From Eqn. 2.7, τ_j can be seen to be inversely proportional to sample viscosity and is consequently proportional to sample temperature. The temperature dependence of the spin-rotation mechanism is therefore the reverse of that predicted for the dipole-dipole relaxation mechanism (Sec. 2.3.1). μ_j is seen to be proportional to the rotational velocity, V, and therefore the spin-rotation interaction is of prime importance for small symmetric molecules with little or no intermolecular interactions.

Spin-rotation is very significant in the gas phase (61) and at high temperature. Spin-rotation interactions are also important for nuclei with large chemical shift ranges (62) as both chemical shift range and spin-rotation interactions depend on the electronic distribution within the molecule. The mechanism has been shown to be important in ^{13}C spectroscopy where it is the

primary relaxation mechanism for ^{13}C in CS_2 (63) at low fields and high temperatures. The mechanism is also important for ^{13}C in methyl groups (64) which reorientate rapidly, even in large molecules.

2.4.4 Chemical Shift Anisotropy Relaxation

In Sec. 1.7 it was noted that the nucleus was effectively screened due to the electron density around the nucleus. This screening was quantified in terms of a screening factor, σ, in Eqn. 1.42. σ is a tensor property and the anisotropy in σ was shown to have a pronounced effect on the observed chemical shift (Sec. 1.7.4). The anisotropy in σ may also furnish a mechanism for relaxation, since as the molecule tumbles in solution, the field at the nucleus is constantly changing in magnitude. As discussed in Sec. 2.3 the components of random tumbling motion at the Larmor frequency can then lead to nuclear relaxation.

If σ is axially symmetric, (the general case is discussed by Abragam (65)) then T_1 is given by,

$$\frac{1}{T_1} = \frac{2}{15} \gamma^2 B_0^2 (\sigma_\parallel - \sigma_\perp)^2 \frac{\tau_c}{1 + \omega_0^2 \tau_c^2} \qquad (2.30)$$

where $\sigma_\parallel$ and $\sigma_\perp$ refer to the components of the shielding tensor parallel and perpendicular to the axis of symmetry. The mechanism is unusual in two ways, in the extreme narrowing region $T_2 = 6T_1/7$ and $1/T_1$ is quadratically dependent on the size of the applied field. The chemical

shift anisotropy is obviously dependent on the chemical shift range of the nuclei under examination. Hence it is not likely to occur in ^{1}H NMR but has been reported for several nuclei with large ranges of chemical shift (^{31}P and ^{113}Cd). In ^{13}C spectroscopy the mechanism is usually very inefficient (66), but has been reported to be significant for diphenylbutadiene (64) and in CS_2 at high fields and low temperatures (63). With the increasing use of high field NMR the mechanism is likely to become more important. T_1's and nOe's for several large molecules have been measured at two different fields (67). The results show the expected quadratic dependence on field strength and result in reasonable values for the shielding anisotropy. The chemical shift anisotropy mechanism can be a nuisance at high fields by causing unacceptable broadening of resonance lines. A typical case is that of the ^{205}Tl linewidth for Me_2TlNO_3 in D_2O. In a field of 9.4T the linewidth is 140 Hz which falls quite markedly to 4 Hz in a field of 1.41T (68).

2.4.5 <u>Scalar Relaxation</u>

Consider two spin $\frac{1}{2}$ nuclei I and S which are spin coupled with a coupling constant J. As noted in Sec. 1.8, J determines the magnitude of the magnetic field at I due to the orientation of S with respect to the applied field. As S relaxes, I experiences a fluctuating field and vice-versa. Similarly if J changes, due to the covalent bond being broken between I and S, such as in chemical exchange, I

experiences a similar fluctuating field. If this fluctuation occurs with a frequency of the order of the Larmor frequency then relaxation can occur. There are three situations where relaxation may occur due to perturbation of a scalar coupling.

If a spin $\frac{1}{2}$ nuclei, I, is coupled with a moderately large coupling constant to a quadrupolar nucleus, S, that relaxes rapidly (Sec. 2.4.5), then the scalar contribution to the relaxation of I is

$$\frac{1}{T_1} = \frac{8\pi^2 J^2}{3} S(S+1) \frac{T_1{}^s}{1 + (\omega_i - \omega_s)^2 T_1{}^{s2}} \qquad (2.31)$$

$$\frac{1}{T_2} = \frac{4\pi^2 J^2}{3} S(S+1) \left[T_1{}^s + \frac{T_1{}^s}{1 + (\omega_i - \omega_s)^2 T_1{}^{s2}} \right] \qquad (2.32)$$

The mechanism only becomes significant for T_1 relaxation when $\omega_i \approx \omega_s$. The situation is rare but has been observed between ^{13}C and ^{79}Br where $\omega_c - \omega_{Br} = 0.054$ MHz. For example in bromobenzene (64), scalar relaxation leads to a non exponential relaxation process for Carbon 1. This is because the scalar relaxation of ^{13}C by ^{79}Br is more efficient than the corresponding scalar relaxation of ^{13}C by ^{81}Br. Consequently, the observed relaxation rate is a combination of the two exponential decays. A similar situation occurs in bromocyclohexane (64) except that in this case the dipole-dipole relaxation mechanism competes with the scalar relaxation for the ^{79}Br bonded ^{13}C but dominates the relaxation of the ^{81}Br bonded ^{13}C. Once again the observed

relaxation rate of the ipso carbon is non exponential. In bromomethanes (69) both the ^{79}Br and ^{81}Br bonded ^{13}C relaxation rate is dominated by scalar relaxation due to the inefficiency of the dipole-dipole relaxation mechanism for rapidly tumbling small molecules.

T_2 relaxation is generally more readily affected by the scalar relaxation mechanism. Inspection of Eqn 2.32 shows that the T_2 relaxation rate depends on a second W_0 term which does not contain (ω_1 - ω_s) in the denominator. This differential significance of scalar relaxation is well known as it accounts for the broad lines which are often observed for protons attached to nitrogen. Freeman and Hill (70) measured ^{13}C T_1 and $T_1\rho$ for ortho-dichlorobenzene, the proton bearing carbons had values of T_1 approximately equal to $T_1\rho$ (Sec. 2.3). The T_1 for the chlorine bearing carbons were long (66 s) due to inefficient dipole-dipole relaxation, however, the $T_1\rho$ value for the chlorine bearing carbons was short (4.2 s) due to efficient scalar relaxation.

The contribution of scalar relaxation to carbon T_2 relaxation is important especially where ^{1}H decoupling is used. From Eqn. 2.31 if, as is normal, $(T_1H)^{-1} \ll J_{CH}^2$ then T_2C must always be shorter than T_2H. For example in ^{13}CH$_3$COOCD$_3$ where J=130Hz T_1H=12.5 s, T_1C=19.2 s, T_2C only equals 6.1 s (71). The ^{13}C T_1 and T_2 relaxation rates would have been expected to be equal if relaxation was only due to the dipole-dipole relaxation mechanism. At low decoupling

powers where $T_1H^{-1} \approx J$, the carbon resonance lines become very broad. At higher decoupling powers, however, $T_1H^{-1} \ll J$ and the scalar relaxation mechanism once again becomes inefficient causing $T_1C=T_2C$ (71).

J can become a function of time as bonds are made and broken in chemical exchange reactions causing J to fluctuate between J and zero. This is in effect identical to the situation discussed above, with the exchange rate τ_e replacing T_1S in Eqn's 2.30 and 2.31 above.

2.4.6 Quadrupolar Relaxation

For nuclei with a spin quantum number greater than or equal to one, the quadrupolar relaxation mechanism usually dominates its relaxation. This mechanism is not available to spin $\frac{1}{2}$ nuclei directly (see Sec. 2.4.4) as it depends on the nucleus having a non spherical nuclear charge distribution. Spin $\frac{1}{2}$ nuclei have spherical charge distributions whereas nuclei with spin quantum numbers greater than $\frac{1}{2}$ can have prolate or oblate charge distributions (72). This non-spherical charge distribution results in the nuclei possessing a quadrupole moment, Q. In the presence of an electric field gradient they precess about the nett electric field causing the normal NMR energy levels to be perturbed by the modification of the interaction hamiltonian (Sec. 1.3.2.). The electric field gradients are modulated by molecular motion which gives rise to relaxation amongst the modified energy levels. The

expressions for T_1 and T_2 relaxation in the extreme narrowing limit are presented as Eqn 2.33.

$$\frac{1}{T_1} = \frac{1}{T_2} = \frac{3}{40} \frac{2I + 3}{I^2(2I - 1)} (1 + \eta^2/3) \frac{e^2 qQ^2}{h} \tau_c \qquad (2.33)$$

where η is the asymmetry parameter and q is the electric field gradient at the nucleus. The electric field gradient at the nucleus is actually a tensor property and η is a measure of its anisotropy. The term $e^2 qQ^2/h$ is referred to as the quadrupole coupling constant where Q, is a constant for a particular nucleus and values for the more common nuclei can be found in reference (72). The $e^2 q$ part depends on the electric field gradient at the nucleus and can show a range of values even for the same nucleus in different compounds. For example in the highly symmetric $^{14}NH_4^+$ ion the quadrupolar coupling constant is zero (73) and relaxation occurs via the dipole-dipole relaxation mechanism giving a T_1 of approximately 50 s. On the other hand in $CH_3 C^{14}N$, the quadrupole coupling constant is 4 MHz, and the ^{14}N relaxation is dominated by the quadrupolar relaxation mechanism, and T_1 equals 22 ms (74).

Quadrupolar relaxation rates are extremely sensitive to the electrical symmetry of the molecule. A case in point is the $AsMe_4^+$ ion. In aqueous solution the arsenic relaxation time is fairly long due to the low value of the quadrupolar coupling constant. In chloroform, however, the arsenic relaxation time becomes very short, implying a larger quadrupolar coupling constant. This was explained (75) by

the formation of the ion pair $AsMe_4^+$ X^- in chloroform which lowered the electrical symmetry of the molecule. When quadrupolar relaxation dominates the relaxation process, it can provide a good measure of τ_c from Eqn. 2.32. if the quadrupolar coupling constant is known. Such measurements can often be made using NQR spectroscopy.

2.5 Applications of NMR Relaxation Times

Much has all ready been stated on the potential use of relaxation processes in the above description of the various mechanisms of NMR relaxation. In most cases the relaxation of a nucleus is governed by more than one relaxation process and the total rate of relaxation, R_T, for a given nucleus is given by

$$R_T = R_{intra} + R_{inter} + R_{EN} + R_{SR} + R_{CSA} + R_{SC} + R_Q \qquad (2.34)$$

where R is the relaxation rate and the subscripts represent the relaxation mechanisms discussed above. The contributions from the various mechanisms can often be isolated from the total relaxation rate due to the different properties of the various mechanisms. For example the dipole-dipole relaxation rate can be separated from the total relaxation rate by measuring the nuclear Overhauser enhancement (Eqn. 2.21). The inter and intra contributions can be separated by dilution studies (55,56) or by intermolecular $^1H-^1H$ n.O.e's (54) (Sec 2.4.1). The electron nuclear relaxation rate may be determined by subtraction of the observed relaxation

rates in non doped and doped solutions (Sec. 2.4.2). Contributions to the total relaxation rate due to a spin-rotation interaction can be determined due to its unique temperature dependence (Sec. 2.4.3). Similarly a chemical shift anisotropy contribution can be determined due to its unique field dependence (Sec. 2.4.4). Scalar relaxation can often be confirmed by its differential effects on T_1 and T_2 measurements (Sec. 2.4.5). If quadrupolar relaxation is present the mechanism is very efficient and is likely to dominate the relaxation rate (Sec 2.4.6).

2.5.1 ^{13}C-^{1}H Dipolar Relaxation

Many of the applications of NMR relaxation have arisen from studies of ^{13}C-^{1}H dipolar relaxation times. Such applications have become popular due to the dominance of dipolar relaxation for the ^{13}C nucleus and its ease of separation from other relaxation mechanisms via the n.O.e. Intermolecular dipole-dipole relaxation for ^{13}C is often inefficient and does not therefore contribute to the n.O.e significantly (Sec. 2.4.1). In general applications of the dipolar relaxation rate fall into three categories: the determination of molecular structure, molecular dynamics and molecular interactions.

2.5.1.1 Determination of Molecular Structure

In ^{13}C spectroscopy carbons bearing attached protons

are often solely relaxed by the intramolecular dipole-dipole
contribution from the attached proton (Sec. 2.4.1). In the
case of more than one attached proton, Eqn. 2.23 can be
modified to

$$\frac{1}{T_1} = \frac{n\gamma^2_H \gamma^2_C \hbar^2}{r^6_{CH}} \tau_c \qquad (2.35)$$

where all the symbols have their usual meaning and n
represents the number of attached protons. In a ^1H noise
decoupled ^{13}C spectrum, therefore, the measurement of the
relaxation times can provide information on the number of
attached protons for each resonance. If n=0 the observed T_1
is considerably longer as relaxation is dominated by another
mechanism (Spin rotation). In cases where the molecule
tumbles isotropically in solution CH, CH_2 and CH_3 carbons
can, in principle, be distinguished due to the expected
3:2:1 ratio of their relaxation times. This method, however,
assumes isotropic rotation which is not often realistic and
has been superseded by spectral editing techniques such as
D.E.P.T (38). Comparison of the relaxation times of
non-protonated carbons can be used to correlate the ^{13}C NMR
spectrum with the structure based on the distance of a
non-protonated carbon to a C-H dipole. Such reasoning
facilitated spectral assignment for codeine and brucine
(76). In cholesterol chloride, Allerhand (77) observed ring
^{13}C T_1's of the order 2:1 for for the CH and CH_2 ring
carbons. The CH_3 side chain carbons, however showed longer
than expected T_1's. This was attributed to rapid internal

rotation of the CH_3 group, thus modifying the τ_c for CH_3. If a proton on a ^{13}C nucleus is replaced by a deuteron then the measured ^{13}C relaxation time will increase due to the small magnetic moment of the deuteron. Such isotopic substitution will effect the T_1 values of non-protonated carbons close to the isotopic substitution site. This technique has been used in the spectral assignment of alkaloids (78).

The use of electron-nuclear relaxation agents can be used as an aid to assignment. Eqn. 2.24 can be rearranged to define a quantity $[R_1^e]$ which is the specific electron-nuclear relaxation rate ($1/T_1^e$ divided by the product of the viscosity and concentration of the paramagnetic species, where $1/T_1^e$ is the spin-lattice relaxation time due to electron-nuclear relaxation). For the paramagnetic relaxation agent Fe $(acac)_3$, $[R_1^e]$ is usually of the order of 50 units, but this value can increase quite significantly when there is a significant amount of intermolecular interaction present. Intermolecular interactions result in the effective increase in the concentration of the paramagnetic additive at the site of intermolecular interaction. In such cases a collision complex is formed and the value of $[R_1^e]$ is expected to fall with distance from the complexation site. Borneol (79) was studied using this technique and a full spectral assignment was possible on the basis of the variation of the value of $[R_1^e]$ with distance from the OH group.

2.5.1.2 Molecular Dynamics and Interactions

Many small molecules tend to tumble anisotropically in solution. Preferential tumbling along a particular axis may result from inertial, electrostatic, or intra-and intermolecular interactions (80). Peripheral molecular fragments in large molecules may have shorter correlation times than the overall correlation time of the whole molecule because of rapid internal rotations. This was observed for the peripheral methyl groups in cholesterol chloride (77). Monosubstituted benzenes show anisotropic tumbling in solution (65) with preferential tumbling occurring about the C2 symmetry axis. This observation was based on the consistently shorter T_1 values for the para carbons in monosubstituted benzenes over the ortho and meta carbons. Rotation about the C2 symmetry axis does not lead to any modulation in the dipole-dipole interaction of the para carbon and its associated proton. However, such rotation does lead to longer relaxation times for the ortho and meta carbons because the C-H bonds make angles of 60° and 120° with the C2 axis. Levy et al (65) were able to calculate the approximate preferential tumbling ratio about the C2 axis in monosubstituted benzenes from the ratio T_{1ortho}/T_{1para}. They concluded that the anisotropy in the tumbling increased with the size of the para substituent and that in the limit of much faster rotation about the C2 axis the ratio T_{1ortho}/T_{1para} would equal 64. Tumbling anisotropy has been used to study solvation processes on molecular motion. For example when phenol is diluted with CCl_4 the

phenol molecular aggregates begin to dissociate, this was demonstrated by the increase in the ^{13}C relaxation times (i.e. lower τ_c) and the decrease in the ratio $T_{1 ortho}/T_{1 para}$ with increasing dilution (81). Anisotropic tumbling has also been used in the study of "ring whizzing" in organometallic sandwich complexes (82).

T_1 measurements also provide a way of studying localised motion along aliphatic chains. Segmental rotation has been observed in 1-decanol (83) and along some shorter chains in some aliphatic amides and oximes (84). To observe segmental motion the local motion must be equal to or greater than the overall motion of the molecule. It is possible to calculate $\tau_{c eff}$ for the individual carbons along the chain provided that the C-H internuclear distance is assumed constant. Hence $\tau_{c eff}$ for C1 in decanol is seven times longer than $\tau_{c eff}$ for C10. This is attributed to intermolecular hydrogen bonds restricting the motion of the hydroxylic end of the alcohol chain, and thus the method may prove of use in the study of intermolecular interactions. Studies of the ion $n-BuNH_3^+$ $CF_3CO_2^-$ in various solvents (85) showed that in non polar solvents the ion pair anchored the molecule, consequently the measured T_1's were low and segmental rotation was pronounced in the butyl chain. In polar solvents, however, the T_1's increased and the amount of segmental motion in the butyl chain decreased. This was attributed to the higher dielectric constant of the polar solvent more effectively separating the ion pairs.

2.6 Relaxation Times in Exchanging Systems

The measurement of exchange rates in NMR has been dominated by the method of total lineshape analysis. With the advent of pulsed NMR the use of relaxation times in the determination of exchange rate constants has increased. Methods have been developed which can supplement lineshape analysis and extend the range of rate constants measured by the NMR technique. A review article by Lambert et al (86) has examined the applicability of relaxation data to dynamic NMR.

2.6.1 Intermediate Energy Barriers

$T_1\rho$ studies are potentially useful in the intermediate energy barrier region as they are sensitive to exchange processes occurring at rates governed by γB_1 as opposed to γB_0 for T_1. In such studies the parameter $T_1\rho(exch)$ is measured which is given by Eqn. 2.36.

$$\frac{1}{T_1\rho(exch)} = \frac{1}{T_1\rho(obs)} - \frac{1}{T_1} \tag{2.36}$$

For exchange between two sites with equal populations, the net $T_1\rho(exch)$ is related to the spin-lock frequency, ω_1, the mean lifetime, $\tau = 1/k$, of a molecule in one of the sites, and the chemical shift difference between the exchanging sites $\Delta\nu$, where k is the rate constant. The measurement of the rate constant at various temperatures allows the thermodynamic properties of the system to be calculated.

$$\frac{1}{T_{1\rho}(exch)} = \pi^2 (\Delta\gamma)^2 \frac{1}{1 + \omega_1^2 \tau^2} \qquad (2.37)$$

It is not, however, as implied in Eqn. 2.37 necessary for the exchange rate to be in the slow exchange region. A plot of $T_{1\rho}(exch)$ against ω_1^2 will give values for τ and $\Delta\gamma$ from the slope and intercept. Stilbs et al (87) have obtained the energy barrier to amide rotation in urea and by variation in the temperature were able to measure $\Delta\gamma$ well above the coalescence temperature using the technique. The ring reversal barrier in cis-decalin (88) has been measured as has the C-C rotational barrier between the aldehyde group and the phenyl moiety in benzaldehyde (89). The practical kinetic range for the method is about $10^2 - 10^6$ s^{-1} and thus it slightly extends the lower field limit of lineshape methods. Due to its high accuracy and its applicability to fast kinetics without the necessity of slow exchange the method should gain wide spread use in the future.

2.6.2. High Energy Barriers

In a two spin system saturation of one resonance (S) causes magnetization transfer to another nucleus (I) in a chemically exchanging system. Forsen and Hoffman (90) showed that analysis of the perturbations at I can provide relaxation and exchange data for the system. The rate of magnetization change at (I) can be written as

$$\frac{dM_z^I}{dt} = \frac{M_z^I t(0)}{T_1^I} - \frac{M_z^I(t)}{\tau_1^I} \qquad (2.38)$$

where $\dfrac{1}{\tau_1{}^I} = \dfrac{1}{\tau^I} + \dfrac{1}{T_1{}^I}$

where τ_I is the reciprocal of the rate constant and $T_1{}^I$ is the spin-lattice relaxation time of I. Eqn. 2.38 can be solved to give

$$M_z{}^I(t) = M_z{}^I(0) \left[\frac{\tau_1{}^I}{\tau_I} \exp\ (-t/\tau_1{}^I)\ +\ \frac{\tau_1{}^I}{T_1{}^I} \right] \qquad (2.39)$$

Hence from values of $M_z{}^I(t)$ at various values of t and an independent measure of T_1, τ_I can be obtained. A similar experiment but with the I spin saturated permits the value of τ_S to be obtained. The method did not become popular until the advent of pulse techniques due to experimental difficulties (86). For ^{13}C applications in Fourier transform spectroscopy, instead of saturating the resonance S a selective 180° pulse is applied to it. This places a limit on the experiment that $T_1{}^I = T_1{}^S$, despite this Boekelheide (91) measured the barrier to ring reversal in [2,2]metaparacyclophanes from ^1H NMR and Mann (92) measured the ring reversal rate in cis-decalin. Mann (93) has also extended the method to provide exchange data when $T_1{}^I \neq T_1{}^S$. With the possibility of selective spin saturation on spectrometers for nuclei other than ^1H the method should prove useful in the determination of exchange rates that do not attain the fast exchange lineshape regime.

2.7. NMR Relaxation in Medicine

In the early 1970's Damadian (94) established that there were significant differences in the measured ^{1}H NMR relaxation times (T_1 and T_2) of normal and malignant tissues in rats. It was also established in this series of experiments that each soft tissue organ had its own characteristic T_1 and consequently the idea of NMR body scanning was born. Similar observations were reported in human tissues (95). Damadian (95) explained these observations by concluding that tumour tissue had less intercelluar water structure than normal tissue, and consequently there is more diffusion and hence longer relaxation times. Weismann et al (96) showed that the measurements could be made in vivo as well as in vitro in a study on mice. Zaner et al. (97) have extended the study to the ^{31}P nucleus and showed that the measured T_1 values were generally longer than those observed for protons. A full discussion is beyond the scope of this thesis but from the early investigations, NMR body scanning on human subjects has become a reality, and a useful non invasive diagnostic tool. Damadian (98) has edited a collection of early papers on the subject.

2.8 Conclusions

The discussion in Sec. 2.3 presented a simplistic view of relaxation processes. In particular the use of Eqn. 2.7 to define τ_c has been much criticised (55,99) and improved theories investigated. Eqn. 2.7 assumed isotropic rotation of a sphere of radius, r, in a medium of viscosity

η. It has been shown in Sec. 2.5.1.2 that isotropic motion is not a reality. Woessner et al. (100) have treated the case of an anisotropic system based on rotational diffusion about a C3 axis and equal rotational diffusion about the two perpendicular axes, (a symmetric top molecule). The approach has been further extended to anisotropic rotation about three perpendicular axes (an asymmetric top molecule) (101). Using Woesnner's equations Grant et al (102) were able to obtain the diffusional rotation constants about the three perpendicular axes and show that adamantane is an isotropic tumbler, bicyclooctane a symmetric top molecule and trans-decalin an asymmetric top molecule. Woessner et al (103) have also treated the case of rapid internal motion imposed on isotropic overall motion for a methyl group. This approach has allowed the rate of internal rotation for methyl groups to be calculated. In cases where the methyl group is not a free rotor temperature studies have allowed the potential barrier to methyl rotation to be calculated. A review of such calculations and its further extension to symmetric and asymmetric top molecules is given by Lambert et al (86). The applications presented in this chapter are by no means exhaustive but serve to illustrate the great potential use of NMR relaxation times in chemistry, biology and medicine. The routine use of NMR relaxation times, however, tends not to be popular due to the excessive time these measurements often take (Chap 4). This thesis is primarily concerned with the reduction in this time and the consequent use of NMR relaxation data in routine NMR.

CHAPTER 3

FOURIER TRANSFORM NMR

3.1 Introduction

Nuclear magnetic moments can absorb energy from an oscillating electromagnetic field applied perpendicular to the direction of the static field, B_0, provided that the Larmor condition of Eqn's 1.7 and 1.12 is fulfilled. For most practical static magnetic fields the Larmor condition is fulfilled when the applied electromagnetic radiation is in the radio frequency range of the electromagnetic spectrum.

From the Larmor expression it is evident that if the field is swept whilst the frequency is kept constant or vice-versa then at a certain combination of field and frequency the Larmor condition will be fulfilled. At this point energy will be absorbed from the electromagnetic field and an NMR signal observed. If the field or frequency are swept through the chemical shift range of the nucleus being observed then absorptions will occur at different fields or frequencies governed by σ for each chemically shifted nucleus in the molecule (Eqn. 1.42). Hence, using these continuous wave techniques it is possible to observe a high resolution NMR spectrum. In order for the time derivatives of Eqn. 1.38 to equal zero and consequently give the lineshape represented by Eqn. 1.41, the sweep of the field or frequency has to be very slow (slow passage). Faster sweep rates result in line distortions and hence the continuous wave excitation method is very time inefficient.

It is obviously better if, in a static field, all the frequencies in the chemical shift range of the nucleus can be applied to the sample at the same time. Bloch et al. (104) realised that this was possible by subjecting the sample to a short intense electromagnetic field pulse, perpendicular to the static field, of frequency close to that predicted for the Larmor condition to be fulfilled for the observed nucleus. Provided that the duration of the pulse is sufficiently short, such a pulse provides all possible excitation frequencies across the chemical shift range of the nucleus (Sec. 3.3.1). This approach, although considerably more efficient than the continuous wave method produces a complicated interferogram (Free Induction Decay,(FID)) composed of all the precessional frequencies in the rotating frame (Sec. 1.6.2) corresponding to the various chemically shifted nuclei in the sample. The FID decays with a time constant equal to T_2^*. Initially, therefore pulse (free precession) techniques were not useful for high resolution NMR, but found use in the study of relaxation times (105). The FID contains the same information as the high resolution, slow passage, continuous wave spectrum (16) but the observed signal is a variable of time rather than frequency. Ernst and Anderson (16) showed that the FID and the high resolution spectrum were a fourier pair and hence, one could be obtained from the other by the technique of fourier transformation (Sec 3.2). The mathematical requirements for a fourier transformation can be readily handled by a computer and, consequently, since about 1970 pulse fourier transform NMR spectrometers have superseded

continuous wave spectrometers. This has opened the way to make the NMR technique possibly the most versatile analytical technique available to the modern chemist.

3.2 Fourier Transformation

The Fourier transformation between the time domain and the frequency domain can be expressed as

$$F(\gamma) = \int_{-\infty}^{+\infty} f(t) \exp (2\pi i \gamma t) \, dt \tag{3.1}$$

The converse transformation between the frequency and time domains is given by

$$f(t) = \int_{-\infty}^{+\infty} F(\gamma) \exp (-2\pi i \gamma t) \, dt \tag{3.2}$$

where $f(t)$ is the time domain function and $F(\gamma)$ is the corresponding frequency domain function. If the time domain function only exists for a finite time then the situation can be further simplified.

$$f(t) = \int_{-\infty}^{+\infty} F_c(\gamma) \cos 2\pi \gamma t \, dt \tag{3.3}$$

$$f(t) = \int_{-\infty}^{+\infty} F_s(\gamma) \sin 2\pi \gamma t \, dt \tag{3.4}$$

where

$$F_c(\gamma) = \int_{-\infty}^{+\infty} f(t) \cos 2\pi \gamma t \, dt \tag{3.5}$$

$$F_s(\gamma) = \int_{-\infty}^{+\infty} f(t) \sin 2\pi \gamma t \, dt \tag{3.6}$$

$F_c(\gamma)$ and $F_s(\gamma)$ are known as the cosine and sine

transformations of f(t). These transformations are very important in pulsed NMR as the cosine transformation of the time domain signal gives the v mode signal and the sine transformation gives the u mode signal (Sec. 1.6.3 and Fig. 1.4). Several other properties of fourier transforms are worth noting:-

1) Change of Origin

If the zero time of a function is changed by an amount δt, then the twin function is multiplied by exp (2πiνδt)

$$f(t+\delta t) = F(\nu) \exp (2\pi i\nu\delta t) \qquad (3.7)$$

2) Area

The total area under a function is equal to its transform at the origin

$$\int_{-\infty}^{+\infty} F(\nu) \ d\nu = f(0) \qquad (3.8)$$

3) Digitisation

If a function f(t) is sampled and can therefore be considered as a series of δ functions τ s apart then its transform is also a series of δ functions 1/τ Hz apart

$$\sum_{n=-\infty}^{\infty} \delta(t-n\tau) \ f(t) = \frac{1}{\tau} \sum_{n=-\infty}^{\infty} F(\nu-n/\tau) \qquad (3.9)$$

Hence, if the time domain function is digitised then the

resultant is simply a digitised frequency domain function.

4) Addition and Subtraction

The addition or subtraction of two functions g(t) and f(t) in the time domain is equivalent to the addition or subtraction of the two corresponding frequency domain functions.

$$F[f(t) \pm g(t)] = F[f(t)] \pm F[g(t)] \qquad (3.10)$$

5) Multiplication

The multiplication of a time domain function by a constant, a, results in the multiplication of the corresponding frequency domain signal by a.

$$F \; af(t) = aF[f(t)] \qquad (3.11)$$

The above results are important when one considers the fourier transform of the FID (time domain) to give the slow passage NMR spectrum equivalent (frequency domain). Time averaging of signals in one domain is equivalent to time averaging in the other domain [4]. If the size of the FID is doubled then so is the signal in the frequency domain [5]. The value of a function at zero in one domain is equal to the area under the function in the co-domain [2], hence the choice of the origin is very important [1]. In FTNMR the FID is never immediately sampled (Sec. 3.4.5) and hence from [1]

this introduces a phase shift in the time domain signal. On fourier transformation the resultant spectrum cannot be observed directly as its sine and cosine transformations, and hence as u and v mode signals, without this phase shift being corrected (Eqn's 3.3 to 3.6 and Sec. 3.4.9).

3.2.1 Digital or Discrete Fourier Transforms

The FID is converted into a regular series of discrete values when it is digitised. Such digitisation is necessary in order for a computer to carry out the fourier transformation. The continuous function f(t) can therefore be rewritten as

$$f(t) = \sum_{n=0}^{N-1} f_n \, \delta(t-n\tau) \qquad (3.12)$$

where f_n is the digitised function, N the number of sampling points and τ represents the time between sampling points. Sampling theory dictates that for a frequency domain spectrum ΔHz wide, $\tau=(2\Delta)^{-1}$, and hence for a specified number of data points, N, the total acquisition time (T_{ac}) can be defined. Eqn. 3.9 showed that such a discrete function in one domain could be fourier transformed into the co-domain. The integration must now be replaced by a sum over a finite series of values (N), and the fourier transformation is thus rewritten as

$$F(\gamma) = 1/N \sum_{n=0}^{N-1} f(t) \, \exp \, (-2\pi i n\gamma/N) \qquad (3.13)$$

The finite nature of the sampling time now results in a

limiting resolution which is observable in the fourier transformed spectrum. The spectral resolution, Sres, is given by

$$Sres = 2\triangle/N \qquad\qquad (3.14)$$

This defines the frequency interval between each data point in the fourier transformed spectrum. The fourier transform is normally carried out using the fast fourier transform (FFT) method of Cooley and Tukey (106). This depends on symmetrising a matrix and thus carries out the calculations more quickly. The Cooley-Tukey algorithm speeds up a fourier transformation of a 32K (N=32x1024) data matrix by about 1500 times. The only limitation is that $N=2^n$ where n is an integer, this is not really a problem as computers are binary based. One note of caution is that the transform is usually carried out in place and therefore it will overwrite the FID it is transforming. If signal to noise (S/N) enhancement or resolution enhancement (Sec. 3.4.9) is required then a copy of the FID must have been previously saved.

3.3 Pulsed Excitation FTNMR

3.3.1 Pulsed Excitation in the Rotating Frame

It was stated in Sec 3.1 that a short intense radio frequency pulse of frequency, ν_c, close to the Larmor frequency of the observed nucleus was sufficient to cause

the individual chemically shifted magnetic moments to absorb energy. For this to occur it is apparent from Eqn. 1.42 combined with 1.7 that the pulse must contain frequency components across the entire chemical shift range of the observed nucleus for a fixed static field. This can be understood by the fourier transformation of a square wave. Fig. 3.1 shows that the fourier transformation of a square wave of amplitude, B_1 and duration τ gives a sinc curve in the frequency domain. The effective range of frequencies covered by such a pulse is $1/\tau$, which for a pulse of $10\mu s$ is equivalent 10^5 Hz. This is easily enough to cover the entire ^1H or ^{13}C chemical shift range. A flat distribution of B_1 over the frequencies of interest is required and so it is usually prudent to allow τ^{-1} to be one or two orders of magnitude greater than the chemical shift range under study. From Sec. 1.6.2., when the rotational velocity of the rotating frame is equal to ω_o, then resonance occurs and the on resonance magnetization component along the z axis is tipped through the zy plane at a frequency γB_1. For a pulse of τ s in duration the total flip angle, θ in radians, is given by

$$\theta = \gamma B_1 \tau \qquad (3.15)$$

When τ is such a length that $\theta=\pi/2$ the on resonance magnetization component will lie along the y' axis of the rotating frame. Such a condition is called a 90° pulse. Similarly after a 180° pulse the magnetization component will lie along the -z axis (Fig. 3.2). Obviously after a 90°
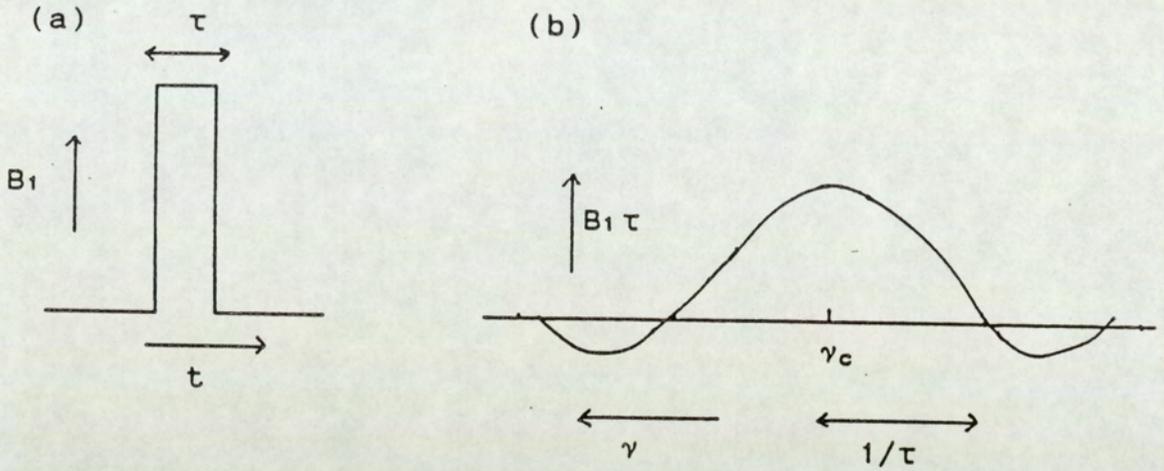
Fig. 3.1 (a) A Square Wave Pulse of Radiation at Frequency γ_c in the time domain (b) Its Fourier Transform in the Frequency Domain
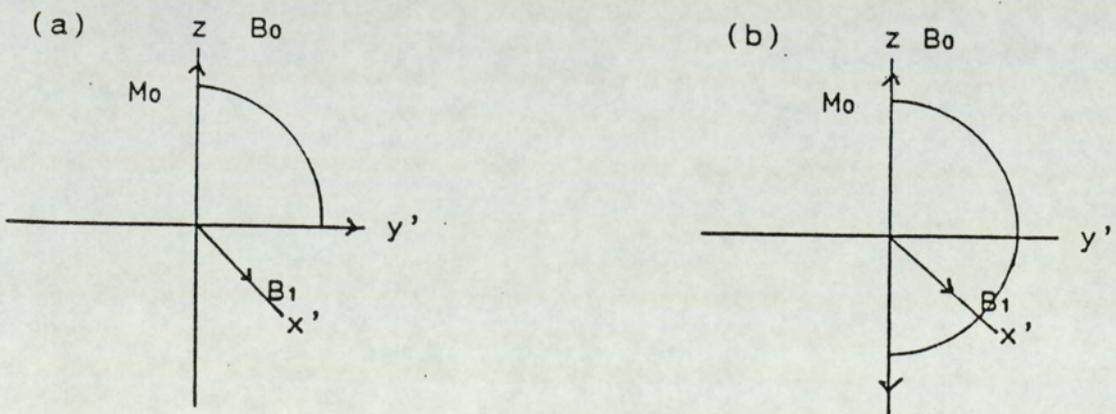
Fig. 3.2 The Effect of (a) a 90° Pulse and (b) a 180° Pulse on a Magnetization Component, M_0, in a Frame of Reference Rotating at ω_1

pulse the rate of change in M_y will be greatest and a 90°
pulse will give the maximum v mode signal. In pulse NMR all
chemically shifted nuclear moments are flipped away from the
z axis, but off resonance moments (ie those precessing about
the field direction at rate different to that of the
rotating frame of reference) (Sec. 1.6.2 and Fig. 1.5) are
nutated about B_{eff} (the resultant field in the rotating
frame of reference) (Sec 1.6.2 and Fig. 1.5) by an angle a,
which is larger than θ, during the period τ. As B_{eff} is not
coincident with the x' axis then when a=90°, off resonance
vectors do not lie along the y' axis but are flipped towards
the x'y' plane (Sec 5.3.2) and thus the detected signal will
be a mixture of u and v mode signals. In pulse NMR the
angular frequency of the rotating frame is identical to the
frequency of the electromagnetic field which is gated to
produce the pulse. The departure of off-resonance
magnetization components from the y' axis of the rotating
frame is usually small unless the chemical shift is
exceedingly large. Consequently, the use of pulses enables
the magnetization, M, to be placed in any chosen direction
without any relaxation during the pulse provided $\tau \ll T_1, T_2^*$.

3.3.2. The Free Induction Decay (FID)

Folowing a nutation pulse the Boltzmann equilibrium
is restored via relaxation processes (Chap 2). The M_z
component of the magnetization after the pulse M_z^+ relaxes
exponentially towards M_o and after a time, t, the M_z magnet-
ization, $M_z(t)$ is given by,

$$M_z(t) = M_0 - (M_0 - M_z^+) \exp(-t/T_1) \tag{3.16}$$

Similarly the M_y component immediately after the pulse, M_y^+, will decay exponentially with a time constant T_2^* towards zero. The M_y component after a time, t, $M_y(t)$ is given by,

$$M_y(t) = M_y^+ \exp(-t/T_2^*) \tag{3.17}$$

where $1/T_2^* = 1/T_2 + 1/T_{inhom}$ and $1/T_{inhom}$ is the rate of decay of the M_y component due to inhomogeneities in the static field, B_0. Immediately after the pulse the observed signal induced in the detector coil will be proportional to M_y^+, which will be attenuated as transverse (T_2^*) relaxation occurs. If the component represented by M_y is on resonance then the plot of signal against time (the FID) will be simply an exponential decay. If the component represented by M_y is off resonance by γ Hz then the observed plot of signal against time will be an exponentially decaying sinusoidal wave of frequency γ Hz. In cases where there are several off-resonance components the exponentially decaying sinusoidal waves will constructively and destructively interfere causing the production of a complicated interferogram.

3.4 Instrumental Considerations

The spectrometer used for the work in this thesis was a Jeol FX 90Q spectrometer (107). This section on instrumental considerations will therefore be based on the

Jeol FX   90Q   spectrometer.

FTNMR spectrometers have many common features and hence much of what is written in this section is applicable to other spectrometers.   Fig.   3.3   shows a schematic representation of the basic units in the Jeol FX 90Q spectrometer.

3.4.1 The Magnet

An NMR magnet must provide a stable and homogeneous field across the sample. The homogeneity of such a field must be of the order of 1 in 10^9. The magnet in the Jeol FX 90Q spectrometer (1.07) is a water cooled electromagnet which provides a field of 2.11 T and enables a proton resonance to be observed at a frequency of 90 MHz. The magnetic field is produced by passing a current through wires wrapped around an iron core. The largest field that can be produced by an electromagnet is approximately 2.3 T due to saturation of the iron core. To achieve the required homogeneity the magnet is temperature stabilised via the cooling system. Also, the diameter of the pole caps must be considerably larger than the sample length and they must be metallurgically uniform and almost optically flat. Even with the appropriate engineering the required homogeneity cannot be achieved. The homogeneity of the field is increased by opposing any field gradients present in the principal field with field gradients produced by varying the current
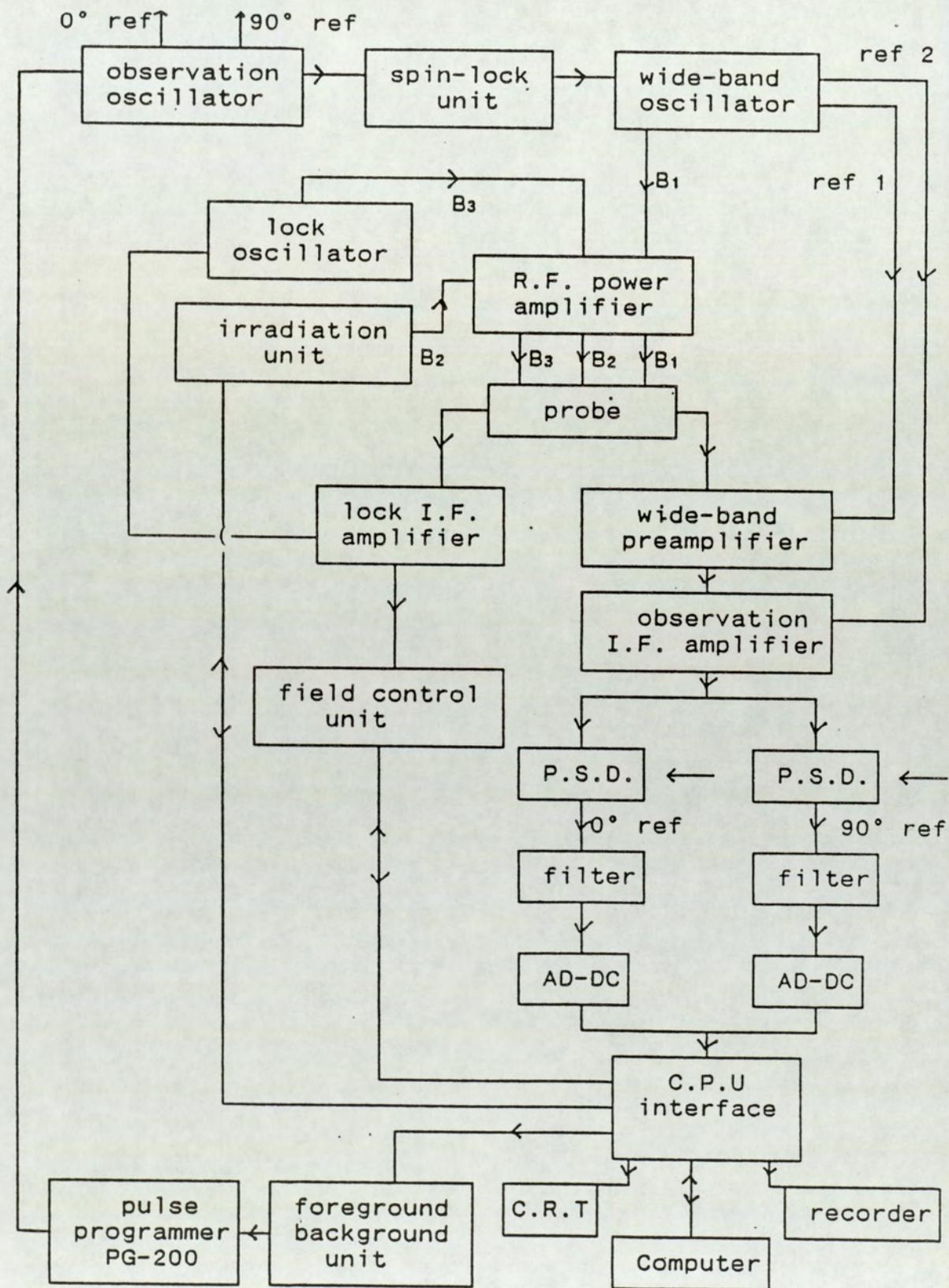
Fig. 3.3 Schematic Representation of a JEOL FX90Q Spectrometer

flowing in coils geometrically placed in the pole pieces of the magnet. Such coils are called Golay shim coils and can correct first order (x,y,z) gradients, second order gradients xy, yz, xz, z^2, c and higher order gradients. Homogeneity is further increased by causing the sample to spin rapidly (>15 Hz) about the y axis; this can cause modulation of any residual field gradients and lead to spinning side bands in the spectrum. The use of the procedures outlined above allows the required homogeneity to be achieved. The quality of the resulting NMR spectrum is very sensitive to field inhomogeneity along the y axis and so the Jeol FX 90Q spectrometer has a resolution stabilser which constantly adjusts the y axis field gradient to retain the homogeneity of the field.

The magnet must also be stable over long periods of time with the field required to be constant to about 1 part in 10^8/Hr. Such stability is achieved for an electromagnet in three stages. The first stage is by the use of a high precision current stabiliser which maintains a constant current flowing through the coils of the electromagnet. The second stage is via the use of a flux stabiliser. Pick up coils are mounted on the pole caps, the voltage induced in the coils due to fluctuations in the field are amplified, integrated and fed as a correction signal to the current stabiliser. The final stage of stabilisation is via the use of a field-frequency lock which is discussed below.

3.4.2 The Field-Frequency Lock

The field-frequency lock on the Jeol FX 90Q spectrometer (107) operates by observing the NMR signal of a heteronucleus. On the Jeol FX 90Q spectrometer a lock oscillator at a constant frequency observes the dispersion mode signal of either a deuterium or lithium nucleus. The deuterium lock is called an internal lock as separate coils on the probe assembly (Sec. 3.4.3) sweep the field through the deuterium resonance of the NMR solvent contained in the sample tube on a time-share basis. Initially the signal is brought to the centre of the oscilloscope screen by adjusting the field, B_0. The lock circuit is then switched on and receives a voltage corresponding to the signal strength at the centre of the oscilloscope screen. Owing to the shape of the dispersion signal (Fig. 1.4), deviation of the resonance from the centre of the oscilloscope screen will cause a positive or negative voltage to be detected. This voltage is converted to a current which is then fed to the current stabiliser and hence provides a correction to the B_0 field and brings the lock signal back to exact resonance. The lithium lock operates in a similar way except that it is an external lock. The resonant lithium nucleus is situated away from the analytical sample tube and hence is external to the sample. This provides a correction in a similar way but due to the difference in distance between the lock and the sample the correction is not as accurate. External locks are useful when the sample contains no deuterium. It should be noted that field-frequency locks can

only compensate for small variations in stability and the above three stage correction procedure is required to maintain sufficient overall stability.

3.4.3. The Probe

The main function of the probe is to position the sample between the poles of the magnet. The probe on the Jeol FX 90Q (107) is of the "omni" type and is composed of a fixed permabody section, replaceable rf modules and a sample insert. The fixed permabody section is non magnetic and houses replaceable rf modules for external lock, observation and double irradiation. The permabody section houses a double walled dewar for variable temperature studies on which the double irradiation coils and a thermocouple are mounted. An air line is also provided which acts on a turbine placed on the sample tube to spin the sample; a photosensor mounted close by records the spinning rate. On either side of the permabody section the current shim boards and the external lock sweep coils are attached. The probe body is maintained at a constant temperature by the circulation of cooling water around it. The Jeol FX 90Q system used in the current work was the broadband multinuclear model and as such has a tuneable rf module. Different tuning ranges plus coarse and fine tuning controls are provided to enable the transmitter/receiver coil to be tuned over a wide range of frequencies. The sample insert supporting the transmitter/receiver coil and the deuterium lock coils, plugs directly jnto the permabody section. The

advantage of such a probe is that different sample inserts for 5mm, 10mm or low frequency operation can be plugged into the probe without having to change the whole assembly. The permabody section also houses a ^1H irradiation module which is used for tuning the irradiation circuit. Due to the high powers required for pulse spectroscopy (100 W) the probe must be very carefully designed to avoid over heating and pulse break through in the observed NMR signal.

3.4.4 The RF Transmitter

In multinuclear instruments the resonant frequency is synthesised by a frequency synthesiser. The output from the frequency synthesiser is phase locked (to provide stability) to the master clock unit which consists of a highly stable RF crystal oscillator in which temperature effects are internally compensated for. Due to the range of frequencies required for multinuclear NMR it would be necessary to have an independent rf amplifier for each nuclear frequency. This problem is circumvented by amplifying the rf signal at an intermediate frequency. An rf signal of correct frequency and power is supplied to the transmitter coil by frequency modulation of the intermediate frequency signal with a local signal for the nucleus being studied. This approach would require a separate local oscillator for each nucleus studied but the local signal can be derived from the frequency synthesiser for the observation nucleus. In order to provide lock and double irradiation facilities separate local oscillators for these

functions are used.

3.4.5. The Receiver Circuit

The probe on the FX 90Q spectrometer is of the single coil type (transmitter and receiver use the same coil). The B_1 field normally has a value of ca. 10^{-3} T whereas the field induced in the receiver coil due to the precession of the nuclear magnets is ca. 10^{-12} T. Hence before a nuclear signal can be detected the field due to the transmitter pulse must have decayed towards zero. This is achieved by the introduction of a delay time after the pulse and prior to detection. There are several problems associated with this viz (1) the FID decays with time constant T_2^* and consequently signal is lost, (2) the area under the frequency domain function is determined by the value of the time domain function at the origin (Eqn. 3.8) and (3) the change of origin (Eqn. 3.7) results in the mixing of the sine and cosine transformations and hence in a mixture of dispersion and absorption signals in the transformed spectrum. The delay time can be reduced to a minimum by temporary degradation of the tuning of the rf circuit (108). The resulting rf signals are amplified by the use of a wideband amplifier once again using the intermediate frequency technique and output to the phase sensitive detector. The Jeol FX 90Q spectrometer uses quadrature detection (Sec. 3.4.8) and hence two phase sensitive detectors are required.

3.4.6 Phase-Sensitive Detector

The phase-sensitive detector compares the output from the receiver coil with the frequency of the B_1 field or the intermediate frequency by cross-correlating the two. Cross-correlation is a measure of whether any correlation exists between two functions. The output from the detector is a voltage which depends on the frequency and phase difference between the two signals. If the frequency and phase of the nuclear signal are identical to those of the drive frequency then an exponentially decaying d.c. voltage with time is observed. If the signals are of the same frequency but of a different phase then a decaying d.c. output is still observed, but the initial magnitude of the output is dependent on the phase difference between the signals; signals 90° out of phase result in no output at all. If the frequency of the drive signal and the nuclear signal are different then an a.c. output is derived, the frequency of which is the difference between the drive and nuclear signals. The sinusoidal output starts at a maximum if the drive and nuclear signals are in phase and at a minimum if they are 90° out of phase. The output from the phase sensitive detector is then the FID. As it contains only difference frequencies the audio signal produced can readily be sampled and stored for fourier transformation. Before sampling, the output from the phase sensitive detector is filtered to remove any high frequency noise associated with the nuclear signal.

3.4.7 The Analogue to Digital Converter (ADC)

The analogue to digital converter converts the analogue output of the phase sensitive detector to the digital information required by the computer to complete the fast fourier transform (Sec. 3.2.1). The signal is sampled at regular intervals, τ, and converted into a binary number which is then stored in the computer. The time, τ, between sampling intervals is determined by the spectral width of the fourier transformed spectrum (Sec. 3.2.1). Any frequencies which are sampled which are lower than the spectral width (Nyquist frequency) will be accurately represented by the digitisation process. If, however there are spectral absorptions of frequency higher than the spectral width (Nyquist frequency) then such frequencies will not be accurately represented. If the Nyquist frequency is F and there is a spectral absorption lying at $F+\Delta F$ then the digitisation process will result in the spectral absorption appearing in the spectrum at the position $F-\Delta F$. This feature is called folding or aliasing and must be avoided by making sure the spectral width contains all the absorptions present in the spectrum. This obviously presents another problem as all the absorptions in the spectrum must be less than or higher than the carrier frequency for them to be correctly sampled by the A.D.C. It would obviously be better if the carrier could be positioned at the centre of the spectrum and so increase the signal to noise ratio by the elimination of folded high frequency noise and extend the range of an even B_1 field across the spectrum (Sec.

3.3.1). This situation can be achieved by the use of quadrature detection (Sec. 3.4.8).

The dynamic range of the A.D.C. is also of great importance in NMR spectroscopy. The Jeol FX 90Q spectrometer (107) has a 12 bit A.D.C. If the signal from the phase sensitive detector completely fills the A.D.C. then the lowest signal that can be detected is represented by the voltage required to activate the first bit of the A.D.C., and hence for a 12 bit A.D.C. the dynamic range is limited to 1 in 2^{11}. The situation is obviously worsened if the signal is not sufficient to fill all the bits of the A.D.C. which results in the effective measurable dynamic range being reduced. If the signal is too large then the first part of the FID will not be represented properly and distortion in the resulting spectrum will appear. It is, therefore, very important to set the receiver gain accurately. The dynamic range represented is probably quite adequate for most samples, and indeed the situation is not quite as described because for very weak signals where the noise is larger than the signal, signal averaging can often cause a peak to be detected even if its intensity is below the dynamic range of the A.D.C. This is because during signal averaging the signal to noise ratio increases with the square root of the number of scans. There is a further dynamic range problem which must be addressed. The JEC 980B is a 16 bit computer and hence it is only possible to collect 16 time averaged scans until the computer is full using 12 bit A.D.C. digitisation. If further sample

averaging is required then the data must be scaled down in the computer and the incoming data from the A.D.C. must be scaled down thus reducing the dynamic range that can be measured.

3.4.8. Quadrature Detection

In Sec. 3.4.7. it was noted that it would be advantageous if the carrier could be positioned at the centre of the spectrum. This is only possible, however, if two phase sensitive detectors are used whose reference frequencies are identical but whose phases differ by 90°. Although it is not true, it is convenient to think of one detector that is set to detect the cosine transformation and the other that is set to detect the sine transformation. The two signals can then be separately digitised, and treated as real and imaginary parts of a complex spectrum. On fourier transformation positive and negative frequencies are correctly distinguished.

Fourier transformation preserves the symmetry of functions eg if $f(-x) = f(x)$ then the function is said to be even whereas if $f(-x) = -f(x)$ the function is said to be odd. On fourier transformation even functions remain even and odd functions odd; cosine and sine are readily seen to be even and odd respectively. Hence the absorption part of an odd function in the frequency domain will give rise to a positive and negative absorption at $\pm\delta$ where δ is the offset frequency from the carrier whereas the absorption part of an

even function will give rise to two positive peaks at $\pm\delta$ in the frequency domain. Thus when both components are transformed, one line in the frequency domain is reinforced whereas the other is cancelled giving rise to the required distinction. Quadrature detection has several advantages. It improves the S/N ratio in a spectrum by $\sqrt{2}$ as high frequency noise is no longer folded in. Also it reduces the required speed of the A.D.C by a factor of 2 (although 2 A.D.C's are now required) and produces a more even B_1 field across the spectral width.

Quadrature detection can lead to quad images in a spectrum which result from incomplete cancellation of the unwanted folded peak. Such images result from slightly different characteristics of the $0°$ and $90°$ phase channels in amplification, filtering etc. This can be reduced by alternating the $0°$ and $90°$ channels and adding the resultants in the computer. In practice this is achieved by incrementing the phase of the B_1 field and the receiver after each successive scan with appropriate data routing in the computer. Such a phase cycle is called CYCLOPS and is extensively used in FTNMR (109). The Jeol FX 90Q spectrometer uses an 8 step phase cycle which reduces the quad images usually below the noise in the spectrum. For accurate data acquisition, however, this means that acquisitions should be carried out in multiples of 8 repetitions (110).

3.4.9 <u>The Computer</u>

The computer essentially controls the FTNMR spectrometer. One part of its memory is concerned with the FTNMR program which contains the algorithms required for fourier transformation of the data, phase correction, base line correction, integration, smoothing, spectral expansion and data reduction. When the above processes are carried out on a data set is controlled by the operator who converses with the computer. Whilst on most NMR spectrometers this occurs via a keyboard, the Jeol FX 90Q spectrometer permits conversation via a light pen. On the Jeol FX 90Q spectrometer the program running in the computer can be varied to allow automatic data analysis for T_1 and $T_{1\rho}$ or the auto stacking of data with certain parameters changed; alternative programs are loaded via cassette tape. With the aid of the digital to analogue converter, fourier transformed data can be displayed on a plotter, monitor 'scope or stored for future reference on cassette tape. The computer also permits foreground background working which allows data to be processed (ie fourier transformed, plotted etc) whilst new data is being accumulated from a continuing run. The computer along with the pulse programmer (Sec. 3.4.10) also controls the timing of the pulse sequences, data acquisition, the use of decoupling and many other spectrometer functions. Although a full description of the use of the computer is beyond the scope of this thesis two particularly important features, resolution enhancement and phase correction, will be discussed in more detail.

Resolution Enhancement

In Sec. 3.3.2 the FID of a single magnetization component was shown to be an exponentially decaying function of the time constant T_2^*. Fourier transformation of such a function results in the production of a Lorentzian line of half height width equal to $1/\pi T_2^*$ (Sec. 1.6.3 and Eqn. 1.31). The data which is required for fourier transformation is stored digitally in the computer and hence can easily be multiplied (scaled) by any desired function. A common function used is an exponentially decaying function with increasing number of stored data points. Multiplication of the FID by such a function enhances the earlier part of the FID whilst decreasing the contribution of the latter part of the FID. As the S/N ratio is largest at the beginning of the FID this results in a higher S/N ratio in the fourier transformed spectrum. The cost of this is that the line widths in the spectrum increase and thus some resolution is lost. However, in many cases the technique can be very useful. A commonly used multiplication function is the matched filter which multiplies the FID by an exponentially decaying function equal to its own, this provides the optimum increase in S/N ratio with an acceptable loss of resolution. The technique is equivalent to the convolution of a Lorentzian curve with another Lorentzian curve in the frequency domain which is difficult without fourier transform techniques. The reverse window function can be used to enhance resolution at the expense of S/N ratio when the observation of small spectral splittings is required. Similar functions can be used to

eliminate pulse breakthrough, A.D.C. overload and apodization in FTNMR spectra. The data table can also have 8K of zeros attached to the end of it prior to fourier transformation. This technique of zero filling does not improve resolution as such but can lead to a smoother looking spectrum due to the absorptions being better digitised.

Phase Correction

Phase errors occur in NMR spectra for various reasons. For example the phase of the reference signal in the phase sensitive detector cannot be accurately adjusted to observe the sine or cosine transformation. Such an error causes a frequency independent phase error across the spectrum, and in the resulting fourier transformed spectrum results in a mixture of absorption and dispersion mode signals. The absorption and dispersion parts of the spectrum can be separated by taking linear combinations of the real and imaginary parts of the data. On the Jeol FX90Q spectrometer this is achieved by adjusting the PO parameter (107). Frequency dependent phase errors can also occur due to the size of the offset from the carrier frequency (Sec. 3.3.1) and due to the necessary delay in the sampling of the FID because of the power of the nutation pulse (Sec. 3.4.5). Other frequency dependent phase errors can occur in the receiver electronics especially in the audio frequency filters. Such errors are all lumped together and adjusted in the final spectrum as though they were linearly dependent on

the frequency. This is achieved on the Jeol FX 90Q spectrometer by the adjustment of the parameter P1. These phase corrections would be very difficult to carry out without the aid of the computer.

3.4.10 The Pulse Programmer

The pulse programmer in use on the Jeol FX 90Q spectrometer is the PG 200 pulse programmer (110). The PG 200 pulse programmer has 13 output bits which control the observation, irradiation and receiver gates. The phases of the irradiation and observation pulses can also be controlled via the pulse programmer as can the use of external parameters such as the homospoiling pulse and the spin-lock unit. Pulse sequences can be written which control these functions of the spectrometer and stored for future reference on cassette tape. The programming language used permits time delays, conditional and unconditional jumps and loops to be inserted into pulse programs. The programs can be up to 64 steps in length and this has been found to be quite sufficient for most applications. The use of the pulse programmer has allowed new pulse sequences to be written for the determination of T_1 (Chap 4) and $T_{1\rho}$ (Chap 7) and also has extended the capability of the Jeol FX 90Q spectrometer to use DEPT (37) and similar pulse sequences. A more complete discussion of the PG-200 pulse programmer is presented in Appendix 1.

CHAPTER 4

MEASUREMENT OF T_1

4.1 <u>Introduction</u>

NMR spin-lattice relaxation times have been shown to be very useful in solving many chemical and biological problems. Prior to the advent of pulse fourier transform techniques, T_1 measurements were carried out either by the use of pulse techniques on simple one line spectra (111,112) or by adiabatic rapid passage techniques using continuous wave spectrometers (113). T_1 measurements were therefore restricted to abundant nuclei (^1H and ^{19}F) and compounds with resonances that were well separated. Vold et al. (114) showed that the T_1's of individual resonances could be obtained from a fourier transformed NMR spectrum based on the original $180°-\tau-90°$ technique of Carr et al. (112) (Sec. 4.2.1). Although the use of NMR spin-lattice relaxation times has increased enormously since the experiments of Vold et al, relaxation times are not usually measured routinely due to the excessively long time such measurements can take. Many methods have been introduced to reduce the time such relaxation measurements take with varying amounts of success (Sec. 4.2). This thesis aims to describe the implementation of the variable nutation angle (DESPOT) technique (115,116) which can reduce the time T_1 measurements take by a factor of up to 100 (Sec. 4.3).

4.1.1 <u>Transverse Magnetization Component Destruction</u>

In many of the T_1 measurement techniques to be discussed in the following section it is essential to

destroy the transverse component of the magnetization in the middle of the pulse sequence. This can be achieved by allowing T_2^* relaxation to occur. Often, however the magnetization component needs to be destroyed more quickly than this method allows. Markley et al (123) destroyed the transverse component of the magnetization by presaturating the system with a burst of non selective $90°(x)$ pulses (saturating comb). The saturating comb dephases the coherent magnetization in the xy plane by making use of inhomogeneities in the B_0 and B_1 fields. Markley et al. claimed a 60-80 db reduction in signal after a 0.5 s burst of $250°$ pulses separated by 10 ms. Care should be taken though, because similar experiments in our laboratory yielded a significantly smaller signal reduction. McDonald et al. (67) replaced the saturating comb with a z-field gradient spoiling pulse. This essentially degrades the B_0 homogeneity for a short time causing the coherent magnetization to spread out in the xy plane very quickly due to the temporarily very small value of T_{inhom} (Sec. 3.3.2). After such a pulse it is essential to allow the homogeneity of the B_0 field to recover prior to measuring $M_z(\tau)$ with the read pulse. On most spectrometers this takes approximately 1 s and thus imposes a lower limit on τ. Z-field gradient spoiling pulses (124), however, will not necessarily prevent Hahn type echo formation (105), which will cause the results to be inaccurate. Fortunately, in ^{13}C proton noise decoupled spectroscopy, echo formation is destroyed by the incoherent decoupling (124). The use of z-field gradient spoiling pulses also tends to preclude the use of resolution

stabilisation circuitry.

4.2   Classical T_1 Measurement Sequences

4.2.1   The 180°-τ-90° (Classical) Sequence

All the techniques for measuring T_1 are based on the same basic idea. The spin system is first perturbed, this perturbation places the system in a known non equilibrium position. The recovery from this non equilibrium position towards the Boltzmann equilibrium position is then monitored. T_1 is then obtained via the appropriate modification of Eqn. 1.28. This approach assumes exponential recovery of the system (Sec 2.4.1) towards the Boltzmann distribution, where this assumption is not valid the actual meaning of the results obtained must be carefully examined.

The 180°-τ-90° technique perturbs a spin system which has attained the Boltzmann thermal equilibrium by a non selective 180° pulse. This causes the M_z magnetization component, M_0, to be placed along the -z axis (Sec. 3.3.1 and Fig. 3.2). The system is then allowed to recover back towards the Boltzmann equilibrium position for a known time τ. After the time τ the z magnetization component $M_z(\tau)$ is subjected to a non selective 90°(x) pulse which places the magnetization along the y' axis of the rotating frame and the resulting FID is then sampled and stored. After a waiting time of $5T_1-\tau$ to allow the Boltzmann equilibrium to be re-established the pulse sequence can be repeated.

Several pulse repetitions for each τ value can be used to give the appropriate S/N ratio and separate FID's for various τ values can be obtained. A schematic diagram of the pulse sequence is presented as Fig. 4.1. The T_1 value can then be obtained from

$$\ln(M_0 - M_z(\tau)) = -\tau/T_1 + \ln(2M_0) \qquad (4.1)$$

For each separate accumulation a time of $5T_1$'s must elapse using this sequence. If a sample containing varying T_1's is used the wait time must be equal to 5 times the longest T_1 value. Hence, if considerable signal averaging is required the time to obtain the partially relaxed spectrum for each τ value can become prohibitive. For an accurate semilog plot it is also necessary to have greater than 3 τ values lying in the range 0.3 to 1.2 T_1 and a measured value of M_0 with which to plot the data. For ^{13}C where T_1's can be as long as 100 s in liquid samples such a measurement can take an extremely long time. There is a further drawback to the technique in that the value of the longest T_1 must be estimated prior to analysis. To ensure that the analysis is accurate this estimation is usually made on the long side which results in the experiment taking an even longer time. As the experiment takes a long time to perform Freeman et al. (117) modified the pulse sequence to give an independent measure of M_0 for each τ value to take into account any errors caused by spectrometer drift during the experiment. Although this results in a more accurate determination of T_1, the experiment takes a longer time to perform.
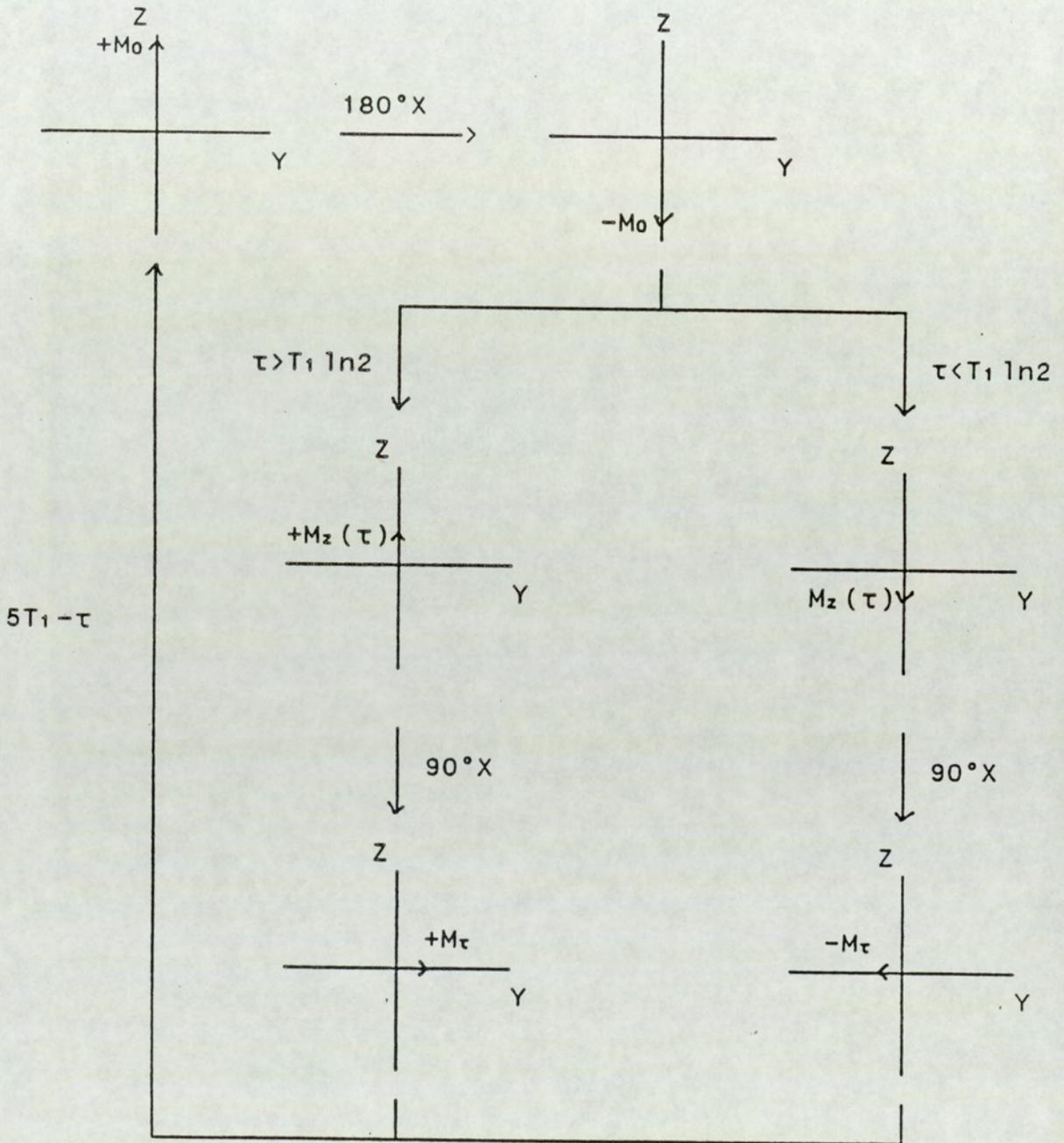
Fig. 4.1 The 180°-τ-90° pulse sequence for T₁ measurement

Several methods based on the sequence have been used to attain values of T_1 more quickly. Inspection of Eqn. 4.1 reveals that at the null point when $M_z(\tau)=0$, Eqn. 4.1 can be rearranged to give

$$\tau_{null} = T_1 \ln 2 \qquad (4.2)$$

Hence if τ_{null} can be obtained, T_1 can be obtained in a one shot experiment. This method has been used quite successfully (98) to measure T_1 but is prone to error. In cases where the sample is weak, the detection of the null point is difficult. The analysis is also quite prone to errors caused by off-resonance effects (118) (Sec. 5.3). Levy and Peat (119) demonstrated that the waiting time after acquisition could be reduced to $3.5T_1-\tau$ with little error and used this as the basis of the fast inversion recovery modification (120). Freeman et al. (121) suggested an intensity ratio method to speed up the determination. Values of $M_z(\tau)$ are measured at two different τ values and from the ratio of the $M_z(\tau)$ values, T_1 can be obtained. This method, therefore, requires only two τ values and no value of M_0 need be measured thus providing a rapid measure of T_1. The choice of the values of τ is quite critical for accuracy and any non exponential decay will not show up in such a two point analysis. De Fontaine et al (122) extended the intensity ratio approach by taking several τ values and fitting them to a non linear least squares routine. This method required no measurement of M_0, although a value of M_0 could be obtained from the data, and reduced the error in T_1

measurement associated with small intensity variations in the ratio method.

4.2.2 The Saturation Recovery Sequence

The saturation recovery (123,67) sequence operates by allowing the z magnetization to grow from zero instead of $-M_0$ as used in the classical sequence. A $90°(x)$ pulse shifts the nett z magnetization onto the y axis. The application of a z-field gradient pulse (Sec. 4.1.1) dephases the magnetization in the xy plane reducing the effective magnetization to zero. After the spin system has relaxed for a time, τ, the magnetization vector $M_z(\tau)$ is sampled by the application of a $90°(x)$ read pulse. After acquiring the resulting FID the z-field gradient spoiling pulse is reapplied thus eliminating any coherent magnetization in the xy plane. After a period, τ, a $90°(x)$ read pulse can be reapplied thus alleviating the need to wait $5T_1$'s between sequence acquisitions. A value for T_1 can now be obtained using Eqn. 4.3 with various τ values in the range $0.3T_1$ to $1.2T_1$.

$$\ln(M_0 - M_z(\tau)) = -\tau/T_1 + \ln(M_0) \qquad (4.3)$$

Once again a value of M_0 is needed which requires one value of τ greater than or equal to five times the longest T_1. The method presents a significant time saving over the classical sequence, especially where long T_1's are involved. Comparison of Eqn. 4.3 with Eqn. 4.1 shows that the dynamic

range of the technique is half that of the classical sequence but the S/N ratio deficit is made up in the measurement of long T_1's by the rapid repetition rate of the sequence. As noted in Sec 4.1.1 it is essential to allow the homogeneity of the magnet to recover before acquisition after the application of a z-field gradient spoiling pulse. This places a lower limit of ca. 1 s on the value of τ that can be used in a saturation recovery sequence. Consequently the sequence is not applicable to the measurement of short relaxation times.

4.2.3 The Progressive Saturation Sequence

The progressive saturation (124) technique is different to the classical and saturation recovery sequences in that it only uses a single pulse sequence. The whole sequence may be written as $(90°-\tau)_n$ where τ represents the total time between 90° pulse repetitions and n is the number of pulse repetitions. As in the saturation recovery sequence a z-field gradient spoiling pulse is included after acquisition to ensure complete T_2^* decay. The progressive saturation technique drives the z-magnetization to an equilibrium value, M_{zeq} which is dependent upon the ratio τ/T_1. M_{zeq} is given by,

$$M_{zeq(\tau)} = M_0 (1-\exp(-\tau/T_1)) \qquad (4.4)$$

The magnetization does not reach the equilibrium position immediately and as such a number of dummy (non acquisition)

sequences are required prior to acquisition. Freeman et al. (124) suggest that four such dummy sequences are required. Once the system is at the equilibrium position further acquisitions can be added immediately without any extra waiting periods. It should be noted that during the interval, τ, the data are acquired and as such the minimum value of τ is determined by the acquisition time plus the time required for recovery from the z-field gradient pulse. It should also be noted that even though no data are acquired during the dummy sequences the total time, τ, remains the same. The data are plotted as the usual semi logarithmic plot

$$\ln(M_0 - M_{zeq}(\tau)) = -\tau/T_1 + \ln(M_0) \qquad (4.5)$$

The method presents no real saving over the saturation recovery sequence. The progressive saturation technique is limited to long relaxation times due to the fact that data are acquired during the period, τ. For ^{13}C acquisition this places a lower limit on τ of about 2 s including the z-field gradient spoiling pulse which means that T_1 values less than about 5 s are not suitable for measurement by this technique. For ^1H spectroscopy where acquisition times of the order of 4 s are common, the applications of progressive saturation are limited.

In common with all the techniques discussed so far a value for M_0 must be obtained to plot the data. This can be avoided by adapting the intensity ratios technique (121) or

the non linear least squares analysis technique (122) (Sec. 4.2.1) to either saturation recovery or progressive saturation. Both progressive saturation and saturation recovery present a worthwhile time saving over the classical technique for the measurement of long relaxation times. Even so for long T_1's, because it is necessary for τ to cover the approximate T_1 range, the experiments can still be very time consuming.

4.3 The Variable Nutation Angle (DESPOT) Method

4.3.1 Introduction

The DESPOT (Driven Equilibrium Single Pulse Observation of T_1) method, in common with the progressive saturation tecnhique, relies on driving the z magnetization to a known equilibrium position, and letting the z magnetization relax towards M_0 during the acquisition time. The difference between the DESPOT and progressive saturation techniques is that instead of using a fixed θ pulse and a variable τ period, the DESPOT sequence uses a fixed τ period and a variable θ pulse. The DESPOT sequence can be represented as $(\theta-\tau)_n$ where θ represents a variable nutation pulse and the period τ is determined by the acquisition time and the B_0 field homogeneity recovery time. The method was first used by Christensen et al. (125) and later revised by Gupta (126). These early papers, however contained some theoretical flaws which made the results obtained by the technique unreliable. The method has been extensively

revised and re-evaluated in a series of papers (115,116,118) by Homer et al and has been shown to be an accurate rapid method for the determination of NMR spin-lattice relaxation times.

4.3.2 The DESPOT Sequence

The DESPOT method relies on driving the z magnetization to a known equilibrium value by the repetition of θ pulses at a fixed time interval, τ. The time interval τ is made up of the acquisition time (T_{ac}), and the time T_{HS} which is the time required for the homogeneity of the B_0 field to recover after the z-field gradient spoiling pulse (Sec. 4.1.1). DESPOT gains over the other T_1 measurement sequences, in that τ remains a constant which is determined by the spectral width, number of data points and B_0 homogeneity recovery time and not by the length of the T_1 being measured. Hence even where T_1's are as long as say 100 s a τ value of 4 s could be used. In the other T_1 measurement techniques, however, in order to get an accurate representation of the relaxation curve τ values up to 100 s and beyond may well be required. The repetition of θ pulses separated by a time, τ, drives the z-magnetization to an equilibrium position, M_{zeq}, which is dependent on the parameters τ/T_1 and θ. A schematic diagram of the pulse sequence is presented as Fig. 4.2

$$M_{zeq} = \frac{M_0 \ (1-\exp(-\tau/T_1))}{1 - \cos \theta \ \exp (-\tau/T_1)} \qquad (4.6)$$

Magnetization being driven
to equilibrium
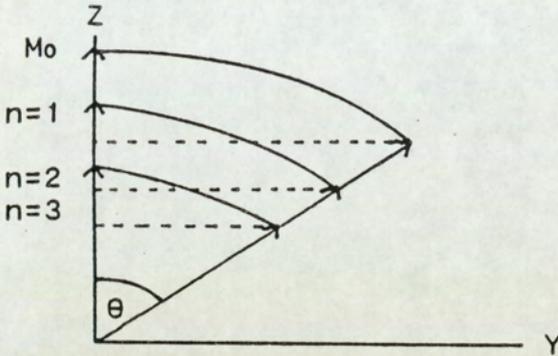
Magnetization at
equilibrium
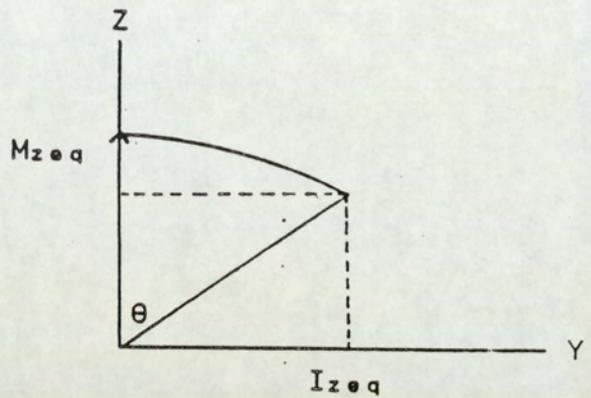
At equilibrium

$$I_{zeq} = \frac{K M_0 \sin \theta \, (1-\exp(-\tau/T_1))}{1-\cos \theta \, \exp(-\tau/T_1)}$$

$$\cos \theta = \exp(-\tau/T_1)$$
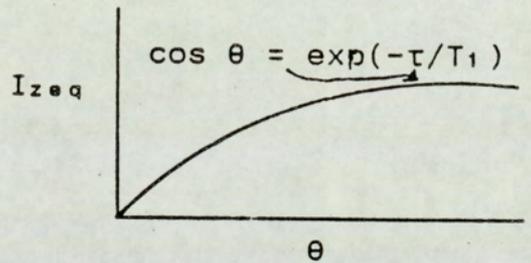
In the above equation K is a spectrometer proportionality
constant.

The equilibrium equation can be rearranged into a linear
form which T_1 can be measured without a knowledge of the
value of M_0

$$\frac{I_{zeq}}{\sin \theta} = \frac{I_{zeq} \cos \theta \, \exp(-\tau/T_1)}{\sin \theta} + K M_0 \, (1-\exp(-\tau/T_1))$$
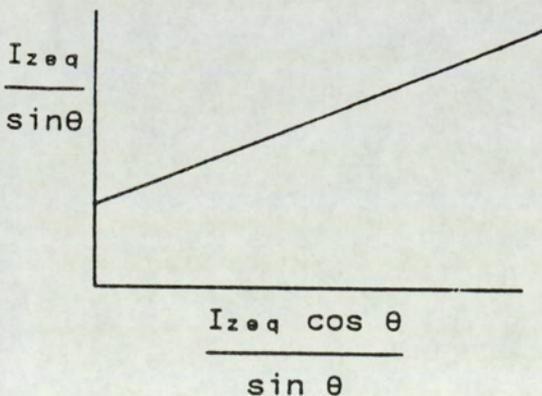
slope $= \exp(-\tau/T_1)$

Intercept $= M_0 \, (1-\exp(-\tau/T_1))$

Fig. 4.2 The DESPOT Pulse Sequence

The measured signal, I_{eq}, due to the projection of M_{zeq} in the xy plane after the θ pulse is given by

$$I_{eq} = \frac{KM_0 \sin \theta \exp(-\tau/T_1))}{1 - \cos \theta \exp(-\tau/T_1)} \qquad (4.7)$$

where K is a spectrometer proportionality constant. The derivations of Eqn's 4.6 and 4.7 are presented as Appendix 2

As shown in Fig. 4.2, Eqn. 4.7 can be readily rearranged to yield a straight line plot of gradient $\exp(-\tau/T_1)$ and a y axis intercept of $KM_0(1-\exp(-\tau/T_1))$

$$\frac{I_{eq}}{\sin \theta} = \frac{I_{eq} \cos \theta \exp(-\tau/T_1)}{\sin \theta} + KM_0 (1-\exp(-\tau/T_1)) \qquad (4.8)$$

A plot of I_{eq} against θ yields a maximum when the Ernst condition is fulfilled (Fig. 4.2 and Appendix 7).

$$\cos \theta = \exp(-\tau/T_1) \text{ when } dI_{eq}/d\theta = 0 \qquad (4.9)$$

It can be seen readily, therefore, that T_1 can be evaluated by obtaining I_{eq} for several different values of θ and either plotting the data as in Eqn. 4.8 or finding the maximum of a plot of I_{eq} against θ. In common with the other T_1 measurement techniques, T_1 can be found from two values of I_{eq}, measured in this case, at different values of θ.

$$\ln \left[\frac{(I_1 \sin \theta_2 - I_2 \sin \theta_1)}{(I_1 \sin \theta_2 \cos \theta_1 - I_2 \sin \theta_1 \cos \theta_2)} \right] = \frac{-\tau}{T_1} \qquad (4.10)$$

where $I_1 = I_{eq}$ at θ_1 and $I_2 = I_{eq}$ at θ_2

It should also be noted that a measured value of M_0, or more accurately a measured value of KM_0 (ie the measured NMR signal when the spin system has attained the Boltzmann equilibrium distribution) is not required to obtain the value of T_1 as it is in the other T_1 measurement sequences. The KM_0 value, however, is still available from the intercept of the linear plot (Eqn.4.8 and Fig. 4.2).

4.3.3 Advantages of the DESPOT Technique

The DESPOT sequence has two particular time saving advantages over the other T_1 measurement sequences. For a DESPOT analysis a value of KM_0 need not be separately obtained in order to plot the data and hence where long T_1's are measured DESPOT presents an immediate advantage. The time, τ, in the DESPOT sequence is determined by data acquisition time and not necessarily by the measured T_1. In most cases, however, where long T_1's are measured it is beneficial to ensure that the ratio τ/T_1 lies in the range 0.1 to 0.5 (Sec. 4.4.1). For a τ value of 4 s this equates to a T_1 measurement range of 8 to 40 s which is sufficient for most ^{13}C applications. It is very difficult to present an appraisal of the time saving aspects of DESPOT as the time an experiment will take is dependent on the S/N ratio of the absorption being measured, the value of τ/T_1 used the nutation angle range used and the number of data points collected.

Table 4.1

Experimental Times Required for T_1 Measurement

T_1/s	100	80	60	40	20	10	5	2
Sequence			Experimental time/s					
180°-τ-90°	47500	38000	28500	19000	9500	4750	2375	950
Sat. Recov	15680	12544	9408	6272	3136	1568	784	314
Prog. Sat.	17120	13696	10272	6848	3424	1712	856	342
DESPOT	1140	932	868	780	640	532	476	412

In order to present some idea of the relative times required to perform T_1 measurements using the 4 methods discussed a table of representative experimental times is presented as Table 4.1. The conditions under which the data in table 4.1 were calculated requires further discussion. For the 180-τ-90 sequence $5T_1$'s was allowed between each pulse sequence. The data are based on 6 different τ values with a seventh τ value of $5T_1$ in order to obtain an experimental M_0. Each partially relaxed spectrum was obtained after 16 accumulations. The saturation recovery data are based on 6 τ values of $0.3T_1$, $0.5T_1$, $0.7T_1$, $0.9T_1$, $1.1T_1$ and $1.3T_1$. A seventh τ value of $5T_1$'s was used to calculate M_0 and each partially relaxed spectrum was obtained after 16 accumulation sequences. The progressive saturation results use the same criteria as the saturation recovery results except that a further 3 non acquisition pulses were added to the sampling pulses for all τ values except when τ=$5T_1$ for the determination of M_0. The DESPOT results were based on

$\tau_{DESPOT} = 4$ s with 6 θ values of 20°, 30°, 40°, 50°, 60° and 70°. The numbers of required non-acquisition sequences were calculated using the equilibrium compromise position of Eqn. 4.13 (Sec. 4.4.1) and each partially relaxed spectrum was obtained after 16 sampling accumulations.

The data in Table 4.1 show the potentially great savings in experimental time that the DESPOT sequence can provide for short values of τ/T_1. It should be noted that where more sampling pulses are required the efficiency of the DESPOT technique compared with the other T_1 measurement techniques will increase. The data in the table do not compare the ratio techniques, but certainly where T_1's are considerably longer than the acquisition time a 2 point DESPOT analysis will be performed more quickly than the corresponding two point ratio analyses for the other techniques. The analysis presented above also does not consider the final S/N ratio of the observed signals, this will be discussed further in Chap. 6. A recent paper (147) based on ^{13}C T_1 measurements of the polysaccharide pullulan stated, "The DESPOT experiment proves in theory and in practice to be at least an order of magnitude faster than inversion recovery for the measurement of T_1. The ^{13}C T_1 magnitudes of pullulan determined by the two methods are found to have comparable precision and there are no discrepancies in T_1 values."

4.4 Conditions for Measuring DESPOT T_1's

4.4.1 The Driven Equilibrium Condition

The equations presented in Sec. 4.3.2 rely on the z-magnetization being driven to the equilibrium value, M_{zeq}. As in the progressive saturation technique this is achieved by the use of a specified number of non acquisition (dummy) sequences. Christensen et al (125) and Gupta (126) assumed that this position could be achieved by the use of 4 non-acquisition pulses similar to the progressive saturation technique (124). Homer et al. (115, 116) showed that this assumption was incorrect and calculated the number of non acquisition pulses required to drive the magnetization to an equilibrium compromise position for various combinations of θ and τ/T_1. The number of non-acquisition sequences which are required to drive the system to the actual equilibrium position, M_{zeq}, can be prohibitively large. Fig. 4.3 shows the variation in M_z with the number of non-acquisition sequences for the conditions $\tau/T_1 = 0.02$ and $\theta = 15°$. It can be seen from the figure that the equilibrium position is approached in an exponential like manner with increasing number of non-acquisition sequences. Hence a compromise condition is sought which reduces the required number of non-acquisition sequences whilst introducing negligible errors into the analysis of the experimental results. The original condition chosen was (115)

$$1.005 \ M_z \ (n-1) \geq M_z \ (n) \geq 0.995 \ M_z \ (n-1) \qquad (4.11)$$
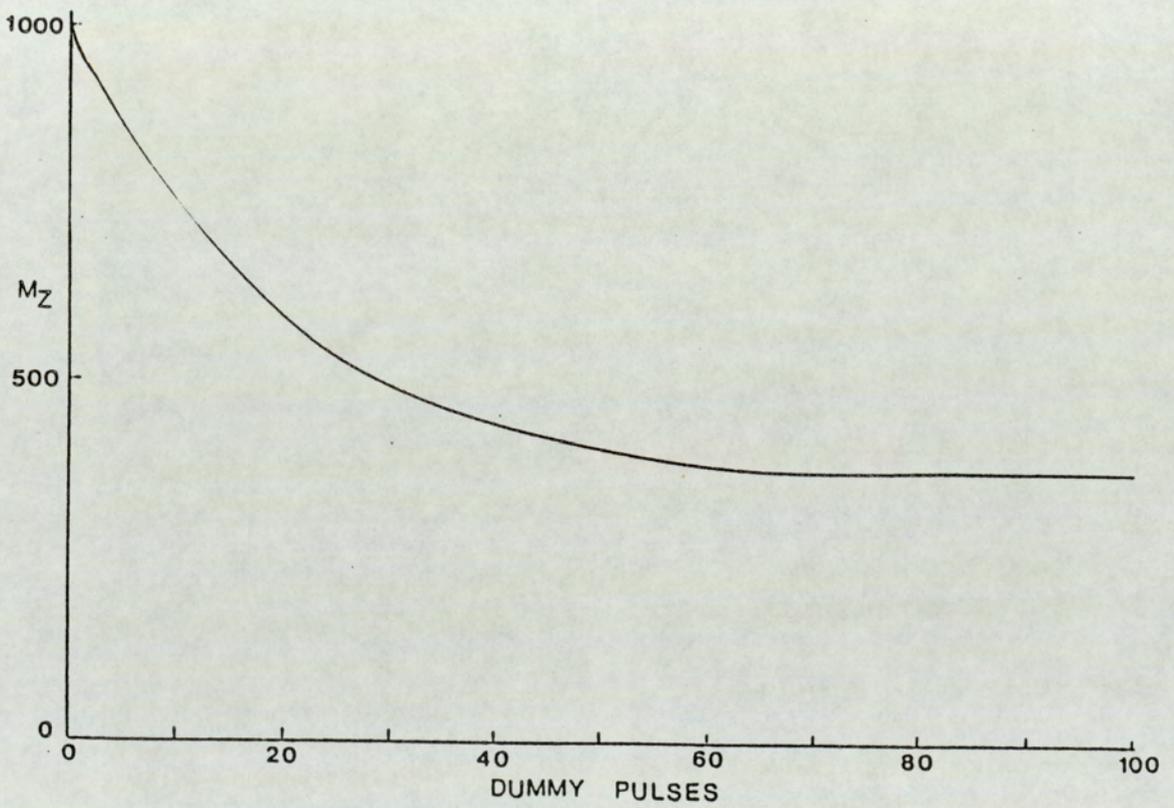
Fig. 4.3 <u>Variation of the Magnetization Vector, M_Z, with the</u>
<u>Number of dummy DESPOT sequences;</u> $\tau/T_1 = 0.02$, $\theta = 15°$

where M_z (n) is the theoretical z-magnetization after n non-acquisition sequences. Such calculations are carried out by a computer simulation of the effect of repetitive non-acquisition sequences on the spin system via

$$M_z \ (n) = M_0 - (M_0 - M_z \ (n-1) \cos \theta) \exp \ (-\tau/T_1) \quad (4.12)$$

Calculations of the number of non-acquisition pulses to satisfy this condition differed quite dramatically from 4 where the ratio τ/T_1 is small and where nutation angles outside the range 45° to 135° were used. If the ratio τ/T_1 is greater than 0.3, however, the use of 4 non-acquisition pulses in the nutation angle range 20° to 120° with a relatively large number of acquisition sequences will yield reasonably accurate results. It is for this reason that the straight line plots of reference (126) yield data comparable with the inversion recovery sequence. It is noticeable in Figs. 5 & 6 of reference (125) that the data show considerable scatter from the fitted curves at small nutation angles and small values of the ratio τ/T_1.

It can be seen by inspection of the data in Table 4.2 that the numbers of non-acquisition pulses required in the nutation angle range 10° to 45° to fulfil the condition in Eqn. 4.11 is very large. Consequently, it was suggested that DESPOT analyses in the nutation angle range 45° to 120° may prove to be more time efficient. Experimental data based on the two nutation angle ranges, 10° to 80° and 45° to 135°, however, yielded different T_1 values especially when the

ratio τ/T_1 was small. This was attributed to the inadequacy of the equilibrium compromise condition of Eqn. 4.11 (116) especially at small nutation angles and small values of τ/T_1. Consequently, a new equilibrium compromise position is presented as,

$$1.005 \, M_z \, (n) \geq M_{zeq} \geq 0.995 \, M_z \, (n) \qquad (4.13)$$

The use of this new condition is found to reduce the discrepancy in the measured T_1 values between the two nutation angle ranges. Table 4.2 shows the z magnetization achieved after the quoted number of non-acquisition sequences which are required to fulfil the equilibrium compromise positions discussed above. A more extensive version of Table 4.2 can be found in reference (116), a copy of which can be found at the back of this thesis.

Inspection of the data in Table 4.2 shows the noticeable departure of the M_{z4} values from the M_{zeq} values at both small and large nutation angles. The error becomes larger as the ratio τ/T_1 becomes smaller. Linear plots based on Eqn 4.8 over the nutation angle range 10° to 140° for τ/T_1 values less than about 0.5, using the 4 pulse equilibrium compromise, will show U shape plots. The observation of this non linearity in DESPOT type plots is indicative of insufficient non-acquisition sequences or off resonance effects (118) (Sec. 5.3). If U shaped plots are noted in the nutation angle range 10° to 140° when condition 4.13 is

Table 4.2

The Numbers of Dummy Sequences Required to Achieve the Quoted z-magnetizations Approximating the DESPOT Equilibrium Condition for Selected Values of τ/T_1

τ/T_1		0.05						0.20				
	Eqn. 4.13		Eqn. 4.11		4 pul	Equil	Eqn. 4.13		Eqn. 4.11		4 pul	Equil
$\theta/°$	n	M_z	n	M_z	M_{z4}	M_{zeq}	n	M_z	n	M_z	M_{z4}	M_{zeq}
10	63	775.2	20	833.3	947.4	771.4	13	939.7	6	953.4	962.9	935.8
20	49	461.7	30	478.2	804.6	459.5	16	789.1	11	797.9	860.9	785.9
30	33	278.0	25	282.5	609.8	276.8	14	626.1	12	629.1	718.3	623.0
40	22	180.5	19	181.8	411.0	179.8	12	488.1	11	489.3	565.7	486.2
50	15	126.1	14	126.4	247.7	125.5	9	384.6	9	384.6	430.0	382.6
60	11	93.3	11	93.3	139.4	93.0	7	308.2	8	307.5	326.3	306.9
70	7	72.6	8	72.4	82.7	72.3	6	252.1	6	252.1	256.4	252.8
80	5	58.5	6	58.4	59.1	58.4	4	211.6	5	211.4	211.6	211.3
90	1	48.8	1	48.8	48.8	48.8	1	181.3	1	181.3	181.3	181.3
100	5	41.7	6	41.9	42.6	41.9	4	159.0	5	158.7	159.0	158.7
110	8	36.9	9	36.8	47.6	36.8	6	142.0	7	141.5	146.9	141.6
120	12	33.2	14	33.1	82.5	33.1	9	128.3	10	128.7	153.1	128.6
130	18	30.4	20	30.3	165.8	30.3	12	119.2	14	118.9	186.4	118.8
140	28	28.4	31	28.2	302.2	28.2	16	111.9	18	111.6	248.9	111.4

The numbers of dummy sequences stated are calculated on the assumption that the M_z magnetization was driven from M_0. This may not always be the case if long T_1's are measured. In such cases conditions 4.11 and 4.13 will be fulfilled with less dummy sequences, thus improving the accuracy of the measurement.

fulfilled and off resonance effects have been taken into account (Sec 5.3) then this is indicative of setting the 90° pulse width incorrectly. The use of condition 4.11 is revealed to be adequate except at nutation angles less than 30°. The DESPOT regression, however, shows the greatest variation in M_{zeq} with θ in the region 10° to 90° and hence the use of condition 4.11 in this nutation angle range will lead to high values of T_1. The equilibrium compromise position based on Eqn. 4.13 is shown to follow M_{zeq} quite closely.

It seemed prudent to assess theoretically the implications of the various equilibrium compromise positions on the results of a DESPOT analysis. It is obvious that for such an assessment to be made, the number of acquisition sequences must also be taken into account. This is due to the fact that during acquisition the z-magnetization will be driven further towards its equilibrium value, M_{zeq}, with increasing number of acquisition sequences. It is also obvious that the error in the analysis due to the equilibrium compromise condition chosen will be dependent upon the actual range and size of the nutation angles chosen to carry out the analysis. The results in Table 4.3 present the theoretical error in a DESPOT analysis for various values of τ/T_1 over the nutation angle ranges 10° to 80° and 40° to 130° for the three equilibrium compromises discussed, after one acquisition pulse. Table 4.4 contains the same data but the number of acquisition pulses is increased to fifty.

Table 4.3

Parameters calculated by regressional analysis appropriate to Eqn. 4.8 for various equilibrium compromise positions. The data are based on one acquisition sequence.

Equilibrium		Eqn 4.11		Eqn 4.13		4-pulse	
τ/T_1	M_0	τ/T_1	M_0	τ/T_1	M_0	τ/T_1	M_0
		(nutation angle range 10° to 80°)					
0.050	1000.0	0.0445	1116.3	0.0499	1005.8	0.0360	2103.6
0.100	1000.0	0.0952	1046.5	0.0998	1005.0	0.0290	114.7
0.200	1000.0	0.1954	1020.3	0.1995	1005.1	0.1883	1118.1
0.500	1000.0	0.4961	1005.8	0.4979	1004.9	0.4950	1012.4
		(nutation angle range 40° to 130°)					
0.050	1000.0	0.0464	1076.3	0.0491	1020.0	0.1900	570.8
0.100	1000.0	0.0965	1034.9	0.0970	1028.4	0.1874	784.9
0.200	1000.0	0.1968	1015.1	0.1981	1010.3	0.2435	948.6
0.500	1000.0	0.4971	1004.9	0.4958	1007.3	0.5005	1012.8

See footnote to Table 4.2

Table 4.4

Parameters calculated by regressional analysis appropriate to Eqn. 4.8 for various equilibrium compromise positions. The data are based on fifty acquisition sequences.

Equilibrium		Eqn 4.11		Eqn 4.13		4-pulse	
τ/T_1	M_0	τ/T_1	M_0	τ/T_1	M_0	τ/T_1	M_0
(nutation angle 10° to 80°)							
0.050	1000.0	0.0484	1029.3	0.0499	1002.0	0.0445	1165.0
0.100	1000.0	0.0991	1007.5	0.0999	1001.0	0.0970	1041.5
0.200	1000.0	0.1995	1001.3	0.1999	1000.5	0.2070	979.8
0.500	1000.0	0.4997	1000.4	0.4999	1000.2	0.5000	1000.5
(nutation angle range 40° to 130°)							
0.050	1000.0	0.0498	1004.3	0.0499	1001.5	0.028	1766.0
0.100	1000.0	0.0998	1002.1	0.0999	1001.1	0.091	1096.3
0.200	1000.0	0.1998	1000.7	0.1999	1000.6	0.197	1015.9
0.500	1000.0	0.4999	1000.2	0.4999	1000.1	0.500	1000.4

See footnote to Table 4.2

Several recommendations can be made from an analysis of the data presented in Tables 4.3 to 4.4. It can be seen from Tables 4.3 and 4.4 that the equilibrium compromise position represented by Eqn 4.13 provides an acceptably accurate analysis over the complete τ/T_1 range. The equilibrium compromise position represented by Eqn. 4.11 provides an acceptably accurate analysis as τ/T_1 increases and as the number of acquisition sequences increases. The 4-pulse equilibrium compromise position is shown to be inadequate for DESPOT analysis unless the τ/T_1 range is $\geq$ 0.5. These comments are based on the use of a maximum of 50 acquisition pulses but if a much larger number of acquisition sequences were required for signal to noise ratio reasons the error introduced into the analysis by the use of the 4-pulse equilibrium compromise positon will obviously fall. It is suggested that the analysis is carried out in the nutation angle range 10° to 80°. In this range the greatest rate of change of M_z with θ occurs (Table 4.2) and hence leads to a more accurate analysis than over the range 40° to 130°. It is further suggested that the τ/T_1 range studied is maintained within the range 0.1 to 0.5. A recent paper by Hoffman et al (147) has suggested that the DESPOT method is most efficient when the τ/T_1 ratio lies between 0.5 and 1.0. It can be seen from Table 4.2 and reference (116), however, that the rate of change of M_z with θ falls as τ/T_1 increases thus the accuracy of the analysis becomes more prone to experimental error at larger values of τ/T_1. As τ/T_1 increases, the efficiency of a DESPOT analysis falls with respect to the other T_1 measurement techniques (Sec 4.3.3).

The lower limit of 0.1 is suggested as a compromise between the rapid rate of change of M_z with θ at low values of τ/T_1 and the large number of non acquisition sequences required at low values of τ/T_1. The use of very small values of τ/T_1 usually means that the absorptions are poorly digitised and consequently the results of such an analysis are prone to a larger than acceptable experimental error. Also at small values of τ/T_1 a small change in the gradient of a plot appropriate to Eqn. 4.8 leads to a large change in the calculated value of T_1.

4.4.2 DESPOT Intensity Measurements

Experimental results using the DESPOT sequence also invariably show differing T_1's depending on whether peak heights or integrated peak areas are used for the analysis. The T_1 values obtained, during this work, using peak heights were higher than those using the corresponding integral values. As the JEOL FX 90Q spectrometer is based on an electromagnet, the resolution over long periods of time is susceptible to degradation. This degradation in the resolution of the spectrometer with time was further enhanced by the fact that the use of the resolution stabilisation circuit was precluded due to the z-field gradient spoiling pulse. Fig. 4.4 shows the change in peak width at half height with and without resolution stabilisation with time. The figure shows that the spectrometer resolution decays quite rapidly with time. Consequently, the variation in the measured peak heights in
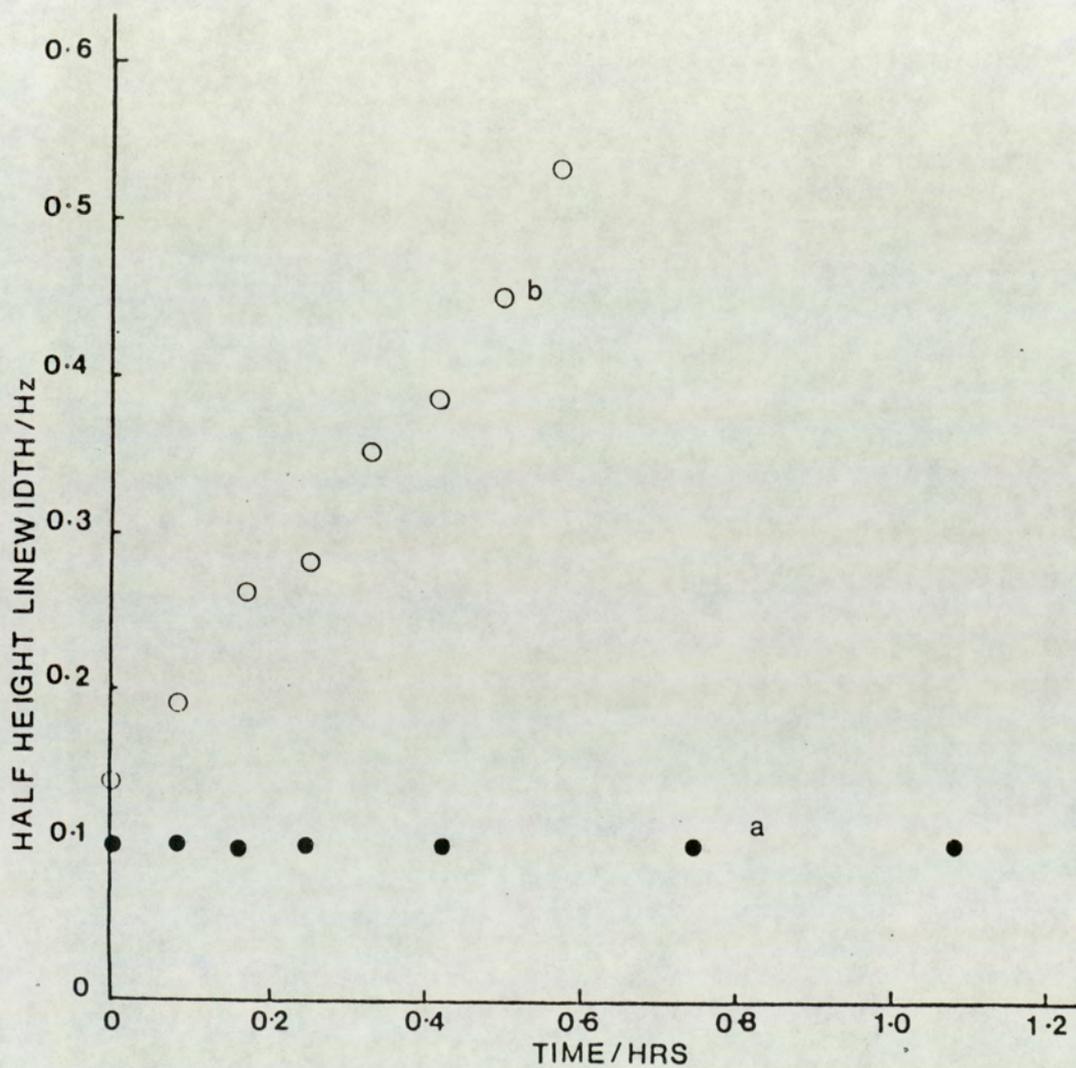
Fig 4.4 <u>Variation in the half height peak width for the ipso carbon of ethyl benzene with time (a) with resolution stabilisation and (b) without</u>

an ongoing DESPOT analysis not only reflect the T_1 of the nuclei under investigation but also the resolution degradation of the spectrometer. This problem could be circumvented by the use of electronic integration of the absorption but this requires that the absorption is better digitised, more accurately phased and has sufficient absorption free baseline (5 times the peak width at half height) around its centre.

Armitage et al. (127) suggested that peak heights could still be used provided that the FID was first multiplied by an exponential weighting function. This produces a symmetrical broadening of the resonance greater than that arising from field inhomogeneity. Experiments using this approach were carried out and the results are presented in Table 4.5.

Table 4.5

^{13}C Spin-Lattice Relaxation Times for ^1H Decoupled Benzene with Various Exponential Line Broadening Functions from Peak Heights and Integral Areas.

line broadening/Hz							
0		0.21		0.50		1.01	
T_1(int)	T_1(h)	T_1(int)	T_1(h)	T_1(int)	T_1(h)	T_1(int)	T_1(h)
17.97	14.42	17.23	14.24	16.79	14.02	16.36	13.95

all T_1 values measured in seconds

Examination of the data in Table 4.5 shows that although the peak height T_1 values show a much larger change with increasing exponential broadening function than the integral T_1 values, the two methods never give identical results even with large broadening functions. The larger change in the peak height T_1 values with increasing exponential broadening function over the integral height T_1 values is probably due to the reduction of resolution degradation effects in the peak height analysis. The difference in the calculated T_1's between the integral and peak height experiments coupled with the observed variation in the T_1 obtained from the integration experiments implies that the peak width is changing throughout the experiment. Fig. 4.5 shows the change in the ratio peak height/integral area with time for an absorption at a fixed and a variable nutation angle. The experimental results show clearly that the line width at half height is dependent on the nutation angle with the bottom curve showing a more pronounced degradation of the ratio peak height/integral area with time than the top curve. This is analogous to the saturation effect that is observed in CW NMR at high B_1 fields. In FTNMR a reduction in the peak intensity due to saturation is caused by insufficient waiting times (ie $<5T_1$) between pulse sequence repetitions (Chap 6) hence the names saturation recovery and progressive saturation for the T_1 measurement sequences. In CW NMR saturation is accompanied by line broadening. Such line broadening is not observed in FT NMR (16) if the observation time of each free induction decay is constant.
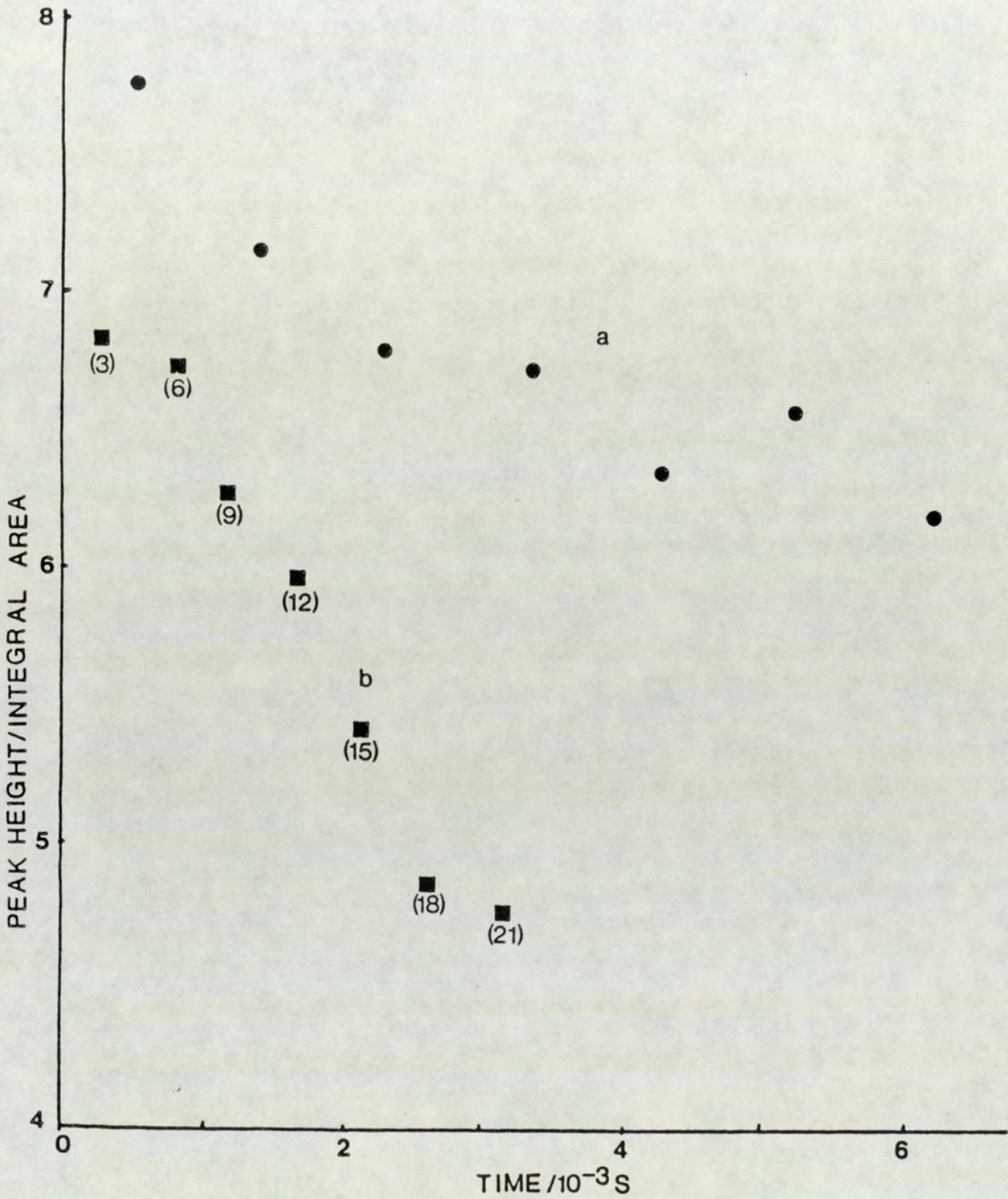
Fig 4.5 <u>Variation in the ratio peak height/integral area with time for an absorption at (a) a fixed nutation angle (9 μs) and (b) at the nutation angles shown in the parentheses</u>

Ernst and Morgan (128) noted that if the pulse spacing, τ, is varied and if the free induction decay is observed during the total available time between two pulses the signal shape becomes dependent upon $1/\tau$. In the DESPOT sequence it is noticeable that the time τ will change throughout the experiment due to the change in the length of the pulse width to provide the different nutation angles. It would be expected that the effect would be negligibly small compared with the acquisition time and z-field gradient recovery times. The experimental results, however, suggest that the line broadening effect due to the change in the pulse width is significant and as such it is suggested that integral areas should be used for DESPOT analysis. It should be noted that the other T_1 measurement sequences will not be affected by absorption broadening due to a change in pulse width but will be affected by a broadening due to resolution degradation, as such broadening is time dependent.

4.4.3. The Effect of Diffusion

Diffusion in liquid samples can cause a measured T_1 value to be low (127, 119) especially if the T_1 under consideration is long. Diffusion of molecules in and out of the effective excitation range of the coil can affect the measured result in two ways. Firstly, during the nutation pulse, molecules at different parts of the sample may experience different B_1 fields due to B_1 inhomogeneity. Diffusion of the molecules during the pulse can take molecules to different regions of the sample and hence to

regions of differing B_1 homogeneity. The upshot of this is that the signal observed is not solely proportional to $M_z \cos \theta$ but is a function of the B_1 inhomogeneity and the diffusion constant as well. Secondly during the FID acquisition molecules contributing to the observed signal can diffuse away from the receiver coil and be replaced by solvent molecules etc which will lead to a reduction in the observed signal height. Diffusion of molecules during the rf pulse was thought likely to be particularly important for DESPOT analysis as the length of the rf pulse was varied in the experiment and the 90° pulse width was calibrated using the null in the DESPOT equation at 360° (115).

The effect of diffusion on the calibration was tested by measuring the intensity of the absorption with varying nutation angle using a sample whose volume was constrained within the excitation region of the coil and a sample whose volume was not constrained. Rather than rely on the unproven DESPOT method of calibration (115) use was made of Eqn 4.14

$$I = K M_0 \sin \theta \qquad (4.14)$$

where K is a spectrometer proportionality constant.

Eqn 4.14 is only valid if a time, $\tau \geq 5T_1$, is allowed between pulse repetitions. The equation is expected to provide a maximum in I when $\theta = 90°$, the 90° pulse could then be

calibrated by fitting the observed curve to a quadratic equation and differentiating to find the maximum. The plots of I against pulse width for the ^1H resonance of cyclohexane are shown in Fig. 4.6 and the corresponding plots of I against sin θ are shown as Fig. 4.7. The unconstrained sample plot in Fig. 4.6A is noticeably asymmetric which leads to the offset apparent in Fig. 4.7A. On constriction, however, the well behaved plots of Figs. 4.6B and 4.7B are observed. These results effectively demonstrate the necessity of minimizing the effects of diffusion which become appreciable at long pulse widths. When this was done no significant difference was noted between the DESPOT method of calibration and the more conventional method used here. In both cases the minimization of diffusion essentially eliminated the pulse offset which was apparent in Fig. 4 of Ref (115). The results of Figs. 4.6 and 4.7 were obtained using 10mm NMR tubes, similar results obtained in 5mm NMR tubes showed considerably less evidence of diffusion effects on the calibration. This was presumably due to the increase in the homogeneity of the B_1 field across the sample volume when using a smaller diameter NMR tube.
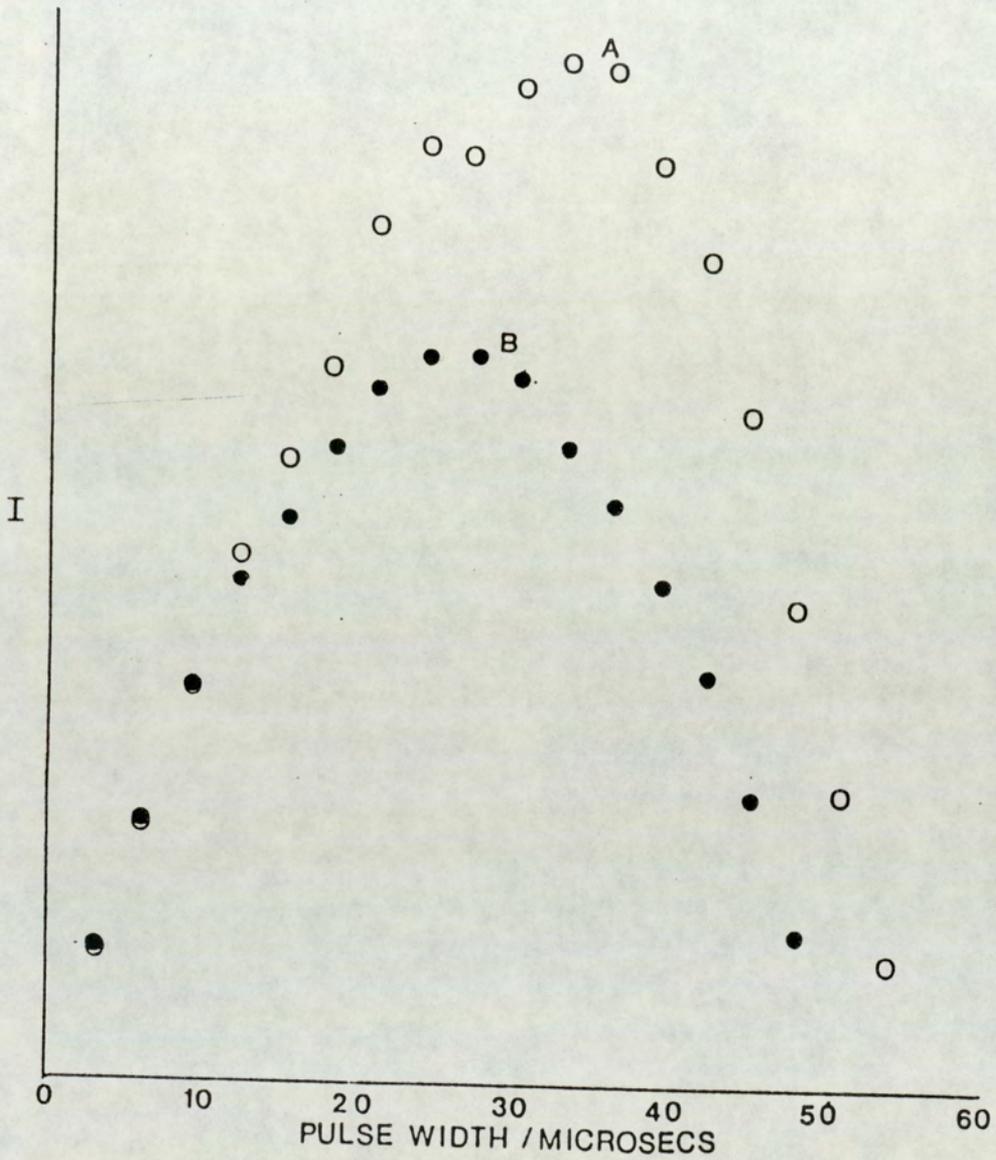
Fig. 4.6 <u>Variation in intensity, I, (arb. units) with pulse
width for the ¹H resonance of cyclohexane in a
10mm tube. (A) Open circles represent the
nonconstricted case; (B) full circles represent the
constricted case</u>
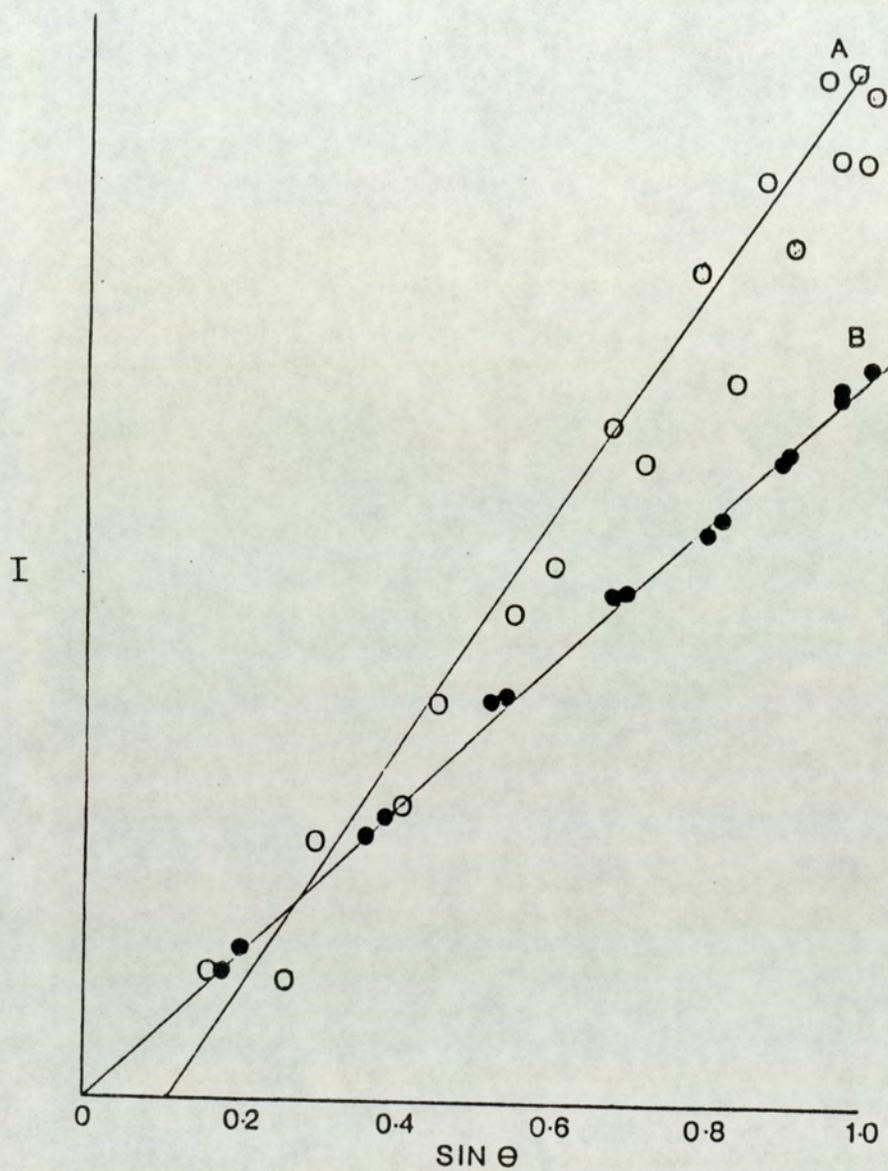
Fig. 4.7 <u>Variation in intensity, I, (arb. units) with sin θ
for the ¹H resonance of cyclohexane in a 10mm tube.
(A) Open circles represent the nonconstricted case;
(B) full circles represent the constricted case</u>

CHAPTER 5

DESPOT T_1

5.1 Introduction

The measurement of T_1 was discussed in Chapter 4 and the DESPOT sequence was shown to be considerably more time efficient than the other T_1 measurement sequences. Chapter 4 also contained discussions of the importance of the driven equilibrium position, the use of peak areas and the effect of sample diffusion on T_1 measurements using the DESPOT technique. In order to obtain the greatest efficiency and accuracy in a DESPOT T_1 determination it is necessary to address some other factors. From an accuracy point of view, the effect of incomplete T_2^* relaxation and off-resonance effects in the rotating frame will be discussed. From an efficiency point of view the use of single non-acquisition pulses in the attainment of the DESPOT equilibrium position and the use of a suite of computer programs to aid in the analysis of DESPOT data will be discussed.

5.2 Incomplete T_2^* Relaxation

It was noted in Sec. 4.1.1 that it is necessary to destroy the transverse component of the magnetization in the measurement of T_1. If the transverse component of the magnetization is not destroyed the equilibrium magnetization value becomes dependent on T_2^* as well as T_1. Consequently, the T_1 measurement sequences presented in Chapter 4 cannot yield a T_1 value without a knowledge of the value of T_2^* and a modification to the equations. T_2^* is obtained readily by

the measurement of the absorption width at half height (Sec. 1.5.2). In view of the fact that the use of the z-field spoiling pulse precludes the use of the resolution stabilisation circuitry it is worthwhile to assess the implications of incomplete T_2^* relaxation on a DESPOT analysis. This analysis yielded a new DESPOT type equation with Eqn. 4.7 being modified to,

$$I_{eq} = \frac{KM_0 \sin \theta (1-A)}{1 - \cos \theta(A + B) + (A \times B)} \qquad (5.1)$$

where $A = \exp (-\tau/T_1)$ and $B = \exp (-\tau/T_2^*)$. The derivation of Eqn 5.1 is presented as appendix 3.

The modified version of Eqn. 5.1 presented in reference (129) is in error with the plus and minus signs interchanged in the denominator. Eqn 5.1 can be readily rearranged to give a DESPOT type linear regressional plot

$$\frac{I_{eq}}{\sin \theta} = \frac{I_{eq} \cos \theta (A + B)}{\sin \theta (1 + (A \times B))} + \frac{KM_0 (1 - A)}{1 + (A \times B)} \qquad (5.2)$$

Hence providing a value of T_2^* can be measured independently a DESPOT type analysis can still provide a value of T_1 thus removing the necessity for the z-field gradient pulse in the DESPOT sequence.

It is evident by inspection of Eqn. 5.1 that when B tends to zero, Eqn. 5.1 tends towards Eqn. 4.7, the normal DESPOT equation. This situation arises when $\tau \geq 5T_2^*$. During

the period τ in a DESPOT analysis the FID is acquired, which usually means that τ is of the order of $3T_2^*$ for most absorptions. If τ is greater than $3T_2^*$ then B is small in comparison with the value of A and hence has only a small effect on the equilibrium position and the measured value of T_1. If, however, the value of B becomes appreciable in comparison with the value of A then the effect of incomplete T_2^* relaxation can become pronounced and cause the numbers of non-acquisition sequences required to fulfil Eqn. 4.13 and, the driven equilibrium magnetization achieved, to be radically altered. Table 5.1 shows some representative data.

Table 5.1

Variation in I_{eq} with τ/T_2^* for Eqn. 5.1 with $\tau/T_1 = 0.1$. The Numbers of Dummy Sequences Required to Fulfil Condition 4.13 Based on Eqn 5.1. and Driven From M_0. $M_0 = 1000$.

τ/T_2^*	10		5		3		1		0.5	
$\theta/°$	I_{eq}	n	I_{eq}	n	I_{eq}	n	I_{eq}	n	I_{eq}	n
10	151.7	30	152.5	30	157.5	30	207.9	32	273.6	29
20	217.4	30	217.7	30	219.9	29	237.7	22	253.1	20
30	219.9	23	219.6	23	217.9	22	206.3	10	198.3	19
40	199.3	17	198.7	17	195.0	16	170.9	10	156.4	19
50	174.2	13	173.5	12	169.0	11	141.6	11	126.3	22
60	150.5	9	149.8	9	145.2	7	118.2	10	103.9	25
70	129.5	7	128.8	6	124.5	5	99.6	13	86.7	20
80	111.2	4	110.5	4	106.6	5	84.3	11	72.9	23

Inspection of the data in Table 5.1 shows that incomplete T_2^* relaxation causes a significant departure of the equilibrium intensities from those predicted by Eqn. 4.7 which assumes complete T_2^* relaxation. It can be seen from the data in Table 5.1 that if the ratio τ/T_2^* is less than 5 then the effects of incomplete T_2^* relaxation on the analysis must be taken into account. It can also be seen from table 5.1 that when the ratio τ/T_2^* is less than 3, the required numbers of non sampling sequences increases quite dramatically towards higher nutation angles. This should be taken into account when analysing data obtained under these conditions if accurate values are to be obtained. Table 5.2 represents the error in a DESPOT analysis based on Eqn. 4.7 which will occur if T_2^* relaxation is not accounted for.

Table 5.2

The Values of τ/T_1 Obtained from Eqn. 4.7 for various values of τ/T_2^*. Calculations Based on Equilibrium Intensities.

τ/T_2^*	10		5		3		1		0.5	
τ/T_1	M_0	τ/T_1	M_0	τ/T_1	M_0	τ/T_1	M_0	τ/T_1	M_0
0.1	1000	0.099	994	0.091	957	0.046	750	0.024	646
0.5	1000	0.493	996	0.451	971	0.227	818	0.12	731

From the results in Table 5.2 it is evident that a substantial error can occur in a DESPOT analysis if the effects of T_2^* relaxation are not taken into account. If no

z-field spoiling pulse is used in the sequence to aid resolution then analysis must be carried out via Eqn. 5.1 unless $\tau \geq 5T_2^*$. It should also be pointed out that the above analysis does not take into account echo formation which is a possibility under incomplete T_2^* relaxation conditions. The noise decoupling in $^{13}C-\{^1H\}$ spectroscopy should prevent such echo formation.

5.3 Off-Resonance Effects

5.3.1. Introduction

In Sec. 1.6.2 the rotating frame of reference was discussed. In this discussion the idea of an effective field B_{eff} and the off-resonance parameter $(\omega_0 - \omega)$ were introduced. In Sec. 3.3.1 this discussion was extended qualitatively to the situation that occurs in pulse NMR.

5.3.2 The Off-Resonance Effect

A typical magnetization component whose resonant position is $\Delta \gamma$ Hz from the carrier frequency in the rotating frame of reference will be nutated perpendicular to an effective field B_{eff} (Fig. 1.5)

$$B_{eff} = \sqrt{(B_1^2 + \Delta B^2)} \qquad (5.3)$$

where B_1 is the pulse field strength and $\Delta B = (2\pi \Delta \gamma / \gamma)$ is the residual z field due to the off-carrier frequency shift at

the resonance. B_{eff} is also tilted with respect to the x' axis at an angle ϕ in the x'z plane.

$$\phi = \tan^{-1}(\Delta B/B_1) \tag{5.4}$$

For a pulse width, t_p, an on-carrier frequency component ($\Delta\gamma=0$) will be nutated through an angle θ about the x' axis of the rotating frame (Sec 3.3.1).

$$\theta = \gamma B_1 t_p \tag{5.5}$$

Off carrier frequency components ($\Delta\gamma\neq0$) will be nutated through a larger angle, α, in a plane perpendicular to B_{eff}

$$\alpha = \gamma B_{eff} t_p = \theta/\cos\phi \tag{5.6}$$

The effect of this (124) on an M_z component prior to the pulse, M_z^-, and immediately after the pulse, M_z^+ is given by

$$M_z^+ = (\sin^2\phi + \cos\alpha\cos^2\phi) M_z^- = kM_z^- \tag{5.7}$$

with the detected signal in the xy plane being given by

$$M_{xy} = M_z^-\cos\phi\sqrt{\{(1-\cos\alpha)^2\sin^2\phi + \sin^2\alpha\}} = \beta M_z^- \tag{5.8}$$

The derivations of Eqn's 5.6 to 5.8 are presented in appendix 4.

Obviously this will have an effect on the measurement of T_1.

It can be seen from Eqn. 5.7 that a 90° pulse which will nutate an on resonance component onto the y' axis, leaving no residual z magnetization, will leave a finite z magnetization when the magnetization component is off resonance and nutate the component into the xy plane. Freeman et al (121) noted that the off-resonance effect would not effect a 180°-τ-90° T_1 determination provided that a value of M_0 was measured, but would effect an analysis carried out by the ratio method. They concluded that such an analysis was very sensitive to the ratio $\Delta B/B_1$ but very tolerant of a missetting of the 180° pulse. For the progressive saturation sequence the recovery of the magnetization was non exponential unless the value of k equalled zero (i.e the absorption was on-resonance, and the excitation pulse was 90°). Levy and Peat (119) illustrated the sensitivity of the progressive saturation sequence to the nutation angle. The saturation recovery technique, on the other hand, appeared quite insensitive to missetting the nutation angle and to the size of $\Delta B/B_1$. As the DESPOT technique is closely related to the progressive saturation technique, it seemed prudent to carry out an analysis of the off-resonance effect on the DESPOT sequence.

5.3.3 DESPOT and Off-Resonance

Combination of Eqn. 4.6 with Eqn. 5.7 yields a new equation for the DESPOT equilibrium

$$M_{zeq} = \frac{M_0 \, (1 - \exp(-\tau/T_1))}{1 - k \, \exp(-\tau/T_1)} \qquad (5.9)$$

M_{zeq}, however cannot be measured directly but only as a projection in the xy plane. Hence by combination of Eqns. 4.7, 5.8 and 5.9, the new DESPOT linear regression equation can be written as

$$\frac{I_{eq}}{\beta} = \frac{I_{eq} \exp(-\tau/T_1) k}{\beta} + M_0 (1-\exp(-\tau/T_1)) \qquad (5.10)$$

The derivations of Eqn's 5.9 and 5.10 are also presented in appendix 4. It should be noted that Eqn. 5.10 should really contain the spectrometer constant, K, in the intercept.

It is apparent from an inspection of Eqn. 5.10 that unless $\phi=0$, the normal DESPOT regression of $I_{eq}/\sin\theta$ on $I_{eq} \cos\theta/\sin\theta$ will not yield a straight line of gradient $\exp(-\tau/T_1)$ and intercept $M_0(1-\exp(-\tau/T_1))$. A plot, however, of I_{eq}/β against $I_{eq}k/\beta$ will yield the appropriate slope and intercept.

Fig. 5.1A represents theoretical DESPOT plots with an offset parameter $(\Delta B/B_1) = 0.45$ (a) plotted normally and (b) plotted appropriate to Eqn. 5.10. Fig. 5.1B represents the corresponding experimental plots for the ^{1}H decoupled ^{13}C resonance of air saturated benzene. It can be seen by inspection of the plots that the off-resonance effect is more marked towards larger nutation angles. The observed non linearity in the plots is similar to that observed when the 90° pulse is misset or the number of non-acquisition sequences is grossly under estimated (Sec. 4.4.1). In this respect the DESPOT sequence provides an in built check on
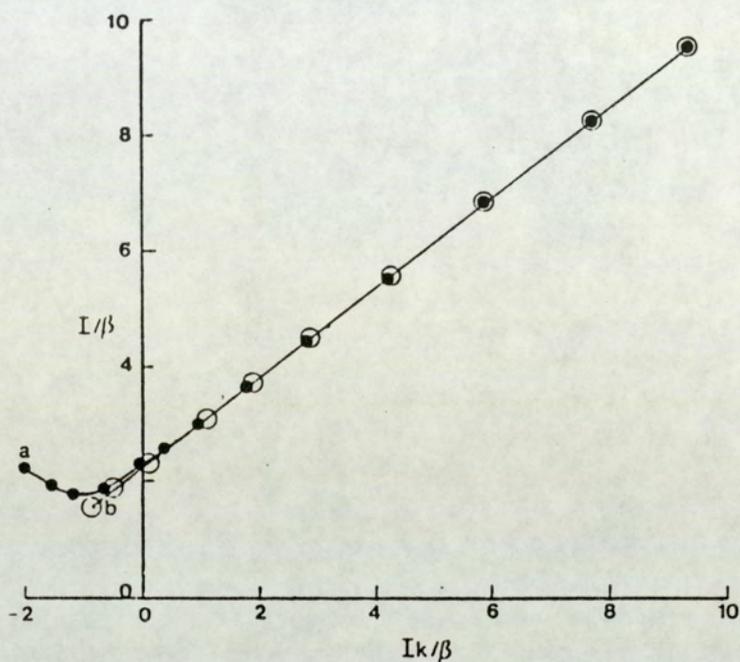
Fig. 5.1(A) <u>Theoretically derived DESPOT type regressional plots of I/ß on Ik/ß with τ/T₁=0.5 and nutation angle range = 10° to 160° (a) without correction for offset parameter with ß and k taken as sin θ and cos θ repectively and (b) plotted appropriate to Eqn. 5.10 with ΔB/B₁=0.45.</u>
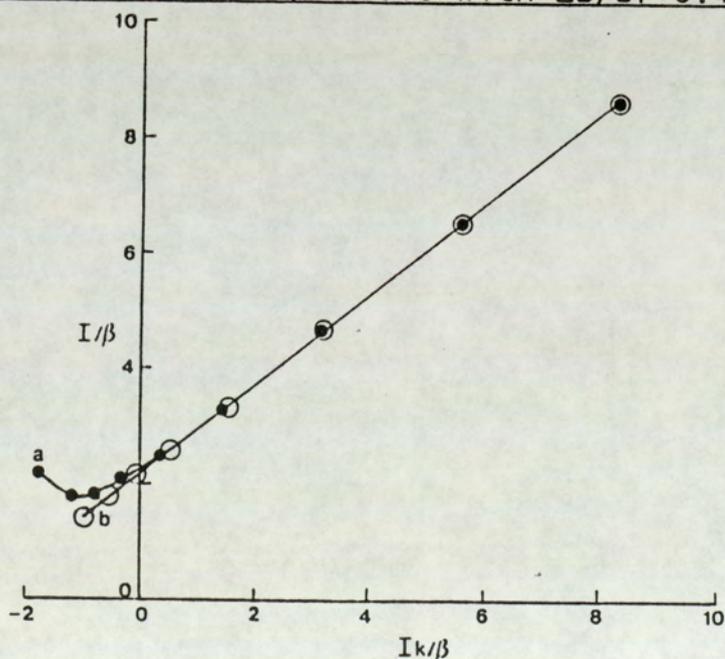
Fig. 5.1(B) <u>Experimental plots for the ¹H decoupled ¹³C resonance of air saturated benzene with the parameters identical to those in (A).</u>

the adequacy of the selected parameters. It should be noted that, when using the DESPOT technique, if the 90° pulse is incorrectly set any data obtained may still be used to calculate an accurate T_1 value provided the correct 90° pulse value is used in the calculations. In the progressive saturation technique, however, the 90° pulse must be determined accurately in order to obtain meaningful data in the first place. Also, at the small nutation angle side of the plots the observed gradient and the corrected gradient are very similar. Fig. 5.2 presents the percentage error in a DESPOT T_1 determination with nutation angles in the range 10° to 80° against the offset parameter for various values of τ/T_1. It can be seen that with an offset parameter as large as 0.5, the percentage error in a T_1 determination obtained using Eqn. 4.7 can be constrained to less than 5% in the τ/T_1 range 0.1 to 0.5.

The off-carrier frequency effect also changes M_{zeq} for a given τ/T_1 and θ and therefore will change the numbers of non-acquisition sequences required to drive the system to the equilibrium position. Table 5.3 presents the numbers of non-acquisition sequences required to establish the equilibrium condition, Eqn. 4.13, for various values of the offset parameter. As would be expected from Fig. 5.1 the numbers of non-acquisition sequences required in the nutation angle range 10° to 80° is almost independent of the offset parameter. In the range 100° to 180° the required number of non-acquisition sequences falls markedly with increasing offset. The slight increase in the number of non-acquisition
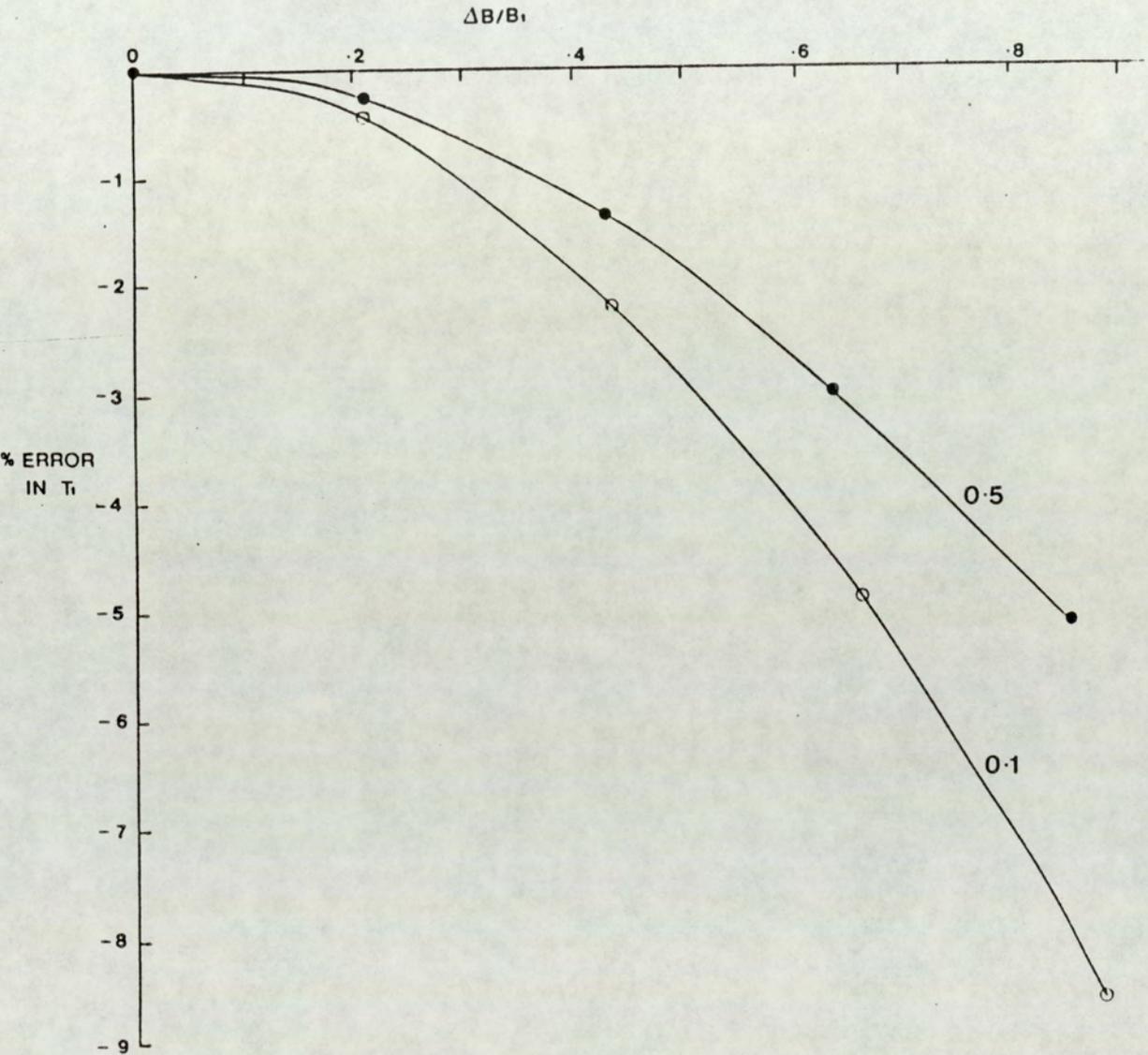
Fig. 5.2 <u>% error in a DESPOT T_1 determination with the nutation angle range constrained between 10° and 80° from Eqn. 4.8 against offset parameter for various values of τ/T_1.</u>

Table 5.3

Variation in the Required Numbers of Non-Acquisition
Sequences for $\theta=10°$ to 180° Against the Offset Parameter.
$\tau/T_1 = 0.1$

Offset	(Number of Non-Acquisition Sequences)			
Parameter	0	0.215	0.430	0.860
θ/Degs				
10	30	30	30	30
20	30	30	30	30
30	23	23	23	23
40	17	17	17	17
50	13	13	13	13
60	9	9	9	10
70	7	7	7	7
80	4	5	5	6
90	1	2	3	4
100	5	4	4	3
110	7	7	6	3
120	11	10	8	4
130	15	14	11	4
140	23	19	13	4
150	34	27	16	4
160	51	35	17	3
170	72	42	17	2
180	83	42	16	4

sequences in the range 80° to 100° must be taken into account in a DESPOT analysis if accurate data are to be obtained.

It was stated above that the 180°-τ-90° sequence is not effected by the offset parameter if the usual semilog plot is used to obtain the T_1. The null method for the rapid determination of T_1, however, is affected by the off-resonance effect. Off-resonance effects cause the null equation (Eqn. 4.2) to be modified to

$$\tau_{null} = T_1 \ln (1-k) \qquad (5.11)$$

Obviously if the null method is used for a rapid T_1 determination then this should be taken into account.

5.4 Single Pulse Driven Equilibrium

5.4.1 Introduction

The DESPOT sequence is dependent on a magnetization component, M_z being driven to an equilibrium position, M_{zeq}. The magnetization has thus far been driven to this equilibrium position by a number of non-acquisition sequence repetitions. It was noted in Sec. 4.4.1 that this process can often be quite inefficient and, therefore, reduce the efficiency of the DESPOT sequence. The use of repetitive non-acquisition pulses in the establishment of the DESPOT driven equilibrium was therefore examined.

5.4.2 Single Pulse Driven Equilibrium

From Eqn. 4.6 it is obvious that the equilibrium driven magnetization for an M_z component can be calculated if the values of τ/T_1 and θ are known. It is also obvious that if the equilibrium position is already known then the magnetization can be driven to this position using only one non-acquisition sequence with an appropriate nutation angle θ_2. The required nutation angle θ_2 can be obtained from Eqn 5.12, the derivation of which is presented in appendix 5.

$$\theta_2 = \cos^{-1} \frac{(1 - \exp(-\tau/T_1)) \; (\cos \theta \; \exp(-\tau/T_1))}{(1 - \cos \theta \; \exp(-\tau/T_1)) \; \exp(-\tau/T_1)} \qquad (5.12)$$

Hence for an absorption with a known value of T_1, the equilibrium position can be reached with only one non-acquisition sequence thus increasing the efficiency of the determination. The above theory requires that a nutation pulse, θ_2, is applied as a single non-acquisition sequence at the beginning of the DESPOT pulse sequence. This was achieved practically by writing a pulse program using the programming facilities of the PG 200 pulse programmer. The program, 1pdum, is presented as appendix 6.

The program and theory were tested using the ^{1}H decoupled ^{13}C resonance of air saturated benzene. In order to establish the initial parameters a normal DESPOT analysis was carried out using the nutation angles shown in Table 5.4, 16 acquisition sequences for each partially relaxed

spectrum and a τ value of 4.2 s. The numbers of non-acquisition sequences, n, required for each partially relaxed spectrum were based on condition 4.13 for a τ/T_1 value of 0.25 at the specified nutation angle, θ. The experimentally derived intensities, I_{meas}, are presented in Table 5.4. A DESPOT analysis of the I_{meas} data in Table 5.4 yields a T_1 value of 11.8 s and a M_0 value of 432.6. The I_{calc} values in Table 5.4 represent the theoretical intensities calculated from the values of θ, the derived values of τ/T_1 and M_0, the equilibrium position achieved after the stated number of non-acquisition sequences, n, and after 16 acquisition sequences.

Table 5.4

Normal and One Pulse DESPOT Analysis for the [1]H Decoupled [13]C Spectrum of Air Saturated Benzene.

	Normal				1-Pulse		
θ/°	n	I_{meas}	I_{calc}	θ_2/°	n	I_{meas}	I_{calc}
15.3	13	99.3	105.4	27.5	1	102.8	105.4
30.6	13	177.4	166.2	50.5	1	170.7	165.9
45.9	9	180.3	181.7	66.8	1	181.8	181.3
61.2	5	173.6	171.6	78.0	1	172.1	171.3
76.5	3	146.3	150.9	85.7	1	142.9	150.6
91.8	2	127.8	126.9	90.8	1	126.5	126.8

From the experimentally derived values of T_1 and M_0 the appropriate value of θ_2 was computed using Eqn. 5.12 for

each value of θ. The experimental, I_{meas}, and theoretical, I_{calc}, intensities for the one pulse driven equilibrium experiment are also presented in Table 5.4. The I_{calc} values for the 1 pulse driven equilibrium experiment were obtained in an identical fashion to those obtained for the normal experiment except that they are based on one non-acquisition sequence of nutation angle θ_2. The I_{meas} values for the one pulse driven equilibrium experiment were obtained under the same experimental conditions as the I_{meas} values for the normal experiment except that only one non-acquisition sequence of nutation angle θ_2 was used for each partially relaxed spectrum obtained at the nutation angle, θ. DESPOT analysis on the 1 pulse I_{meas} values presented in Table 5.4 give a T_1 value of 12.0 s and an M_0 value of 434.5. The results were considered to be consistent with the values obtained from the normal experiment within experimental error. It is worth noting that the total experimental time fell from 592 s to 428 s using the one pulse driven equilibrium conditions. It is of interest to compare the data in Table 5.4 with those produced from a normal DESPOT sequence with one non-acquisition sequence and no non-acquisition sequences at all. Those data are presented in Table 5.5. The I_{meas} and I_{calc} values presented below were obtained in the same way as those in Table 5.4 except for the difference in the non-acquisition sequences.

Table 5.5

DESPOT T_1 Determination for the ^1H Decoupled ^{13}C Resonance of Air Saturated Benzene with One and Zero Non-Acquisition Sequences.

$\theta/°$	n	I_{meas}	I_{calc}	n	I_{meas}	I_{calc}
15.3	1	103.0	106.5	0	103.7	107.1
30.6	1	184.1	171.3	0	192.5	174.9
45.9	1	201.6	189.3	0	204.8	197.4
61.2	1	170.7	178.2	0	191.5	191.5
76.5	1	145.9	154.1	0	171.7	171.0
91.8	1	128.3	126.5	0	145.2	145.6

It can be seen from a comparison of the data in Tables 5.4 and 5.5 that the one pulse driven equilibrium position is only marginally superior to the use of only one normal non-acquisition sequence but certainly better than using no non-acquisition sequences at all. The normal one non-acquisition data presented in Table 5.5 are better than would perhaps be expected. The reason for this is that 16 acquisition pulses were required to obtain a sufficient S/N ratio to carry out the integration. During the acquisition sequences the z-magnetization was driven towards the actual equilibrium position thus reducing the effect on the analysis of the inadequate preconditioning of the z magnetization using only one normal non-acquisition sequence (Sec. 4.4.1). This is borne out by comparison of the I_{calc}

values for the one normal non-acquisition sequence in Table 5.5 and the I_{calc} values for the one pulse driven equilibrium condition in Table 5.4. In order to appreciate fully the difference between the one pulse driven equilibrium position and the use of a single non-acquisition sequence would require the use of a smaller τ/T_1 value or a smaller number of sampling sequences. The I_{meas} values from the one normal non-acquisition pulse data, however, yields a T_1 of 12.7 s and M_0 of 462.6 on DESPOT analysis which is noteably different from the T_1 and M_0 values derived from the data in Table 5.4. Despite the averaging due to the use of 16 acquisition sequences the data in Table 5.5 for the case when no non-acquisition sequences are applied show considerable departure from the equilibrium values. DESPOT analysis on the I_{meas} values for the no dummy case provides a T_1 of 10.5 s and an M_0 of 452.2, which are significantly different from the equilibrium values in Table 5.4.

5.4.3 Use of Single Pulse Equilibrium

From the above discussion it can be seen that the single pulse driven equilibrium is only useful if the T_1 is already known. This is not usually the case, as the idea of the DESPOT sequence is to measure the T_1 accurately with only a prior estimate of the T_1 for the purpose of deciding how many non-acquisition sequences are required. In a modification to the recent application of limited angle excitation to NMR microscopy (129), the use of a single pulse to drive the system to equilibrium prior to obtaining

the image would improve contrast in the images and enable accurate calculations of the spin density in the sample. The single pulse driven equilibrium position is also useful in the NMR determination of T_1. In general for small flip angles and low values of τ/T_1 the number of required non-acquisition sequences required to fulfil condition 4.13 can be large. If a single pulse is used to drive the magnetization vector resulting from a nucleus with a long T_1 value to fulfil condition 4.13 then nuclei with smaller values of T_1 can attain their equilibrium positions with relatively fewer non-acquisition sequences than would have been required if the total magnetization had been drien from M_0. Fig. 5.3 shows the variation in the number of non-acquisition sequences required to fulfil Eqn. 4.13 (a) with conventional sequence repetitions and (b) after a 1 pulse driven equilibrium sequence for $\tau/T_1 = 0.025$ and $\theta = 30°$. It can be seen that the required number of non-acquisition sequences is reduced from a maximum of 45 to 22 across the 0 to 80 s T_1 range for the particular combination of τ and θ.

5.5 The DESPOT Data Analysis Programs

5.5.1 Introduction

The analysis of DESPOT data by hand is a tedious, inaccurate and time consuming business. The manipulation of DESPOT data, however is easily achieved by the use of micro computers. To this end a suite of programs was written to
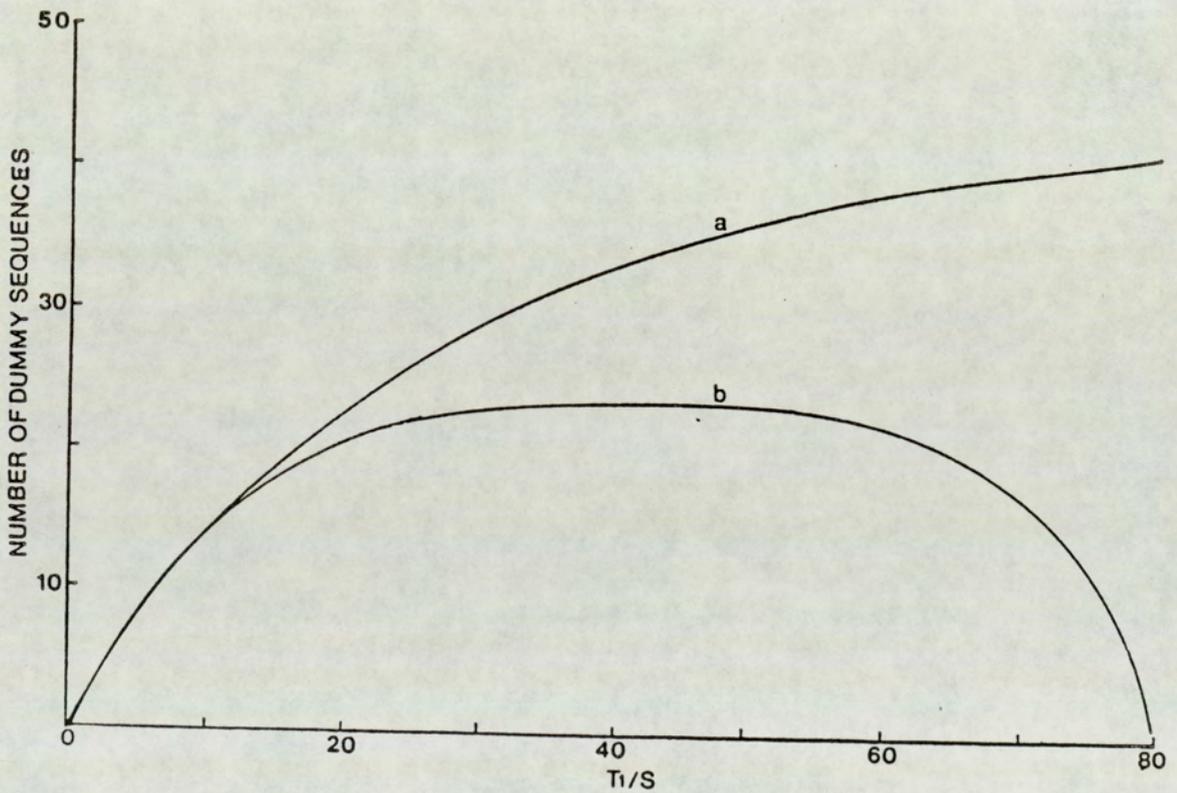
Fig. 5.3 <u>Variation in the number of dummy sequence repetitions required to fulfil Eqn 4.13 (a) with conventional sequence repetitions and (b) after a 1 pulse driven equilibrium sequence for $\tau/T_1 = 0.025$ and $\theta = 30°$</u>

analyse DESPOT data and produce a hard copy of the analysis for future reference. The suite contains 4 programs for the analysis of data.

1) 360° Pulse Determination

2) Numbers of Non-Acquisition Sequences Program

3) DESPOT Analysis via Curve Fitting to the Data

4) DESPOT Analysis via Linear Fitting to the Data

The programs were originally written to run on Apple II BASIC with hard copies being output to the TIGER printers in the department. For convenience, however, versions of the programs are now available to run on the Sinclair Spectrum with microdrive compatability and on P.C. and P.C. clone computers using Locomotive II BASIC operating under the GEM system. The BASIC programming language was used because it is generally understood and thus the programs can easily be modified. Although BASIC is in general a slow language the number of calculations required to carry out a DESPOT analysis is quite small and therefore the programs yield the analysis quite rapidly. On the AMSTRAD PC 1512 a typical DESPOT analysis containing 6 data points can be analysed in well under one minute. The use of the computer programs enables data to be analysed while the experiment is proceeding and, therefore, poor data can be rapidly detected and repeated to ensure optimum accuracy in the determination.

5.5.2 360° Pulse Determination

As noted in Sec 4.4.3, the 90° pulse width is conveniently obtained from a DESPOT analysis around the null in the DESPOT equation at 360°. As long as the equilibrium position is obtained with an appropriate number of non-sampling sequences for various nutation angles between 270° and 450° the null in the plot of I_{eq} against pulse width will yield the 360° nutation angle. Data in this range are fitted to a cubic polynomial from which the intercept on the x axis yields the null position and hence the 360° pulse width. The DESPOT equation should not in reality be modelled by a cubic polynomial but should be modelled by a least squares fit on the actual DESPOT equation. Data around the null point, however, were found to be modelled quite accurately by a cubic polynomial. The cubic polynomial was, therefore, used due to the speed of the computer algorithms and the simplicity of the resulting computer program. The output from the computer program is presented as Fig. 5.4 and shows the validity of the approach used due to the high value of the correlation coefficient. As mentioned in Sec. 4.4.3, when diffusion in liquid samples was reduced to a minimum, no significant difference could be found between 90° pulse widths obtained by this method and via the classical method used in Sec. 4.4.3. It should be noted that the apparent 360° pulse width will be dependent on the offset parameter (Sec. 5.3) and therefore the resonance chosen for calibration purposes should be as close to the carrier frequency as practically possible. In order to use

the program it is necessary that the data used is driven to its equilibrium position. This entails a prior estimate of the ratio τ/T_1. Hence, the 360° pulse width determination program and the program to determine the numbers of non-acquisition sequences are used in conjunction with each other, with the initial estimate of τ/T_1 being smaller than the actual value. It is necessary to check the value of the 90° pulse width quite regularly; different nuclei have differing 90° pulse widths and the 90° pulse width can also often change with time and will change with samples of differing magnetic susceptibility. In order to obtain the most accurate estimation of the spin-lattice relaxation time the pulse calibration should be checked for every sample. As noted in Sec. 4.4.1, the missetting of the 90° pulse width in a DESPOT analysis is often indicated via U shaped plots if nutation angles greater than 90° are used in the analysis.

5.5.3 Numbers of Non-Acquisition Sequences Program

This program calculates the required number of non-acquisition sequences modelled in its simplest form by repetitions of Eqn 4.12 to fulfil condition 4.13 for a given value of τ/T_1 and θ. The program also calculates and displays the z magnetization when condition 4.13 is fulfilled and compares that with the predicted equilibrium magnetization. The program in its most recent version can also take into account, in the calculations, the effect of incomplete T_2^* relaxation (Sec. 5.2) and the effect of

DESPOT 360 degree pulse determination

data fitted to cubic equation

$$y(int.) = a*x^3 + b*x^2 + c*x + d$$

where:-
a= -1.5339079 b= 324.89362
c= -22545.962 d= 511486.7

Data Table

pulse width microsecs	Expt. int	Calc. int.
60	-2878	-2978.0806
62	-3105	-3045.0562
64	-2902	-2795.3384
66	-2394	-2302.5537
68	-1526	-1640.3315
74	855.5	626.69482
76	1218.5	1230.3984
78	1494	1635.3984
80	1561	1768.0791
82	1730	1554.7949

pulse width(y=0)= 72.3±.1us
int.= 12.31543 at 72.3 us

X axis:- p.w/us:x div.=2 us
y axis:- int.:y div.= 2000 units
p.w min=60us:p.w(y=0)=72.3±.1us
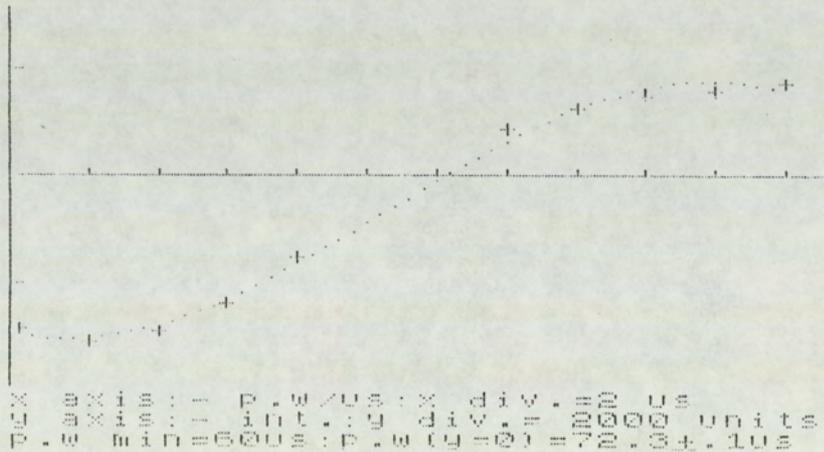
Fig. 5.4 Output from the 360° pulse determination program

off-resonance (Sec. 5.3) on the numbers of required non-acquisition sequences. It should be noted at this point that the program bases its calculations on the assumption that the magnetization is being driven from M_0 for each combination of τ/T_1 and θ. This may not always be the case, especially if τ/T_1 is short or if a magnetization component in the sample is driven to equilibrium by a single non-acquisition sequence. Other programs, not included in the suite, have been written to analyse these situations. In general, however, the magnetization being driven from M_0 presents the worst possible case; any non-acquisition sequences applied to the system after condition 4.13 has been fulfilled will drive the magnetization further towards the equilibrium position, hence improving the accuracy of the determination. An example of the output from the program is presented as Fig. 5.5.

5.5.4. DESPOT Analysis Via Curve Fitting the Data

This program calculates the spin-lattice relaxation time by finding the maximum of a plot of I_{eq} against pulse width. As with the 360° pulse determination program the data are not fitted to a least squares algorithm based on the actual DESPOT equation but rather to a least squares algorithm based on a polynomial. Data in the range 10° to 130° were found to be modelled quite successfully by a quadratic least squares fit. The maximum of the curve, and hence the T_1, is therefore, found by differentiating the

dummy analysis

td/t1 ratio= 0.1

angle (deg)	pw us	dummies reqd	mz	mequ
10	2	30	877.74	873.77
15	3	31	759.05	755.29
20	4	30	638.36	635.55
25	5	27	531.08	528.86
30	6	23	441.83	439.77
35	7	20	369.28	367.7
40	8	17	311.48	310.12
45	9	15	265.11	264.2
50	10	13	228.12	227.45
55	11	11	198.43	197.84
60	12	9	174.44	173.78
65	13	8	154.47	154.08
70	14	7	138.04	137.81
75	15	5	124.88	124.26
80	16	4	113.44	112.9
85	17	3	103.74	103.3
90	18	1	95.16	95.16

*-no.of dummies req'd > 550
  mz value after 550 dummies

Fig. 5.5 Output from dummy program

fitted curve to yield the maximum (Fig. 4.2). The program in its later versions is also capable of calculating the T_1 in the presence of incomplete T_2^* relaxation and when off-resonance effects are thought to be significant. When diffusion is not effectively eliminated in the sample a pulse offset is often noted (Sec. 4.4.3). In the curve fit program the curve is fitted to the data for offsets in the range 0μs to 1μs in steps of 0.1μs. The offset giving rise to the highest correlation coefficient is used to evaluate the experimental data. In constricted 10mm and 5mm sample tubes, however, the best fit usually provides a very small offset (Sec. 4.4.3); unconstricted 10mm tubes can give quite large offset values (115). The curve fit program permits selective insertion and removal of data points so the effect on the results of marginal data can be predicted. The data can also be saved to a text file for insertion into the linear DESPOT program or for retrieval at a later date. A typical output from the program is presented as Fig. 5.6.

5.5.5. DESPOT Analysis Via a Linear Fit to the Data

This program carries out a linear least squares fit to data plotted as $I_{eq}/\sin\theta$ against $I_{eq}\cos\theta/\sin\theta$ and consequently obtains a value of T_1 from the gradient and a value of M_0 from the intercept. As with the curve fit program marginal data can be selectively inserted and removed to assess its effects on the determination and data can be saved for archiving or interchange between analysis programs. The linear fit program is also equipped to deal

despot-t1 from peak max.

C8H10
Ethyl Benzene
15/1/86
para carbon

fitted cubic curve

$$ax^3 + bx^2 + cx + d$$

a= 0.461 b= -35.663

c= 804.857 d= -850.681

90 deg pulse= 27 us
delay time= 4 s
pulse offset = 0.6 us

pulse width us	expt. int	calc int
3	1268	1137.8923
7	3157	3048.3103
11	4325	4257.2641
15	4785	4753.861
19	4694	4731.7473
23	4426	4397.7914

spin lattice relaxation time = 7.233 seconds
equilibrium magnetization(m0)= 9233.0527


```
Y div.=1000:X div.=5 us
y axis units intensity
X axis units pulse width
```
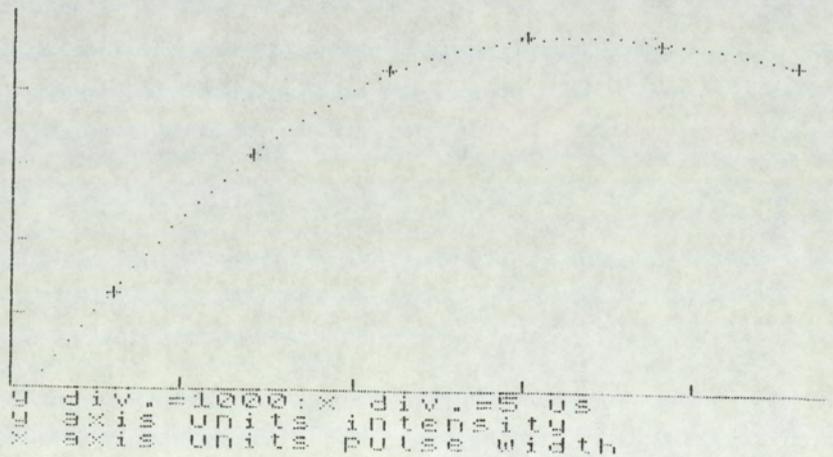
Fig. 5.6 Output from Curve fit Program

with incomplete T_2^* relaxation and off-resonance effects in its later versions. An independent determination of the offset is available using the linear fit program via a two point analysis on the various data points. The offset which produces the smallest variation in the value of T_1 obtained from the various two point analyses is used to obtain the experimental data. As mentioned above in cases where diffusion is effectively eliminated the observed pulse offset is usually very close to zero. A typical output from the program is presented as Fig. 5.7. Obviously in the entire program suite the analysis of the data is very susceptible to the original quality of the data. Poor data due to inadequate S/N ratio, or insufficient consideration of the experimental parameters will yield inaccurate T_1 values.

DESPOT-T1 from Mz vs Mzcos θ

C8H10
Ethyl Benzene
15/1/88
para carbon

fitted line
ax + b = y(int.)

a= 0.571 b= 3940.137
correlation coeff.= 0.9996

90 deg pulse= 27 us
delay time= 4 s
pulse offset= 0.599 us

pulse width/us	intensity
3	1268
7	3157
11	4325
15	4785
19	4694
23	4426

data table

x	y	y calc'd
8819.1337	8909.8229	8980.9107
7885.8048	8494.2666	8447.4457
6073.6127	7456.1649	7411.6468
4146.2261	6331.4624	6310.006
2419.9252	5281.0675	5323.3002
1073.736	4554.3809	4553.8557

spin lattice relaxation time= 7.151 seconds
equilibrium magnetization(MO)= 9196.74


```
y div.=2000:x div.=2000
y axis:-i/sin(theta)
x axis:-i*cos(theta)/sin(theta)
```
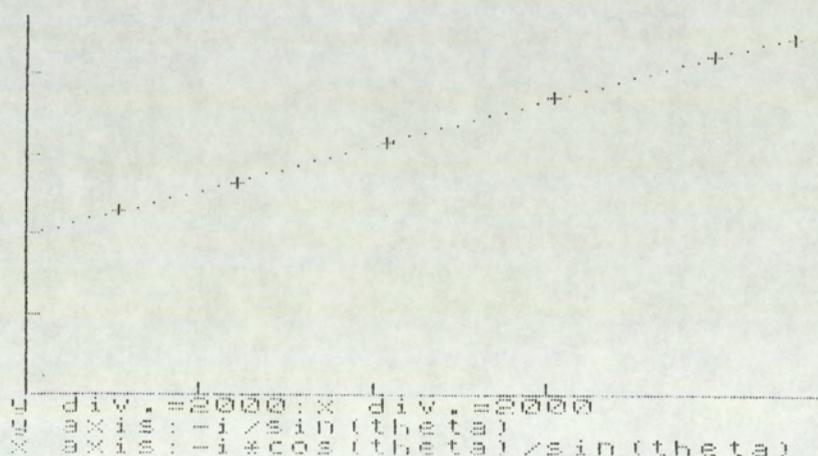
Fig. 5.7 Linear Fit Program Output

CHAPTER 6

NMR RAPID MULTIPULSING

6.1 Introduction

It was noted in Chapter 3 that pulse excited NMR is considerably more time efficient than continuous wave techniques as all the chemically shifted nuclei are excited simultaneously. Due to the short acquisition times required for FTNMR compared with CW NMR the FTNMR technique readily lends itself to multipulse operation. Thus, following a pulse, the FID is sampled and stored sequentially in the memory of the computer. At a suitable point in time a new pulse is applied to the system and the resulting FID is again sampled and co-added to the first. Repetition of this process is continued until the S/N ratio in the resulting fourier transformed spectrum is sufficient for the required analysis. The S/N ratio in the final fourier transformed spectrum is given by

$$S/N(f) = S/N(i) \ N^{\frac{1}{2}} \qquad\qquad (6.1)$$

where S/N(f) is the S/N ratio in the fourier transformed spectrum after N pulse sequence repetitions and S/N(i) is the S/N ratio that would be observed if the spectrum was fourier transformed after only one sequence repetition. A similar process, in which subsequent CW NMR scans are co-added in a computer has been carried out. Due to the length of time a CW scan takes, especially if a slow passage spectrum is required (Sec 1.6.3.1), this is a very time consuming process. Ernst and Anderson (16) have shown that the resulting increase in the S/N ratio of a spectrum

obtained via the FTNMR technique over the CW NMR technique in the same experimental time is of the order of $\sqrt{[F/\Delta\nu\frac{1}{2}]}$ where F is the spectral width examined and $\Delta\nu\frac{1}{2}$ is the width, at half height, of the individual absorptions in the spectrum. The increased sensitivity of the FTNMR technique is high, resulting in the use of FTNMR techniques for less sensitive nuclei and samples of low concentration.

So far, the question of the equilibration of the pulse perturbed magnetization has not been discussed. If each successive FID, generated from a train of equivalent pulses, is to be identical then the interpulse time must be long enough to allow full relaxation to occur. Examination of Eqn's 3.16 and 1.30 shows that the interpulse relaxation time must be $\geq 5T_1$'s. On the other hand, however, the FID actually decays with a characteristic time T_2^* which is usually considerably shorter than T_1. Hence data acquisition beyond $\approx 3T_2^*$ will just add noise to the FID without significantly adding to its information content. It is thus easy to see that there are two ways of acquiring pulsed NMR data. The first is to allow a waiting period of $5T_1$'s, including the acquisition time, between successive pulse repetitions and use 90° pulses. The 90° pulse places the magnetization along the y'axis, giving the maximum detectable signal from the magnetization, M_0 and the subsequent $5T_1$ wait allows the z-component of the magnetization to relax to M_0. This is the so-called classical technique and can give rise to spectra of lower S/N ratio than could be obtained with a shorter waiting

time than $5T_1$. Spectra obtained using the classical technique have relative signal intensities that are proportional to the number of nuclei giving rise to the absorption. The second is to use a waiting period less than $5T_1$'s between pulse repetitions in what will be referred to as a rapid multipulsed approach. This results in attenuation of the signal due to saturation (Sec. 4.4.2). For a given absorption the attenuation of the signal due to saturation can be offset by the increased pulse repetition rate thus giving a higher S/N ratio in a given experimental time than the classical sequence. However, this is not always the case, as the final S/N ratio in a multipulsed spectrum is dependent on the values of θ and τ/T_1. Inadequate care in choosing these parameters can lead to a S/N ratio which is less than that obtained using the classical sequence in the same experimental time. As the S/N ratio obtained for a given absorption is dependent on θ and τ/T_1, absorption intensities in a multipulsed spectrum will not in general be proportional to the number of nuclei giving rise to the absorption. One of the primary objectives of this chapter is to assess the implications of rapid multipulsing on NMR spectra, and present conditions for the more common nuclei which will make the most efficient use of the NMR spectrometer.

6.2 Rapid Multipulsing at the Ernst Angle

Inspection of Fig. 4.2 or differentiation of Eqn. 4.7 with respect to θ shows that the maximum intensity in a

rapid multipulsed spectra is obtained when the condition

$$\cos \theta_e = \exp(-\tau/T_1) \qquad (6.2)$$

is fulfilled for a fixed τ value (Appendix 7). This condition is known as the Ernst angle (16). Combination of Eqn's. 4.7 and 6.1 shows that the signal, S_{mp}, measured at constant spectrometer noise from the rapid multipulsed sequence and obtained in a certain experimental time, E, is given by,

$$S_{mp} = \frac{KM_0 \sin \theta (1-\exp(-\tau/T_1))}{(1-\cos \theta \exp(-\tau/T_1))} \times \left[\frac{(E-(\tau \times m))}{\tau} \right]^{1/2} \qquad (6.3)$$

where K is a spectrometer constant and m is the number of non-acquisition sequences required to satisfy Eqn. 4.13. If rapid multipulsing is carried out at the Ernst angle then Eqn 6.3 can be rewritten as Eqn. 6.4

$$S_{mpe} = \frac{KM_0 \sin \theta_e (1-\cos \theta_e)}{(1-\cos^2 \theta_e)} \times \left[\frac{(E-(\tau \times m))}{\tau} \right]^{1/2} \qquad (6.4)$$

For the classical sequence the signal, S_c, measured at the same noise level relevant to Eqns 6.3 and 6.4, and obtained in the same experimental time, E, is given by

$$S_c = KM_0 \times \left[\frac{E}{5T_1} \right]^{1/2} \qquad (6.5)$$

Becker (130) has shown that rapid multipulsing at the Ernst angle, using 4 non-acquisition sequences, can yield a

maximum S/N advantage of 56% over the classical sequence in the same experimental time. The dependence of this S/N ratio advantage with the ratio τ/T_1 was obtained using Eqn's 6.4 and 6.5. This analysis shows that providing the τ/T_1 range is constricted between 0.1 and 0.5 a 56% S/N ratio advantage over the classical sequence is available at the Ernst angle. The S/N ratio advantage is greater than 55% in the τ/T_1 range 0.07 to 0.6. These figures are slightly different from those that can be interpolated from figure 8 of reference (130) as this figure was derived using the erroneous four pulse equilibrium compromise position (Sec 4.4.1). Outside the τ/T_1 range 0.07 to 0.6 the Ernst condition does not necessarily provide the maximum attainable S/N ratio. For example at $\theta=88°$ the S/N ratio maximum occurs at a τ value of $1.2T_1$ whereas the Ernst condition would predict a τ value of approximately $3.4T_1$. For $\theta=88°$ with $\tau=1.2T_1$ the S/N enhancement over the classical sequence is 43% whereas with $\tau=3.4T_1$ the S/N enhancement over the classical technique falls to 6%. Hence, when using the Ernst condition to predict the maximum S/N ratio available it is not beneficial to allow the value of τ/T_1 to increase beyond 1.2. For τ/T_1 values of less than 1 the difference between the maximum S/N ratio available and that predicted by the Ernst condition is negligible.

6.2.1 Time Saving Aspects of Rapid Multipulsing

It is obvious that a given S/N ratio can be obtained in a shorter time using rapid multipulsing rather than the

classical sequence. At the Ernst angle, it can be shown
that, providing the τ/T_1 is constrained within the limits
0.07 to 0.6 the S/N ratio obtained using the classical
sequence in an experimental time, E, can be obtained using
rapid multipulsing in 43% of the time. Obviously with
departure from the Ernst condition within the prescribed
limits or with multipulsing at the Ernst angle outside the
prescribed limits the time saving will fall. It is
incorrect, however, to assume that there is a linear
relationship between time saving and S/N enhancement with
the former being slightly greater than the latter. The above
discussion, however, assumes that the number of sampling
pulses far outweighs the required numbers of non-acquisition
pulses required to drive the system to equilibrium. In cases
where the numbers of required non-acquisition pulses are
large, but the sample is concentrated and requires few
sampling pulses to produce a sufficient S/N ratio for
analysis, the time saving using rapid multipulsing will be
greatly reduced. Indeed it is possible that the classical
sequence will be more time economic in such cases and the
classical sequence will of course provide quantitative data.
It is worth pointing out that it is not strictly necessary,
if a qualitative spectrum only is required, to use
non-acquisition sequences at all. If non-acquisition
sequences are not used, however, it is not possible to use
Eqns 6.3 or 6.4 to say anything about the relaxation times
or the intensity ratios in the spectrum. Often for a
qualitative analysis such a situation is acceptable and in
such cases the S/N ratio obtained at the end of the

experimental time, E, will be greater than that obtained if the non-acquisition sequences were used. All the figures, however, in this chapter are based on the magnetization being previously driven by repetitive pulses to satisfy Eqn. 4.13. If the spin abundance and/or the receptivity is low such that the number of required sampling pulses far outweighs the number of non-acquisition pulses then the error introduced into the final spectrum due to the omission of the non-acquisition sequences is likely to be negligible and the resulting spectrum should model Eqn. 6.3 quite closely.

6.3 Nutation Angles Other Than the Ernst Angle

Samples submitted for NMR analysis invariably have nuclei with different spin-lattice relaxation times contained within them. It is therefore not possible to choose a nutation angle that will fulfil the Ernst condition for each nucleus in the sample. It is worthwhile, therefore, considering the effect on the S/N ratio of nutation angles other than the Ernst angle over the expected T_1 range of the nucleus under investigation. Fig. 6.1 shows the variation in the S/N ratio enhancement using rapid multipulsing, over the classical technique, against $\ln \tau/T_1$ for various nutation angles. Fig. 6.1 shows that by the judicious choice of nutation angle, the measured intensities due to specific T_1 regions of the spectrum can be selectively enhanced for a chosen τ. For example, the choice of a small nutation angle will selectively enhance the S/N ratio for slowly relaxing
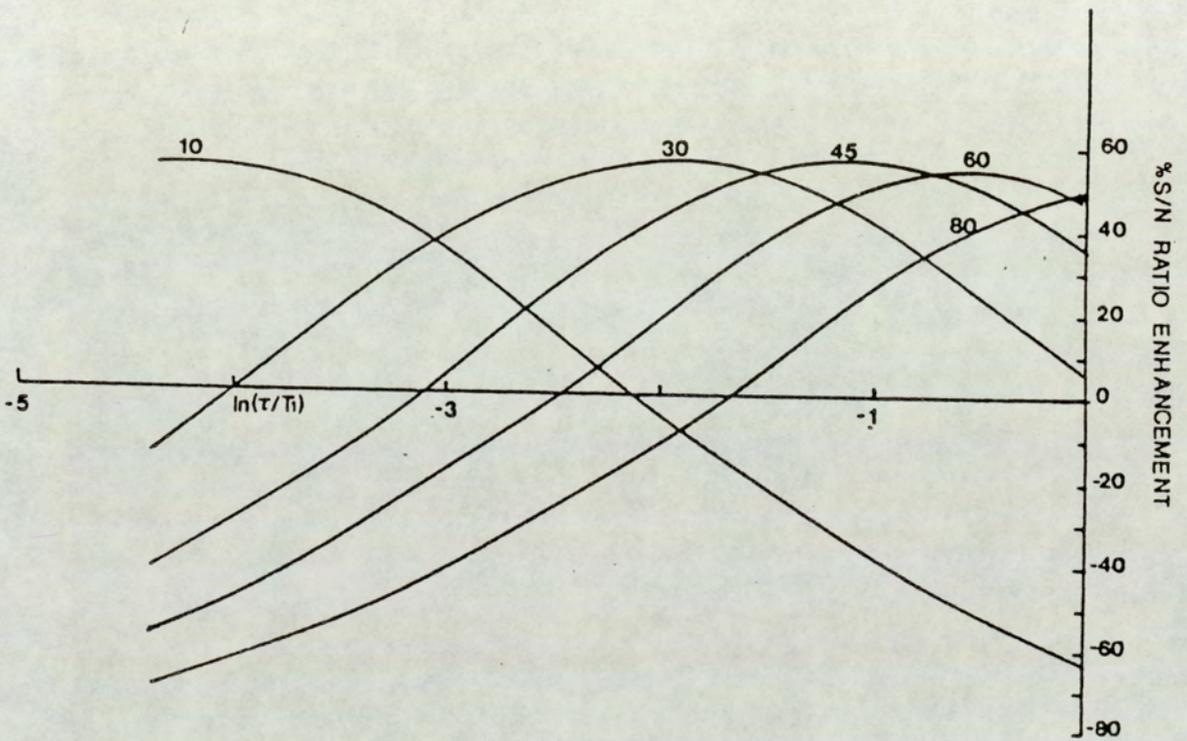
Fig. 6.1 <u>Variation in the S/N ratio enhancement using rapid
multipulsing, relative to the classical sequence,
against ln(τ/T₁) for various nutation angles.</u>

nuclei such as the ipso carbons in ^{13}C spectra. Such absorptions may otherwise (ie at larger θ's) be reduced relative to the higher S/N ratio for the shorter T_1 nuclei, in the worst cases the absorption may not be noted at all. Inspection of Fig. 6.1 also reveals that for pulse repetition times of the order of 2 s for ^{13}C spectra a nutation angle of 30° will give a minimum enhancement of 20% in the S/N ratio over the classical method for T_1's in the range 2.8 to 70 s ($\ln \tau/T_1 = -0.35$ to -3.55). In cases where a value of 2 s is impractical for τ due to other factors interpolation between the plots of Fig. 1 will allow the optimum value of θ to be selected for differing τ values. For example, for a pulse repetition time of 4 s for ^{13}C spectroscopy a good choice of θ is 45° which will give a similar enhancement over the ^{13}C T_1 range as $\tau=2$ s and $\theta=30°$ does.

In ^1H spectroscopy where τ values of the order 4 s are often used, a better choice of nutation angle for optimum S/N ratio reasons will be 60° (Fig. 6.1). In cases where the T_1 values are very short this choice may well rise as high as 80°. Such conditions give a good S/N ratio enhancement over the classical sequence for the typical proton T_1 range of 2 to 10 s ($\ln \tau/T_1 = 0.69$ to -0.92). The choice of a nutation angle of 60° or higher, however, will not allow for quantitative determination from a proton spectrum. Hence, this condition should only be used when a good S/N ratio is required rapidly and where quantitative data are not required. In the recent application of rapid

multipulsing to MR imaging (129) the main criterion was to obtain the highest S/N ratio in the shortest possible time. Consequently, the conditions were optimised to give a high S/N ratio rather than quantitative data.

Fig. 6.2 shows the variation in the S/N enhancement, over the classical sequence, against θ for various values of the ratio τ/T_1. It can be seen readily from this figure that the maxima of the curves become broader as the ratio τ/T_1 increases. Hence, for shifted nuclei where the τ/T_1 ratio is small the measured enhancement is very sensitive to the precise value of θ chosen. For example at $\tau/T_1 = 0.05$ the S/N ratio enhancement over the classical sequence falls from 54% at the Ernst angle to 13% at the Ernst angle minus 10° and to 40.4% at the Ernst angle plus 10°. When $\tau/T_1 = 0.5$, however, the enhancements over the classical sequence at the Ernst angle, the Ernst angle minus 10° and the Ernst angle plus 10° are 56%, 52% and 53% respectively. Hence when choosing a small nutation angle to specifically enhance the S/N ratio for a shifted nucleus with a long T_1 (ie τ/T_1 is small) the chosen value of θ is critical and the choice should err to larger values of θ rather than smaller ones. In cases where the required nutation angle would be exceptionally small it would probably be beneficial to increase the value of τ.

The above proposals have been confirmed practically using the ^1H noise decoupled ^{13}C resonance of air saturated benzene. The T_1 of the ^{13}C nucleus at 30°C was measured
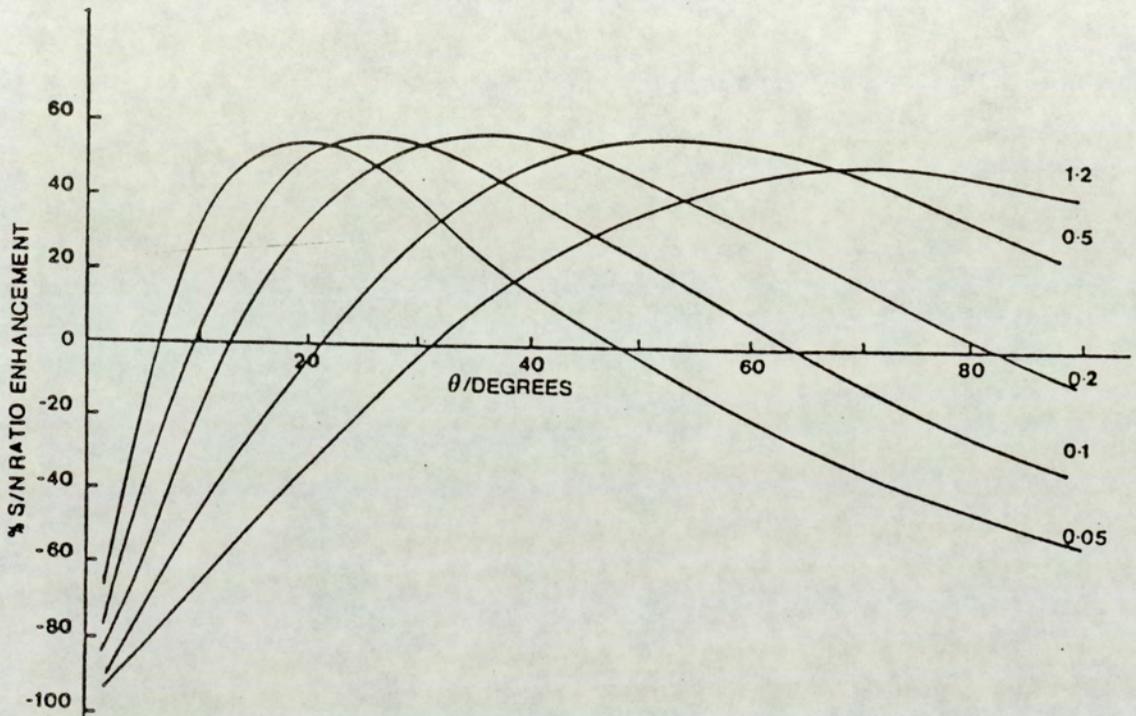
Fig. 6.2 <u>Variation in the S/N ratio enhancement, relative to the classical sequence, using rapid multipulsing against the nutation angle for various values of the parameter τ/T_1.</u>

using the DESPOT sequence with a τ value of 4.2 s and found to be 14.4 s. The S/N ratios were obtained from the following formula (131)

$$S/N = \frac{\text{Measured peak height}}{(\text{peak to peak noise})/2.5} \qquad (6.6)$$

and the results are presented in Table 6.1

Table 6.1

Comparison of Rapid Multipulsed and $(90°-5T_1)_n$ Spectral Analyses

Experiment	Expt. time /secs	S/N ratio	% Enhancement Expt.	Theoretical
$90°-5T_1$	3384	137:1	–	–
Ernst angle	3385	212:1	55	56
Ernst angle	1457	137:1	0	0
90° multipulsed	3385	141:1	3	4

$T_1 = 14.4$ s, $\tau = 4.2$ s in all multipulsed experiments

The results in Table 6.1 illustrate the validity of the above theoretical proposals. Rapid multipulsing is seen to be considerably more efficient than the classical sequence with the theoretical and practical enhancements being in close agreement. The proposal that rapid multipulsing could attain the same S/N ratio in 43% of the time required

classically is also apparent from the data in Table 6.1. The 90° multipulsed experiment is of some interest, it should be stressed that in the practical experiment the only condition that was changed from the experiments at the Ernst angle was the value of θ. In practice θ changed from 42° to 90°, which resulted in a dramatic fall in the measured S/N ratio. The theoretical enhancements can be predicted by interpolation between the plots of Figs 6.1 and 6.2. The 90° multipulsed condition used here is not the same as the 90° multipulsed condition used by Becker (130) where the τ/T_1 ratio is 1.2. If this condition is fulfilled then a 43% enhancement over the classical sequence is available in the same experimental time as can be seen from Fig. 6.2. Such a condition has found considerable use in setting up the conditions for polarization transfer experiments such as D.E.P.T (38). It should be noted that for a nutation angle of 90°, deviation from the ideal condition of $\tau=1.2T_1$ will result in a rapid fall in the expected S/N enhancement over the classical sequence (Table 6.1, Fig. 6.1).

6.4 Boltzmann Equilibrium Intensity Distortions

Integrated intensities are influenced by the values of τ, T_1 and θ in a particular experiment. This is possibly not a great disadvantage for ^{13}C spectra, when ^1H broadband decoupling is used, because the intensities are already distorted from their equilibrium values due to the nuclear Overhauser enhancement (Sec. 2.4.1). In ^1H spectroscopy, however, where many chemists rely on ^1H NMR integrations for

structural information, the systematic errors produced by rapid multipulsing could lead to errors in the spectral analysis. Fig. 6.3 shows the theoretical spectral intensity ratio of two shifted nuclei with differing τ/T_1 ratios plotted against the nutation angle. It can be seen that the true intensity ratio (unity) between the two absorptions cannot be expected unless the nutation angle is small. For example for a τ value of 4 s and two shifted nuclei with T_1's of 4 s and 10 s respectively the integration error at a nutation angle of 30° is 18% but this falls to 2% at a nutation angle of 10°. However, cross referencing with Fig. 6.1 shows that at a nutation angle of 10° for the above two specified shifted nuclei the classical sequence would be far more economical based on the $T_1 = 10$ s nucleus (for $\tau/T_1 = 0.4$, $\ln(\tau/T_1) = -0.92$, the S/N ratio multipulsed enhancement is -40%). At a nutation angle of 30°, however, for the same nucleus a 46% S/N ratio enhancement over the classical technique is observed but the 18% error in the relative intensities between the two shifted nuclei is unacceptably large for analytical applications. The case described above is obviously only pertinent to this specific example. In the general case, inspection of Fig. 6.3 in conjunction with with Fig. 6.1 will give an idea of the expected S/N ratio enhancements over the classical sequence along with the expected intensity ratio distortion. In cases where the T_1's in the sample are known to be relatively similar then a nutation angle of 30° with a τ value of 4 s will give a reasonable S/N enhancement and reasonably quantitative
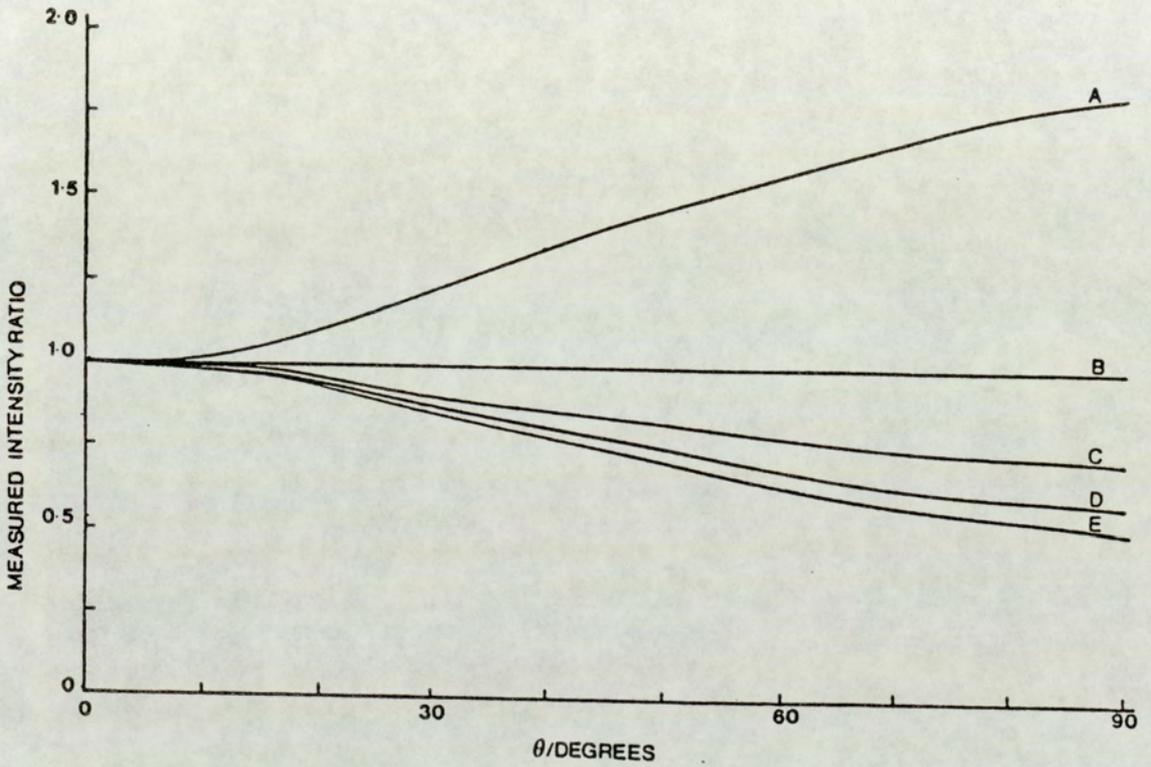
Fig. 6.3 <u>Variation in the observed intensity ratio for two resonances, 1 and 2, with nutation angle for $(\tau/T_1)_1=0.4$ with A) $(\tau/T_1)_2=0.2$; B) $(\tau/T_1)_2=0.4$; C) $(\tau/T_1)_2=0.6$; D) $(\tau/T_1)_2=0.8$ and E) $(\tau/T_1)_2=1.0$. True M_0 ratio=1.0. Non-acquisition pulses for each nutation angle are based on $\tau/T_1=0.4$.</u>

spectra. Obviously if the two absorptions have identical T_1's then the spectra should be obtained by multipulsing at the appropriate Ernst angle. In cases where accurate integrals are required for structural analysis it is probably prudent to use the classical sequence as accurate integrals are assured.

6.5 Rapid Multipulsing with Incomplete T_2^* Relaxation

As noted in Sec. 5.2 rapid multipulsing with incomplete T_2^* relaxation can modify the driven equilibrium intensity, I_{eq}, and the number of non-acquisition sequences required to fulfil condition 4.13. It was thought prudent therefore to assess the implications of incomplete T_2^* relaxation on rapid multipulsed spectra. It should be pointed out that spectra from samples submitted for analysis are in the main obtained by rapid multipulsing without the inclusion of a z-field gradient spoiling pulse immediately after F.I.D. acquisition. Spectra obtained in this way are likely to be affected by incomplete T_2^* relaxation.

Fig. 6.4 presents the variation in the S/N enhancement by rapid multipulsing over the classical sequence against $\ln (\tau/T_1)$ at a nutation angle of 30° for various values of the parameter τ/T_2^*. Inspection of the figure immediately reveals two points which require further discussion. Firstly, it can be seen that the maxima of the curves appear at more positive values of the parameter
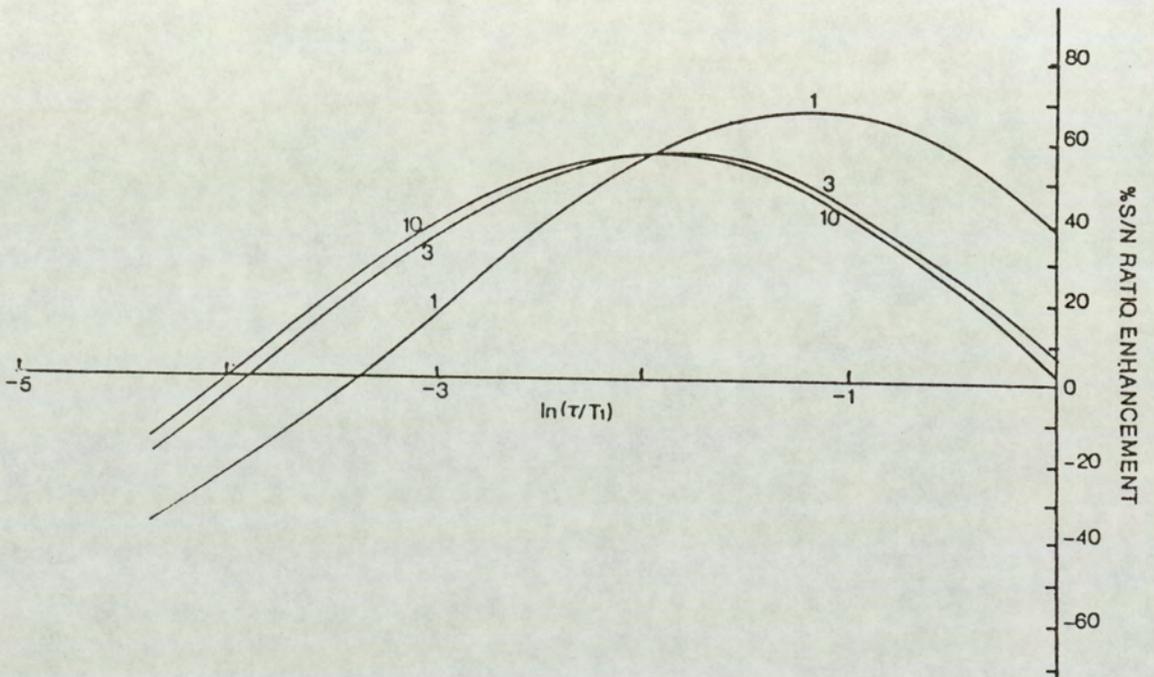
Fig. 6.4 <u>Variation in the S/N ratio enhancement using rapid
multipulsing, relative to the classical technique,
against ln (τ/T_1) for a nutation angle of 30° and
various values of the parameter τ/T_2^*.</u>

ln (τ/T_1), and consequently at higher values of the parameter τ/T_1, for a given nutation angle. This implies that the maxima of the curves no longer appear when the Ernst condition (Eqn. 4.9) is fulfilled. The maxima of such curves now appear when a modified Ernst condition is fulfilled which can be readily found by differentiation of Eqn. 5.1 with respect to θ (appendix 7) and can be expressed as

$$\cos \theta = \frac{\exp (-\tau/T_1) + \exp (-\tau/T_2{}^*)}{1 + \exp (-\tau/T_1) \exp (-\tau/T_2{}^*)} \qquad (6.7)$$

Inspection of Eqn. 6.7 shows that when the value of $\tau/T_2{}^*$ is greater than 5, Eqn. 6.7 reduces to Eqn. 4.9 which is the Ernst condition. This is apparent by noting that the curve representing a nutation angle of 30° on Fig. 6.1 and the curve representing a $\tau/T_2{}^*$ value of 10 on Fig. 6.4 are identical. As the value of $\tau/T_2{}^*$ falls the effect of incomplete $T_2{}^*$ relaxation becomes more noticeable and the maxima of the curves on Fig. 6.4 shift to larger values of the parameter τ/T_1. It can be seen from Fig. 6.4 that if the parameter $\tau/T_2{}^*$ is greater than 3 then the effect of incomplete $T_2{}^*$ relaxation on the multipulsed experiment becomes almost negligible.

Secondly, it can be seen from inspection of Fig. 6.4 that the maximum S/N ratio enhancement using rapid multipulsing with incomplete $T_2{}^*$ relaxation over the classical sequence is greater than 56% when the ratio $\tau/T_2{}^*$ falls below 3. The curve representing a $\tau/T_2{}^*$ ratio of 1 shows a 69% enhancement over the classical sequence at its

maximum represented by condition 6.7. It is noticeable from the figure that the enhancement at the Ernst angle condition $(\cos \theta = \exp(-\tau/T_1))$ is independent of the value of τ/T_2^* with the three curves intersecting at this point, yielding an enhancement of 56% over the classical sequence. The effect of incomplete T_2^* relaxation is similar to increasing the nutation angle (compare the curve for $\theta=30°$ and $\tau/T_2^* =1$ on Fig. 6.4 with the $\theta=45°$ curve on Fig.6.1) with the maximum enhancement occurring for a smaller value of T_1 for a given θ and τ. It should be emphasised, however, that the observed enhancement of 69% over the classical sequence at $\ln(\tau/T_1)=-1.16$ is greater than the enhancement that would have occurred, (56%) if rapid multipulsing with complete T_2^* relaxation had been carried out fulfilling the Ernst condition (Eqn. 4.9) for this τ/T_1 value. Hence, the effect of incomplete T_2^* relaxation is to provide a greater enhancement over the classical sequence than would be expected if T_2^* relaxation was complete for an absorption multipulsed at the Ernst angle on the short T_1 side of the Ernst condition. Similarly a smaller enhancement over the classical sequence than would be predicted if T_2^* relaxation was complete is noted on the long T_1 side of the Ernst condition. Consequently, incomplete T_2^* relaxation will adversely effect the S/N ratio of slowly relaxing nuclei which are more prone to incomplete T_2^* relaxation (Sec. 3.3.2). Hence, where a z-field gradient spoiling pulse is not included in rapid multipulsed experiments and $\tau \leq 3T_2^*$ it is prudent to multipulse at a smaller nutation angle than would be predicted from Fig. 6.1. For example for ^{13}C

acquisition with a τ/T_2^* ratio equal to one, multipulsing at a nutation angle of 20° gives a S/N ratio enhancement curve over the classical sequence similar to that obtained when multipulsing at a nutation angle of 30° when T_2^* relaxation is complete (Fig. 6.1).

6.6 Summary

In conclusion it is possibly worth summarising the conditions for rapid multipulsing discussed so far. For ^{13}C spectra a nutation angle of 30° and a pulse repetition time of 2 s will provide a good S/N ratio enhancement over the classical sequence across the usual ^{13}C T_1 range. In cases where a τ value of 2 s is impractical the nutation angle can be changed to ensure a reasonable enhancement across the usual ^{13}C T_1 range (Fig. 6.1). If a z-field gradient spoiling pulse is not applied and the τ value chosen causes the ratio τ/T_2^* to be less than 3 then it may be worth reducing the nutation angle slightly to ensure that slowly relaxing ^{13}C nuclei are subject to a reasonable S/N ratio enhancement over the classical sequence.

For ^1H spectroscopy the choice of the conditions $\theta=60°$ and $\tau=4$ s will provide a good S/N ratio enhancement across the proton T_1 range 2 to 10 s. In cases where the T_1 values are expected to be less than 4 s with τ still set at 4 s a good S/N ratio enhancement over the classical sequence will be achieved with a nutation angle of 70 to 80°. It must be stressed that the above conditions provide for optimum

S/N ratio and not for quantitative spectra. For truly quantitative proton spectra the classical sequence should be used. If a compromise is sought between a reasonable S/N enhancement over the classical sequence and a reasonably quantitative spectrum then the multipulsed conditions $\tau=4$ s and $\theta=30°$ are suitable. For rapid multipulsed spectra where τ/T_2^* is less than 3 the maximum S/N ratios wll be achieved with nutation angles slightly shorter than quoted above. In this case it may also be beneficial to reduce the nutation angle slightly if the conditions $\theta=30°$ and $\tau=4$ s are used as a compromise between S/N ratio enhancement and a quantitative spectrum.

6.7 Quantitative NMR Using Rapid Multipulsing

6.7.1 Introduction

It is apparent from the discussion in Sec. 6.4 that rapid multipulsed spectra are inherently non quantitative unless the nutation angle is very small or the T_1's of the absorptions in the spectrum are very similar. The use of small nutation angles to obtain quantitative rapid multipulsed spectra has been shown to be uneconomic in comparison with the classical sequence. In general one has to choose a trade off between S/N ratio enhancement over the classical sequence and the tolerable level of deviation from the expected Boltzmann equilibrium ratios in a rapid multipulsed spectrum: Hence the use of the conditions $\tau=4$ s and $\theta=30°$ in the routine acquisition of ^{1}H NMR spectra in

Sec. 6.4. Although rapid multipulsed spectra are inherently non quantitative, the actual degree of distortion from the Boltzmann equilibrium value is dependent on the parameters τ, T_1 and θ. In any rapid multipulsed spectra the parameters τ and θ are known hence the degree of Boltzmann equilibrium intensity distortion is dependent on the value of T_1. Consequently, if the value of T_1 for a given absorption is known then the true Boltzmann equilibrium intensity can be calculated.

6.7.2 <u>Theoretical</u>

Assuming for the moment that the value of $\tau > 5T_2^*$ in a rapid multipulsed spectrum then rapid multipulsing at two different nutation angles θ_1 and θ_2 for a constant number of acquisition sequences, m, will produce two spectra providing intensities showing deviations from the Boltzmann equilibrium. Provided that the magnetization is driven to its equilibrium value for each nutation angle then the T_1 of each absorption in the spectrum can be obtained by substitution of the relevant parameters into Eqn. 4.10. From this point it is obviously possible to obtain a value of M_0 for each absorption in the spectrum by substitution of the relevant parameters into Eqn. 6.8

$$M_0 = \frac{I_x \ (1 - \cos \theta_x \exp (-\tau/T_1))}{\sin \theta_x \ (1 - \exp(-\tau/T_1))} \tag{6.8}$$

where the subscript x denotes whether the intensity and

nutation angle data were taken from the spectrum obtained at
a nutation angle θ_1 or θ_2. The ratio of the M_0 values for
two particular absorptions in the spectrum will yield the
true Boltzmann equilibrium ratio between the two
absorptions. The same information can be obtained by
measuring the integration ratio R_1 between any two
absorptions 1 and 2 in the same spectrum. The Boltzmann
equilibrium ratio between the two absorptions can then be
given directly by substitution of the appropriate parameters
into Eqn. 6.9.

$$\frac{M_0(1)}{M_0(2)} = \frac{R_1 \ (1 - A \cos \theta_x) \ (1 - B)}{(1 - B \cos \theta_x) \ (1 - A)} \tag{6.9}$$

where $A = \exp(-\tau/T_1)$ for absorption (1), $B = \exp(-\tau/T_1)$
for absorption (2) and the subscript x denotes whether the
spectrum used to obtain the measurement of R_1 was that
obtained at the nutation angle θ_1 or θ_2.

It should be noted that the derivation of the
equations above does not take into account the effects of
incomplete T_2^* relaxation or off-resonance effects. As the
results are dependent upon ratioing the integrals of two
absorptions of often differing line widths and differing
chemical shifts, the accuracy of the results may well be
significantly improved by rederiving the equations taking
Secs. 5.2 and 5.3 into account.

The above proposals can obviously only account for
spectral intensity distortions caused by saturation due to

rapid multipulsing. Equilibrium magnetization distortions can also arise from other sources, the most common of these being the nuclear Overhauser enhancement in proton decoupled heteronuclear NMR spectroscopy. In such cases, if the actual unperturbed M_0 ratios in the molecule are all ready known then the deviation from these ideal ratios after correction using Eqn's 6.7 or 6.8 will be due to the nuclear Overhauser enhancement only. Owing to the nature of the equations it is not possible to directly derive the actual η values, only the ratio $(1+\eta_1)/(1+\eta_2)$ can be evaluated. In the case of $\{^1H\}-^{13}C$ spectroscopy (65) it is often possible to approximate the actual η values by assuming that the largest $1+\eta$ value measured corresponds with the maximum nuclear Overhauser enhancement of approximately 2.

The above theory was tested using the ^1H and $\{^1H\}-^{13}C$ spectra of ethyl and methyl benzene. The ^1H results for methyl benzene are presented in Table 6.2 with the corresponding results for ethyl benzene presented in Table 6.3. Tables 6.4 and 6.5 contain the corresponding $\{^1H\}-^{13}C$ results. The expected intensity ratio results presented in Tables 6.4 and 6.5 were obtained by measuring the values of η using the Harris-Newman approach (132) and correspond to the intensity ratio between the two specified absorptions that would be observed in a spectrum where the nuclei giving rise to the absorptions had identical values of T_1.

Table 6.2

^{1}H Results for Methyl Benzene

Absorptions Ratioed	R_1 at 12°	R_1 at 58°	Calc. M_0 Ratio	Expected M_0 Ratio
Ar-CH$_3$	1.653	1.562	1.659	1.666

Spin-lattice relaxation times, from a two point analysis of the data, were calculated to be 2.9 s for the aromatic protons and 2.54 s for the methyl protons

Table 6.3

^{1}H Results for Ethyl Benzene

Absorptions Ratioed	R_1 at 18°	R_1 at 71°	Calc. M_0 Ratio	Expected M_0 Ratio
Ar-CH$_3$	2.621	2.400	2.552	2.500
Ar-CH$_2$	1.720	1.479	1.683	1.666
CH$_2$-CH$_3$	0.656	0.616	0.659	0.666

Spin-lattice relaxation times, from a two point analysis of the data, were calculated to be 3.9 s for the aromatic protons, 4.6 s for the methylene protons and 4.5 s for the methyl protons.

Table 6.4

^{13}C Results Methyl Benzene
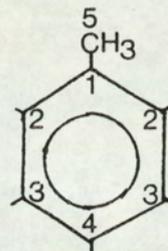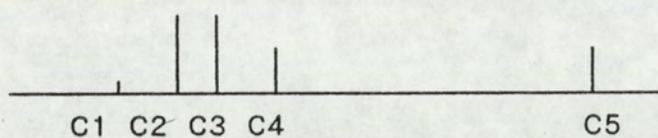
Absorptions Ratioed	R_1 at 13°	R_1 at 64°	Calc. Int Ratio	Expected Int Ratio*
C1-C2	0.204	0.116	0.217	0.278
C1-C3	0.229	0.122	0.244	0.278
C1-C4	0.475	0.227	0.511	0.543
C1-C5	0.648	0.324	0.694	0.854
C2-C3	1.119	1.051	1.124	1.000
C2-C4	2.325	1.958	2.353	1.951
C2-C5	3.171	2.798	3.200	3.069
C3-C4	2.078	1.863	2.094	1.951
C3-C5	2.835	2.662	2.848	3.069
C4-C5	1.364	1.429	1.360	1.573

T_1 and nOe* Measurements pertinent to the above data

Absorption	T_1/s	nOe*	Absorption	T_1/s	nOe*
C1	25.0	0.341	C4	6.5	1.470
C2	9.6	1.409	C5	7.3	0.570
C3	8.4	1.409			

* data derived from a Harris-Newman Experiment (132)

Table 6.5

^{13}C Results Ethyl Benzene
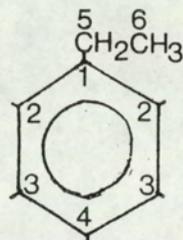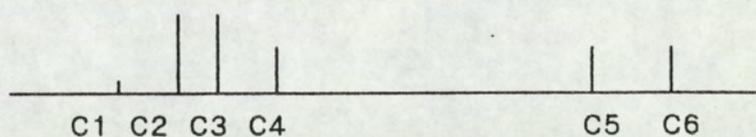
Absorptions Ratioed	R_1 at 15°	R_1 at 80°	Calc. int Ratio	Expected int Ratio*
C1-C2	0.309	0.105	0.417	0.356
C1-C3	0.310	0.103	0.418	0.344
C1-C4	0.623	0.158	0.867	0.664
C1-C5	0.581	0.196	0.784	0.669
C1-C6	0.567	0.136	0.793	0.628
C2-C3	1.002	0.985	1.004	0.964
C2-C4	2.015	1.512	2.081	1.861
C2-C5	1.880	1.867	1.882	1.874
C2-C6	1.833	1.298	1.904	1.762
C3-C4	2.011	1.535	2.073	1.930
C3-C5	1.877	1.895	1.875	1.944
C3-C6	1.830	1.317	1.897	1.826
C4-C5	0.933	1.235	0.904	1.007
C4-C6	0.910	0.858	0.915	0.946
C5-C6	0.975	0.695	1.011	0.939

T_1 and nOe* Measurements pertinent to the data above

Absorption	T_1/s	nOe*	Absorption	T_1/s	nOe*
C1	66.6	0.880	C4	9.6	1.830
C2	14.4	1.634	C5	14.7	1.810
C3	14.1	1.731	C6	8.8	1.990

6.7.3 Aspects of Quantitative Multipulsed Analysis

Inspection of the ^1H data in Tables 6.2 and 6.3 shows the validity of the above approach. The calculated and expected ratios for both ethyl and methyl benzene show good agreement. It should also be noted that the experimental results verify the theoretical predictions made in Sec. 6.4 and Fig. 6.3. Boltzmann equilibrium intensity distortions are shown to be increased with increasing nutation angle. It can be seen clearly by inspection of the data in Tables 6.2 and 6.3 that significant Boltzmann equilibrium intensity distortions can occur at long nutation angles even when the T_1's of the two specified absorptions are quite similar. Such distortion could easily lead to an incorrect spectral analysis. The ^{13}C data in Tables 6.4 and 6.5 show that the equilibrium intensity distortions at long nutation angles can be quite dramatic when there is a significant difference in the T_1's of the two specified absorptions e.g. the C1-C2 absorptions in Table 6.5. In cases where the T_1's are essentially similar (C2-C3 absorptions, Table 6.5), there is very little change in the measured ratio with change in nutation angle. Comparison of the calculated and expected (Harris-Newman derived) intensity data show reasonable, but not exact agreement. Obviously the comparison is between two experimental pieces of data and consequently both pieces of experimental data will have an error associated with them. The Jeol FX 90Q spectrometer used to obtain the results was not equipped to obtain the spectrum of the same sample under two different sets of conditions with the conditions being

changed after each successive acquisition sequence and the resulting FID's being stored separately as is required for the accurate implementation of the Harris-Newman technique (132). Consequently the calculated values of η were subject to a larger error than would have normally been the case. At the time the experiments were carried out the maximum pulse delay time available from the pulse programmer was 409 s, this is insufficient to allow a $10T_1$ wait during the gated decoupling part of the experiment (133). Consequently the value of η obtained for the ipso carbon of ethyl benzene is likely to be slightly low (132,134). Inspection of the results in Table 6.5 show that the expected ratios containing the ipso carbon of ethyl benzene do show slightly smaller values than the calculated values. The equations used to obtain the calculated results were based on the assumption that T_2^* relaxation was complete and that there were no off-resonance effects. Such an assumption is likely to be valid for the ^1H data but is possibly not justified in the case of the ^{13}C data.

For the case of ethyl benzene it is instructive to assume that the largest calculated value of $1+\eta$ corresponds to a η value of 1.998 (maximum nOe for $\{^1H\}-^{13}C$). With the knowledge of the true ratios of the numbers of carbon nuclei giving rise to each pair of absorptions in the NMR spectrum it is possible to calculate η values for the other absorptions in the spectrum. The results are presented in Table 6.6, based on the C5 absorption giving the maximum nOe.

Table 6.6

Comparison of Calculated η Values from Multipulsed Sequence
and the Harris-Newman Experiment Assuming η=1.998 for C5

Absorption	Multipulsed η	Harris-Newman η
C1	1.350	0.880
C2	1.821	1.634
C3	1.813	1.731
C4	1.710	1.830
C5	1.998	1.810
C6	1.966	1.990

The results obtained in this way yield η values that are
comparable with those from the Harris-Newman experiment for
carbons 2 to 6. The differences observed are possibly due to
the error associated with making the measurements in both
the Harris-Newman technique and the multipulsed technique.
The data is good enough, however, to give an indication of
the magnitude of η for a given absorption within ±0.2. It is
noticeable that the predicted order of increasing η is not
the same between the two techniques. This discrepancy may
once again be attributable to the small difference in the
measured value of η over the C2 to C6 range compared with
the predicted error in the value of η obtained from the
experiment. The measured η values for C1 are vastly
different. This difference is thought to be due in part to
the fact that it was not possible to wait $10T_1$'s in the
measurement of η for C1 using the Harris-Newman technique.

The results as presented, although not presenting a method for obtaining η values sufficiently accurately do indicate in both the methyl and ethyl benzene analysis that the ipso carbons are relaxed to a considerable extent by a mechanism other than dipole-dipole; probably in this case a spin-rotation interaction. The CH_3 group in toluene using the multipulsed technique is shown to have a low value of η and is therefore shown to have a large spin-rotation contribution to its relaxation mechanism. The low value of η is confirmed by the Harris-Newman approach.

So far the fact has been ignored that the T_1's have also been obtained from the data. In the proton spectra the T_1's are very similar as would be expected for predominantly dipole-dipole relaxation in the samples chosen. The similarity in the T_1's measured, however, serves to emphasise the fact that considerable Boltzmann equilibrium intensity distortion can occur even when the T_1's of the two specified absorptions are similar (Tables 6.2 and 6.3). The ^{13}C T_1 data are as would be expected for the samples chosen. The ipso carbons in both methyl benzene and ethyl benzene show considerably longer T_1's than the other carbons in the sample due to the inefficient relaxation field at the ipso site. The ring carbons C2 and C3 show similar T_1's whereas the C4 carbons show shorter T_1's indicative of preferential tumbling about the C2 axis of symmetry (Sec. 2.5.1.2). The C5 carbon in toluene has a shorter T_1 than the ring protons as would be expected due to the increase in the number of protons attached to it. The fact that the decrease is not by

a factor of three is indicative of the fact that the $\tau_{c\,eff}$ value for the CH_3 group is lower than that for the ring protons. From the nOe data it should also be remembered that there is a significant spin-rotation contribution to the relaxation rate. The C5 and C6 carbons in ethyl benzene are shown to have a lower $\tau_{c\,eff}$ value than the ring protons and the side chain is shown to tumble isotropically as the T_1 values of the C5 and C6 carbons are in the ratio 3:2 which is inversely proportional to the numbers of attached protons. For this to occur both carbons must be primarily relaxed by the dipole-dipole relaxation mechanism, this is confirmed by the size and similarity of their η values.

The above discussion has shown that rapid multipulsing need not be inherently non quantitative and that by the use of the above new technique useful T_1 information can be gained from a spectrum as well. For ^1H decoupled heteronuclear spectra the use of two rapid multipulsed spectra has also given some information on the relative sizes of the nOe's in the spectrum. At this point it seems worthwhile to assess the time saving implications of using two multipulsed spectra for the approach proposed above. It was shown in Sec 6.2.1. that by rapid multipulsing at the Ernst angle a given spectral S/N ratio could be obtained in 43% of the time that would be required classically. Consequently two multipulsed spectra of a given S/N ratio could be obtained in approximately the same time as it would take to obtain one classical spectrum provided that the chosen nutation angles are close to the Ernst

condition. In practice, however, in order to attain the required accuracy in the T_1 determination it is necessary to use two nutation angles that are quite different. Inspection of the experimental results shows that a reasonable choice for the two nutation angles is approximately 20° and 70°. Such a choice, however, is quite arbitrary, the main criteria are that the angles should be quite well separated, usually by greater than 30°, and that at the two nutation angles chosen the value of $dI/d\theta$ should be quite small. Obviously to fulfil these criterion for absorptions of differing T_1's in a spectrum will be a matter of compromise. In fulfilling these criteria it is likely that two multipulsed spectra at the same S/N ratio will take longer to attain than one classical spectrum. It should also be noted that it is erroneous to talk of two multipulsed spectra at the same S/N ratio as a classical spectrum. The important point is that two multipulsed spectra at different nutation angles must be obtained with a S/N ratio which is large enough to provide accurate integral ratios. These spectra should be obtained with the same number of acquisition sequences after being previously driven to equilibrium.

It should be noted that although two multipulsed spectra will probably take slightly longer to obtain than one classical spectrum, the multipulsed technique will provide T_1 information as well. Hence the real time comparison should be made between the time it would take to obtain two multipulsed spectra at differing nutation angles

and two classical 180°-τ-90° sequences at different τ
values. It is difficult to make a direct S/N ratio
comparison between the spectra as the τ values require a
reasonable separation to provide accurate data. The data in
Table 6.7 are based on the time it would take to obtain the
spectrum of an absorption for a nucleus with $T_1 = 25$ s
classically, via two multipulsed spectra at nutation angles
of 30° and 64° with a τ value of 6 s, and by two 180°-τ-90°
sequences of differing τ values. The chosen τ values are
$0.5T_1$ and T_1 which provide a representative range. The
time it takes to obtain the spectra at a nutation angle of
64° and a τ value of $0.5T_1$ were chosen so that the S/N
ratio resulting from these spectra was equal to that
obtained from the classical sequence. Obviously the data
given in Table 6.7 are somewhat arbitrary but they do
provide some idea of the time savings which are available by
the use of rapid multipulsing.

Table 6.7

Comparison of Experimental Times for Classical, Multipulsed
and 180°τ-90° Spectral Acquisitions

	S/N ratio	Time/s
Classical	120:1	1875
Multipulsed 30°	137:1	1194
Multipulsed 64°	120:1	1158
180°-τ-90° τ=$0.5T_1$	120:1	44125
180°-τ-90° τ=T_1	149:1	44125

The above data were calculated using the parameters described in the above text together with $M_0 = 30$ and assuming 16 classical acquisitions. The times for the multipulsed experiments differ due to the differing numbers of non-acquisition sequences required to drive the system to equilibrium.

The data in Table 6.7 show that under these conditions, two multipulsed spectra can be obtained in approximately 25% more time than it takes to obtain one classical ($90°-5T_1$) spectrum. Although the time required is slightly longer the extra T_1 information available in the given time may be deemed worthwhile. It is of interest to note that the T_1 and M_0 information is gained from two multipulsed spectra in 2.7% of the time required to gain the same information by the use of two $180°-\tau-90°$ spectra at $\tau=0.5T_1$ and $\tau=T_1$. Obviously the above figures are only pertinent to the conditions described in the text. The time required for the $180°-\tau-90°$ sequence could be reduced by using a τ value less than $0.5T_1$ and a τ value greater than T_1. Similarly the times required for the multipulsed sequence could be reduced by using two angles closer to the Ernst condition. The data used to construct Table 6.7 were based on the ipso carbon of methyl benzene in Table 6.4. It should be noted that by using a nutation angle of 13°, the experimental time required to obtain a S/N ratio of 120:1 is 2352 s. This emphasises the need for care in choosing the parameters if the experimental time is going to be comparable with that of a single classical sequence. It

should also be noted, however, that even with the two nutation angles used in Table 6.4 the total experimental time is only 5.3% of the time required for two $180°-\tau-90°$ sequences with $\tau=0.5T_1$ and $\tau=T_1$.

CHAPTER 7

MEASUREMENT OF $T_{1\rho}$

7.1 <u>Introduction</u>

The discussion in Sec. 2.3 and Fig. 2.2 show that T_1 falls as τ_c increases only so long as the extreme narrowing condition is fulfilled. Outside the extreme narrowing condition T_1 must be predicted from Eqn 2.10 which predicts a minimum value for T_1 which is dependent on the spectrometer operating frequency. Consequently, where molecules have long correlation times or the exchange rate between two sites is less than γB_0 (Sec. 2.6.1), T_1 data cannot be used readily to obtain correlation times and exchange rates. Fig. 2.2, however, shows that the parameters T_2 and $T_{1\rho}$ effectively extend the extreme narrowing condition and consequently are of use in studies of large molecules and intermediate exchange rates. The extension of the extreme narrowing range in the measurement of $T_{1\rho}$ is sufficient to make $T_{1\rho}$ and T_2 equal for the values of τ_c encountered in liquid samples. The measurement of both parameters can be time consuming due to the fact that thermal equilibrium is required to be re-established between repetitive pulse sequences. This combined with other experimental difficulties associated with the measurements has meant that the applications of $T_{1\rho}$ and T_2 in solving chemical problems have been severely limited. This chapter is concerned with the application of a rapid multipulsed technique to the measurement of $T_{1\rho}$ and it is hoped that with further development this technique will enable $T_{1\rho}$ measurements to be exploited more widely in chemical analysis.

7.2 The Measurement of T_2

Although the main aim of this chapter is not to apply rapid multipulsing to the measurement of T_2, it is beneficial to look at the measurement of T_2. The spin-lock technique used to measure $T_{1\rho}$ is really a limiting case of the Carr-Purcell technique for the measurement of T_2. Consequently, a full understanding of the principles behind the measurement of T_2 and the practical difficulties associated with this measurement enable a better understanding of the principles and problems associated with the measurement of $T_{1\rho}$.

Following a θ pulse the transverse component of the magnetization decays with a time constant T_2^* (Sec. 3.3.2). The time constant T_2^* is made up of two contributions and is given by

$$\frac{1}{T_2^*} = \frac{1}{T_2} + \frac{1}{T_{inhom}} \tag{7.1}$$

where T_{inhom} is the decay in the transverse magnetization component due to the inhomogeneity of the applied field. The Carr-Purcell technique for the measurement of T_2 (112) relies on the fact that the inhomogeneity contribution to the decay is reversible. Such a decay occurs because nuclei in the sample experience slightly different B_0 fields due to the inhomogeneity in the applied field. Consequently, the nuclei precess about the average value of the applied field

at different rates and thus the transverse component of the magnetization starts to "smear" itself out in the xy plane. Some components travel faster and some slower than the average precessional rate. T_2 is measured by applying a 90°(x) pulse followed by an evolution time τ during which the transverse component of the magnetization decays with a time constant T_2^* (i.e due to both T_2 and T_{inhom}). At the time τ the transverse component of the magnetization is subjected to a 180°(x) pulse, which effectively causes the magnetization components travelling faster than the average precessional rate to be behind the magnetization components travelling slower than the average precessional rate in the rotating frame of reference. Consequently, after a further time, τ, provided that no nuclei diffuse to regions of different applied field, the smearing out of the transverse magnetization in the xy plane will be reversed. Hence at a time 2τ the transverse magnetization component will be refocussed along the -y axis and its decay will only be a function of T_2.

T_2 is usually measured using a slight modification of the above technique proposed by Meiboom and Gill (135). In the modified experiment the 180° refocussing pulses are applied along the y axis. There are two beneficial effects, the first is that the measured echoes are all positive (i.e. occur along +y axis) and the second is that the modification compensates for any cumulative errors which may build up due to the mis-setting of flip angles or inhomogeneity in the radio frequency field (135, 136). A similar compensation is

possible by alternating the phase of the refocussing pulses along the ±x directions in the rotating frame (137). Owing to the possibility of diffusion of nuclei to regions of varying B_0 it is essential that the period τ is kept as short as possible, hence, τ is usually set around 50 ms. As T_2 values in liquid samples often have values in the seconds region, many sequence repetitions are required before the transverse magnetization decays to a measurable extent via T_2 relaxation. T_2 values are measured in practice by using differing numbers of refocussing pulses to give different overall relaxation times, t. The values of t chosen usually cover the range $0.3T_2$ to $1.2T_2$. Fourier transformation of the resulting half echo after the time, t, gives the partially relaxed high resolution spectrum. Integration measurements on the absorptions in a series of such spectra obtained at different t values can then be used to obtain a value of T_2 via a linear regressional plot on Eqn. 7.2

$$\ln I(t) = (-t/T_2) + \ln I_0 \qquad (7.2)$$

where $I(t)$ is the measured intensity at time (t) and I_0 is the measured intensity when t=0.

7.2.1. J Coupling in spin-echo formation

There is one serious drawback to the Carr-Purcell-Meiboom-Gill (C.P.M.G) sequence for the measurement of T_2 and this occurs when the shifted nucleus under consideration is J coupled to another nucleus.

Consider the A nucleus of a homonuclear AX system where the coupling constant J_{AX} has the value z Hz. After the initial 90° pulse the two components of the A doublet will precess in the rotating frame at $\nu_a \pm z/2$ Hz and the magnetization due to both components of the doublet will "smear" out in the xy plane due to static field inhomogeneities. When the refocussing pulse is applied, however, it will effect the X spins as well as the A spins. As a result of this the component of the A doublet rotating at $\nu_a + z/2$ Hz prior to the 180° refocussing pulse will rotate at $\nu_a - z/2$ Hz afterwards. This component, however, will now be behind the component rotating at $\nu_a + z/2$ Hz and, therefore, after the refocussing pulse the two components of the A doublet will continue to diverge. Even though the smearing out of the magnetization in each component of the doublet due to static field inhomogeneities will be refocussed at the time 2τ the doublet itself will not refocus along the y axis of the rotating frame. Obviously as many thousands of refocussing pulses are often required and where more than two groups are often spin-coupled together, echo modulation can become quite complex causing difficulties in the determination of individual spin-spin relaxation times (138). This problem can be circumvented to some extent by viewing the power spectrum (136,139) or by the use of selective pulses (140), neither method, however, provides a perfect solution.

7.2.2 ^{13}C T_2 Measurements with Noise Decoupling

There is a further complication to the measurement

of ^{13}C T_2's using the C.P.M.G sequence when ^{1}H noise decoupling is used. In Sec. 2.4.5 it was shown that ^{13}C T_2 measurements were affected by the power of the decoupling field. In cases where the power of the decoupling field is insufficient to fully decouple the protons from ^{13}C the resulting ^{13}C absorptions are broad. The residual randomly modulated coupling inhibits the refocussing process essential to spin-echo formation (124). This problem can, however, be circumvented by higher decoupling powers at the expense of potential heating of the sample. Rotating frame resonance effects can also occur when the Hartmann-Hahn condition (141) of Eqn. 7.3 is fulfilled.

$$\gamma_C B_1 / 2\pi = \gamma_H B_2 / 2\pi \qquad\qquad (7.3)$$

The effect of this is to provide a mechanism for energy to be exchanged between the two spin reservoirs with the saturated protons heating (over populating the higher energy state) the ^{13}C spins via the spin-spin coupling between the nuclei. Consequently the measured spin-spin relaxation times are very low. With incoherent (noise) decoupling, even when condition 7.3 is not fufilled the exchange of energy beyween the two spin systems cannot be avoided. Consequently during echo formation noise decoupling must be not be used. In order to maintain the steady state nOe the decoupler is switched to coherent mode and only switched to incoherent mode when the FID is sampled (136).

7.3 The Spin-Lock Experiment

From the discussion in Sec. 7.2 it is obvious that
the time τ must be kept short to eliminate diffusion
effects. It is interesting to note that as τ decreases so do
the phase differences in spin-echo spectra of J-coupled
systems (Sec. 7.2.1). In the limit, therefore, the time τ
can approach zero and the Carr Purcell sequence then bears a
close resemblance to the spin-locking experiment. In such an
experiment the transverse component of the magnetization is
held along the y axis of the rotating frame by a B_1 field
applied along this y axis for a certain time, t (142,143).
From the discussion relating to the rotating frame in Sec.
1.6.2 it is apparent that an on-resonance magnetization
component, M, will be rotated onto the y' axis of the
rotating frame by a 90°(x') pulse. If the B_1 field is now
applied along the y' axis the on-resonance magnetization
component will be "locked" along this axis with the
individual nuclear moments precessing around the y' axis at
a rate γB_1 as $B_{eff}=B_1$ for an on-resonance component. The B_1
field is much smaller than the B_0 field and consequently
cannot sustain a magnetization component which is
proportional to the size of the B_0 field (Sec. 1.4). Hence
the magnetization component "locked" along the y' axis will
decay to a value B_1M/B_0 with a characteristic time which is
known as the spin-lattice relaxation time in the rotating
frame ($T_1{}_\rho$). In practice the ratio B_1/B_0 is virtually zero
and hence the decay may be written as

$$M_\tau = M_0 \exp(-\tau/T_1\rho) \tag{7.4}$$

where τ is the time for which the locking field is applied. Consequently, spectra obtained by fourier transformation after varying locking times, τ (0.3 to $1.2T_1\rho$), yield partially relaxed spectra from which $T_1\rho$ can be obtained. $T_1\rho$ values obtained using the spin-lock method have been used to solve a variety of chemical problems (70,87-89).

7.4 Problems Associated with Spin-Locking

7.4.1 Off-Resonance Effects

From the above discussion it is apparent that the magnetization vector will only be effectively locked on the y-axis after an exact on-resonance 90° pulse. Inexact on-resonance 90° pulses will produce a ±z magnetization component. The only effect of mis-setting the 90° pulse will be a slight loss of S/N in the final fourier transformed spectrum which will not unduly effect the results obtained. It is essential, however, to wait somewhere in the region of $5T_1$'s to ensure that the nucleus is fully relaxed between repetitive pulse sequences in order to obtain accurate results.

Off-resonance effects have a more serious effect on the experimentally derived values of $T_1\rho$. When a magnetization component ν Hz from resonance is subjected to

a 90°(x) pulse its final position will not lie along the y' axis of the rotating frame but rather in a direction given by Eqns 5.7 and 5.8. When the phase shift occurs placing the B_1 field along the y' axis, B_{eff} will not lie along this axis but rather at an angle θ to the y' axis in the zy' plane. The component of the magnetization parallel to B_{eff} will be locked along the direction of B_{eff} but will decay via $T_{1\rho}$ and T_1 relaxation. Measurements of $T_{1\rho}$ based on Eqn. 7.2, show that the measured values of $T_{1\rho}$ are lower than the actual $T_{1\rho}$ for absorptions with resonance frequency higher than the carrier frequency and vice-versa, with the true $T_{1\rho}$ value only being observed for on-resonance magnetization components (88). Ohuchi et al. (88) have shown that the error in the measurement of $T_{1\rho}$ is less than ±5% provided that the angle $1/\phi = \tan^{-1}(B_1/\Delta B)$ (Eqn. 5.4) is within ±15% of the on-resonance condition ($\phi=0$). The definitions of ΔB, ϕ, and B_1 are identical to those used in Sec. 5.3 except that B_1 is now applied along the y'axis. For a 1 KHz spectral width with quadrature detection the above condition is satisfied provided that a 90° pulse on the B_1 locking field is no longer than 128 μs. For locking fields that do not fulfil this criterion the spectral width must be reduced. An equation to correct for off-resonance effects in the determination of $T_{1\rho}$ using the spin-locking technique has been proposed by Leipert et al.(144).

7.4.2 <u>J Coupling and Decoupling with Spin-Locking</u>

Homonuclear J coupling is not a problem in the

determination of $T_{1\rho}$ using the spin-lock technique. As was noted in Sec. 7.2.1, as the time, τ, during a spin-echo sequence falls so does the phase distortion in the final signal due to J coupling. The spin-lock technique essentially represents a spin-echo experiment with $\tau=0$. Wells and Guttowsky (145) have shown both practically and theoretically that there is no modulation of the signal due to J coupling in the spin-locking experiment.

The effects of Hartmann-Hahn matching must be carefully avoided in the measurement of heteronuclear $T_{1\rho}$'s using the spin-locking technique with ^1H decoupling (Sec. 7.2.2). This condition is possibly best avoided by measuring the field strength of the ^1H decoupler by the use of the D.E.P.T sequence (38). Noise decoupling is not permissible during spin-locking, and so for the same reasons as detailed in Sec. 7.2.2., it is necessary to switch the decoupler to coherent mode whilst spin-locking occurs. Freeman et al. (70) obtained good $T_{1\rho}$ values for the $\{^1H\}-^{13}C$ spectrum of ortho-dichlorobenzene using this decoupler switching technique. One of the principal disadvantages of the spin-locking technique is that the locking field must be strong enough to effectively cover the chemical shift range of the absorptions being studied and minimise off-resonance effects but must also be sufficiently weak so as to prevent sample heating during the locking pulse. In the case of very long $T_{1\rho}$ values, where long locking pulses are required, such conditions may be difficult to achieve. In such cases it is possibly advantageous to measure T_2 using the C.P.M.G

sequence with very small τ values.

7.5 Rapid Multipulsed $T_1\rho$ Measurements

7.5.1 Introduction

The use of DESPOT sequence for T_1 determination in Sec. 4.3.3. was shown to provide a considerable time saving over the other well established methods for measuring T_1. The increased efficiency of the DESPOT technique stems from driving the magnetization to an equilibrium position dependent on nutation angle and τ/T_1. The consequence of this is to alleviate the need for long intersequence delays required by the other T_1 measurement techniques, and thus popularize the use of routine T_1 measurements in NMR analysis (Chap 4). Similar reasoning can be applied to the measurement of $T_1\rho$ using the spin-locking technique. The classical spin-lock experiment depends only on $T_1\rho$ provided that a sufficient relaxation time ($5T_1$'s) is left between pulse sequences, whereas any driven equilibrium analogue would necessarily depend on T_1 also. The pulse sequence presented below, however, does not require an independent measurement of T_1 to be carried out as both T_1 and $T_1\rho$ can be obtained from one set of experimental data provided that an independent measure of M_0 is available.

7.5.2. Theoretical

It is obviously not possible to rapid multipulse a

spin system at an angle θ and just apply a spin-locking pulse prior to acquisition as any z magnetization present will rotate about the B_1 locking field in the zx' plane. Hence during the spin-locking pulse it is necessary that the magnetization component present must lie solely along the y' axis. In order to make the magnitude of the locked magnetization vector dependent upon θ it is necessary to pre-condition a z-magnetization vector and then apply a $90°(x)$ pulse to place that vector along the y' axis of the rotating frame. In our experiments this was achieved using the pulse sequence presented as Fig 7.1.

Analysis of the evolution of the magnetization component during the above pulse sequence yields an expression for the measured intensity, I_y, (See Fig. 7.1) as

$$I_y = KM_0 \cos \theta (1 - E1) \, E1 \, E1\rho + KM_0 (1 - E1) \, E1\rho \qquad (7.5)$$

where $E1 = \exp(-T/T_1)$, $E1\rho = \exp(-\tau/T_1\rho)$ and K is an instrumental proportionality constant. Inspection of Eqn. 7.5 shows that a plot of I_y against $\cos \theta$ will yield a linear plot of gradient $KM_0 (1 - E1) \, E1 \, E1\rho$ and an intercept of $KM_0 (1 - E1) \, E1\rho$. It is apparent, therefore, that the ratio of the gradient and the intercept will yield a value for $\exp(-T/T_1)$ and hence a value for T_1. Now, providing that an independent measure of the value of M_0 is available, a value of $T_1\rho$ can be determined from either the slope or the intercept of the straight line plot.

z

$M_z = M_z$
$I_y = 0$

——————(1)
y'

$\downarrow$ 90°(x)

z

$M_z = 0$
$I_y = KM_z$

——————(2)
y'

$\downarrow$ HS

z

$M_z = 0$ if pulses so far are
$I_y = 0$ perfect

——————(3)
y'

$\downarrow$ 90°(x)

z

$M_z = 0$
$I_y = 0$

——————(4)
y'

$\downarrow$ HS

z

$M_z = 0$ steps 4 and 5 should
$I_y = 0$ effectively remove any
           residual magnetization
           components

——————(5)
y'

$\downarrow$ T

z

$M_z = M_0(1-E1)$
$I_y = 0$

——————(6)
y'

$\downarrow$ to (7)

Fig 7.1 DESPOT T₁ Pulse Sequence (Steps 1 to 6)

From (6)

$M_z = M_0(1-E1)\cos\theta$
$I_y = KM_0(1-E1)\sin\theta$

$\theta°(x)$

z

θ

————————— (7)

y'

HS

$M_z = M_0(1-E1)\cos\theta$
$I_y = 0$

z

————————— (8)

y'

T

$M_z = M_0(1-E1) + M_0(1-E1)E1\cos\theta$
$I_y = 0$

z

————————— (9)

y'

$90°(x)$

$M_z = 0$
$I_y = KM_0(1-E1) + M_0(1-E1)E1\cos\theta$

z

————————→ (10)

y'

locking pulse τ

$M_z = 0$
$I_y = KM_0(1-E1)E1\rho + M_0(1-E1)E1E1\rho\cos\theta$

z

———→———— (11)

y'

acquire
HS

$M_z = M_z$
$I_y = 0$

z

————————— (12)

y'

→ To step (1)
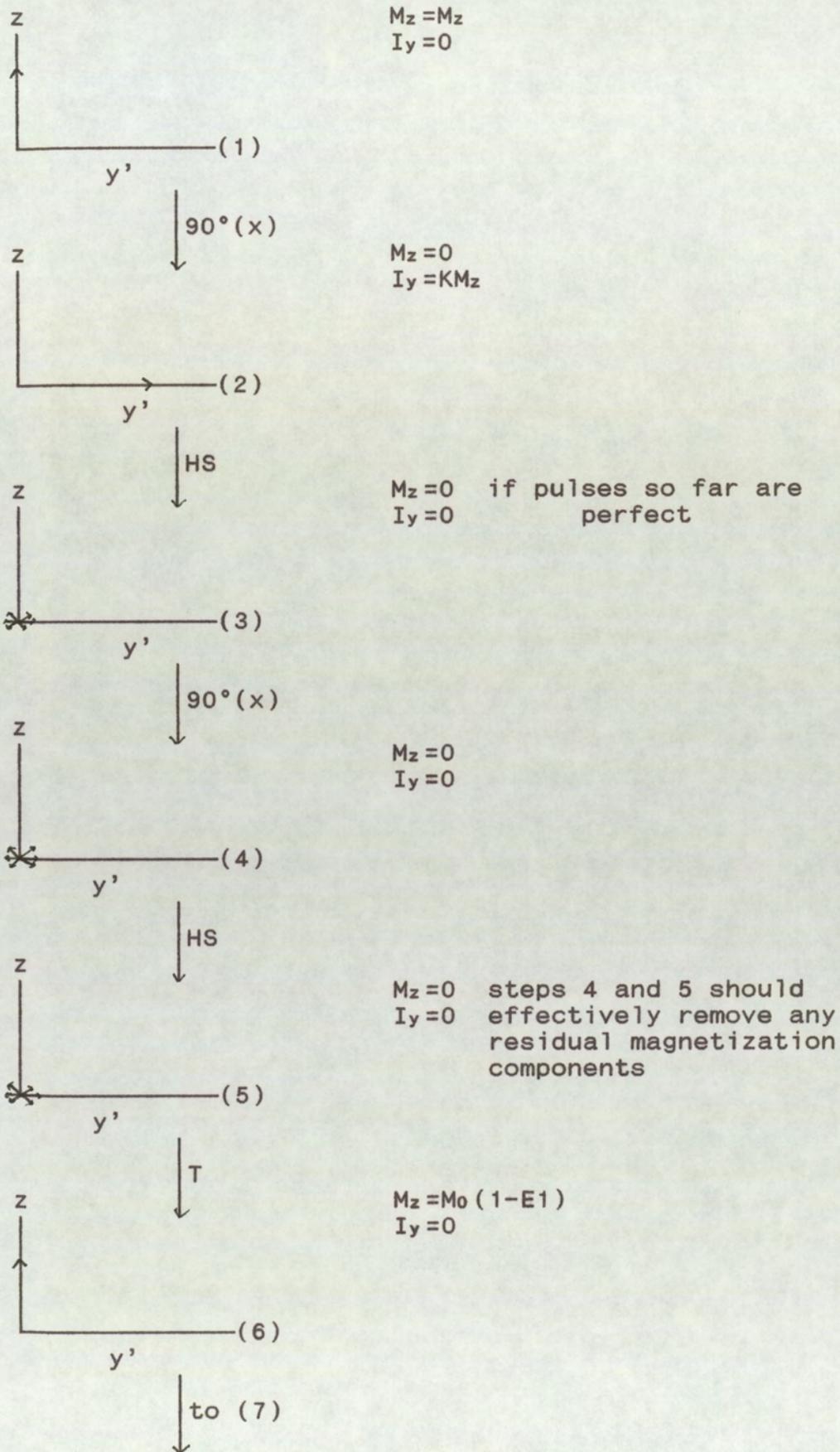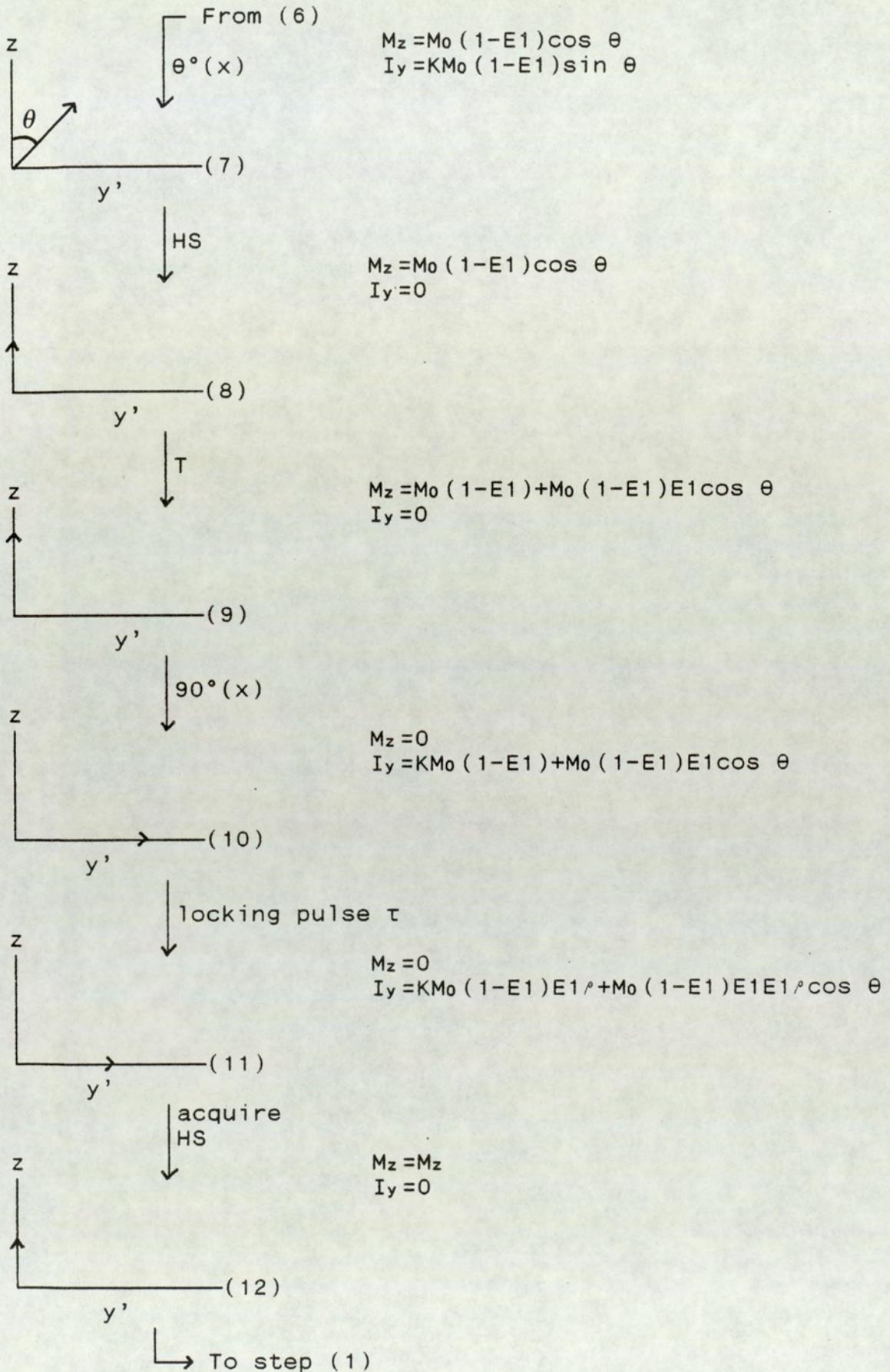
Fig.7.1 DESPOT $T_1\rho$ Pulse Sequence (Steps 7 to 12)

It is worth making some remarks about the choice of
the experimental parameters to obtain accurate values for T_1
and $T_{1\rho}$ from the above equation. Firstly, there is no need
to drive the magnetization to an equilibrium position with
non-acquisition sequences as in the DESPOT sequence. In the
above sequence any z-magnetization which is present at step
1 in the sequence will be effectively destroyed by the
90°(x) and z-field gradient spoiling pulses of steps 2,3 and
4. Consequently the sequence can be repeated immediately
after acquisition without waiting for thermal equilibrium to
be re-established. The choice of of the ratio T/T_1 is also
worth some consideration. It is inadvisable to allow the
ratio T/T_1 to become too small (<0.3). When the value of
$\exp(-T/T_1)$ approaches unity, the observed gradient becomes
very dependent on exact 90° nutation pulses. At higher T/T_1
ratios this dependence is reduced to a large extent although
the required experimental time is increased. The value of τ,
the spin-locking time, chosen is not as critical as the
value chosen for T. In our experiments it has been
sufficient to make sure that the ratio $\tau/T_{1\rho} > 0.25$ which
has enabled the gradient and intercept of the plot to be
sufficiently sensitive to the value of $T_{1\rho}$. Although it is
only strictly necessary to obtain an independent value of M_0
in order to obtain values for T_1 and $T_{1\rho}$, in our experiments
it proved convenient to measure the value of M_0 using a
DESPOT T_1 measurement. In this way the value of T_1 obtained
from the DESPOT sequence and from the DESPOT $T_{1\rho}$ plot could
be compared.

7.5.3 <u>Experimental</u>

The pulse sequence proposed in Fig. 7.1 was converted into a pulse program to run on the PG200 pulse programmer (Appendix 8). In accordance with the instrument manufacturer's recommendations (146) the B_1 spin-locking field was set at half the field strength of the normal B_1 field and its phase accurately adjusted (Appendix 9). Experiments were carried out with the recommendations of Ohuchi et al.(88) (Sec. 7.4.1) taken into account. In our experiments though, a greater than 1 KHz spectral width could have been tolerated as the 90° spin-locking pulse width was approximately 70 μs for ^1H and 45 μs for ^{13}C. The $T_1\rho$ measurements obtained were compared with values obtained on the same sample and under otherwise the same conditions using the classical sequence (70). In the case of ^{13}C measurements, ^1H noise decoupling was switched to coherent decoupling during the spin-locking process and the field strength of the decoupler was checked using the D.E.P.T sequence (38) (Appendix 10) to avoid Hartmann-Hahn matching (Sec. 7.2.2). Proton results based on a two point analysis for the aryl and methyl protons of methyl benzene are presented in Table 7.1. ^{13}C results for the three proton decoupled resonances of 1,2-dichlorobenzene are presented in Table 7.2. Fig. 7.2 shows typical experimental plots of I_y against cos θ for the ^1H resonances of methyl benzene.

Table 7.1

^{1}H $T_1\rho$ Results for Methyl Benzene

	Aromatic			Methyl		
Sequence	T_1/s	$T_1\rho$/s	M_0	T_1/s	$T_1\rho$/s	M_0
DESPOT $T_1\rho$	5.67	4.81	–	4.17	5.32	–
DESPOT	5.29	–	384	3.84	–	223
Spin Lock	–	4.71	390	–	5.00	222

The DESPOT $T_1\rho$ data presented above is based on a two point analysis at 31° and 72°. Each point was an average of 3 separate readings using 8 scans per reading, T=4 s and τ=1.5 s. The DESPOT results were based on a similar two point analysis with τ=4.396 s. The classical spin-lock results are based on 6 separate τ readings between 0 and 7 s with an interpulse interval=44 s. The two point analyses were carried out, in order to obtain results quickly so as to minimise the effects of spectrometer drift. The quoted DESPOT $T_1\rho$ results are based on gradient values.
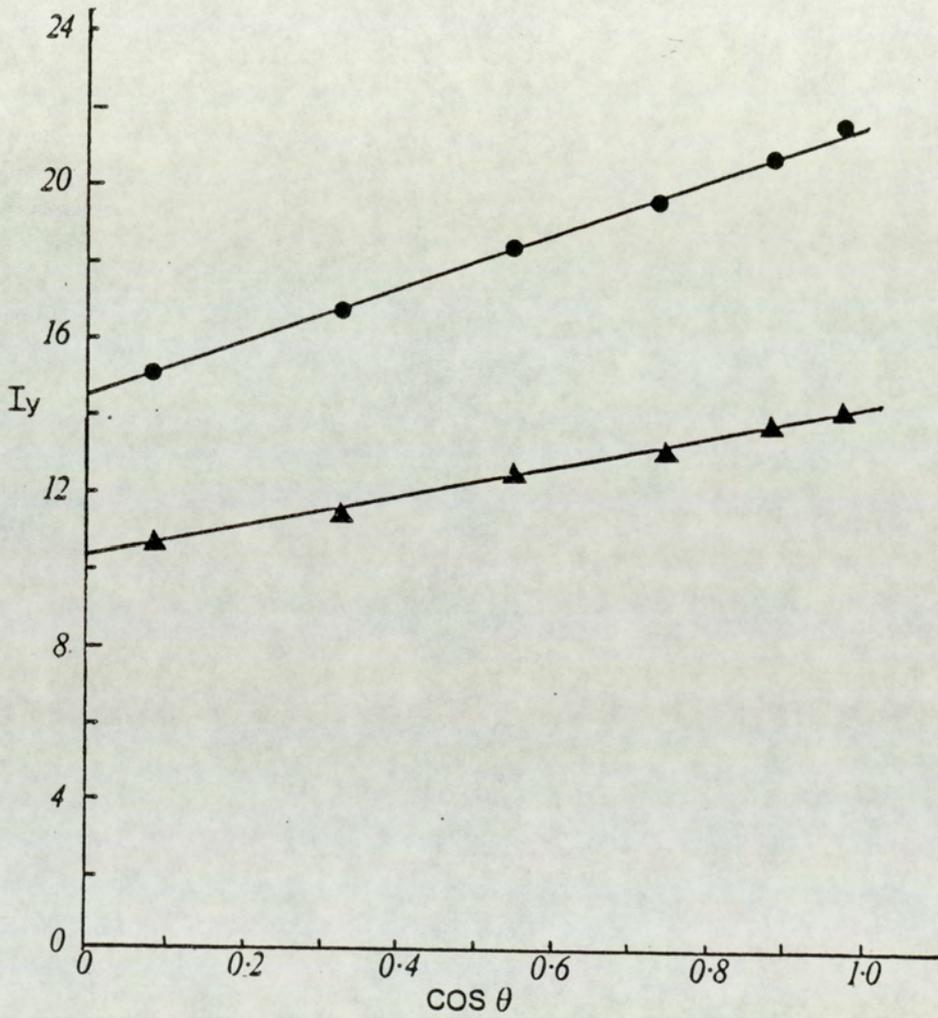
Fig. 7.2 <u>Variation in I_y with cos θ for the DESPOT $T_{1\rho}$ determination of methyl benzene. Circles represent the aryl protons and triangles the methyl protons.</u>

Table 7.2

$^{13}C\ T_{1\rho}$ Results for 1,2-dichlorobenzene
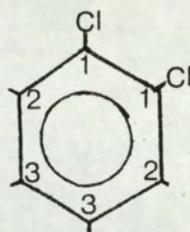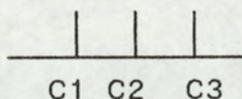
	DESPOT		DESPOT $T_{1\rho}$		Spin-Lock	
	T_1/s	M_0	T_1/s	$T_{1\rho}/s$	$T_{1\rho}/s$	M_0
C1	41.7	2500	42.3	2.4	3.1	2606
C2	7.3	2311	7.4	4.4	4.8	2128
C3	5.8	2148	6.8	5.3	4.6	2135

The DESPOT $T_{1\rho}$ results for C2 and C3 were obtained from a two point analysis with nutation angles of 37° and 74°. Each point was an average of 3 readings with 16 accumulations per reading, T=6 s and τ=2 s. The DESPOT results for C2 and C3 were based on a similar two point analysis with τ=4.396 s. The classical spin-lock results for C2 and C3 were based on 6 separate τ readings between 0 and 7 s with a waiting time of 44 s between sequence repetitions and 8 repetitions per data point. The quoted DESPOT $T_{1\rho}$ results are based on gradient values.

The DESPOT $T_{1\rho}$ data for C1 were obtained from a linear regressional analysis on four data points between 25° and 74° with T=40 s and τ=2 s. The DESPOT data are based on a linear regression on four data points between 25° and 74° with τ=25 s. The spin-lock data were based on 6τ values between 0 and 7 s with a pulse repetition time of 254 s.

For the ^{13}C results the 90° decoupler pulse width was found to be 32 μs using the DEPT sequence. The 90° spin-lock field pulse was set to 44 μs using the SPINCAL program (Appendix 9); the rotation rate of the protons in their rotating frame equalled 7.8×10^3 Hz compared with 5.7×10^3 Hz for carbon nuclei in their rotating frame. Hence, it was considered that erroneous $T_{1\rho}$ values due to Hartmann-Hahn matching (Sec. 7.2.2) were avoided under these conditions.

The results presented in Tables 7.1 and 7.2 show reasonable agreement between the DESPOT $T_{1\rho}$ sequence and the DESPOT and spin-locking classical sequence. In most cases the measured $T_{1\rho}$ and the T_1 values show quite close agreement as would be expected for molecules with short correlation times in the extreme narrowing region (Sec 2.3 and Fig. 2.2). The chloro containing carbons of 1,2-dichlorobenzene yielded the expected large difference between T_1 and $T_{1\rho}$ due to the difference in the magnitudes of the spectral density at γB_0 and γB_1. This difference is due to scalar relaxation because of the high quadrupolar relaxation rate of ^{35}Cl and ^{37}Cl (Sec.2.4.5). The ^{13}C results for the resonances C2 and C3 show a larger than expected difference between the T_1 and $T_{1\rho}$ values. The fact that the $T_{1\rho}$ values are lower than the T_1 values both classically and with the use of the DESPOT $T_{1\rho}$ sequence implies that there is a long range J coupling between the proton bearing carbons and the chlorine nuclei or that the carbon spin system is being heated by the proton spins or

that there is a sizeable off-resonance effect. Measurements were carried out with all absorptions within 200 Hz of the carrier frequency with the absorptions C1 and C3 equally spaced about the carrier frequency. Consequently, the observed difference in the measured values of T_1 and $T_{1\rho}$ were not thought to be attributable to off-resonance effects. It is also worthwhile pointing out that the difference in the precessional rates of protons and carbons in their respective rotating frames in this work was 2.1 KHz compared with 0.6 KHz in the original work by Freeman et al. (70). The T_1 and $T_{1\rho}$ values in reference (70) for C2 and C3, however, are in close agreement which implies that the long range coupling between the proton bearing carbons and the chlorine nuclei has little effect on the measured $T_{1\rho}$'s for the proton bearing carbons. A further experiment was carried out with the B_1 spin-locking field strength reduced in order to further separate the precessional rates of the protons and carbons in their respective rotating frames of reference. The results of this analysis are presented in Table 7.3. The quoted DESPOT $T_{1\rho}$ results are based on values obtained from the gradient of the regression.

<div align="center">

Table 7.3

^{13}C $T_1\rho$ Results for 1,2-dichlorobenzene

</div>
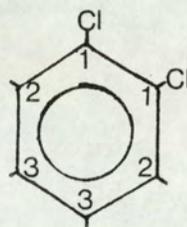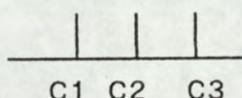
	DESPOT		DESPOT $T_1\rho$		Spin-Lock	
	T_1/s	Mo	T_1/s	$T_1\rho/s$	$T_1\rho/s$	Mo
C2	7.0	500	7.3	6.1	6.6	483
C3	5.7	510	6.4	5.8	5.9	501

The results in the above table were obtained with a ^{13}C 90° spin-lock pulse equal to 85μs and a proton 90° decoupler pulse measured at 29.5μs using the D.E.P.T sequence. This gives a difference in the precessional rates of the protons and carbons in their respective rotating frames of 5.53 KHz. It can be seen that with the increased difference in the precessional rates of the proton and carbon nuclei in their respective rotating frames, the measured $T_1\rho$ results obtained both classically and using the DESPOT $T_1\rho$ sequence increase towards the expected extreme narrowing values. The observed increase in both the classical $T_1\rho$ and DESPOT $T_1\rho$ derived values, in this experiment, virtually rules out the possibility of a long range J coupling between C2 and C3 and the chlorine nuclei as a cause for the difference in the observed values of T_1 and $T_1\rho$. Even with the difference in the precessional rates being almost ten times that used by Freeman et al (70), however, the expected extreme narrowing equivalence of the

T_1 and $T_{1\rho}$ values is not observed. As the classical sequence and the DESPOT $T_{1\rho}$ sequence have been shown to give comparable results the problem was thought to be a hardware problem and could possibly be due to inadequate suppression of the incoherent decoupling during the spin-locking part of both sequences.

7.5.4 Sensitivity of the Sequence to Experimental Parameters

As with all pulse sequences it is necessary to carefully set up the experimental parameters prior to an analysis if an acceptably accurate analysis is to be obtained. In the case of the above sequence there are three parameters which require consideration, τ, T and the range of θ values chosen.

τ is the time for which the spin-locking field operates, and its length is therefore dependent upon the size of $T_{1\rho}$ being measured. τ must be long enough to ensure that significant $T_{1\rho}$ relaxation has occured during the spin-locking pulse. It is not beneficial to allow τ to become too long as the S/N ratio of the resulting spectrum decreases as τ increases and also sample heating can be a problem at long τ values. On the JEOL FX 90Q spectrometer the maximum value of τ which should be set is 25% of the whole sequence time. τ values greater than this run the risk of damaging the excitation coils on the probe insert. In connection with this, a table in reference (146) details the maximum spin-locking field strengths that should be used for

a particular nucleus at different τ values in order to prevent damage to the probe insert. Consequently, it is prudent to set τ as short as is practically possible. In our experiments a reasonable value for τ is approximately $0.25T_{1\rho}$ which represents a 22% fall in the signal intensity compared with an identical spectrum obtained with no spin-lock pulse. It should be noted that in this respect the multipulse sequence scores over the classical sequence as in the classical sequence lock times of the order of $T_{1\rho}$ are often used.

As mentioned above the accuracy of the results can be quite dramatically effected by inaccurately set 90° pulses. The problem occurs because the rate of change of cos θ around 90° is quite high. Consequently after an inaccurately set 90° pulse there can remain quite a large $\pm M_z$ component which can readily give rise to anomalous results. The combination of two 90°(x) pulses and two z-field gradient spoiling pulses at the beginning of the sequence is designed to remove any $\pm M_z$ magnetization at step 5 in the pulse sequence of Fig. 7.1. The size of the anomalous M_z component is dependent on two factors, the first is the degree of mis-setting of the 90° pulses and the second is the original size of the M_z component at step 1. During the first sequence it is possible that the M_z component at step 1 has a value of M_0 and consequently, it is possibly beneficial to insert one non-acquisition sequence at the beginning of the experiment. The inaccuracy in the experimental results due to mis-setting the pulse

angle decreases with increase in the ratio T/T_1. However, an increase in the ratio T/T_1 results in an experiment with a set number of pulse repetitions taking a longer time to perform. As the DESPOT $T_{1\rho}$ sequence is a rapid multipulsed sequence it is worth considering the conditions of θ and T/T_1 which will give rise to the maximum S/N ratio in a given experimental time. The results of such an analysis for a fixed value of the ratio $\tau/T_{1\rho}$ is presented in Table 7.4.

<u>Table 7.4</u>

Values of the ratio T/T_1 giving the maximum S/N ratio in a DESPOT $T_{1\rho}$ experiment in 1000 s for different values of θ with $\tau/T_{1\rho}=0$. $M_0=1$ and $T_1=10$ s.

$\theta/°$	T/T_1 (max)*	S/N ratio at T/T_1 (max)
10	0.630	6.35
20	0.645	6.25
30	0.665	6.09
40	0.695	5.87
50	0.745	5.62
60	0.815	5.33
70	0.920	5.04
80	1.065	4.76
90	1.255	4.51

* In the above table T/T_1 (max) represents the value of the ratio T/T_1 which gives the maximum spectral S/N ratio in the given experimental time under the specified conditions.

Examination of the data presented in Table 7.4 shows that the ratio T/T_1 (max) increases with increasing nutation angle and that the maximum attainable S/N ratio in a given time falls with increasing nutation angle. Bearing in mind the small change in $\cos \theta$ in the region 10° to 30° and the small S/N ratio values obtained at larger nutation angles it is possibly most efficient to carry out a DESPOT $T_{1\rho}$ analysis in the nutation angle range 10° to 75° with well spaced data points at the small nutation angle side of the range and a T/T_1 value of somewhere around 0.75. It should be stressed, however, that where the sample under consideration gives a strong signal and requires relatively few pulses to obtain a sufficient S/N ratio it may well be preferable to use a smaller T/T_1 ratio.

7.5.5 Time Saving Aspects of the Sequence

The time saving aspects of the pulse sequence can be looked at in two ways. It is possible to compare the times required to obtain a measurement of $T_{1\rho}$ using the DESPOT $T_{1\rho}$ sequence and the classical sequence over a given number of acquisition pulses. Alternatively the time required to achieve similar S/N ratio values in the final spectrum can be considered. In view of this the data presented in the tables below give the resulting average S/N ratios (taken as an average over the spectra acquired) as well as the total times required to make the measurement. In the following table all the results are based on a T_1 value of

10 s, a $T_1\rho$ value of 10 s, an M_0 value of 1000 and a τ value in the DESPOT $T_1\rho$ results of 2.5 s. Linear regression results for the DESPOT $T_1\rho$ sequence are based on 6 nutation angles of 10°, 25°, 40°, 50°, 60° and 70°. Linear regression results for the classical sequence are based on 6τ values between $0.2T_1\rho$ and $1.2T_1\rho$ incrementing in steps of $0.2T_1\rho$. The M_0 value required using the DESPOT $T_1\rho$ sequence can be obtained via a DESPOT analysis using the same nutation angles as used for the DESPOT $T_1\rho$ sequence, with the pulse repetition time, τ, being determined by the acquisition time or via a classical $(90-5T_1)_n$ sequence. The former method obviously provides a check on the value of T_1 obtained. The data pertinent to a linear regressional analysis are presented in Table 7.5. DESPOT $T_1\rho$ two point analyses are based on two nutation angles of 25° and 60° with M_0 obtained via a two point DESPOT analysis at 25° and 60° or via a classical $90-5T_1$ sequence. Corresponding two point classical $T_1\rho$ values are obtained using τ values of $0.4T_1\rho$ and $1.0T_1\rho$. Classical T_1 values relate to the use of the $180°-\tau-90°$ technique with the same τ values as used to derive the classical $T_1\rho$ values. The two point analysis data are presented in Table 7.6.

Table 7.5

Comparison of the time required and average S/N ratio predicted for the evaluation of $T_1\rho$ using the DESPOT $T_1\rho$ sequence and using the Classical sequence, from linear regression.

Sequence	Time/s	S/N ratio average
DESPOT $T_1\rho$ $(T/T_1)=0.3$	600	862.9
DESPOT $(\tau/T_1)=0.4$	332	981.0
Classical spin-lock	2736	1487.9
$(90°-5T_1)$	400	2828.0
$180°-\tau-90°$	2800	1141.7
DESPOT $T_1\rho$ $(T/T_1)=0.75$	1032	1541.3

The above data are calculated using the conditions described above and assuming that 8 acquisition sequences were required for each spectrum. The DESPOT sequence was based on the numbers of non-acquisition sequences required to fulfil condition 4.13. The acquisition time was assumed to be 4 s with τ_{DESPOT} being set equal to this.

Table 7.6

Comparison of the time required and the average S/N ratio predicted for the evaluation of $T_1\rho$ using the DESPOT $T_1\rho$ sequence and using the Classical sequence, from two point analyses.

Sequence	Time/s	S/N ratio average
DESPOT $T_1\rho$ $(T/T_1)=0.3$	200	868.3
DESPOT $(\tau/T_1)=0.4$	116	1109.4
Classical spin-lock	912	1468.2
$(90°-5T_1)$	400	2828.0
$180°-\tau-90°$	800	855.4
DESPOT $T_1\rho$ $(T/T_1)=0.75$	344	1548.3

The above data are calculated using the conditions described above and assuming that 8 acquisition sequences were required for each spectrum. The DESPOT sequence was based on the numbers of non-acquisition sequences required to fulfil condition 4.13. The acquisition time was assumed to be 4 s with τ_{DESPOT} being set equal to this.

The data presented in Tables 7.5 and 7.6 show that the DESPOT $T_1\rho$ sequence is more efficient than the classical sequence. From Table 7.5 using a DESPOT sequence to obtain M_0, and a T/T_1 value of 0.3 for the DESPOT $T_1\rho$ sequence, values of T_1, M_0 and $T_1\rho$ can be obtained in 34% of the time it would take to obtain $T_1\rho$ and M_0 classically or in 16.8% of the time it would take to obtain the classical T_1 values as well. If the value of T/T_1 is increased to 0.75 the above

two time savings increase to 50% and 25% respectively. It should be noted, however, that when $T/T_1 = 0.75$ the average S/N ratio in the recorded spectrum has increased beyond that recorded by the classical $T_1\rho$ sequence. The two point analysis results in Table 7.6 show similar savings in the experimental time. The results obviously only give a rough guide to the available time saving using the DESPOT $T_1\rho$ sequence as they are only appropriate to the particular case studied. It should also be noted that when the value of T in the DESPOT $T_1\rho$ sequence is greater than the acquisition time it should be possible to make use of the acquisition time as one of the relaxation periods, T. This will cause the sequence to become more efficient depending on the magnitudes of T and the acquisition time.

7.6 Conclusions

The DESPOT $T_1\rho$ sequence has been shown above to provide a rapid and accurate method for measuring T_1 and $T_1\rho$ in NMR liquid samples. As with any rapid method there are some draw backs and the most notable of these is the decrease in the rate of change of the intensity with θ compared with the rate of change of intensity with spin-locking time in the classical sequence. The susceptibility of the sequence to imperfect 90° pulses is also a potential problem but the error associated with this can be reduced by careful determination of the 90° pulse and sample constriction (Sec. 4.4.3). Throughout this chapter

all the quoted DESPOT $T_1\rho$ results have been derived from gradients of the straight line plots. Gradient values were used as they are less sensitive to small numerical changes than the corresponding intercept values. The intercept values, however, are useful as they provide a check on the derived $T_1\rho$ value from the gradient and combined with a DESPOT T_1 analysis provide a check on the determined T_1 value. In this way the DESPOT $T_1\rho$ sequence is self checking, and with the aid of a computer program enables poor data or inadequate experimental conditions to be identified before a considerable amount of spectrometer time is wasted. The efficiency of the DESPOT $T_1\rho$ sequence can be improved by allowing the growth of the z-magnetization vector during the acquisition time to be one of the relaxation times, T, required in the sequence.

The DESPOT $T_1\rho$ sequence should lend itself readily to dynamic NMR studies of intermediate energy barriers based on a measurement of $T_1\rho$(exch) (Sec. 2.6.3). The method should be especially useful as it provides T_1 as well as $T_1\rho$ information which is required in the calculation of $T_1\rho$(exch). There is also a possibility that the sequence could be used in medical imaging where the $T_1\rho$ values measured may well give further useful information compared with that already available from T_1's and spin densities.

REFERENCES

1) W. Pauli, Jr. "The theoretical significance of the sattelites of some spectrum lines and the effect on them of magnetic fields," Naturwissenschaften 12, 741-3 (1924)

2) I. Estermann and O. Stern," Magnetic Deviation of Hydrogen molecules and the Magnetic Moment of the Proton Part II," Z. Phys. 85, 17-24 (1933)

3) J.M.B. Kellogg, I.I. Rabi, N.F. Ramsey, Jr., and J.R. Zacharias, " The Magnetic Moment of the Proton and Deuteron," Phys. Rev., 56 728-43 (1939)

4) E.M. Purcell, H.C. Torrey, and R.V. Pound, "Resonance Absorption by Nuclear Magnetic Moments in a Solid ," Phys. Rev., 69, 37-8 (1946)

5) F. Bloch, W.W. Hansen, and M. Packard, "Nuclear Induction," Phys. Rev., 69, 127 (1946)

6) W.D. Knight, "NMR shifts in Metals," Phys. Rev., 76, 1259-60 (1949)

7) J.T. Arnold, S.S. Dharmatti, and M.E. Packard, "Chemical Effects on Nuclear Induction Signals for Organic Compounds," J. Chem. Phys., 19, 507 (1951).

8) P.L. Corio, "Structure of High Resolution NMR Spectra," pp. 60-62. Academic Press, New York, 1966

9) H. Goldstein, "Classical Mechanics," Addison-Wesley, Reading, Massachusetts, 1950.

10) J.A. Pople, W.G. Schneider, and H.J. Bernstein, "High Resolution Nuclear Magnetic Resonance," p. 27 McGraw-Hill, New York, 1959.

11) D.E. Leyden and R.H. Cox, "Analytical Applications of NMR," Wiley, New York, 1977

12) B.E. Lasarew, and L.W. Schubnikow,"Magnetic Moment of the Proton," Physik. Z. Sowjetunion, 11, 445-57 (1937)

13) A. Einstein,"On the Quantum Theory of Radiation," Phys. Z., 18, 121-8 (1917)

14) E.M. Purcell,"Spontaneous Emission Probabilities at Radio Frequencies," Phys. Rev., 69, 681 (1946)

15) F. Bloch, "Nuclear Induction," Phys. Rev.,70, 460-74 (1946)

16) R.R. Ernst and W.A. Anderson, "Applications of Fourier Transform Spectroscopy to Magnetic Resonance," Rev. Sci. Instrum. 37, 93-102 (1966)

17) G.V.D Tiers,"Proton NMR Spectroscopy XII TMS: Some Observations Concerning Line Width and Line Shape,"J. Phys. Chem. 65, 1916-8 (1961)

18) I.U.P.A.C. Recommendations for the Presentation of NMR Data for Publication in Chemical Journals, Pure Appl. Chem. 29, 627-8 (1972);ibid, 45, 217-9, (1976)

19) E.D. Becker, "High Resolution NMR Theory and Chemical Applications 2nd ed.," pp. 59-61, Academic Press, New York (1980)

20) J. Homer, "Dispersed Liquid Phase Referencing of NMR Spectra," J. Magn. Reson., 54, 1-8 (1983)

21) J.W. Emsley, J. Feeney, and L.H. Sutcliffe, "High Resolution NMR Spectroscopy," pp. 1115-36. Macmillan, New York, (1965)

22) G.C. Levy and G.L. Nelson "^{13}C NMR for Organic Chemists," Wiley, New York, (1972)

23) G.A. Webb, and M. Witanowski, "Nitrogen NMR," Plenum Press, New York, (1973)

24) L. Cavalli, "Fluorine Chemical shifts and F-F Coupling Constants," in, "Nuclear Magnetic Resonance Spectroscopy of Nuclei Other Than Protons," (Edited by T. Axenrod and G.A. Webb) Wiley, New York, (1974)

25) R.A.Y. Jones, and A.R. Katritzky,"Phosphorus NMR Spectroscopy," Angew. Chem., Int. Ed. 1, 32-41 (1962)

26) N.F. Ramsey, "Electron Coupled Interactions Between Nuclear Spins in Molecules," Phys. Rev.,91, 303-7 (1953)

27) H. Spiesecke, and W.G. Schneider, "Effect of Electronegativity and Magnetic Anisotropy of Substituents on ^{13}C and ^1H chemical Shifts in CH_3X and CH_3CH_2X Compounds," J. Chem. Phys. 35, 722-30 (1961)

28) S. Castellano, R. Kostelnik, and C. Sun,"NMR Spectral Parameters of Monosubstituted Benzenes: Halobenzenes Tetrahedron Lett., 4635-9 (1967)

29) e.g. J. Homer, and D. Callaghan, "Intramolecular Screening Effects on NMR Chemical Shifts. Part 1. The Anisotropy in the Magnetic Susceptibility of the C-C and C-H bonds" J. Chem. Soc. A. 439-44, (1968) and references therein

30) C.E. Johnson, Jr. and F.A. Bovey, "Calculation of NMR Spectra of Aromatic Hydrocarbons," J. Chem. Phys. 29, 1012-4 (1958)

31) A.A. Bothner-By, and R.E. Glick,"Medium Effects in NMR Spectra of Liquids III: Aromatics," J. Chem. Phys., 26, 1651-4 (1957)

32) J. Homer and C. Percival, "Reaction Fields, van der Waals Forces and Related Nuclear Magnetic Resonance Chemical Shifts," J. Chem. Soc. Faraday Trans. II, 80, 1-29 (1984)

33) F.A. Bovey, "NMR Spectroscopy," Academic Press, New York (1969)

34) N.F. Chamberlain "The practice of NMR Spectroscopy," Plenum Press, New York, (1974)

35) N.F. Ramsey and E.M. Purcell,"Interactions Between Nuclear Spins in Molecules," Phys. Rev., 85, 143-4 (1952)

36) A.A Bothner-By and R.H. Cox,"The Estimation of Vicinial ^{31}P-^{1}H and ^{14}N-^{1}H Spin-Spin Coupling Constants in Single Conformers," J. Phys. Chem., 73, 1830-4 (1969)

37) M. Karplus,"Contact Electron Spin Coupling of Nuclear Magnetic Moments," J. Chem. Phys.,30, 11-5 (1959)

38) D.M. Doddrell, D.T. Pegg, and M.R. Bendall, "Distortionless Enhancement of NMR Signals by Polarization Transfer," J. Magn. Reson. 48, 323-7, (1982)

39) A. Bax, R. Freeman, and S.P. Kempsell,"Natural Abundance ^{13}C-^{13}C Coupling Observed via Double Quantum Coherence," J. Amer. Chem. Soc. 102, 4849-51 (1980)

40) N. Bloembergen, E.M. Purcell and R.V. Pound, "Relaxation Effects in NMR Absorption," Phys. Rev., 73, 679-712 (1948)

41) P. Debye, "Polar Molecules," Dover Publications, New York, 1945

42) D. Shaw, "Fourier Transform NMR Spectroscopy (2nd ed),"
    Chapters 3 & 9, Elsevier, New York, 1984

43) R.K. Harris, "Nuclear Magnetic Resonance Spectroscopy, "
    p 97, Longman, U.K., 1986

44) I. Solomon, "Relaxation Processes in a System of Two
    Spins," Phys. Rev. **99**, 559-65, (1955)

45) J.H. Noggle and R.E. Schirmer, "The Nuclear Overhauser
    Effect," p 25, Academic Press, New York, 1971

46) I.D. Campbell and R. Freeman, "Influence of Cross
    Relaxation on NMR Spin-Lattice Relaxation Times," J.
    Magn. Reson., 11, 143-62 (1971)

47) A. Overhauser, "Paramagnetic Relaxation in Metals,"
    Phys. Rev., 89 689-700 (1953)

48) G. Chiarotti and L. Guilotto, "Proton Relaxation in
    Water," Phys. Rev., **93**, 1241 (1954)

49) R. Kaiser, "Intermolecular nOe in Liquid Solutions," J.
    Chem. Phys., **42**, 1838 (1965)

50) J.A. Pople, W.G. Schneider and H.J. Bernstein,
    "High-Resolution Nuclear Magnetic Resonance," p 203,
    McGraw Hill, London, 1959

51) R.K. Harris, "Nuclear Magnetic Resonance Spectroscopy, "
    p 100, Longman, U.K., 1986

52) H.S. Gutowsky and D.E. Woessner, "Nuclear Magnetic
    Spin-Lattice Relaxation in Liquids, " Phys. Rev., **104**,
    843-4 (1956)

53) Topics in Carbon 13 NMR Spectroscopy Vol. 1 ed. G.C.
    Levy, p 107, Wiley, New York, 1974

54) J. Homer and E.R. Valdiviesco-Cedeno, "Use of Intermolecular ^1H-^1H noe Measurements to Isolate Intramolecular and Intermolecular Contributions to ^1H NMR Spin-Lattice Relaxation Times," J. Chem. Soc., Faraday Trans. 2, **80**, 375-82 (1984)

55) R.W. Mitchell and M. Eisner, "Nuclear Spin-Lattice Relaxation in Liquids," J. Chem. Phys., **33**, 86-91 (1960)

56) J.G. Powles and R. Figgins, "Molecular Motion in Liquid Benzene by NMR," Mol. Phys., **10**, 155-61 (1966)

57) O.A. Gansow, A.R. Burke and G.N. LaMar,"A Shiftless Relaxation Agent for the Carbon-13 Magnetic Resonance of Carbonyl Compounds," J.C.S. Chem. Comm., 456-7 (1972)

58) G.C. Levy and J.D. Cargioli,"Spin-Lattice Relaxation in Solutions Containing Cr(III) Paramagnetic Relaxation Agents," J. Magn. Reson. **10**, 231-4 (1973)

59) A. Abragam "The principles of Nuclear Magnetism," Oxford University Press, Oxford, 1961, Chap. 9

60) P.S. Hubbard, "Theory of NMR Relaxation by Spin-Rotation Interactions in Liquids," Phys. Rev., **131**, 1155-65 (1963)

61) J.R. Lyerla and D.M. Grant in C.A. McDonell (Ed.), International Rev. Science, Phys. Chem. Series, Vol. 4, Ch. 5, Medical and Technical Publishing Co., 1972

62) A.A. Maryott, T.C. Farrar and M.S. Malmberg, "^{35}Cl and ^{19}F NMR Spin-Lattice Relaxation Time Measurements and Rotational Diffusion in Liquid ClO_3F," J. Chem. Phys. **54**, 64-71 (1971)

63) H.W. Spiess, D. Schweitzer, U. Haeberlen and K.H. Hausser, "Spin-Rotation Interaction and Anisotropic Chemical Shift in Carbon-13 Disulphide," J. Magn. Reson., 5, 101-8 (1971)

64) G.C. Levy, J.D. Cargioli and F.A. Anet, "Carbon 13 Spin-Lattice Relaxation in Benzene and Substituted Aromatic Compounds," J. Am. Chem. Soc., 95, 1527-35 (1973)

65) A. Abragam, "The Principles of Nuclear Magnetism," p 316, Oxford Univ. Press. 1961

66) G.G. McDonald and J.S. Leigh, Jr, "New Method for Measuring Longtitudinal Relaxation Times," J. Magn. Reson., 9, 358-62 (1973)

67) G.C. Levy and U. Edlund, "Carbon-13 Chemical Shift Anisotropy Relaxation in Organic Compounds," J. Am. Chem. Soc., 97, 5031-2 (1975)

68) F. Brady, R.W. Matthews, M.J. Forster and D.G. Gillies, "^{205}Tl Spin-Lattice Relaxation in Dialkylthallium III Derivatives: Importance of Chemical Shift Anisotropy Relaxation and Effects on NMR Spectra of Coupled Nuclei," Inorg. Nucl. Chem. Lett. 17, 155-9 (1981)

69) J.R. Lyerla, Jr, D.M. Grant and R.K. Harris, "Dipolar Contribution to Carbon-13 Relaxation Times," J. Phys. Chem., 75, 585-8 (1971)

70) R. Freeman and H.D.W. Hill, "Fourier Transform Study of NMR Spin-Spin Relaxation," J. Chem. Phys., 55, 1985-6 (1971)

71) R.R. Shoup and D.L. Vanderhart, "Effect of Scalar Coupling on ^{13}C Transverse Relaxation Times," J. Am. Chem. Soc., **93**, 2053-4 (1971)

72) R.K. Harris, "Nuclear Magnetic Resonance Spectroscopy," pp. 131-41, Longman, U.K., 1986

73) R.A. Ogg and J.D. Ray, "Quadrupole relaxation and Structures in Nitrogen Magnetic Resonances of Ammonia and Ammonium Salts," J. Chem. Phys., **26**, 1339-40 (1957)

74) W.B. Moniz and H.S. Guttowsky, "Nuclear Relaxation of ^{14}N by Quadrupole Interaction in Molecular Liquids," J. Chem. Phys., **38**, 1155-62 (1963)

75) A.G. Massey, E.W. Randall and D. Shaw, "NMR Studies of Tetraalkyl Compounds of Group III and Group V Elements 1," Spectrochim. Acta., **20**, 379-83 (1964)

76) F.W. Wehrli, "Carbon-13 NMR Spectral Assignments in Large Molecules with the aid of Spin-Lattice Relaxation Data," J.C.S. Chem. Commun., **1973**, 379-80

77) A. Allerhand, D. Doddrell and R. Komoroski, "Natural Abundance Carbon-13 Partially Relaxed FTNMR Spectra of Complex Molecules," J. Chem. Phys., **55**, 189-98 (1971)

78) Topics in Carbon-13 NMR Spectroscopy Volume 1 (Ed. G.C. Levy) p112 Wiley, New York (1974)

79) J. Briggs, F.A. Hart, G.P. Moss and E.W. Randall, "Ready Method of Assignment of Carbon-13 NMR Spectra: Complete Assignment of the Carbon-13 Spectrum of Borneol," J. Chem. Soc. (D), 1971, 364-5

80) G.C. Levy, D.M. White and F.A.L. Anet," Carbon-13 Spin-Lattice Relaxation in Phenylacetylenes: Effect of Anisotropic Molecular Motion and Chemical Shift Anisotropy," J. Magn. Reson., 6, 453-5 (1972)

81) G.C. Levy," Carbon-13 Spin-Lattice Relaxation and Intermolecular Interactions:Phenol and Aniline," J. Magn. Reson., 8, 122-5 (1972)

82) G.C. Levy," Carbon-13 Spin-Lattice Relaxation: Internal Motions in Substituted Ferrocenes," Tetrahedron Lett., 3709-12 (1972)

83) Y.K. Levine, N.J.M. Birdsall, A.G. Lee and J.C. Metcalfe," ^{13}C NMR Relaxation Measurements of Synyhetic Lecithins and the Effect of Spin-Labelled Lipids," Biochemistry, 11, 1416-21 (1972)

84) G.C. Levy and G.L. Nelson," Carbon-13 Study of Aliphatic Amines and Oximes: Spin-Lattice Relaxation Times and Fast Internal Motions," J. Am. Chem. Soc., 94, 4897-901 (1972)

85) G.C. Levy, "Carbon-13 Spin-Lattice Relaxation and Solvation of Organic Ions: n-Butylamine and n-Butylammonium Ion J.C.S. Chem. Commun. 1972, 768-9

86) J.B. Lambert, R.J. Neinhuis and J.W. Keepers, "The Kinetics of Intramolecular Reactions from Relaxation Times Measurements," Angew. Chem. Int. Ed., 20, 487-616 (1981)

87) P. Stilbs and M.E. Moseley," Chemical Exchange Rates from Fourier Transform Measurements of Nuclear Spin-Lattice Relaxation in the Rotating Frame: Application to Hindered Rotation in Ureas," J. Magn. Reson. 31, 55-61 (1978)

88) M. Ohuchi, T. Fujito and M. Imanari," Spin-Lattice Relaxation of Carbon-13 in the Rotating Frame," J. Magn. Reson., 35, 415-27 (1979)

89) D.M. Doddrell, M.R. Bendall, P.F. Baron and D.T. Pegg," Use of ^{13}C T_1/ Measurement to Study Dynamic Processes in Solution," J.C.S. Chem. Commun. 1979, 77-9

90) S. Forsen and R.A. Hoffman, " Study of Moderately Rapid Chemical Exchange Reactions by Means of Nuclear Magnetic Double Resonance," J. Chem. Phys., 39, 2892-901 (1963)

91) V. Boekelheide and S.A. Sherrod, " An Unusually Large Conformational Kinetic Isotope Effect in [2.2,] metaparacyclophane," J. Am. Chem. Soc., 94, 5513-5 (1972)

92) B.E. Mann, " The Application of the Forsen-Hoffman Method of Measuring Rates of Exchange to the Carbon-13 NMR Spectrum of cis-Decalin," J. Magn. Reson., 21, 17-23 (1976)

93) B.E. Mann, "The Application of the Forsen-Hoffman Spin Saturation Method of Measuring Rate of Exchange to the Carbon-13 NMR Spectrum of N-N,dimethylformamide," J. Magn. Reson., 25, 91-4 (1977)

94) R. Damadian," Tumour Detection by Nuclear Magnetic Resonance," Science, 171, 1151-3 (1971)

95) R. Damadian, K. Zaner, D. Hor and T. Dimaio," Human Tumours by NMR," Physiol. Chem. and Phys., 5, 381-402 (1973)

96) I.D. Weisman, L.H. Bennett, L.R. Maxwell, Sr. and D.E. Henson, "Cancer Detection by NMR in the Living Animal, " NMR Basic Principles and Progress 19 (Ed. R. Damadian), Springer-Verlag, New York, 1981 pp17-37

97) K.S. Zaner and R. Damadian," Phosphorus-31 as a Nuclear Probe for Malignant Tumours," Science, 189, 729-31 (1975)

98) NMR Basic Principles and Progress 19 (Ed. R. Damadian), Springer-Verlag, New York, 1981

99) Topics in Carbon-13 Spectroscopy Volume 3 (Ed. G.C. Levy), Wiley, New York 1979 p119

100) D.E. Woessner and B.S. Snowden, Jr." Magnetic Relaxation Under Hindered Motion in Fluids," Advan. Mol. Relaxation Processes, 3, 181-97 (1972)

101) D.E. Woessner," Nuclear Spin Relaxation in Ellipsoids Undergoing Rotational Brownian Motion," J. Chem. Phys., 37, 647-54 (1962)

102) D.M. Grant, K.F. Kuhlmann and R.K. Harris," Nuclear Overhauser Effects and ^{13}C Relaxation Times in ^{13}C-{H} Double Resonance Spectra," J. Chem. Phys., 52, 3439-48 (1970)

103) D.E. Woessner, B.S. Snowden, Jr. and G.H. Meyer," Nuclear Spin-Lattice Relaxation in Axially Symmetric Ellipsoids with Internal Motion," J. Chem. Phys.,50, 719-21 (1969)

104) F. Bloch, W.W. Hansen and M. Packard, "The Nuclear Induction Experiment," Phys. Rev., **70**, 474-85 (1946)

105) E.L. Hahn, "Spin Echoes," Phys. Rev., **80**, 580-94 (1950)

106) J.W. Cooley and J.W. Tukey, "An Algorithm for the Machine Calculation of Complex Fourier Series," Math. Comput., **19**, 297-301 (1965)

107) Jeol FX 90Q Instruction and Service manuals, Jeol Ltd., Tokyo, Japan

108) I.J. Lowe and C.E. Tarr, " A Fast Recovery Probe for Pulsed NMR Spectroscopy," J.Phys. E 1, 320-2 (1968)

109) A. Derome, "Modern NMR Techniques for Chemistry Research," Pergamon, Oxford (1987), p81

110) "PG 200 Programmable Pulse Generator", Jeol Ltd., Tokyo, Japan

111) E.L. Hahn,"Spin Echoes," Phys. Rev., **80**, 580-94 (1950)

112) H.Y. Carr and E.M. Purcell,"Effects of Diffusion on Free Precession in NMR Experiments," Phys. Rev., **94**, 630-8 (1954)

113) J.A. Pople, W.G. Schneider and H.J. Bernstein,"High Resolution Nuclear Magnetic Resonance," McGraw-Hill, New York pp. 82-85

114) R.L. Vold, J.S. Waugh, M.P. Klein and D.E. Phelps, "Measurement of Spin Relaxation in Complex Systems," J. Chem. Phys., **48**, 3831-2 (1968)

115) J. Homer and M.S. Beevers, "Driven-Equilibrium Single Pulse Observation of T_1 Relaxation. A Reevaluation of a Rapid "New" Method for Determining NMR Spin-Lattice Relaxation Times," J. Magn. Reson., **63**, 287-97 (1985)

116) J. Homer and J.K. Roberts, "Conditions for the Driven Equilibrium Single Pulse Observation of Spin-Lattice Relaxation Times," J. Magn. Reson., **74**, 424-32 (1987)

117) R. Freeman and H.D.W. Hill, "High Resolution Studies of Nuclear Spin-Lattice Relaxation," J. Chem. Phys., 51, 3140-1 (1969)

118) J. Homer and J.K. Roberts, "The Effects of Carrier to Absorption Frequency Shift on the DESPOT Evaluation of Spin-Lattice Relaxation Times," J. Magn. Reson. 80, 116-8 (1988)

119) G.C. Levy and I.R. Peat,"The Experimental Approach to Accurate Carbon-13 Spin-Lattice Relaxation Measurements,"J. Magn. Reson., **18**, 500-21 (1975)

120) D. Canet, G.C. Levy and I.R. Peat,"Time Saving in Carbon-13 Spin-Lattice Relaxation Measurements by Inversion Recovery," J. Magn. Reson., **18**, 199-204 (1975)

121) R. Freeman, H.D.W. Hill and R. Kaptein, "An Adaptive Scheme for Measuring NMR Spin-Lattice Relaxation Times," J. Magn. Reson., 7, 82-98 (1972)

122) D.L. De Fontaine, D.K. Ross and B. Ternai, "A Fast Nonlinear Least Squares Method for the Calculation of Relaxation Times," J. Magn. Reson., **18**, 276-81 (1975)

123) J.L. Markley, W.J.Horsley and M.P. Klein, "Spin-Lattice Relaxation Measurements in Slowly Relaxing Complex Spectra," J. Chem. Phys., **55**, 3604-5 (1971)

124) R. Freeman and H.D.W. Hill,"Fourier Transform Study of NMR Spin-Lattice Relaxation by "Progressive Saturation"," J. Chem. Phys., **54**, 3367-77 (1971)

125) K.A. Christensen, D.M. Grant, E.M. Schulman and C. Walling, "Optimal Determination of Relaxation Times of FTNMR. Determination of Spin-Lattice Relaxation Times in Chemically Polarized Species," J. Phys. Chem., 78, 1971-7 (1974)

126) R.K. Gupta, "A New Look at the Method of Variable Nutation Angle for the Measurement of Spin-Lattice Relaxation Times Using FTNMR," J. Magn. Reson., 25, 231-5 (1977)

127) I.M. Armitage, H. Huber, D.H. Live, H. Pearson and J.D. Roberts, "NMR Spectroscopy. Concentration Dependence of the T_1 Relaxation Time for ^{13}C in Dioxane-D_2O. Some Experimental Problems with T_1 Measurements," J. Magn. Reson., 15, 142-9 (1974)

128) R.R. Ernst and R.E. Morgan, "Saturation Effects in Fourier Spectroscopy," Mol. Phys., 26, 49-74 (1973)

129) J.P. Karis, G. Allan Johnson and G.H. Glover, "Signal-to-Noise Improvements in Three-Dimensional NMR Microscopy Using Limited-Angle Excitation," J. Magn. Reson., 71, 24-33 (1987)

130) E.D. Becker, J.A. Ferretti and Prem N. Gambhir, "Selection of Optimum Parameters for Pulse Fourier Transform Nuclear Magnetic Resonance, " Anal. Chem., 51, 1413-20 (1979)

131) R.R. Ernst, in "Advances in Magnetic Resonance" (J.S. Waugh, Ed.), Vol. 2 p.1, Academic Press, New York, 1966

132) R.K. Harris and R.H. Newman, "Choice of Pulse Spacings for Accurate T_1 and NOE Measurements in NMR Spectroscopy," J. Magn. Reson., **24**, 449-56 (1976)

133) R. Freeman, H.D.W. Hill, and R. Kaptein, "Proton Decoupled NMR Spectra of Carbon-13 with the Nuclear Overhauser Effect Suppressed," J. Magn. Reson., **7**, 327-9 (1972)

134) D. Canet, "Systematic Errors Due to Improper Waiting Times in Heteronuclear Overhauser Effect Measurements by the Gated Decoupling Technique," J. Magn. Reson., **23**, 361-4 (1976)

135) S. Meiboom and D. Gill, "Modified Spin-Echo Method for Measuring Nuclear Relaxation Times," Rev. Sci. Instrum., **29**, 688-91 (1958)

136) R. Freeman and H.D.W. Hill, "Determination of Spin-Spin Relaxation Times in High Resolution NMR," in Chap. 5 of "Dynamic Nuclear Magnetic Resonance Spectroscopy," Ed. LLoyd M. Jackman and F.A. Cotton, Academic Press, New York, 1975

137) R. Freeman and S. Wittekeok, "Relaxation Measurements in High Resolution NMR," Proc. Colloq. Ampere (At. Mol. Etud. Radio Elec.,) **15**, 205-20 (1969)

138) A. Allerhand, "Analysis of Carr-Purcell Spin-Echo NMR Experiments on Multiple Spin Systems. (1) The Effect of Homonuclear Coupling," J. Chem. Phys., **44**, 1-9 (1966)

139) A.C. McLaughlin, G.G. McDonald and J.S. Leigh, "Measurement of Transverse Relaxation Rates for Individual Protons in First Order Spin-Coupled NMR Spectra," J. Magn. Reson., **11**, 107-9 (1973)

140) R. Freeman and S. Wittekeok, "Selective Determination of Relaxation Times in High Resolution NMR," J. Magn. Reson., 1, 238-76 (1969)

141) S.R. Hartmann and E.L. Hahn, "Nuclear Double Resonance in the Rotating Frame," Phys. Rev., 128, 2042-53 (1962)

142) A.G. Redfield,"Nuclear Magnetic Resonance Saturation and Rotary Saturation in Solids," Phys. Rev., 98, 1787-809 (1955)

143) I. Solomon," Measurement of Magnetic Resonance Relaxation in the Presence of a Driving Field," C.R. Acad. Sci., 248, 92-4 (1959), "Magnetic Relaxation in Liquids in the Presence of a High Frequency Field," ibid., 249, 1631-2 (1959)

144) T.K. Leipert, J.H. Noggle, W.J. Freeman and D.L. Dalrymple, "Rotating Frame Nuclear Relaxation of Phosphorus Tribromide. Off-Resonance Studies by Fourier Transform NMR," J. Magn. Reson., 19, 208-21 (1975)

145) E.J. Wells and H.S. Gutowsky, "NMR Spin-Echo Train for a Coupled Two-Spin System," J. Chem. Phys., 43, 3414-5 (1965)

146) Spin-lock unit manual NM-3960, JEOL Ltd., Tokyo, Japan

147) R.E. Hoffman and D.B. Davies, "Evaluation of the Inversion-Recovery and DESPOT Methods for Measurement of T_1 of the Polysaccharide Pullulan," J. Magn. Reson., 80, 318-23 (1988)

APPENDICES

APPENDIX 1

The PG200 Pulse Programmer

A1.1 Introduction

The PG200 is a programmable pulse sequence generator which may be programmed via the use of the light pen on the monitor oscilloscope of the FX 90Q spectrometer. The pulse sequence programs are stored in RAM (random access memory) prior to accumulation and any individual program may contain up to 64 words, each word consisting of 18 bits. Thirteen of the 18 output bits are used to control the output of the spectrometer and may be changed independently to produce the desired pulse programs (Sec. A1.2). In order to generate the pulse program various commands are available which control timing, loops, conditional and unconditional program jumps the triggering of the A.D.C.(Sec. A1.3). The pulse programmer also controls the accumulation phase program so that quadrature images are cancelled out using the cyclops sequence (Sec. 3.4.8). These accumulation phase programs can be input with up to 16 different accumulation phases consisting of 0°,90°,180° and 270° phases before repetition of the phase sequence. At any time three pulse programs may be stored in memory which are designated PUMOD 1 to 3. PUMOD 1 and 2, however, are always set aside for the single and double pulse sequences respectively, hence at any time only one user pulse program can be accessed directly from the spectrometer RAM. User programs may be stored on cassette

tape so different programs may be loaded, written and saved as required. Overall the pulse programmer is quite easy to use but the program editing techniques are very limited with small changes to a program requiring the program to be virtually rewritten.

A1.2 Spectrometer Output Control

As stated in Sec. A1.1 each word in a pulse program consists of 18 bits and each 18 bit word is equivalent to one line in a pulse program of up to 64 lines (Address 0 to 63). Of these 18 bits, 5 bits are allotted to internal control of the program storing information required for timing, loop counting, program line addressing and program advance on the completion of one command. The remaining 13 bits, 12 of which can be changed independently, control the output of the spectrometer at any given time. Bit 13 is the sampling trigger and is automatically controlled by bit 7 which triggers the A.D.C. Table A1.1 lists the output bits with a description of their operation.

Table A1.1

Output bits controlled via PG200 Pulse Programmer

Bit Nos.	Contents
1	Opens Observation gate when selected
2	Observation phase 0°(off) 180°(on)
3	Observation phase 0°(off) 90° (on)
4	Observation phase reset
5	Opens Receiver gate when selected
J(6)	Irradiation phase 0°(off) 180°(on)
7	Triggers A.D.C. for sampling
8	Opens Irradiation Gate when selected
A(9)	External 1
B(10)	External 2
C(11)	External 3
K(12)	Irradiation phase 0°(off) 90°(on)

As can be seen from Table A1.1, 3 of the output bits are reserved for external operations. There are 5 external operations which may be controlled via the output bits 9-11. The number associated with each operation maybe attributed to bits 9 to 11 by placing that number opposite that bit on the DEVICE screen. Table A1.2 lists the external operations, their identification numbers, mnemonics and their operation.

Table A1.2

External Devices Identification and Operation

No.	Mnemonic	Contents
1	HS	Selects z-field spoiling pulse
2	OBSLV	Selects B_1 field controlled via spin lock unit. Turns off decoupler noise
3	IRSE2	Selects triple irradiation mode
4	IRMO2	Reverses irradiation mode gating
5	IRPO2	Selects second irradiation power

In a pulse program the various output bits are selected by placing a * under the appropriate bit in the appropriate line in the program. An example of a pulse program with a description of its operation is given in Sec. A1.4.

A1.3 Pulse Program Commands

In order to facilitate programming, several commands are available to control loops, timing intervals, conditional and unconditional jumps and sampling. These commands along with their descriptions are presented in Table A1.3. A letter x following a command indicates that other parameters are often added.

Table A1.3

PG200 Programming Commands

Command	Description
PUL	Activates Sampling Trigger
LD1 x	Loads loop 1, the parameter x (2-10) determines which loop parameter (Loop,LO3-LO10) is used. The number of loops carried out equals the value of (Loop,LO3-LO10) plus 2.
LD2 x	Loads loop 2, identical to above except the number of loops carried out equals 64*(Loop, LO3-LO10+1). If x=1 then the number of loops is automatically determined by the number of sampling points.
TIM x	TIM represents a time which can have up to 40 different values between 0.5µs and 4095s. TIM 1-10 are controlled from the main spectrometer program (Table A1.4)
JC1 x	Decrements the value of LD1 loop and jumps to address x if LD1 loop is non zero
JC2 x	As above but operates on LD2 loop
JMP x	Unconditional jump to address x
INT x	Automatically calculated time to ensure correct A.D.C. sampling sequence

---

As mentioned in Table A1.3 the times TIM1 to TIM 10 are associated with operations in the main spectrometer program. These times and their associated mnemonics are

presented in Table A1.4.

Table A1.4

Mnemonics for TIM 1 to 10 in Main Spectrometer Program

TIM	Mnemonic	COMMENT
1	PW1**	Sets Observation pulse width time PW1**
2	PW2**	Sets Observation pulse width time PW2**
3	PI***	Sets pulse interval between PW2** and PW1** in double pulse (PUMOD=2) program
4	PD***	Sets Relaxation time
5	INTVL	Calculated Digitisation time interval
6	DELAY	Time between pulse end and sampling
7	PREDL	Time to open irradiation gate (200 μs)
8	DEADT	Receiver dead time (50 μs)
9	INIWT	Initial wait before program start (1 s)
10	SPOIL	length of z-field gradient pulse (1 ms)

A1.4 Single Pulse Program

In order to help to understand a pulse program the program for a single pulse sequence is presented below with comments. Further information on all aspects of PG200 programming can be found in reference (110).

Address	K	C	B	A	8	7	J	5	4	3	2	1	Command	Parameter
0	.	.	.	.	.	.	.	.	.	.	.	.		
1													TIM	9
2	.	.	.	.	*	.	.	.	.	.	.	.		
3													TIM	7
4	.	.	.	.	*	.	.	.	.	.	.	*		
5													TIM	1
6	.	.	.	.	*	.	.	.	*	.	.	.		
7													TIM	8
8													PUL	
9													LD2	1
10	.	.	.	.	*	.	.	*	*	.	.	.		
11													TIM	6
12	.	.	.	.	*	*	.	*	*	.	.	.		
13													INT	5
14	.	.	.	.	*	.	.	*	*	.	.	.		
15													INT	5
16													JC2	12
17	.	.	.	*	.	.	.	.	.	.	.	.		
18													TIM	10
19	.	.	.	.	.	.	.	.	.	.	.	.		
20													TIM	4
21													JMP	2

Address 1 is an initial wait prior to commencing program. Steps 2 and 3 ensure that irradiation gate is open, if an irradiation mode is selected. A θ(x) pulse is applied for time PW1 at steps 4&5. Step 6 resets the phase in order to make the spectrometer noise constant whilst sampling

leaving irradiation gate open. Step 7 gives the coil chance to recover from the B_1 pulse. Step 8 primes the A.D.C. for sampling. Step 9 loads LD2 to loop automatically for the number of sampling sequences. Step 10 ensures that the receiver gate is open ready to sample data with the phase reset and the irradiation gate open. Step 11 is a further delay time ensuring that the receiver coil is not saturated by the B_1 pulse. At Step 12 sampling takes place. Step 13 allows sampling for the required time. At step 15 the particular sampling is terminated and the result stored appropriately in the computer at step 15. The JC2 command at step 16 decrements 1 from LD2 and causes a jump to address 12 to sample the next data point whilst LD2>0. If LD2 is zero then sampling is finished and the program moves to step 17. A z-field spoiling pulse is applied for a time TIM 10 as HS is selected as external device A. Step 20 is a relaxation time before an unconditional jump at step 21 back to step 2. The steps 6 to 16 are associated directly with data sampling and maybe input into a program directly by the SC command on the sequence page.

APPENDIX 2

Derivation of the DESPOT Equation

After the appropriate number of non-acquisition DESPOT sequences $(\theta-t-HS)_n$ where $t+HS=\tau$, the thermal equilibrium z-magnetization, M_0 will be driven to an equilibrium position, M_{zeq}, assuming complete T_2^* relaxation in the time, τ. The equilibrium position is shown in Fig A2.1.
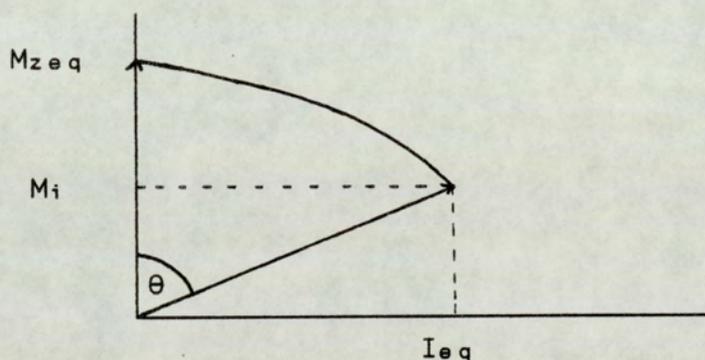
Fig. A2.1 Magnetization Vector at DESPOT Equilibrium

$$(M_0-M_i)\ exp(-\tau/T_1) = (M_0-M_{zeq}) \qquad (A2.1)$$

At equilibrium $M_i=M_{zeq}\cos\theta$, consequently (A2.1) can be rearranged to give

$$M_{zeq} = M_{zeq}\ \cos\theta\ exp(-\tau/T_1) + M_0(1-exp(-\tau/T_1)) \quad (A2.2)$$

A2.2 is then readily rearranged to give Eqn. 4.6. Due to the configuration of the receiver coils in most commercial spectrometers the intensity of the signal measured at equilibrium equals

$$I_{eq} = KM_{zeq} \sin \theta \qquad (A2.3)$$

where K is a spectrometer constant.

Hence, (A2.3) can be readily rearranged to give Eqn 4.7 and the linear DESPOT equation, equation 4.8.

Combining (A2.2) with (A2.3) gives

$$I_{eq} = \frac{KM_0 \sin \theta (1-\exp(-\tau/T_1))}{(1-\cos \theta \exp(-\tau/T_1))} \qquad (A2.4)$$

cf Eqn 4.7 which is readily rearranged to give the linear form

$$\frac{I_{eq}}{\sin \theta} = \frac{I_{eq} \cos \theta \exp(-\tau/T_1)}{\sin \theta} + KM_0 (1-\exp(-\tau/T_1)) \qquad (A2.5)$$

cf Eqn. 4.8.

APPENDIX 3

Incomplete T_2^* Relaxation and DESPOT T_1

The DESPOT equation of Sec 4.3.1 is only valid
provided that there is no transverse component of the
magnetization left when the $\theta(x)$ pulse is applied. When a
z-field gradient spoiling pulse is not included this may not
be the case and the DESPOT equation under these
circumstances must be modified to account for incomplete T_2^*
relaxation. The derivation of the modified equation is
presented below based on Fig A3.1.
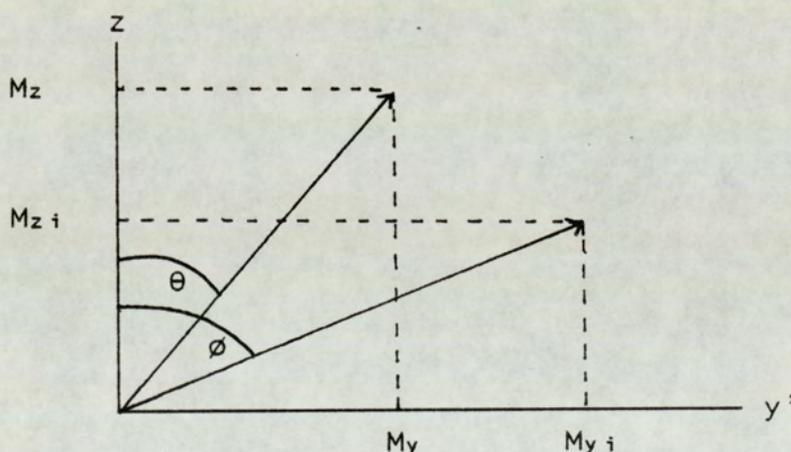
Fig. A3.1 Magnetization Component, M_z, at Equilibrium with
incomplete T_2^* relaxation

The above figure assumes that the system has been driven to
an equilibrium position where θ represents the nutation
pulse and where the total pulse repetition time equals τ.

My Component

$M_y = M_{yi} \exp(-\tau/T_2^*)$

$$M\sin(\emptyset-\theta) = M\sin\emptyset \exp(-\tau/T_2^*)$$

therefore

$$\cos\theta - \frac{\cos\emptyset}{\sin\emptyset} \sin\theta = \exp(-\tau/T_2^*) \qquad (A3.1)$$

M_z Component

$$(M_0 - M\cos(\emptyset-\theta)) = (M_0 - M\cos\emptyset)\exp(-\tau/T_1)$$

$$M_0 - M(\cos\emptyset\cos\theta + \sin\emptyset\sin\theta) = (M_0 - M\cos\emptyset)\exp(-\tau/T_1)$$

$$M_0 - M\cos\emptyset\left[\cos\theta + \frac{\sin\emptyset}{\cos\emptyset}\sin\theta\right] = (M_0 - M\cos\emptyset)\exp(-\tau/T_1)$$

substitute (A3.1)

$$M_0 - M\cos\emptyset\left[\cos\theta + \frac{\sin^2\theta}{\cos\theta - \exp(-\tau/T_2^*)}\right] = (M_0 - M\cos\emptyset)\exp(-\tau/T_1)$$

$$M_0(1 - \exp(-\tau/T_1)) = M\cos\emptyset\left[\cos\theta + \frac{\sin^2\theta}{\cos\theta - \exp(-\tau/T_2^*)} - \exp(-\tau/T_1)\right]$$

Combine with A3.1 noting that $M\cos\emptyset = I_{eq}\cos\emptyset/\sin\emptyset$ and putting $A = \exp(-\tau/T_1)$ and $B = \exp(-\tau/T_2^*)$

$$M_0(1-A) = I_{eq}\left[\frac{\cos\theta-B}{\sin\theta}\right]\left[\cos\theta + \frac{\sin^2\theta}{\cos\theta-B} - A\right]$$

$$M_0(1-A) = I_{eq}\left[\frac{\cos^2\theta-\cos\theta B}{\sin\theta} + \sin\theta - \frac{A\cos\theta + AB}{\sin\theta}\right]$$

$$M_0(1-A) = \frac{I_{eq}}{\sin\theta}\left[\cos^2\theta - \cos\theta B + \sin^2\theta - A\cos\theta + AB\right]$$

$$M_0(1-A) = \frac{I_{eq}}{\sin\theta}\left[1 - \cos\theta(A+B) + AB\right] \qquad (A3.2)$$

Eqn. A3.2 can then be rearranged to give Eqn 5.1

$$I_{eq} = \frac{M_0 \sin\theta(1-A)}{1 - \cos\theta(A+B) + AB} \qquad (A3.3)$$

Eqn. A3.3 can also be readily rearranged to give the linear form of Eqn 5.1

$$\frac{I_{eq}}{\sin\theta} = \frac{I_{eq}\cos\theta\ (A+B)}{\sin\theta\ (1+(AB))} + \frac{M_0(1-A)}{1+(AB)} \qquad (A3.4)$$

APPENDIX 4

Off-Resonance Effects in DESPOT T_1 Determinations

A4.1 Magnetization components after off-resonance nutation pulse

A typical magnetization component whose resonant position is $\Delta\nu$ Hz from the carrier frequency in the rotating frame of reference will be nutated perpendicular to an effective field B_{eff} (Fig. A4.1)
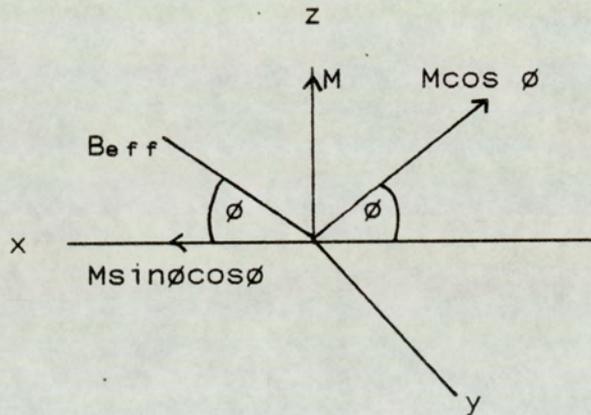
Fig. A4.1 Nutation of magnetization component, M, perpendicular to B_{eff}

$$B_{eff} = \sqrt{(B_1^2 + \Delta B^2)} \qquad (A4.1)$$

where B_1 is the pulse field strength and $\Delta B = (2\pi\Delta\nu/\gamma)$ is the residual z-field due to the off-carrier frequency shift at the resonance. B_{eff} is also tilted with respect to the x' axis at an angle ϕ in the x'z plane (Fig A4.1)

$$\phi = \tan^{-1}(\Delta B/B_1) \qquad (A4.2)$$

For a pulse of duration, t_p, an on-carrier frequency component ($\Delta\nu=0$) will be nutated through an angle θ perpendicular to the x' axis in the zy' plane.

$$\theta = \gamma B_1 t_p \qquad (A4.3)$$

For a pulse duration, t_p, off-carrier components will be nutated through a larger angle, α, in a plane perpendicular to B_{eff}

$$\alpha = \gamma B_{eff} t_p \qquad (A4.4)$$

Combining A4.4 with A4.1

$$\alpha = \gamma t_p \sqrt{(B_1{}^2 + \Delta B^2)} \qquad (A4.5)$$

Combining (A4.5) with (A4.2)

$$\alpha = \gamma t_p B_1 \sqrt{(1+\tan^2\phi)} \qquad (A4.6)$$

but $\sqrt{(1+\tan^2\phi)} = 1/\cos\phi$

therefore $\alpha = \gamma B_1 t_p / \cos\phi = \theta/\cos\phi$ (from A4.3) $\qquad$ (A4.7)

From Fig A4.1, B_{eff} rotates the component of M ($M\cos\phi$) through the angle α perpendicular to the direction of B_{eff}. Fig A4.2 shows the situation looking in the plane perpendicular to the direction of B_{eff} and along the B_{eff} axis.
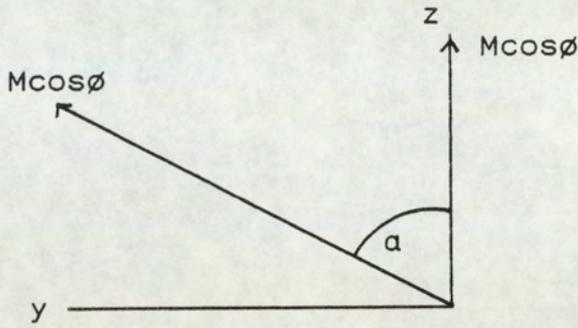
Fig. A4.2 <u>Nutation of magnetization component, M, by α° looking in the plane perpendicular to B_{eff} and along B_{eff} axis</u>

From Fig A4.2 the component of the magnetization along the y axis after rotation by an angle, α, perpendicular to B_{eff} is given by

$$M_y = M\cos\emptyset\sin\alpha \qquad (A4.8)$$

From Fig A4.2, after the α pulse the z-component that may be acted on by B_{eff} will equal Mcos∅cosα. Referring back to Fig A4.1 shows that this represents a total magnetization component along B_{eff} equal to Msin∅-Mcos∅cos α. Resolving this component along the x' axis of the rotating frame gives

$$M_x = M\sin\emptyset\cos\emptyset - M\cos\emptyset\sin\emptyset\cos\alpha \qquad (A4.9)$$

Now the component M_z can be found via vector addition as

$$M_z^2 = M^2 - M_x^2 - M_y^2 \qquad (A4.10)$$

therefore

$M_z{}^2 = M^2 - M^2 \sin^2\emptyset\cos^2\emptyset(1-\cos\alpha)^2 - M^2\cos^2\emptyset\sin^2\alpha$

$M_z{}^2 = M^2\{1-\sin^2\emptyset\cos^2\emptyset(1-2\cos\alpha+\cos^2\alpha)-\cos^2\emptyset\sin^2\alpha\}$

$M_z{}^2 = M^2(1-\sin^2\emptyset\cos^2\emptyset+2\sin^2\emptyset\cos^2\emptyset\cos\alpha-\sin^2\emptyset\cos^2\emptyset\cos^2\alpha$
$\phantom{M_z{}^2 = M^2(1} -\cos^2\emptyset\sin^2\alpha)$

$M_z{}^2 = M^2(1-2\sin^2\emptyset\cos^2\emptyset+2\sin^2\emptyset\cos^2\emptyset\cos\alpha+\cos^2\emptyset\sin^2\alpha(\sin^2\emptyset-1))$

$M_z{}^2 = M^2(1-2\sin^2\emptyset\cos^2\emptyset+2\sin^2\emptyset\cos^2\emptyset\cos\alpha-\cos^4\emptyset\sin^2\alpha)$

$M_z{}^2 = M^2(1-2\sin^2\emptyset+2\sin^4\emptyset+2\sin^2\emptyset\cos^2\emptyset\cos\alpha-\cos^4\emptyset+\cos^4\emptyset\cos^2\alpha)$

but $\cos^4\emptyset = 1-2\sin^2\emptyset+\sin^4\emptyset$

$M_z{}^2 = M^2(\sin^4\emptyset+2\sin^2\emptyset\cos^2\emptyset\cos\alpha+\cos^4\emptyset\cos^2\alpha)$

therefore taking roots and denoting M_z before and after the pulse as $M_z{}^-$ and $M_z{}^+$ respectively

$M_z{}^+ = M_z{}^-(\sin^2\emptyset+\cos\alpha\cos^2\emptyset) = kM_z{}^-$ (cf Eqn. 5.7)   (A4.11)

Now the signal detected in the xy plane, M_{xy} can be found by vector addition of the M_x and M_y components from Eqns A4.8 and A4.9

$M_{xy}{}^2 = M^2\cos^2\emptyset\sin^2\alpha+M^2\sin^2\emptyset\cos^2\emptyset(1-\cos\alpha)^2$

$M_{xy}{}^2 = M^2\cos^2\emptyset(\sin^2\alpha+\sin^2\emptyset(1-\cos\alpha)^2)$

Therefore, denoting the M_{xy} component after the pulse as $M_{xy}{}^+$

$M_{xy}{}^+ = M_z{}^-\cos\emptyset\sqrt{(\sin^2\alpha+\sin^2\emptyset(1-\cos\alpha)^2)} = \beta M_z{}^-$ (cf Eqn 5.8) (A4.12)

A4.2 <u>Off-Resonance and DESPOT</u>

        Fig. A4.3 shows the situation for a DESPOT analysis when equilibrium has been achieved
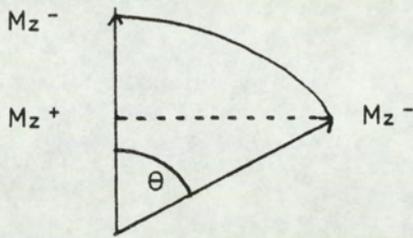
Fig. A4.3 Off-resonance vector at DESPOT equilibrium

During the total pulse repetition time, τ, M_z^+ will relax to M_z^-, hence from Eqn A4.11 kM_z^- relaxes to M_z^- in the time, τ. From the derivation of appendix 2 substituting M_{zeq} for M_z^- and kM_z^- for $M_{zeq}\cos\theta$

$$M_{zeq} = M_z^- = \frac{M_0(1-\exp(-\tau/T_1))}{(1-k\exp(-\tau/T_1))} \quad \text{(cf Eqn. 5.9)} \qquad \text{(A4.13)}$$

M_{zeq} cannot be measured directly, but only as a component in the xy plane, hence the measured intensity, I_{eq}, from Eqns A4.12 and A4.13 can be rewritten as

$$M_{xy} = I_{eq} = \frac{\beta M_0(1-\exp(-\tau/T_1))}{1-k\exp(-\tau/T_1))} \qquad \text{(A4.14)}$$

Eqn A4.14 can be rearranged readily to give a form suitable for a linear plot

$$\frac{I_{eq}}{\beta} = \frac{I_{eq}\,\acute{e}xp(-\tau/T_1)k}{\beta} + M_0(1-\exp(-\tau/T_1)) \qquad \text{(A4.15)}$$

APPENDIX 5

Derivation of the One Pulse Dummy DESPOT Equation

The equilibrium z-magnetization for an absorption with a known T_1 value can be calculated via Eqn. (A2.2) for given values of τ(the total pulse sequence repetiton time) and nutation angle θ. If we assume that the z-magnetization is initially at thermal equilibrium and we apply a nutation pulse θ_2 to the spin system then immediately following the θ_2 pulse the z-magnetization, M_z^+, is given by

$$M_z^+ = M_0 \cos \theta_2 \qquad (A5.1)$$

If the resulting z-magnetization is allowed to relax towards M_0 for a time, τ, the resulting z-magnetization, $M_z(\tau)$ will be given by

$$M_z(\tau) = M_0 - ((M_0 - M_z^+) \exp(-\tau/T_1)) \qquad (A5.2)$$

therefore combining Eqn's A5.1 and A5.2 and rearranging gives

$$M_z(\tau) = M_0 \{1 - [\exp(-\tau/T_1)(1 - \cos \theta_2)]\} \qquad (A5.3)$$

If $M_z(\tau)$ is set equal to M_{zeq} for a known value of τ and θ then Eqn. A5.4 can be written

$$M_0\{1-[\exp(-\tau/T_1)(1-\cos\theta_2)]\} = \frac{M_0(1-\exp(-\tau/T_1)}{1-\cos\theta\,\exp(-\tau/T_1)} \qquad (A5.4)$$

Eqn. A5.4 can now be rearranged after cancelling out the M_0 values in terms of θ_2 to give

$$\theta_2 = \cos^{-1}\left[\frac{(1-\exp(-\tau/T_1))\,(\cos\theta\,\exp(-\tau/T_1))}{(1-\cos\theta\,\exp(-\tau/T_1))\,\exp(-\tau/T_1)}\right] \qquad (A5.5)$$

cf Eqn. 5.12

APPENDIX 6

One Pulse Dummy Pulse Program

During a DESPOT analysis the equilibrium condition for specified values of τ/T_1 and θ can sometimes require many non-acquisition sequences of the type $(\theta-t-HS)_n$ where n is the number of repetitions required to reach equilibrium and $t+HS=\tau$. The use of one preconditioning sequence of the type (θ_2-t-HS) causes equilibrium to be established after only one sequence provided that θ_2 is obtained from Eqn. 5.12. As θ_2 is invariably different to θ it is not possible to use the single pulse sequence (Sec. A1.4). Consequently a new pulse sequence had to be written to allow the preconditioning pulse to be applied. This pulse sequence was called 1pdum and is presented below. Details of the PG200 pulse programmer can be found in appendix 1

The 1pdum Pulse Sequence

Address	K C B A 8 7 J 5 4 3 2 1	Command	Parameter
0	. . . .		
1		TIM	9
2	. . . . *		
3		TIM	2
4	. . . *		
5		TIM	10
6	. . . .		
7		TIM	11

1pdum pulse sequence(cont.)

Address	K	C	B	A	8	7	J	5	4	3	2	1	Command	Parameter
8	.	.	.	.	*	.	.	.	.	.	.	.		
9													TIM	7
10	.	.	.	.	*	.	.	.	.	.	.	*		
11													TIM	1
12	.	.	.	.	*	.	.	.	*	.	.	.		
13													TIM	8
14													PUL	
15													LD2	1
16	.	.	.	.	*	.	.	*	*	.	.	.		
17													TIM	6
18	.	.	.	.	*	*	.	*	*	.	.	.		
19													INT	5
20	.	.	.	.	*	.	.	*	*	.	.	.		
21													INT	5
22													JC2	18
23	.	.	.	*	.	.	.	.	.	.	.	.		
24													TIM	10
25	.	.	.	.	.	.	.	.	.	.	.	.		
26													TIM	4
27													JMP	8

It can be seen by examination of the above sequence
that the required preconditioning pulse is applied at lines
2 and 3 using the PW2** parameter. The time TIM 11
(address7) enables the time, τ, to be accurately set. At
address 27 the program jumps to address 8 which is the
beginning of the single pulse sequence (Sec. A1.4). Device A

is set as a z-field gradient spoiling pulse in the DEVICE
pattern.

APPENDIX 7

Differentiation of DESPOT Type Equations

The DESPOT equation and its variant that compensates for incomplete T_2^* relaxation have the general form (cf Eqn's 4.8 and 5.2)

$$\frac{I_{eq}}{\sin \theta} = \frac{I_{eq}\cos \theta \, A}{\sin \theta} + B \qquad (A7.1)$$

where I_{eq} is the measured intensity at equilibrium, θ is the on-resonance nutation angle and A and B are constant terms. Multiplication of A7.1 by $\sin \theta$ followed by differentiation with respect to θ yields

$$\frac{dI_{eq}}{d\theta} = A \left[-I_{eq} \sin\theta + \frac{dI_{eq}}{d\theta} \cos \theta \right] + B\cos \theta \qquad (A7.2)$$

Now at the turning point (maximum) $dI_{eq}/d\theta=0$ and Eqn. (A7.2) reduces to

$$I_{eq}A\sin \theta = B\cos \theta \qquad (A7.3)$$

Rearranging Eqn. A7.1 yields

$$I_{eq} = \frac{B\sin \theta}{(1- A\cos \theta)} \qquad (A7.4)$$

Rearranging and combining Eqn. (A7.4) with Eqn. (A7.3) yields

$$AB\sin^2 \theta = B\cos\theta - AB\cos^2 \theta \qquad (A7.5)$$

Rearranging and recalling that $\sin^2\theta + \cos^2\theta =1$

$$A = \cos \theta \qquad (A7.6)$$

Hence the maximum of a plot of I_{eq} against θ will occur when the relationship of Eqn. A7.6 is fulfilled. Consequently for a normal DESPOT plot with complete T_2^* relaxation between pulse sequence repetitions, the maximum of a plot of I_{eq}

against θ will occur when

$$\cos \theta = \exp(-\tau/T_1) \tag{A7.7}$$

which is the Ernst condition, (Sec. 4.3.2 and 6.2). When $T_2{}^*$ relaxation is incomplete the maximum in a plot of I_{eq} against θ will occur when

$$\cos \theta = \frac{\exp(-\tau/T_1) + \exp(-\tau/T_2{}^*)}{1 + \exp(-\tau/T_1)\ \exp(-\tau/T_2{}^*)} \tag{A7.8}$$

This is the modified Ernst condition of Sec. 6.5

APPENDIX 8

The DESPOT $T_{1\rho}$ Pulse Sequence

The pulse program presented below was used to model the DESPOT $T_{1\rho}$ sequence presented as Fig. 7.1. An explanation of the PG200 pulse programmer is presented in Appendix 1.

The T1RS2 Pulse Sequence

Address	K	C	B	A	8	7	J	5	4	3	2	1	Command	Parameter
0	.	.	.	.	.	.	.	.	.	.	.			
1													TIM	9
2	.	.	.	.	.	.	.	.	.	.	.	*		
3													TIM	2
4	.	.	.	.	.	.	.	.	.	.	.	.		
5	.	.	.	*	.	.	.	.	.	.	.	.		
6													TIM	10
7	.	.	.	.	.	.	.	.	.	.	.	.		
8													TIM	11
9	.	.	.	.	.	.	.	.	.	.	*			
10													TIM	2
11	.	.	.	.	.	.	.	.	.	.	.	.		
12	.	.	.	*	.	.	.	.	.	.	.	.		
13													TIM	10
14	.	.	.	.	.	.	.	.	.	.	.	.		
15													TIM	13
16	.	.	.	.	.	.	.	.	.	.	*			

(T1RS2 Program cont.)

Address	K	C	B	A	8	7	J	5	4	3	2	1	Command	Parameter
17													TIM	1
18	.	.	.	.	.	.	.	.	.	.	.	.		
19													TIM	11
20	.	.	.	*	.	.	.	.	.	.	.	.		
21													TIM	10
22	.	.	.	.	.	.	.	.	.	.	.	.		
23													TIM	13
24	.	.	.	.	.	.	.	.	.	.	.	*		
25													TIM	2
26	.	.	*	.	.	.	.	.	.	*	.	.		
27													TIM	11
28	.	.	*	.	.	.	.	.	.	*	.	*		
29													TIM	3
30	.	.	.	.	*	.	.	.	.	*	.	.		
31													TIM	8
32													PUL	
33													LD2	1
34	.	.	.	.	*	.	.	*	*	.	.	.		
35													TIM	6
36	.	.	.	.	*	*	.	*	*	.	.	.		
37													INT	5
38	.	.	.	.	*	.	.	*	*	.	.	.		
39													INT	5
40													JC2	36
41	.	.	.	*	.	.	.	.	.	.	.	.		
42													TIM	10
43	.	.	.	.	.	(T1RS2 Program	.	.		

(T1RS2 Program cont.)

Address	K C B A 8 7 J 5 4 3 2 1	Command	Parameter
44		TIM	4
45		JMP	2

In the above program TIM 2 (PW2) is a 90°(x) pulse, TIM 1 (PW1) is a θ°(x) pulse, TIM 3 (PI***) is the spin-lock time, τ and TIM 13 is the relaxation time T. TIM 11 is set at 10μs and is a short delay to enable switching of the spectrometer phase.

APPENDIX 9

Spin-Locking on the JEOL FX90Q Spectrometer

A9.1 Introduction

Owing to the nature of the spin-locking experiment it is essential that the strength of the spin-locking field and the phase of the spin-locking pulse are accurately adjusted. The spin-lock unit on the JEOL FX90Q spectrometer allows adjustment of the strength of the spin-locking field via the calibration potentiometer or via the power output control. The function of the calibration level potentiometer is to set the spin-lock field strength to a maximum of half the B_1 field strength. This is the maximum spin-lock field strength recommended by the instrument manufacturers (146) and serves to prevent damage to the probe insert due to excessive heating during long spin-lock pulses. Nevertheless care is still required, it is essential that the air flow through the probe is sufficient ($>15L/min$) to cause extra cooling and that the field strength set is within the limitations for the probe insert and nucleus studied as laid out in reference (146). It is also necessary to ensure that the maximum duty cycle of the spin-lock unit is no greater than $\frac{1}{4}$ of the experimental time. For experiments which involve varying the strength of the spin-lock field (Sec. 2.6.1) this can be achieved readily using the power output control keeping the calibration level control constant.

It is also important in a spin-locking experiment that the spin-locking pulse is applied down the y axis of the rotating frame. In order to set the phase of the spin-locking pulse accurately, adjustments to the phase of the locking pulse can be made via the phase control on the spin-lock unit. The necessary adjustments to the spin-lock field strength and the phase of the locking pulse were made using the SPINCAL program.

A9.2 The SPINCAL Program

The SPINCAL program in essence is identical to single pulse program (Sec. A1.4) except that the nutation pulse is provided by the spin-lock unit down the y axis of the rotating frame. The SPINCAL program is reproduced below. An explanation of some aspects of programming the PG200 pulse programmer can be found in Appendix 1.

Address	K	C	B	A	8	7	J	5	4	3	2	1	Command	Parameter
0	.	.	.	.	.	.	.	.	.	.	.	.		
1													TIM	9
2	.	.	.	.	.	.	.	.	.	.	.	.		
3	.	.	.	.	.	.	.	.	.	.	.	.		
4	.	.	*	.	.	.	.	.	.	*	.	.		
5													TIM	11
6	.	.	*	.	.	.	.	.	.	*	.	*		
7													TIM	3
8	.	.	.	.	*	.	.	.	.	*	.	.		

SPINCAL Program (cont.)

Address	K	C	B	A	8	7	J	5	4	3	2	1	Command	Parameter
9													TIM	8
10													PUL	
11													LD2	1
12	.	.	.	.	*	.	.	*	*	.	.	.		
13													TIM	6
14	.	.	.	.	*	*	.	*	*	.	.	.		
15													INT	5
16	.	.	.	.	*	.	.	*	*	.	.	.		
17													INT	5
18													JC2	14
19	.	.	.	*	.	.	.	.	.	.	.	.		
20													TIM	10
21	.	.	.	.	.	.	.	.	.	.	.	.		
22													TIM	4
23													JMP	4

External 1 (A) is set as HS i.e. a z-field spoiling pulse. External 2 (B) is set as OBSLV. This selects the spin-lock unit and turns the noise off the decoupler. The time TIM 11 is set to 10 μs and allows time for the spin-lock unit to be selected and for the 90° phase shift (address 4 bit 3) to occur. The rest of the program is similar to the single pulse program (Sec A1.4).

A9.3 Use of the SPINCAL Program

A spectrum of the sample is first obtained using the

single pulse program and is phased noting the values of P0 and P1. PW1** is then varied until a value for the 90° pulse has been obtained. This was usually achieved in our laboratory by looking for a null signal at 180° and halving that value to get the 90° pulse. Obtain a spectrum of the sample using the SPINCAL program (PUMOD 3) with PI*** set to 2 times the value of PW1** required to give a 90° pulse using the single pulse program with the cal level potentiometer set to zero and the power level set to max. Phase this spectrum and then increase the value of the cal level until a 90° pulse is obtained (this may be best achieved by looking for a null at 180°). When the 90° pulse width using the SPINCAL program is exactly twice the 90° pulse width using the single pulse program, lock the cal level potentiometer. Switch back to the single pulse program (PUMOD 1) and obtain a spectrum of the sample with a 90° pulse and phase it accurately noting the values of P0 and P1. Now add 90 to the value of P0 and save the phase. Switch back to the SPINCAL program and obtain a spectrum using a 90° pulse. On fourier transformation note the phase of the resulting spectrum. If the spectrum is not in the absorption mode turn the phase knob on the spin-lock unit and reacquire the spectrum until an absorption mode spectrum is obtained. After these adjustments have been made the spin-locking power and phase should be correctly adjusted. When acquiring data using the SPINLOCK (110,146) or the T1RHOD2 program (Sec 7.5.3, Appendix 8) ensure that the setting of P0 is returned to its original noted value.

APPENDIX 10

The D.E.P.T Sequence

A10.1 Introduction

It is well known that the D.E.P.T sequence (38) has gained marked popularity in ^{13}C spectroscopy in recent years due to its potential as a spectral assignment and editing tool. The technique is based on coherence transfer and as such only ^{13}C nuclei with attached protons are detected. The sequence as originally proposed by Doddrell et al. is shown below

^{1}H $\pi/2(y)$ —1/2J——π——1/2J——$\theta(\pm x)$——1/2J——decouple

^{13}C $\pi/2(x)$ π acquire

As can be seen from the above sequence the method relies on applying pulses both on the observation channel (^{13}C) and on the proton decoupler channel. Spectral editing is achieved by varying the length of the θ pulse on the decoupler. The CH, CH$_2$ and CH$_3$ absorptions have the following mathematical dependencies on the angle θ: $\sin \theta$ for CH; $\sin 2\theta$ for CH$_2$ and $\sin \theta + \sin 3\theta$ for CH$_3$. As a consequence, if θ is selected to be 90° then a ^{13}C spectrum should only show absorptions due to CH moieties and therefore the D.E.P.T sequence can be used readily to measure the 90° proton decoupler pulse width. The sequence was used for this purpose in order to prevent Hartmann-Hahn matching in our

spin-locking experiments (Sec. 7.5.3).

A10.2 D.E.P.T on the JEOL FX90Q Spectrometer

The D.E.P.T sequence can be run on the JEOL FX90Q spectrometer by writing the appropriate pulse program for the PG200 pulse programmer (Appendix 1). Such a sequence was supplied by JEOL and is reproduced below. The sequence supplied by JEOL is slightly different to that of Doddrell et al (38) with the original π/2 decoupler pulse being applied along the x axis with the final θ pulse being alternated between the ±y axes. The Jeol sequence also alternates the phase of the spin-echo refocussing π pulses on both the proton and carbon channels in order to reduce cumulative errors due to misset pulse angles (Sec 7.2). The corrected PG200 pulse program presented below has a 180° observation channel phase shift at lines 19 and 21 instead of a 90° phase shift in the original JEOL supplied sequence which was in error.

Address	K	C	B	A	8	7	J	5	4	3	2	1	Command	Parameter
0	.	*	.	.	.	.	.	.	.	.	.	.		
1													TIM	19
2													LD1	3
3	.	*	.	.	*	.	.	.	.	.	.	.		
4													TIM	9
5													TIM	1
6	.	*	.	.	.	.	.	.	.	.	.	.		
7													TIM	3

D.E.P.T Sequence (cont)

Address	K	C	B	A	8	7	J	5	4	3	2	1	Command	Parameter
8													JC1	38
9	.	*	.	.	*	.	*	.	.	.	.	.		
10													TIM	9
11													TIM	9
12													TIM	1
13	.	*	.	.	*	.	*	.	.	.	.	*		
14													TIM	1
15	*	*	.	.	.	.	*	.	.	.	.	.		
16													TIM	3
17	*	*	.	.	*	.	*	.	.	.	.	.		
18													TIM	7
19	.	.	.	.	.	.	.	.	.	.	*	.		
20													TIM	11
21	.	.	.	.	.	.	.	.	.	.	*	*		
22													TIM	2
23	.	.	.	.	.	.	.	*	.	.	.	.		
24													TIM	3
25													PUL	
26													LD2	1
27	.	.	.	.	*	.	.	*	*	.	.	.		
28													TIM	6
29	.	.	.	.	*	*	.	*	*	.	.	.		
30													INT	5
31	.	.	.	.	*	.	.	*	*	.	.	.		
32													INT	5
33													JC2	29
34	.	.	.	.	.	.	.	.	.					

D.E.P.T Sequence (cont)

Address	K	C	B	A	8	7	J	5	4	3	2	1	Command	Parameter
35													TIM	4
36													JC1	3
37													JMP	2
38	.	*	.	.	*	.	.	.	.	.	.	.		
39													TIM	9
40													TIM	9
41													TIM	1
42	.	*	.	.	*	.	.	.	.	.	.	*		
43													TIM	1
44	*	*	.	.	.	.	.	.	.	.	.	.		
45													TIM	3
46	*	*	.	.	*	.	.	.	.	.	.	.		
47													TIM	7
48	.	.	.	.	.	.	.	.	.	.	.	.		
49													TIM	11
50	.	.	.	.	.	.	.	.	.	.	.	*		
51													TIM	2
52													JMP	23

The above program gives the following sequence

^1H $\pi/2(x)$——$1/2J$——$\pi(\pm x)$——$1/2J$——$\theta(\pm y)$——$1/2J$——decouple

^{13}C $\pi/2(x)$——$1/2J$——$\pi(\pm x)$——$1/2J$——acquire

with the differences between this sequence and the original sequence explained above. External 3 (C) was set as OBSLV in the sequence and the decoupling mode is set as NNE. The times delays, mnemonics, functions, and actual times used

in our experiment are detailed below.

Table A10.1

D.E.P.T Sequence Timings

Time	Mnemonic	Function	Time
TIM 1	PW1**	90° ^{13}C Pulse	(23 µs)
TIM 2	PW2**	180° ^{13}C Pulse	(46 µs)
TIM 3	PI***	1/2J	(3.5 ms)
TIM 4	PD***	1.2 T_1 (H) minus acquisition time	(3 s)
TIM 6	DELAY	Delay time prior to sampling	(150 µs)
TIM 7	PREDL	Decoupler θ pulse {90°}	(32 µs)
TIM 9	INIWT	90°^{1}H minus 90°^{13}C pulse width	(9 µs)
TIM 11	-	Time to allow for phase change	(5 µs)
TIM 19	-	Initial Wait	(2 s)

Care should be taken that the 90° and 180° observation pulses are set using the SPINCAL program (Appendix 9) as these pulses are derived via the spin-lock unit and that LO3 is set at 1.

Conditions for the Driven Equilibrium Single Pulse Observation of Spin–Lattice Relaxation Times

JOHN HOMER* AND JOHN K. ROBERTS

Department of Chemical Engineering and Applied Chemistry, Aston University, Aston Triangle, Birmingham B4 7ET, England

Conditions governing the most satisfactory implementation of the DESPOT (*d*riven *e*quilibrium *s*ingle *p*ulse *o*bservation of T_1) method of measuring NMR spin–lattice relaxation times are discussed. The determination of the number of nonacquisition, dummy pulses, required to drive a spin system to the DESPOT equilibrium condition is reexamined. It is shown that an improved condition for the achievement of equilibrium minimizes the errors in experimentally determined values of T_1. Spectrometer pulse width–nutation angle calibration and sample diffusion are discussed. © 1987 Academic Press, Inc.

INTRODUCTION

The recent reevaluation of the "variable nutation angle method" for the rapid measurement of T_1 (for convenience renamed the DESPOT method) (*1*) has been extended. It has been found that where long T_1 values are involved the measurements are sensitive to experimental conditions. This has led to the reevaluation of the number of dummy pulses needed to achieve the DESPOT equilibrium condition. Additionally, investigations of the spectrometer pulse width–nutation angle relationship and the spectrometer "pulse offset" (*1*) have been found to be influenced by diffusion in liquid samples. The purpose of this paper is to present the relevant aspects of these investigations.

THEORETICAL BASIS OF DESPOT

For any single-spin system, the transient magnetization, M_z, during relaxation recovery from an initial value, M_i, toward the Boltzmann equilibrium value, M_0, is given by

$$M_z = M_0 - (M_0 - M_i)e^{-t_i/T_1}, \qquad [1]$$

where t_i is the total pulse repetition time. If a system is subject to rapid multipulsing, using the sequence $(\theta\text{–FS–}t)_n$, at an angle θ followed by a field-spoiling z-gradient pulse (FS), the magnetization, M_z, also follows Eq. [1]. Ultimately the system is driven to equilibrium whereafter the equilibrium magnetization, M_{zeq}, can be acquired (A) by m pulse sequences of the form $(\theta\text{–A–FS–}t^*)_m$. The times t and t^* ensure that the dummy and acquisition sequences have a constant total repetition time such that

* To whom correspondence should be addressed.

$t_i = FS + t$ and $t_i = FS + A + t^*$ in the respective cases. The DESPOT equilibrium magnetization is given by

$$M_{zeq} = M_{zeq}\cos\theta e^{-t_i/T_1} + M_0(1 - e^{-t_i/T_1}).$$ [2]

By determining values for M_{zeq} at various θ's, it is possible to determine T_1 from Eq. [2]. Because of the detector coil configuration of many commercial spectrometers, M_{zeq} can be determined readily from signal intensities (I) using

$$I_{eq} = KM_{zeq}\sin\theta,$$ [3]

where K is a spectrometer constant. T_1 can then be obtained from the regression of $I/\sin\theta$ on $I\cos\theta/\sin\theta$, appropriate to Eq. [2].

The DESPOT method applies rigorously to spin systems for which single exponential relaxation is appropriate. In certain other cases, for example $\{^1H\}-^{13}C$, complete decoupling can make a multiexponential relaxation system obey a single exponential recovery so that DESPOT will be valid for these systems. In other cases where this is not feasible, DESPOT should, in principle, not be applicable (2). However, in such cases it is usual, as when using the (180°–τ–90°) sequence, to take advantage of the fact (2) that the initial magnetization data on recovery of the perturbed system essentially show single exponential behavior. Provided that t_i/T_1 and the acquisition time in the DESPOT method are short, it is possible that the magnetization data for the equilibrium cycles will approximate to single exponential behavior (this is currently the subject of further investigation). In the relevant circumstances DESPOT should be widely applicable.
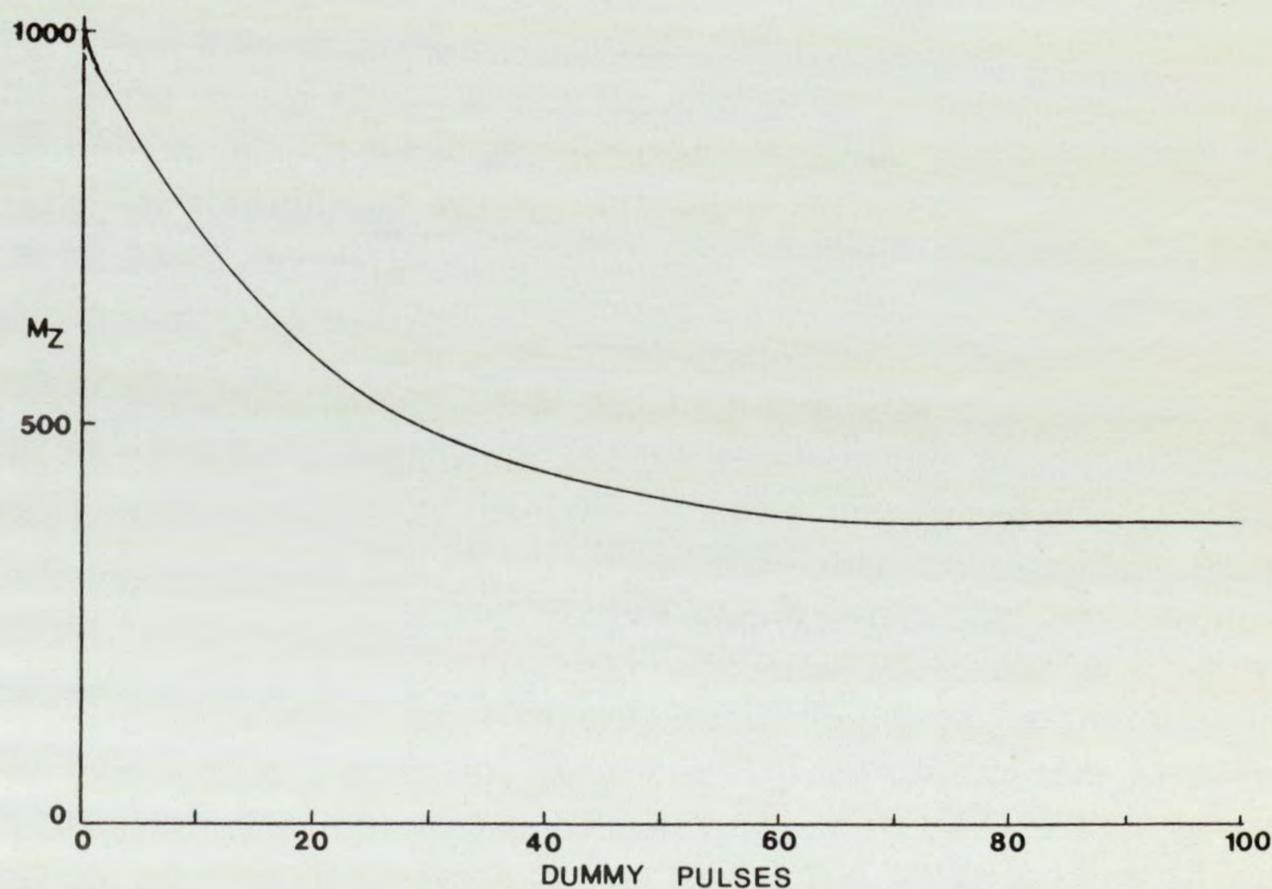

FIG. 1. Variation of the magnetization vector, M_z, with the number of dummy DESPOT sequences; $t_i/T_1 = 0.02$, $\theta = 15°$.

THE NUMBER OF DUMMY PULSES TO ACHIEVE EQUILIBRIUM

Under certain experimental conditions, the equilibrium condition for DESPOT can be approached quite slowly. This is illustrated in Fig. 1. Because it is impractical to wait for the actual equilibrium position to be achieved, a compromise is sought that introduces negligible errors into the analysis of the experimental data. In an earlier paper (*1*) the compromise chosen was such that after n dummy pulses

$$1.005M_{z(n-1)} > M_{zn} > 0.995M_{z(n-1)}. \tag{4}$$

Recent work has revealed that this condition is inadequate in certain circumstances, particularly for the smaller nutation angles. It has been found that in order to overcome this problem an alternative condition should be used, which is

$$1.005M_{zeq} > M_{zn} > 0.995M_{zeq}, \tag{5}$$

where M_{zeq} is the true equilibrium magnetization. The number of dummy pulses required to fulfill this (new) condition and also the original condition (old) are given in Table 1 together with M_{zn} and M_{zeq} (based on $M_0 = 1000$) in order to illustrate the advantages of using condition [5] rather than [4].

It has been suggested elsewhere (*3, 4*) that as few as four dummy pulses can be used to achieve the driven equilibrium condition. This assumption is generally invalid and could lead to large experimental errors. Consequently, Table 1 also contains values for the z magnetization after four dummy pulses (M_{z4}) to illustrate this point.

It is evident from Table 1 that the large error, at small nutation angles, between the actual equilibrium value M_{zeq} and M_z derived from [4] or from M_{z4} is substantially reduced by the use of condition [5]. The use of condition [5], however, causes the number of dummy pulses required to increase markedly and hence prolong the experimental time. Superficially, therefore, it might appear wise when measuring T_1 to avoid the use of small nutation angles. This suggestion will be reviewed later.

Even using the new condition for calculating n, it is evident that true equilibrium need not have been achieved after employing the calculated number of dummy pulses. Consequently, during subsequent acquisition pulses, equilibrium will still be approached slowly. Obviously this will have some effect on the calculated values of T_1. This point has been investigated by computer simulation.

The various theoretical (nonequilibrium) magnetization data given in Table 1 were used to calculate the t_i/T_1 ratio and the value of M_0 that would be obtained using a linear regression analysis appropriate to Eq. [2]. The data were taken at 10° intervals. Table 2 presents the results that would be obtained after one acquisition pulse and with nutation angles varied within the ranges 10° to 80° and 40° to 130°. In both cases it can be seen that the new condition [5] yields the best results, with the four-pulse analysis being quite inadequate. It is interesting to note that the earlier suggestion that small nutation angles should be avoided does not appear to be sustained. The reason for this is that in the range 10° to 80° the greatest rate of change of M_{zeq} with θ occurs and the effect of this is to overwhelm small errors in "M_{zeq}." Table 3 presents similar results to those in Table 2 except that 50 acquisitions have been considered. Very similar conclusions can be drawn from these results, but with the further observation that the new condition [5] gives much improved results. Moreover, whereas

TABLE 1

The Numbers of Dummy Pulses Required to Achieve the Quoted z Magnetizations Approximating the DESPOT Equilibrium Condition for Selected Values of t_i/T_1

| t_i/T_1 | 0.05 | | | | | | 0.10 | | | | | | 0.20 | | | | | |
| angle/degs. | New [5] | | Old [4] | | 4-Pulse | Equil. | New [5] | | Old [4] | | 4-Pulse | Equil. | New [5] | | Old [4] | | 4-Pulse | Equil. |
	n	M_z	n	M_z	M_{z4}	M_{zeq}	n	M_z	n	M_z	M_{z4}	M_{zeq}	n	M_z	n	M_z	M_{z4}	M_{zeq}
5	51	935.4	1	996.4	986.6	930.9	20	969.5	1	996.6	988.1	965.1	7	987.2	2	994.3	990.6	983.1
10	63	775.2	20	833.3	947.4	771.4	30	877.7	11	909.3	953.4	873.8	13	939.7	6	953.4	962.9	935.8
15	58	603.7	29	635.0	885.3	600.7	31	759.1	17	780.1	898.1	755.3	15	870.6	9	882.8	918.8	866.6
20	49	461.7	30	478.2	804.6	459.5	30	638.4	19	652.3	826.0	635.6	16	789.1	11	797.9	860.9	785.9
25	40	355.4	28	363.8	710.7	353.7	27	531.1	19	539.7	741.9	528.9	15	706.0	12	710.9	792.8	702.7
30	33	278.0	25	282.5	609.8	276.8	23	441.8	18	446.7	651.0	439.8	14	626.1	12	629.1	718.3	623.0
35	27	221.8	22	224.1	508.1	220.9	20	369.3	16	373.0	558.5	367.7	13	552.9	11	556.0	641.3	550.4
40	22	180.5	19	181.8	411.0	179.8	17	311.5	15	313.0	469.4	310.1	12	488.1	11	489.3	565.7	486.2
45	18	149.6	16	150.5	323.2	149.0	15	265.1	13	266.4	387.5	264.2	11	431.9	10	432.9	494.5	430.5
50	15	126.1	14	126.4	247.7	125.5	13	228.1	12	228.6	315.9	227.5	9	384.6	9	384.6	430.0	382.6
55	13	107.7	12	108.0	186.4	107.3	11	198.4	11	198.4	256.0	197.8	8	343.3	9	342.5	373.8	341.8
60	11	93.3	11	93.3	139.4	93.0	9	174.4	9	174.4	208.4	173.8	7	308.2	8	307.5	326.3	306.9
65	9	81.8	9	81.8	105.5	81.6	8	154.5	8	154.5	172.2	154.1	6	278.4	7	277.6	287.5	277.2
70	7	72.6	8	72.4	82.7	72.3	7	138.0	7	138.0	145.7	137.8	6	252.1	6	252.1	256.4	252.8
75	6	64.9	7	64.8	68.1	64.5	5	124.9	6	124.4	126.9	124.3	5	230.3	6	230.1	231.6	230.0
80	5	58.5	6	58.4	59.1	58.4	4	113.4	5	113.0	113.4	112.9	4	211.6	5	211.4	211.6	211.3
85	4	53.2	5	53.2	53.2	53.2	3	103.7	4	103.3	103.3	103.3	3	195.5	4	195.2	195.2	195.2
90	1	48.8	1	48.8	48.8	48.8	1	95.2	1	95.2	95.2	95.2	1	181.3	1	181.3	181.3	181.3
95	4	45.1	5	45.0	45.1	45.0	4	88.2	5	88.2	88.2	88.2	3	168.9	4	169.2	169.2	169.2
100	5	41.7	6	41.9	42.6	41.9	5	82.2	6	82.3	82.8	82.2	4	159.0	5	158.7	159.0	158.7
105	7	39.1	8	39.1	42.7	39.1	6	77.3	7	77.1	79.9	77.1	5	149.2	6	149.7	151.3	149.6
110	8	36.9	9	36.8	47.6	36.8	7	72.4	8	72.8	81.2	72.7	6	142.0	7	141.5	146.9	141.6
115	10	34.9	11	34.7	60.0	34.8	9	68.7	10	68.9	88.7	68.8	7	134.2	9	134.6	147.1	134.7
120	12	33.2	14	33.1	82.5	33.1	11	65.4	12	65.6	104.7	65.5	9	128.3	10	128.7	153.1	128.6
125	15	31.4	17	31.5	117.4	31.6	13	62.5	14	62.7	130.7	62.6	10	123.8	12	123.4	166.0	123.3
130	18	30.4	20	30.3	165.8	30.3	15	59.9	17	60.1	167.7	60.2	12	119.2	14	118.9	186.4	118.8
135	23	29.1	25	29.1	227.9	29.2	19	57.8	21	58.0	215.9	58.0	14	115.2	16	114.9	214.2	114.8
140	28	28.4	31	28.2	302.2	28.2	23	56.0	25	56.1	274.1	56.2	16	111.9	18	111.6	248.9	111.4
145	36	27.5	39	27.4	385.9	27.4	28	54.9	31	54.6	340.0	54.7	19	108.1	21	108.3	288.9	108.5
150	46	26.9	50	26.8	475.0	26.8	34	53.6	37	53.2	410.3	53.4	22	106.5	25	105.9	332.0	106.1
155	61	26.1	66	26.2	564.1	26.2	42	52.5	46	52.4	480.9	52.2	25	103.5	28	104.3	375.7	104.1
160	80	25.9	87	25.7	647.7	25.8	51	51.2	56	51.5	547.2	51.4	29	102.0	32	102.7	416.9	102.4
165	106	25.5	115	25.4	720.0	25.4	62	51.0	67	50.7	604.7	50.8	32	101.7	36	101.4	452.8	101.2
170	138	25.3	149	25.1	775.9	25.2	72	50.6	78	50.4	649.1	50.3	35	99.9	39	100.2	480.6	100.4
175	167	24.9	180	25.1	811.2	25.0	80	50.3	87	49.9	677.2	50.0	37	99.4	41	99.6	498.2	99.8
180	180	25.1	194	25.1	823.3	25.0	83	49.7	90	50.1	686.8	50.0	38	100.1	42	99.9	504.2	99.7

TABLE 2

Parameters Appropriate to Eq. [2] Using the Data from Table 1, after One Acquisition Pulse

Equilibrium		Old [4]		New [5]		4-Pulse	
t_i/T_1	M_0	t_i/T_1	M_0	t_i/T_1	M_0	t_i/T_1	M_0
(nutation angle range: 10°–80°)							
0.050	1000.0	0.0445	1116.3	0.0499	1005.8	0.0360	2103.6
0.100	1000.0	0.0952	1046.5	0.0998	1005.0	0.0290	114.7
0.200	1000.0	0.1954	1020.3	0.1995	1005.1	0.1883	1118.1
0.500	1000.0	0.4961	1005.8	0.4979	1004.9	0.4950	1012.4
(nutation angle range: 40°–130°)							
0.050	1000.0	0.0464	1076.3	0.0491	1020.0	0.1900	570.8
0.100	1000.0	0.0965	1034.9	0.0970	1028.4	0.1874	784.9
0.200	1000.0	0.1968	1015.1	0.1981	1010.3	0.2435	948.6
0.500	1000.0	0.4971	1004.9	0.4958	1007.3	0.5005	1012.8

Note. The data presented above are calculated as though the magnetization was driven from M_0 for each nutation angle. This may not always be the case especially if long T_i's are measured. If M_0 is not the initial magnetization, then fewer dummies than presented in Table 1 will fulfill conditions [4] and [5]. Any dummy pulses which are added after these conditions are achieved will drive the magnetization further toward M_{zeq} thus improving the accuracy of the measurement.

the old condition [4] now yields acceptable results, those based on four dummy pulses are still generally far from satisfactory. The reason for these improvements is that progressive acquisitions have the same effect as additional dummy pulses in driving the system more closely to true equilibrium.

TABLE 3

Parameters Appropriate to Eq. [2] Using the Data from Table 1, after 50 Acquisition Pulses

Equilibrium		Old [4]		New [5]		4-Pulse	
t_i/T_1	M_0	t_i/T_1	M_0	t_i/T_1	M_0	t_i/T_1	M_0
(nutation angle range: 10°–80°)							
0.050	1000.0	0.0484	1029.3	0.0499	1002.0	0.0445	1165.0
0.100	1000.0	0.0991	1007.5	0.0999	1001.0	0.0970	1041.5
0.200	1000.0	0.1995	1001.3	0.1999	1000.5	0.2070	979.8
0.500	1000.0	0.4997	1000.4	0.4999	1000.2	0.5000	1000.5
(nutation angle range: 40°–130°)							
0.050	1000.0	0.0498	1004.3	0.0499	1001.5	0.028	1766.0
0.100	1000.0	0.0998	1002.1	0.0999	1001.1	0.091	1096.3
0.200	1000.0	0.1998	1000.7	0.1999	1000.6	0.197	1015.9
0.500	1000.0	0.4999	1000.2	0.4999	1000.1	0.500	1000.4

Note. See the footnote to Table 2.

SPECTROMETER PULSE WIDTH AND OFFSET CALIBRATION

The earlier paper (1) on DESPOT suggested that the relationship between spectrometer pulse width and nutation angle could be found by using the DESPOT sequence itself around 360° where the signal intensity is zero. In Fig. 3 of Ref. (1) it is noticeable that the curves are not symmetrical about the pulse width corresponding to 360°. Subsequent work invariably revealed similarly asymmetric plots. Moreover, plots of I versus pulse width, t_p, invariably revealed zero signal intensity occurring at a finite pulse width, and this was called the pulse offset. Additionally, even after accounting for the pulse offset it has been found that t_p does not appear always to be linearly related to θ.

Superficially the above observations could be attributed to the use of numbers of dummy pulses appropriate to condition [4] rather than the demonstrably better condition [5]. However, when conditions appropriate to [5] are used, similar observations to those mentioned above have been observed. The implication is that the condition (5)

$$\gamma B_1/2\pi \gg \Delta F, \qquad [6]$$

where γ is the gyromagnetic ratio, B_1 is the strength of the nutation field pulse, and ΔF is the spectral frequency range, is not obeyed so that the pulses are imperfect and do not follow the simple linear relationship

$$\theta = \gamma B_1 t_p \qquad [7]$$

between nutation angle and pulse width. However, calibration experiments with a ^{1}H absorption adjusted to resonance show that the situation does not improve significantly.

DIFFUSION AND PULSE WIDTH CALIBRATION

Levy and Peat (6) have pointed out that diffusion of sample molecules into and out of the effective volume of the RF excitation coils can cause errors in the measurement of T_1. Accordingly, the possible effects of diffusion on pulse width calibration have been investigated. Rather than rely on the unproven DESPOT method of calibration (1) use was made of the appropriate form of Eq. [3]

$$I = KM_0 \sin \theta \qquad [8]$$

that applies when the spin system is allowed to relax for a time $>5T_1$ after the application of the nutation pulse. The experimental data were fitted to quadratic equations which were differentiated to find the maximum in I at which $\theta = 90°$. Figure 2A shows a plot of I versus t_p for the ^{1}H resonance of cyclohexane obtained using a JEOL FX 90Q spectrometer operating at 89.56 MHz. The plot is noticeably asymmetric and this leads to the "offset" evident in Fig. 3A. When the experiments were repeated with the sample constrained within the effective excitation volume of the coil, the well-behaved plots shown in Figs. 2B and 3B were obtained. These results effectively demonstrate the necessity of minimizing the effects of diffusion which become appreciable at long pulse widths. When this was done no significant difference could be found between the DESPOT method of calibration and the more conventional method used here. In both cases the minimization of diffusion essentially eliminates the "pulse offset."

THE FIELD-SPOILING PULSE

It is important to note that the DESPOT method is only valid if any $M_{x,y}$ component is destroyed between pulse sequences. This is achieved by using a z-gradient field-spoiling pulse. It is important, therefore, to ensure that the polarizing magnetic field homogeneity is allowed to recover between pulses. On many commercial spectrometers this sets a lower limit of about one second on t_i. Moreover, the use of a homogeneity-spoiling pulse may preclude the use of resolution stabilization circuitry. However, if a T_1 determination is likely to be prolonged due to adverse signal-to-noise, it may prove advantageous to use resolution stabilization and then t_i must be set greater than $5T_2^*$. Unfortunately, the imposition of the last criterion will possibly render the DESPOT method invalid for multiexponential relaxation systems, which, under conditions of short t_i, may provide data that approximate reasonably to the single exponential relaxation system for which DESPOT is specifically applicable.

CONCLUSION

The basic experimental conditions necessary to optimize the use of the DESPOT method of measuring T_1's have been reconsidered. The conditions governing the estimation of the number of dummy pulses required to drive a spin system to equilibrium have been investigated. The previously proposed condition [4] is found to introduce
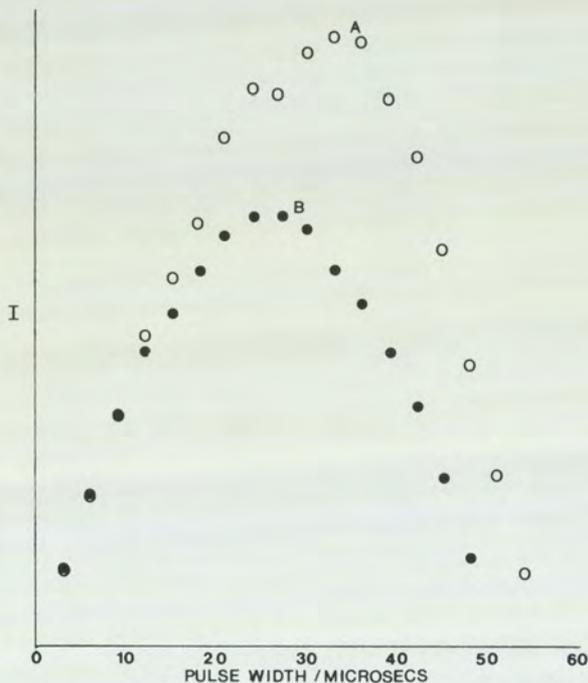

FIG. 2. Variation of intensity, I, (arbitrary units), with pulse width for the ^1H resonance of cyclohexane in a 10 mm tube. (A) Open circles represent the nonconstricted case; (B) full circles represent the constricted case.
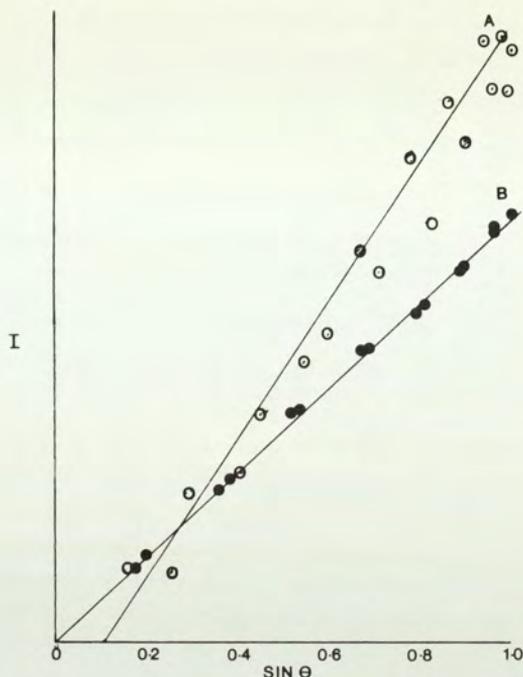
FIG. 3. Variation in intensity, I, (arbitrary units), with sin θ for the ^{1}H resonance of cyclohexane in a 10 mm tube. (A) Open circles represent the nonconstricted case; (B) full circles represent the constricted case.

significant errors into the method when the ratio t_i/T_1 is small, but when larger values of the ratio are employed, the accuracy improves. Nevertheless, the use of the new condition [5] leads to acceptably precise analyses over a wide range of experimental conditions. Suggestions (3, 4) that four dummy pulses are adequate to achieve equilibrium are shown to be incorrect except when θ approaches 90° (5) or when $t_i/T_1 \geqslant 0.5$.

A revised series of steps necessary for the improved implementation of DESPOT is as follows:

1. Ensure that the sample is restricted to the effective volume of the excitation coils to eliminate the effects of molecular diffusion.

2. Accurately determine the relationship between pulse width and nutation angle. This relationship should be checked at regular intervals.

3. Estimate the longest T_1.

4. Select t_i to give a value for t_i/T_1 (about 0.1 to 0.2) that provides a compromise between the adverse features of the large number of dummy pulses required for small values of t_i/T_1 and the small change in M_{zeq} with θ that is found at higher values of t_i/T_1.

5. Select nutation angles in the range 10° to 80° to ensure a good rate of change of M_{zeq} with θ.

6. Calculate the required number of dummy pulses enforced by condition [5].

7. Implement the DESPOT pulse train.

If the above considerations are carefully accounted for, the DESPOT method will provide a fast and accurate method for measuring spin–lattice relaxation times.

REFERENCES

1. J. HOMER AND M. S. BEEVERS, *J. Magn. Reson.* **63,** 287 (1985).
2. I. D. CAMPBELL AND R. FREEMAN, *J. Magn. Reson.* **11,** 143 (1973).
3. R. K. GUPTA, *J. Magn. Reson.* **25,** 231 (1977).
4. E. D. BECKER, J. A. FERRETTI, AND P. N. GAMBHIR, *Anal. Chem.* **51,** 1413 (1979).
5. R. FREEMAN AND H. D. W. HILL, *J. Chem. Phys.* **54,** 3367 (1971).
6. G. C. LEVY AND I. R. PEAT, *J. Magn. Reson.* **18,** 500 (1975).

The Effects of Carrier to Absorption Frequency Shift on the DESPOT Evaluation of Spin–Lattice Relaxation Times

JOHN HOMER* AND JOHN K. ROBERTS

Department of Chemical Engineering and Applied Chemistry, Aston University, Aston Triangle, Birmingham B4 7ET, England

It has been known for some time that the nutation of the magnetization vector is increasingly perturbed from the zy plane as the resonant frequency shift from the carrier frequency increases in pulsed NMR spectroscopy. This effect on the measurement of T_1 using the progressive saturation (*1, 2*) and the inversion recovery (*2*) techniques is well known. It is perhaps not as well known that the perturbation modifies the intercept of the usual inversion recovery semilog plot. This modifies the null equation for the estimation of T_1 (*3*) to $\tau_{\text{null}} = T_1 \ln(1 - k)$, where k is defined later in Eq. [3]. It seemed prudent in the light of the increasing popularity of rapid T_1 measurements to assess the implications of this perturbation on the DESPOT (*4, 5*) technique.

A typical magnetization component, $\Delta\nu$ Hz away from the carrier frequency, is nutated through an angle

$$\alpha = \gamma\sqrt{(B_1^2 + \Delta B^2)}\, t_\text{P} \tag{1}$$

in the plane perpendicular to an axis that is tilted with respect to the x axis and which makes an angle ϕ from x in the zx plane of the rotating frame:

$$\tan^{-1}\phi = \Delta B/B_1. \tag{2}$$

In Eq. [1] γ is the gyromagnetic ratio, B_1 is the pulse field strength, $\Delta B = (2\pi\Delta\nu/\gamma)$ is the residual z field due to the off-carrier frequency shift at the resonance, and t_P is the pulse width.

The effect of this (*1*) on an M_z component prior to the pulse (M_z^-) and immediately after the pulse (M_z^+) is given by

$$M_z^+ = (\sin^2\phi + \cos\alpha\cos^2\phi)M_z^- = kM_z^- \tag{3}$$

with the detected signal in the xy plane being given by

$$M_{xy}^+ = M_z^-\cos\phi\sqrt{\{(1 - \cos\alpha)^2\sin^2\phi + \sin^2\alpha\}} = \beta M_z^-. \tag{4}$$

The above considerations require the normal DESPOT equation (*4*) to be modified to account for the off-carrier frequency effect to

* To whom correspondence should be addressed.

$$I_{eq}/\beta = I_{eq}\exp(-t/T_1)k/\beta + M_0(1 - \exp(-t/T_1)), \qquad [5]$$

where I_{eq} is the measured equilibrium intensity and t is the total pulse sequence repetition time.

Unless $\phi = 0$, the normal DESPOT regression of $I_{eq}/\sin\theta$ on $I_{eq}\cos\theta/\sin\theta$ will not yield a straight line of gradient $\exp(-t/T_1)$ and intercept $M_0(1 - \exp(-t/T_1))$, where
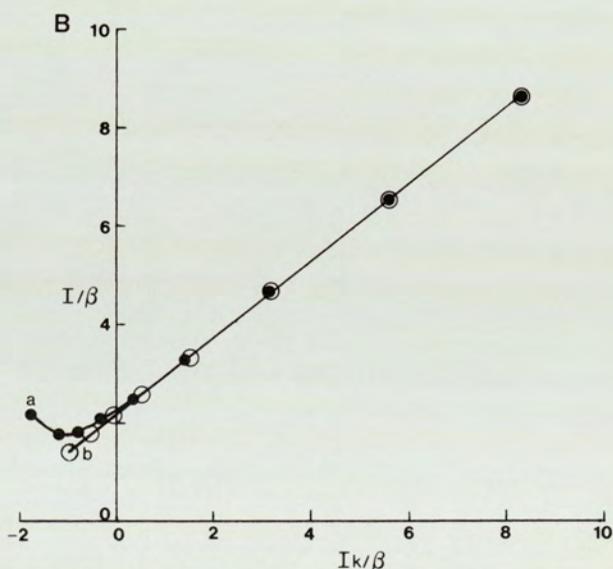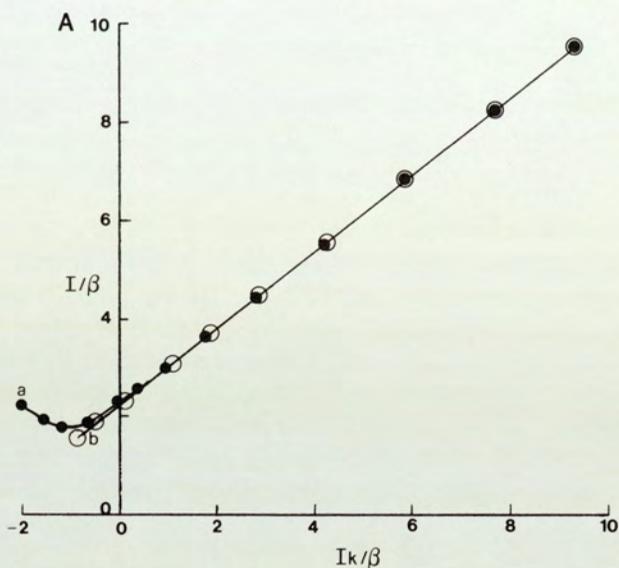

FIG. 1. (A) Theoretically derived DESPOT-type regressional plots of I/β on Ik/β with $t/T_1 = 0.5$ and nutation angle range $= 10°$ to $160°$ (a) without correction for offset parameter with β and k taken as $\sin\theta$ and $\cos\theta$, respectively, and (b) plotted appropriate to Eq. [5] with $\Delta B/B_1 = 0.45$. (B) Experimental plots for the ^{1}H-decoupled ^{13}C resonance of air-saturated benzene with the parameters identical to those in (A).

θ is the on-carrier frequency nutation angle. A plot, however, of I_{eq}/β against $I_{eq}k/\beta$ will yield the above stated slope and intercept.

Figure 1A represents theoretical DESPOT plots with an offset parameter $(\Delta B/B_1)$ = 0.45 (a) plotted normally and (b) plotted appropriate to [5]. Figure 1B represents corresponding experimental plots. It can be seen from Figs. 1A and 1B that the off-carrier frequency shift effect is more marked toward larger nutation angles. The error in the calculation of T_1 values using a normal DESPOT regression with the on-carrier nutation angle range restricted between 10° and 80° (5) is <5% if the offset parameter is maintained below 0.5.

As M_{zeq} depends on the off-carrier frequency shift effect as well as t/T_1, both will affect the number of dummy pulses required to drive the system to equilibrium (5). The required numbers of dummy pulses remain virtually unaffected by offset in the nutation angle range 10° to 75°. In the range 75° to 90° the number of dummy pulses required increases with increasing offset: As a rule of thumb for most practical offsets, an increase in the published number (5) of dummies by four should suffice. The number of dummy pulses required in the range 100° to 180° falls markedly with increasing offset.

Clearly the off-carrier effect will be most pronounced for nuclei with large chemical-shift ranges and in such cases it is important that the appropriate corrected Eq. [5] is used to calculate T_1. The need to correct for the frequency shift from the carrier will also be more pronounced in nonquadrature detection spectrometers where the carrier is positioned at one end of the spectral window.

REFERENCES

1. R. FREEMAN AND H. D. W. HILL, *J. Chem. Phys.* **54**, 3367 (1971).
2. R. FREEMAN, H. D. W. HILL, AND R. KAPTEIN, *J. Magn. Reson.* **7**, 82 (1971).
3. E. FUKUSHIMA AND S. B. ROEDER, "Experimental Pulse NMR: A Nuts and Bolts Approach," Addison–Wesley, Reading, Massachusetts, 1981.
4. J. HOMER AND M. S. BEEVERS, *J. Magn. Reson.* **63**, 287 (1985).
5. J. HOMER AND J. K. ROBERTS, *J. Magn. Reson.* **74**, 424 (1987).

The Advantages of Rapid Multipulsing in the Routine Acquisition of NMR Spectra

JOHN HOMER* AND JOHN K. ROBERTS

Department of Chemical Engineering and Applied Chemistry, Aston University, Aston Triangle, Birmingham B4 7ET, England

The use of rapid multipulsing in the routine acquisition of NMR spectra is shown to provide a maximum increase of 56% in the available S/N ratio over the ideal classical sequence $(90°-5T_1)_n$, in agreement with theoretical prediction. The variation in the S/N ratio over the classical sequence for compounds with varying T_1's is also examined and recommendations about the correct choice of nutation angle and pulse repetition time are presented. The time saving aspects of rapid multipulsing over the classical sequence are also discussed. Rapid multipulsing is shown to be beneficial in the acquisition of the spectra of low receptivity nuclei. Under certain specialized conditions, it is shown that rapid multipulsing can provide essentially quantitative data with a reasonable S/N ratio enhancement over the classical sequence. © 1989 Academic Press, Inc.

Rapid multipulsing (repeated single pulses with short interpulse delays) is used extensively to obtain NMR spectra. Under the correct conditions this can produce a significant S/N ratio advantage over the classical pulse sequence $(90°-5T_1)_n$ (*1*). However, there appears to be widespread evidence that users of NMR for routine analysis are not entirely conversant with a number of pitfalls in the use of rapid multipulsing.

The intensity due to a shifted nucleus in a rapid multipulsed spectrum is dependent on three parameters θ, τ, and T_1, where θ is the nutation angle, τ is the total pulse sequence repetition time, and T_1 is the spin–lattice relaxation time. In any spectrum the parameters τ and θ will be fixed and hence the measured intensity will be dependent only on T_1 for the chosen τ and θ. The shifted nuclei in most samples submitted for analysis relax with differing T_1's and hence rapid multipulsing will produce spectral intensities that are not solely proportional to the number of nuclei giving rise to the absorption. The above statement raises two questions. The first is, what are the best values of τ and θ for a given absorption in a spectrum to achieve a significant S/N enhancement over that available from the classical sequence in the same experimental time? The second is, to what extent will the different absorptions in the spectrum be distorted from their expected equilibrium intensities due to the differences in T_1, and under what conditions can this distortion be reduced to an acceptable minimum? This paper addresses these questions.

---

* To whom correspondence should be addressed.

THEORETICAL

Consider a magnetization component, M_0, subjected to the pulse sequence $(\theta-\tau)_n$, including a z-field spoiling pulse. The magnetization will, after a number of sequence repetitions, n, be driven to an equilibrium M_{zeq}. The corresponding measured intensity, I_{eq}, (2) is given by

$$I_{eq} = KM_0\sin\theta(1 - \exp(-\tau/T_1))/(1 - \cos\theta\exp(-\tau/T_1)), \qquad [1]$$

where K is an instrument proportionality constant. If the z-field spoiling pulse is left out of the pulse sequence the above equation is modified and the measured absorption intensity also becomes dependent on the observed spin–spin relaxation time, T_2^*, according to

$$I_{eq} = \frac{KM_0\sin\theta(1 - A)}{1 - \cos\theta(A + B) + (A \times B)}, \qquad [2]$$

where $A = \exp(-\tau/T_1)$ and $B = \exp(-\tau/T_2^*)$.

It should be emphasised at this point that the measured intensity will only depend on the above two equations when the system is driven to the equilibrium position by the appropriate number of nonacquisition pulse sequences (3). All the figures and recommendations in this paper are based on the assumption that the magnetization has been previously driven to the equilibrium position. If the nonacquisition pulse sequences are left out, the measured intensity will not be represented by Eq. [1].

THE S/N RATIO ENHANCEMENT

The signal, S_{mp}, measured at constant noise from the multipulse sequence, and obtained in a certain experimental time, E, is

$$S_{mp} = \frac{KM_0\sin\theta(1 - \exp(-\tau/T_1))}{(1 - \cos\theta\exp(-\tau/T_1))}\left(\frac{(E - (\tau \times m))}{\tau}\right)^{1/2}, \qquad [3]$$

where m is the number of nonacquisition sequences required to drive the system to equilibrium. Equation [3] is based on Eq. [1]. In cases where $5T_2^* \geqslant \tau$, and where a z-field spoiling pulse is not included, then an analogous equation based on Eq. [2] can be used.

For the classical sequence, the signal, S_c, measured at the same noise level relevant to Eq. [3], and obtained in the same experimental time, E, is

$$S_c = KM_0\left(\frac{E}{5T_1}\right)^{1/2}. \qquad [4]$$

In the experimental time, E, the theoretical maximum increase in the S/N ratio using rapid multipulsing over the classical sequence is 56%. This is attained when rapid multipulsing is carried out at the Ernst angle ($\cos\theta = \exp(-\tau/T_1)$) provided that τ/T_1 is between 0.1 and 0.5. A greater than 55% S/N ratio increase occurs provided that the τ/T_1 ratio is restricted to the range of 0.07 to 0.6 when multipulsing at the Ernst angle. Outside these τ/T_1 ranges the Ernst condition does not provide the maximum attainable S/N ratio. For example, at $\theta = 88°$ the S/N ratio maximum occurs

at $\tau \approx 1.2T_1$ whereas the Ernst condition would predict $\tau \approx 3.4T_1$. For $\theta = 88°$ with $\tau = 1.2T_1$ the S/N enhancement is 43% whereas with $\tau = 3.4T_1$ the S/N enhancement falls to 6%. Hence, when using the Ernst angle to predict the maximum S/N ratio available it is not beneficial to allow the τ/T_1 ratio to increase beyond 1.2.

Although a 56% S/N ratio enhancement is available at the Ernst angle, variations between T_1's for shifted nuclei in a particular sample cause the individual enhancements to differ. Figure 1 shows that by the judicious choice of nutation angle, the measured intensities due to specific T_1 regions of a spectrum can be selectively enhanced for a chosen τ. For example, the choice of a small nutation angle will enhance the S/N ratio for slowly relaxing ipso carbons in ^{13}C spectra, which may otherwise be reduced relative to the higher S/N ratio for the shorter T_1 nuclei. For pulse repetition times of the order of 2 s for ^{13}C spectra it can be seen from Fig. 1 that a nutation angle of 30° will give a minimum enhancement of 20% in the S/N ratio over the classical method for T_1's in the range 2.84 to 70 s ($\ln \tau/T_1 = -0.35$ to -3.55) with a maximum enhancement of 56% for a T_1 of 14 s ($\ln \tau/T_1 = -1.95$). The value of τ is usually determined by the required data point resolution and for different τ values interpolation between the plots of Fig. 1 will allow the optimum conditions of θ to be found.

In ^1H spectroscopy where τ values of the order of 4 s are often used a better choice of nutation angle will be 60° (Fig. 1). This will give a good S/N ratio enhancement over the classical sequence for the typical range of proton T_1's. It must be noted, however, that a choice of 60° will not allow for quantitative determination from proton spectra. Hence, this condition should only be used when a good S/N ratio is required rapidly and where quantitative data are not required.
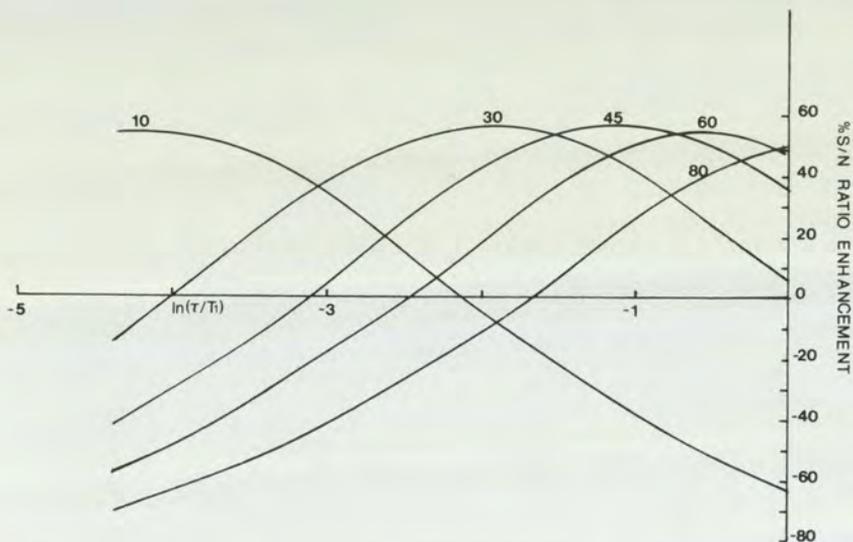

FIG. 1. Variation in the S/N ratio enhancement using rapid multipulsing, relative to the classical sequence, against $\ln(\tau/T_1)$ for various nutation angles.

Figure 2 shows the variation in the S/N enhancement, over the classical sequence, against θ for various values of the ratio τ/T_1. It can be seen readily from this figure that the maxima of the curves become broader as the ratio τ/T_1 increases. Hence, for shifted nuclei where the τ/T_1 ratio is small the enhancement is very sensitive to the value of θ chosen. For example, at $\tau/T_1 = 0.05$ the S/N ratio enhancement falls from 54% at the Ernst angle to 13% at the Ernst angle minus 10° and to 40.4% at the Ernst angle plus 10°. When $\tau/T_1 = 0.5$, however, the enhancements at the Ernst angle, the Ernst angle minus 10°, and the Ernst angle plus 10° are 56, 52, and 53%, respectively. Hence when choosing a small nutation angle to specifically look for shifted nuclei with long T_1's the chosen value of θ will be critical and the choice should err to larger values of θ rather than smaller ones. In cases where the required nutation angle would be exceptionally small it would probably be beneficial to increase the value of τ.

The S/N ratio enhancement obviously leads to a reduction in the time required to obtain spectra. The time saving is particularly worthwhile where considerable signal averaging is required, notably in the observation of low receptivity nuclei or of nuclei at low concentration. Theoretical simulations based on Eq. [3] and Eq. [4] predict that in about 43% of the time required to obtain a given S/N ratio using the classical sequence, the same S/N ratio can be obtained by rapid multipulsing at the Ernst angle provided that τ/T_1 is constrained within the range 0.07 to 0.6. Outside this range or with departure from the Ernst condition within this range the time taken to obtain the classical S/N ratio is increased. For example, when $\tau/T_1 = 2.0$ rapid multipulsing at the Ernst angle gives the same S/N ratio as that produced by the classical sequence in 53% of the time. It should be noted, however, that this time saving will only occur when the number of nonsampling sequences is small compared
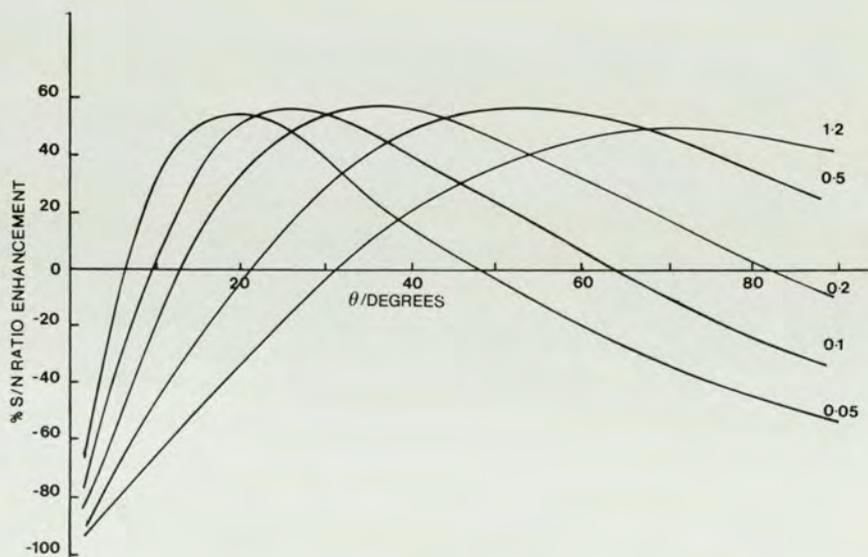

FIG. 2. Variation in the S/N ratio enhancement, relative to the classical sequence, using rapid multipulsing against the nutation angle for various values of the parameter τ/T_1.

to the number of acquisition sequences. In samples where the absorptions are likely to be strong and an adequate S/N ratio can be acquired in only a few pulse sequences the use of the classical sequence is likely to be more economical. The classical sequence will, of course, also provide quantitative data.

DEVIATIONS FROM THE BOLTZMANN EQUILIBRIUM ABSORPTION INTENSITIES

Integrated intensities are influenced by the values of T_1, τ, and θ. This is possibly not a great disadvantage for ^{13}C spectra, when ^1H broadband or composite pulse decoupling is used, because the intensities are already perturbed from their equilibrium magnetization ratios due to the nuclear Overhauser enhancement. In ^1H spectroscopy, however, where many chemists rely on ^1H NMR integrations for structural information, the systematic errors produced by rapid multipulsing could lead to errors in the spectral analysis. Figure 3 shows the theoretical spectral intensity ratio of two shifted nuclei with differing τ/T_1 ratios plotted against nutation angle. This figure shows that the true intensity ratio (unity) cannot be expected unless the nutation angle is small. For example, for a τ value of 4 s and two shifted nuclei with T_1's of 4 and 10 s, respectively, the integration error at a nutation angle of 30° is 18% but this falls to 2% at a nutation angle of 10°. However, cross referencing with Fig. 1 shows that at a nutation angle of 10° for these two shifted nuclei the classical sequence would be far more economical based on the $T_1 = 10$ s nucleus (for $\tau/T_1 = 0.4$, $\ln(\tau/T_1)$ $= -0.92$, the S/N ratio multipulsed enhancement $= -40\%$). At 30° for the same nucleus a 46% S/N ratio multipulsed enhancement is observed but the 18% error in
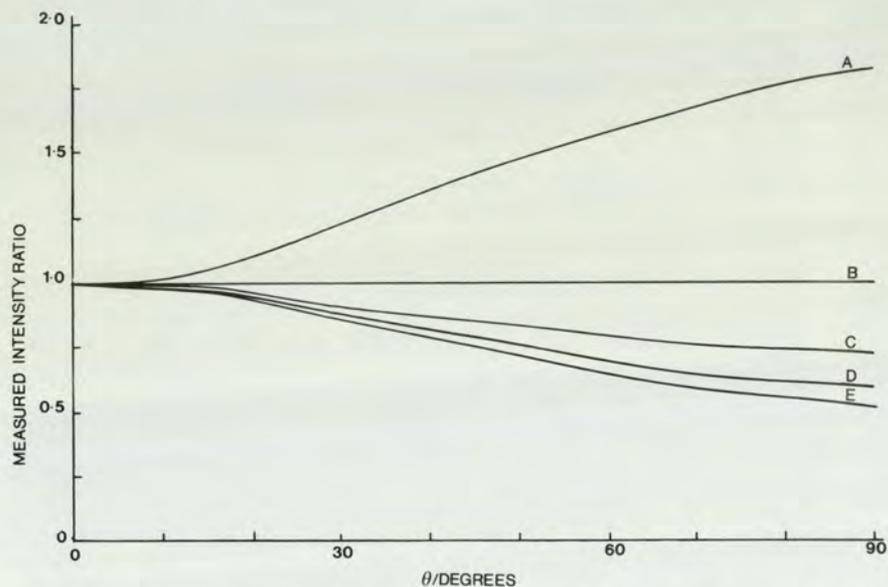

FIG. 3. Variation in the observed intensity ratio for two resonances, 1 and 2, with nutation angle for $(\tau/T_1)_1 = 0.4$ with (A) $(\tau/T_1)_2 = 0.2$; (B) $(\tau/T_1)_2 = 0.4$; (C) $(\tau/T_1)_2 = 0.6$; (D) $(\tau/T_1)_2 = 0.8$; and (E) $(\tau/T_1)_2 = 1.0$. True M_0 ratio $= 1.0$. Nonacquisition sequences for each nutation angle are based on $\tau/T_1 = 0.4$.

the relative intensities between the two shifted nuclei is unacceptably large for analytical applications.

The case described above is obviously pertinent to only one specific example. In the general case, inspection of Fig. 3 in conjunction with Fig. 1 will enable an estimation of the observed intensity ratio errors and the S/N enhancement over the classical sequence. In cases where the T_1's in a sample are known to be relatively similar then a nutation angle of 30° with a τ value of 4 s will give a reasonable S/N enhancement and reasonably quantitative spectra.

EXPERIMENTAL

To test the above proposals, the ^{1}H noise-decoupled ^{13}C spectrum of air-saturated benzene was obtained at 22.5 MHz using a Jeol FX 90Q spectrometer operating at 30°C. The T_1 of the ^{13}C nucleus was measured using the DESPOT (2, 3) sequence and found to be 14.4 s. The results of the experiments are presented in Table 1, the S/N ratios being obtained by the usual method (4). All the multipulsed experiments were carried out with a total pulse repetition time equal to 4.2 s. The results presented in Table 1 illustrate the validity of the theoretical proposals made earlier. It should be noted that during the experiments no evidence of echo formation (5) due to repetitive multipulsing was observed. Freeman et al. (6) have shown that noise decoupling effectively eliminates echo formation. ^{1}H multipulsed experiments have also shown no evidence of echo formation in our experiments, for which $T_2^* \ll \tau$.

CONCLUSIONS

Rapid multipulsing is shown to provide a 56% S/N ratio improvement relative to the classical sequence provided that the τ/T_1 ratio is maintained between 0.1 and 0.5 and the system is multipulsed at the Ernst angle. Although this can equate to a large time saving when acquiring spectra, rapid multipulsing is shown to be most efficient when applied to nuclei of low sample concentration or low receptivity. This is primarily due to the time required to drive the system to its equilibrium position. For ^{13}C acquisition the conditions $\tau = 2$ s and $\theta = 30°$ provide a good S/N improvement across the normal T_1 range relative to the classical sequence. For nonquantitative proton spectra a choice of $\tau = 4$ s and $\theta = 60°$ provides a similarly good enhancement

TABLE 1

Comparison of Rapid Multipulsed and $(90°-5T_1)_n$ Spectral Analyses

No.	Expt	Expt time/s	S/N	% Enhancement	
				Experimental	Theoretical
1	$90°-5T_1$	3384	137:1	—	—
2	Ernst angle	3385	212:1	55	56
3	Ernst angle	1457	137:1	0	0
4	90° multipulsed	3385	141:1	3	4

Note. $T_1 = 14.4$ s, $\tau = 4.2$ s in all multipulsed experiments.

across the normal proton T_1 range. Quantitative spectra, however, are best obtained by the classical sequence unless the T_1's of the shifted nuclei are similar. In such a case for ^1H spectroscopy the conditions $\tau = 4$ s and $\theta = 30°$ provide a good compromise between S/N ratio enhancement and intensity ratio distortion. Other values of τ and θ for various applications may be found from interpretation of the figures.

REFERENCES

1. E. D. BECKER, J. A. FERRETTI AND PREM. N. GAMBHIR, *Anal. Chem.* **51,** 1413 (1979).
2. J. HOMER AND M. S. BEEVERS, *J. Magn. Reson.* **63,** 287 (1985).
3. J. HOMER AND J. K. ROBERTS, *J. Magn. Reson.* **74,** 424 (1987).
4. R. R. ERNST, *in* "Advances in Magnetic Resonance" (J. S. Waugh, Ed.), Vol. 2, p. 1, Academic Press, New York, 1966.
5. E. L. HAHN, *Phys. Rev.* **80,** 580 (1950).
6. R. FREEMAN AND H. D. W. HILL, *J. Chem. Phys.* **54,** 3367 (1971).